NUREG/CR-5024
MEA-2229

Tensile and J-R Curve Characterization of Thermally Aged Cast Stainless Steels

Prepared by A.L. Hiser

Materials Engineering Associates, Inc.

Prepared for
U.S. Nuclear Regulatory
Commission

NOTICE

This report was prepared as an account of work sponsored by an agency of the United States Government. Neither the United States Government nor any agency thereof, or any of their employees, makes any warranty, expressed or implied, or assumes any legal liability or responsibility for any third party's use, or the results of such use, of any information, apparatus, product or process disclosed in this report, or represents that its use by such third party would not infringe privately owned rights.

NOTICE

Availability of Reference Materials Cited in NRC Publications

Most documents cited in NRC publications will be available from one of the following sources:

1. The NRC Public Document Room, 1717 H Street, N.W. Washington, DC 20555

2. The Superintendent of Documents, U.S. Government Printing Office, Post Office Box 37082, Washington, DC 20013-7082

3. The National Technical Information Service, Springfield, VA 22161

Although the listing that follows represents the majority of documents cited in NRC publications, it is not intended to be exhaustive.

Referenced documents available for inspection and copying for a fee from the NRC Public Document Room include NRC correspondence and internal NRC memoranda; NRC Office of Inspection and Enforcement bulletins, circulars, information notices, inspection and investigation notices; Licensee Event Reports; vendor reports and correspondence; Commission papers; and applicant and licensee documents and correspondence.

The following documents in the NUREG series are available for purchase from the GPO Sales Program: formal NRC staff and contractor reports, NRC-sponsored conference proceedings, and NRC booklets and brochures. Also available are Regulatory Guides, NRC regulations in the *Code of Federal Regulations*, and *Nuclear Regulatory Commission Issuances*.

Documents available from the National Technical Information Service include NUREG series reports and technical reports prepared by other federal agencies and reports prepared by the Atomic Energy Commission, forerunner agency to the Nuclear Regulatory Commission.

Documents available from public and special technical libraries include all open literature items, such as books, journal and periodical articles, and transactions. *Federal Register* notices, federal and state legislation, and congressional reports can usually be obtained from these libraries.

Documents such as theses, dissertations, foreign reports and translations, and non-NRC conference proceedings are available for purchase from the organization sponsoring the publication cited.

Single copies of NRC draft reports are available free, to the extent of supply, upon written request to the Division of Information Support Services, Distribution Section, U.S. Nuclear Regulatory Commission, Washington, DC 20555.

Copies of industry codes and standards used in a substantive manner in the NRC regulatory process are maintained at the NRC Library, 7920 Norfolk Avenue, Bethesda, Maryland, and are available there for reference use by the public. Codes and standards are usually copyrighted and may be purchased from the originating organization or, if they are American National Standards, from the American National Standards Institute, 1430 Broadway, New York, NY 10018.

NUREG/CR-5024
MEA-2229
RF, R5

Tensile and J-R Curve Characterization of Thermally Aged Cast Stainless Steels

Manuscript Completed: August 1988
Date Published: September 1988

Prepared by
A.L. Hiser

Materials Engineering Associates, Inc.
9700-B Martin Luther King, Jr. Highway
Lanham, MD 20706-1837

Prepared for
Division of Engineering
Office of Nuclear Regulatory Research
U.S. Nuclear Regulatory Commission
Washington, DC 20555
NRC FIN B8900

ABSTRACT

Although cast stainless steels have excellent properties in the as-received or pre-service condition, significant degradation of the properties, principally fracture toughness (J-R curve), can occur after extended exposure to elevated temperatures typical of service conditions.

The NRC is sponsoring work to study the significance of in-service embrittlement of thermally aged, cast stainless steel. This report summarizes the results of tensile and J-R curve tests of commercial and experimental heats of these steels. The materials were supplied by Argonne National Laboratory (ANL), who have conducted microstructural studies to identify the degradation mechanisms.

The loss in Charpy-V upper shelf energy can be quite large, up to 57% for aging at 450°C for 9980 h. The decrease in fracture toughness, specifically J levels on the J-R curve, can be even more severe, with a reduction of 75% in some cases.

Data from this study are accessible through the NRC's Piping Fracture Mechanics Data Base (PIFRAC), an on-line system available at MEA.

CONTENTS

LIST OF FIGURES

LIST OF FIGURES

LIST OF FIGURES

LIST OF FIGURES

LIST OF FIGURES

LIST OF FIGURES

LIST OF FIGURES

LIST OF TABLES

LIST OF TABLES

FOREWORD

The work reported here was performed at Materials Engineering Associates (MEA) under the program Structural Integrity of Water Reactor Pressure Boundary Components, F. J. Loss, Program Manager. The program is sponsored by the Office of Nuclear Regulatory Research of the U. S. Nuclear Regulatory Commission (NRC). The technical monitor for the NRC is Alfred Taboada.

Prior reports under the current contract are listed below:

1. J. R. Hawthorne, "Significance of Nickel and Copper to Radiation Sensitivity and Postirradiation Heat Treatment Recovery of Reactor Vessel Steels," USNRC Report NUREG/CR-2948, Nov. 1982.

2. "Structural Integrity of Water Reactor Pressure Boundary Components, Annual Report for 1982," F. J. Loss, Ed., USNRC Report NUREG/CR-3228, Vol. 1, Apr. 1983.

3. J. R. Hawthorne, "Exploratory Assessment of Postirradiation Heat Treatment Variables in Notch Ductility Recovery of A 533-B Steel," USNRC Report NUREG/CR-3229, Apr. 1983.

4. W. H. Cullen, K. Torronen, and M. Kemppainen, "Effects of Temperature on Fatigue Crack Growth of A 508-2 Steel in LWR Environment," USNRC Report NUREG/CR-3230, Apr. 1983.

5. "Proceedings of the International Atomic Energy Agency Specialists' Meeting on Subcritical Crack Growth," Vols. 1 and 2, W. H. Cullen, Ed., USNRC Conference Proceeding NUREG/CP-0044, May 1983.

6. W. H. Cullen, "Fatigue Crack Growth Rates of A 508-2 Steel in Pressurized, High-Temperature Water," USNRC Report NUREG/CR-3294, June 1983.

7. J. R. Hawthorne, B. H. Menke, and A. L. Hiser, "Notch Ductility and Fracture Toughness Degradation of A 302-B and A 533-B Reference Plates from PSF Simulated Surveillance and Through-Wall Irradiation Capsules," USNRC Report NUREG/CR-3295, Vol. 1, Apr. 1984.

8. J. R. Hawthorne and B. H. Menke, "Postirradiation Notch Ductility and Tensile Strength Determinations for PSF Simulated Surveillance and Through-Wall Specimen Capsules," USNRC Report NUREG/CR-3295, Vol. 2, Apr. 1984.

9. A. L. Hiser and F. J. Loss, "Alternative Procedures for J-R Curve Determination," USNRC Report NUREG/CR-3402, July 1983.

10. A. L. Hiser, F. J. Loss, and B. H. Menke, "J-R Curve Characterization of Irradiated Low Upper Shelf Welds," USNRC Report NUREG/CR-3506, Apr. 1984.

11. W. H. Cullen, R. E. Taylor, K. Torronen, and M. Kemppainen, "The Temperature Dependence of Fatigue Crack Growth Rates of A 351 CF8A Cast Stainless Steel in LWR Environment," USNRC Report NUREG/CR-3546, Apr. 1984.

12. "Structural Integrity of Light Water Reactor Pressure Boundary Components -- Four-Year Plan 1984-1988," F. J. Loss, Ed., USNRC Report NUREG/CR-3788, Sep. 1984.

13. W. H. Cullen and A. L. Hiser, "Behavior of Subcritical and Slow-Stable Crack Growth Following a Postirradiation Thermal Anneal Cycle," USNRC Report NUREG/CR-3833, Aug. 1984.

14. "Structural Integrity of Water Reactor Pressure Boundary Components: Annual Report for 1983," F. J. Loss, Ed., USNRC Report NUREG/CR-3228, Vol. 2, Sept. 1984.

15. W. H. Cullen, "Fatigue Crack Growth Rates of Low-Carbon and Stainless Piping Steels in PWR Environment," USNRC Report NUREG/CR-3945, Feb. 1985.

16. W. H. Cullen, M. Kemppainen, H. Hanninen, and K. Torronen, "The Effects of Sulfur Chemistry and Flow Rate on Fatigue Crack Growth Rates in LWR Environments," USNRC Report NUREG/CR-4121, Feb. 1985.

17. "Structural Integrity of Water Reactor Pressure Boundary Components: Annual Report for 1984," F. J. Loss, Ed., USNRC Report NUREG/CR-3228, Vol. 3, June 1985.

18. A. L. Hiser, "Correlation of C_v and K_{Ic}/K_{Jc} Transition Temperature Increases Due to Irradiation," USNRC Report NUREG/CR-4395, Nov. 1985.

19. W. H. Cullen, G. Gabetta, and H. Hanninen, "A Review of the Models and Mechanisms For Environmentally-Assisted Crack Growth of Pressure Vessel and Piping Steels in PWR Environments," USNRC Report NUREG/CR-4422, Dec. 1985.

20. "Proceedings of the Second International Atomic Energy Agency Specialists' Meeting on Subcritical Crack Growth," W. H. Cullen, Ed., USNRC Conference Proceeding NUREG/CP-0067, Vols. 1 and 2, Apr. 1986.

21. J. R. Hawthorne, "Exploratory Studies of Element Interactions and Composition Dependencies in Radiation Sensitivity Development," USNRC Report NUREG/CR-4437, Nov. 1985.

22. R. B. Stonesifer and E. F. Rybicki, "Development of Models for Warm Prestressing," USNRC Report NUREG/CR-4491, Jan. 1987.

23. E. F. Rybicki and R. B. Stonesifer, "Computational Model for Residual Stresses in a Clad Plate and Clad Fracture Specimens," USNRC Report NUREG/CR-4635, Oct. 1986.

24. D. E. McCabe, "Plan for Experimental Characterization of Vessel Steel After Irradiation," USNRC Report NUREG/CR-4636, Oct. 1986.

25. E. F. Rybicki, J. R. Shadley, and A. S. Sandhu, "Experimental Evaluation of Residual Stresses in a Weld Clad Plate and Clad Test Specimens," USNRC Report NUREG/CR-4646, Oct. 1986.

26. "Structural Integrity of Water Reactor Pressure Boundary Components: Annual Report for 1985," F. J. Loss, Ed., USNRC Report NUREG/CR-3228, Vol. 4, June 1986.

27. G. Gabetta and W. H. Cullen, "Application of a Two-Mechanism Model for Environmentally-Assisted Crack Growth," USNRC Report NUREG/CR-4723, Oct. 1986.

28. W. H. Cullen, "Fatigue Crack Growth Rates in Pressure Vessel and Piping Steels in LWR Environments," USNRC Report NUREG/CR-4724, Mar. 1987.

29. W. H. Cullen and M. R. Jolles, "Fatigue Crack Growth of Part-Through Cracks in Pressure Vessel and Piping Steels: Air Environment Results, USNRC Report NUREG/CR-4828.

30. D. E. McCabe, "Evaluation of Surface Cracks Embedded in Reactor Vessel Cladding Unirradiated Bend Specimens," USNRC Report NUREG/CR-4841, May 1987.

31. H. Hanninen, M. Vulli, and W. H. Cullen, "Surface Spectroscopy of Pressure Vessel Steel Fatigue Fracture Surface Films Formed in PWR Environments," USNRC Report NUREG/CR-4863, July 1987.

32. A. L. Hiser and G. M. Callahan, "A User's Guide to the NRC's Piping Fracture Mechanics Data Base (PIFRAC)," USNRC Report NUREG/CR-4894, May 1987.

33. "Proceedings of the Second CSNI Workshop on Ductile Fracture Test Methods (Paris, France, April 17-19, 1985)," F. J. Loss, Ed., USNRC Conference Proceeding NUREG/CP-0064, (in publication).

34. W. H. Cullen and D. Broek, "The Effects of Variable Amplitude Loading on A 533-B Steel in High-Temperature Air and Reactor Water Environments," USNRC Report NUREG/CR-4929 (in publication).

35. "Structural Integrity of Water Reactor Pressure Boundary Components: Annual Report for 1986," F. J. Loss, Ed., USNRC Report NUREG/CR-3228, Vol. 5, July 1987.

36. F. Ebrahimi et. al, "Development of a Mechanistic Understanding of Radiation Embrittlement in Reactor Pressure Vessel Steels: Final Report," USNRC Report NUREG/CR-5063, Jan. 1988.

37. J. B. Terrell, "Fatigue Life Characterization of Smooth and Notched Piping Steel Specimens in 288°C Air Environments," USNRC Report NUREG/CR-5013, May 1988.

ACKNOWLEDGMENT

This work was supported in part by the Division of Engineering of the U.S. Nuclear Regulatory Commission (M. Vagins and A. Taboada were NRC Program Managers) and in part by the Argonne National Laboratory (through O. Chopra).

The assistance of the following at MEA is appreciated: E. M. D'Ambrosio, B. H. Menke, L. K. Fletcher, T. B. Ramey and F. J. Loss. J. Phillips and L. Gelzer-Cargill were virtually flawless (as usual) in preparing this manuscript.

1. INTRODUCTION

While the preservice properties of cast duplex stainless steels make them an excellent choice for use in nuclear power plant applications, the mechanical properties of such steels have been found to degrade substantially in some cases after extended exposure to elevated temperatures (Ref. 1-4). Previous work in this regard has been carried out using temperatures above 400°C, with at best Charpy V-notch (C_v) specimens used to assess the embrittlement. As a part of ongoing work for the U. S. Nuclear Regulatory Commission's (NRC) Office of Nuclear Regulatory Research, Argonne National Laboratory (ANL) investigators are studying the significance of in-service embrittlement of cast duplex stainless steels under light-water reactor operating conditions (Ref. 5-9). ANL is using microstructural studies to identify the mechanism(s) of embrittlement, with C_v, tensile, and fracture toughness (in this case J-R curve) tests to assess the extent of embrittlement. The tensile and J-R curve data permit the assessment of the significance of the embrittlement to safety margins under postulated flaw or loading conditions. While safety margins for the "preservice" material properties are thought to be quite high, assessments of the extent of the embrittlement (in terms of degraded properties) for actual material under typical service conditions is required to assure that sufficient safety margins are available in commercial plants.

ANL has studied 19 experimental heats and 6 commercial heats, with specimen blanks aged at temperatures from 290°C to 450°C for times up to 50,000 h. Within and in cooperation with the ANL program, Materials Engineering Associates, Inc. (MEA) has performed tensile and J-R curve tests of some of the heats under study at ANL. This report addresses the results of the MEA work.

2. MATERIALS AND AGING CONDITIONS

Specimens were provided by ANL to MEA from four commercial heats and three experimental heats. An additional commercial heat was obtained independent of ANL. Details on each heat are given in Tables 1 to 8.

The commercial heats are from two heats of centrifugally-cast pipe (Heats P1 and P2), and single heats from a pump casing ring (Heat C1) and a pump impeller (Heat I). The last heat is from a research pressure vessel, made from centrifugally-cast rings (Heat ZP18). Heats P1 and C1 represent CF8 grades, whereas Heats P2 and I represent CF3 grades and Heat ZP18 represents the CF8A grade. Heat C1 has the lowest ferrite content at ~ 2%, with Heats P2 (~ 14.5%), ZP18 (17.4%), I (~ 17.7%) and P1 (~ 23.5%) following in ascending order. Heats C1 and ZP18 were tested in the as-received condition only.

The experimental heats (Heats 68, 69 and 70) were made as static cast slabs, consistent with specification SA 351. Heat 68 represents the CF8 grade, Heat 69 the CF3 grade and Heat 70 the CF8M grade. The ferrite contents are all quite high, from 18.9% (Heat 70) to 23.6% (Heat 69).

Table 1 Information on Commercial Heat P1[a] (Specification: SA 451-C(P)F8 Product Form: Centrifugually Cast Pipe, 890-mm diameter x 63.5-mm wall)

Chemical Composition (Wt. %) from Product Analysis

	C	Mn	P	S	Si	Ni	Cr	Mo	N
I.D.[b]	0.040	0.61	0.024	0.012	1.17	8.20	20.60	0.04	0.060
O.D.[b]	0.032	0.56	0.028	0.014	1.07	8.00	20.38	0.04	0.053
-c-	0.034	0.62	0.023	0.018	0.95	7.68	20.87	0.03	0.051

Hardness: I.D. 85.3 Rockwell-B
O.D. 84.5 Rockwell-B

Ferrite Content: I.D. 19.5%
(Measured) O.D. 27.6%

Description of Grains: Equiaxed

[a] All information courtesy of ANL
[b] I.D. = Inside Diameter; O.D. = Outside Diameter
[c] MEA analysis of fracture toughness specimen P1T-6LC, from the pipe O.D.

Table 2 Information on Commercial Heat P2[a] (Specification: SA 451-C(P)F3 Product Form: Centrifugually Cast Pipe, 930-mm diameter x 73.0-mm wall)

Chemical Composition (Wt. %) from Product Analysis

	C	Mn	P	S	Si	Ni	Cr	Mo	N
H[b]	0.028	0.84	0.021	0.006	1.01	9.66	20.14	0.11	ND[c]
C[b]	0.029	0.83	0.017	0.005	0.98	9.54	20.23	0.11	ND[c]
I.D.[d]	0.019	0.75	0.018	0.006	0.95	9.51	20.20	0.16	0.040
O.D.[d]	0.020	0.72	0.019	0.005	0.92	9.24	20.20	0.16	0.041
-e-	0.028	0.78	0.019	0.001	0.84	8.90	20.87	0.14	0.034

Hardness: I.D. 85.1 Rockwell-B
O.D. 82.4 Rockwell-B

Ferrite Content: I.D. 13.2%
(Measured) O.D. 15.9%

Description of Grains: Equiaxed

[a] All information courtesy of ANL
[b] Vendor analysis with H = Hot or pouring end; C = Cold or opposite end
[c] Not Determined
[d] ANL analysis with I.D. = Inside Diameter; O.D. = Outside Diameter
[e] MEA analysis of fracture toughness specimen P2T-5LC, from the pipe O.D.

Table 3 Information on Commercial Heat I[a] (Specification: SA 351-CF3 Product Form: Static-Cast Pump Impeller)

Chemical Composition (Wt. %) from Product Analysis

	C	Mn	P	S	Si	Ni	Cr	Mo	N
Vanes	0.019	0.47	0.025	0.011	0.82	8.65	20.14	0.45	0.032
Shroud	0.020	0.47	0.036	0.012	0.82	8.64	20.34	0.44	0.029
Hub	0.015	0.48	0.033	0.012	0.84	8.84	20.20	0.46	0.028
-b-	0.034	0.50	0.030	0.016	0.68	8.50	20.35	0.45	0.027

Hardness: Vanes 81.7 Rockwell-B
Shroud 78.1 Rockwell-B
Hub 81.0 Rockwell-B

Ferrite Content (Measured): Vanes 17.2%
Shroud 16.9%
Hub 19.1%

Description of Grains: Mixed columnar and equiaxed

[a] All information courtesy of ANL
[b] MEA analysis of fracture toughness specimen I2-1LC, from the shroud

Table 4 Information on Commercial Heat C1[a] (Specification: SA 351-CF8 Product Form: Static-Cast Pump Casing Ring, 600-mm diameter x 57.2-mm wall)

Chemical Composition (Wt. %) from Product Analysis

	C	Mn	P	S	Si	Ni	Cr	Mo	N
I.D.[b]	0.042	1.22	0.030	0.008	1.17	9.42	18.89	0.65	0.040
O.D.[b]	0.036	1.22	0.036	0.008	1.19	9.32	19.10	0.64	0.041

Hardness: I.D. 78.3 Rockwell-B
O.D. 80.6 Rockwell-B

Ferrite Content (Measured): I.D. 2.3%
O.D. 1.7%

[a] All information courtesy of ANL
[b] I.D. = Inside Diameter O.D. = Outside Diameter

Table 5 Information on Commercial Heat ZP18 (Specification: SA 351-CF8A Product Form: Centrifugually Cast Ring, 813-mm diameter x 57-mm wall)

Chemical Composition (Wt. %) from Product Analysis							
C	Mn	P	S	Si	Ni	Cr	Co
0.06	0.68	0.02	0.02	1.17	8.58	20.42	0.07

Ferrite Content: 17.4%
(measured)

Table 6 Information on Experimental Heat 68[a] (Specification: SA 351-CF8 Product Form: 76-mm thick slab, cast flat)

Chemical Composition (Wt. %) from Product Analysis								
C	Mn	P	S	Si	Ni	Cr	Co	N
0.05	0.67	0.018	0.013	1.13	8.08	20.85	0.06	0.062

Hardness: 84.6 Rockwell-B

Ferrite Content: 23.4%
(Measured)

Description of Grains: Mixed columnar and equiaxed

[a] All information courtesy of ANL

Table 7 Information on Experimental Heat 69[a] (Specification: SA 351-CF3 Product Form: 76-mm thick slab, cast flat)

Chemical Composition (Wt. %) from Product Analysis								
C	Mn	P	S	Si	Ni	Cr	Co	N
0.021	0.62	0.011	0.007	1.10	8.54	20.49	0.027	0.027

Hardness: 83.7 Rockwell-B

Ferrite Content: 23.6%
(Measured)

Description of Grains: Mixed columnar and equiaxed

[a] All information courtesy of ANL.

Table 8 Information on Experimental Heat 70 (Specification: SA 351-CF8M Product Form: 76-mm thick slab, cast flat)

Chemical Composition (Wt. %) from Product Analysis								
C	Mn	P	S	Si	Ni	Cr	Co	N
0.066	0.55			0.72	9.01	19.17		0.049

Hardness: 85.8 Rockwell-B

Ferrite Content: 18.9%
(Measured)

Description of Grains: Mixed columnar and equiaxed

[a] All information courtesy of ANL

Specimen blanks were aged prior to final machining of the specimens. Aging times were 3,000 h and 10,000 h, with aging temperatures of 350°C, 400°C, and 450°C (Table 9). Aging time and temperature is specified for each specimen in the appropriate summary table.

Table 9 Summary of Aging Conditions

Heat ID[a]	Grade	Aging Temperature				
		350°C		400°C		450°C
		(3000 h)	(10000 h)	(3000 h)	(10000 h)	(3000 h)
C1	CF8	-	-	-	-	-
ZP18	CF8A	-	-	-	-	-
I	CF3	-	X	-	-	-
P1	CF8	-	X	-	X	-
P2	CF3	X	X	-	X	-
68	CF8	X	-	X	-	X
69	CF3	X	-	X	-	X
70	CF8M	X	-	X	-	X

[a] Virgir (unaged) specimens were tested from each heat.

3. TENSILE TEST AND DATA ANALYSIS PROCEDURES

Tensile test data are used to analyze J-R curve data (using strength results) and to assess safety margins in structures (using stress-strain data). In this work, tensile specimen tests were designed to provide data matching the loading plane orientation, test temperature, and aging conditions of the J-R curve tests.

Applicable ASTM Standards E 8 (Standard Methods of Tension Testing of Metallic Materials) and E 21 (Standard Recommended Practice for Elevated Temperature Tension Tests of Metallic Materials) were followed in all cases.

3.1 Test Specimen

The tensile specimen design used is a subsized specimen machined from a C_v specimen blank. As indicated in Fig. 1, the specimen design utilized a circular cross-section with a diameter of ~ 5.1 mm (0.2 in.), with threaded ends for gripping purposes.

3.2 Test Procedure

Tensile tests were performed in a servohydraulic test frame, with a maximum loading capacity of 89 kN (20 kips). A contacting axial extensometer was used for continuous measurement of strain, with an initial gage length of 12.7 mm (0.5 in.) typically used. On some specimens, punch marks with a spacing of ~ 20 mm (~ 0.8 in.) were used to assess total elongation after each test. The remaining specimens used the extensometer attachment marks for total elongation evaluation. The latter represents a non-standard measurement.

Load and axial displacement data were digitized using digital voltmeters and stored on floppy disks using a desktop computer. An analog trace of load vs. extensometer displacement was made for each test.

Elevated temperature tests at 290°C (~550°F) were conducted with identical hardware to that used for ambient temperature tests. To achieve the test temperature, a forced-air recirculating furnace was used to enclose the specimen and grips. Thermocouples were mounted on the specimen above and below the extensometer, with monitored temperatures within ± 2°C of the target temperature in most cases.

3.3 Data Analysis Procedures

Engineering stress (σ_E) and strain (ϵ_E) were calculated from the initial gage diameter and length, respectively, as given by:

$$\sigma_E = \frac{P}{A_o} \qquad (1)$$

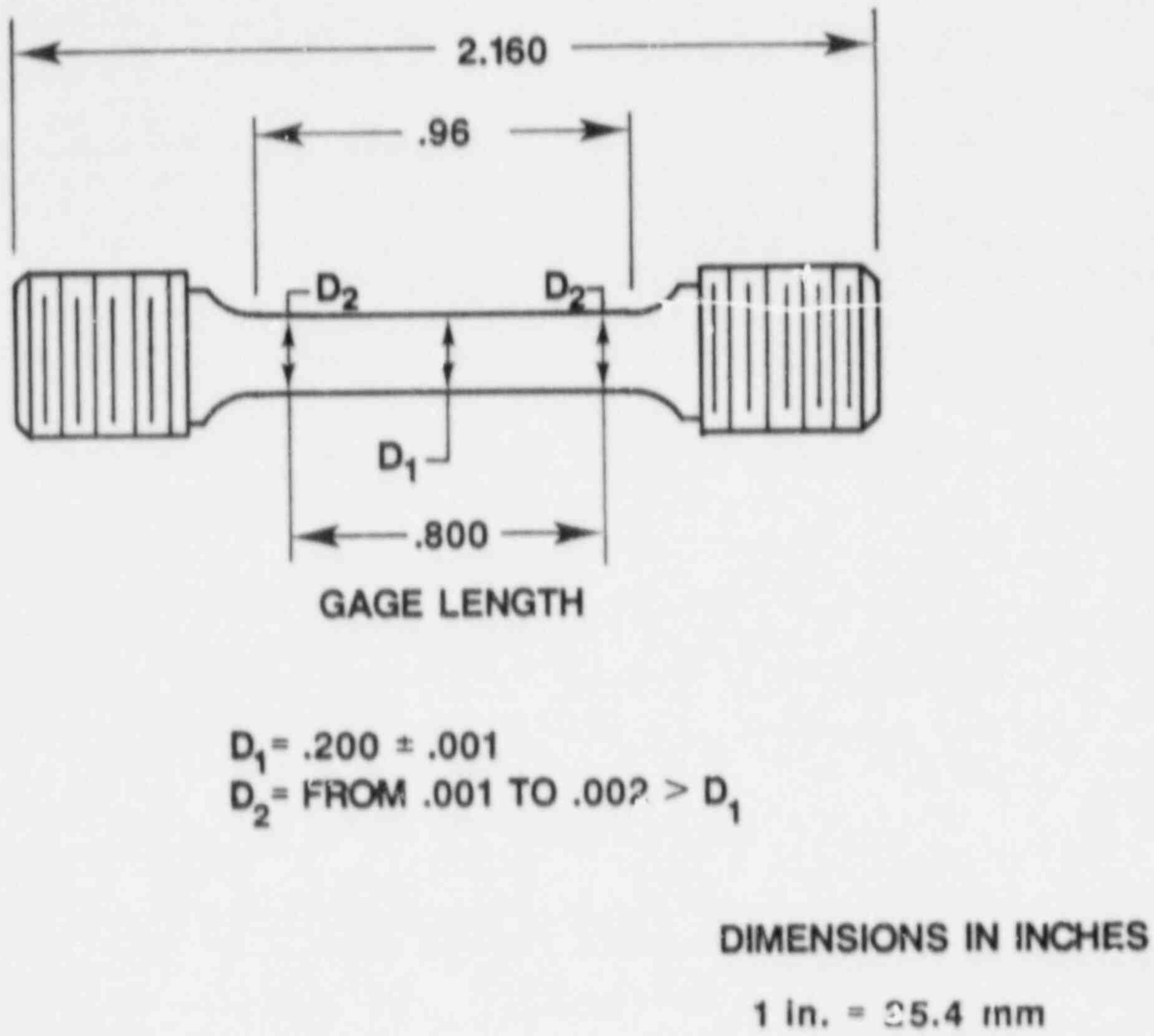

Fig. 1 The tensile specimens were machined from Charpy-V specimen blanks. The gage diameter is ~5.1 mm (0.2 in.).

$$\epsilon_E = \frac{\Delta L}{L_o} \tag{2}$$

where P is the applied load, A_o is the gage section area given by πr_o^2 (where r_o is the initial gage section radius), ΔL is the extensometer displacement and L_o is the initial extensometer gage length.

Because of necking, true stress-strain values are calculated from measured load and extensometer displacement up to maximum load only; the final gage diameter and radius of curvature (of the necked region) are used to obtain values of true stress-strain at fracture. Up to maximum load, true strain (ϵ_T) is calculated from:

$$\epsilon_T = LOG_e\ (\epsilon_E + 1) \tag{3}$$

whereas true stress (σ_T) is calculated from:

$$\sigma_T = \sigma_E\ (\epsilon_E + 1) \tag{4}$$

based on assumptions of constant volume (i.e., incompressibility) and a homogeneous distribution of strain along the gage length (Ref. 10).

The true strain at fracture (ϵ_{Tf}) is calculated from:

$$\epsilon_{Tf} = LOG_e\ (A_o/A_f) \tag{5}$$

where A_f, the final (measured) gage area, is given by πr_f^2. Dimension r_f is the measured final gage section radius.

The true stress at fracture (σ_{Tf}) is calculated using a Bridgman correction (Ref. 11):

$$\sigma_{Tf} = P_f/[A_f\ (1 + 2\ R/r_f)\ LOG_e\ (1 + r_f/2R)] \tag{6}$$

where P_f is the load at fracture and R is the measured radius of curvature of the necked region. This correction, from a mathematical analysis, adjusts the average axial stress to account for the introduction of transverse stresses. The following assumptions were made for the Bridgman correction (Ref. 10):

(1) The contour of the neck is approximated by the arc of a circle.
(2) The cross section of the necked region remains circular throughout the test.

(3) The von Mises' criterion for yielding applies.
(4) The strains are constant over the cross section of the necked region.

With these cast stainless steel specimens, the gage section tended to "orange peel", with a lumpy, irregular surface remaining after fracture. This result is due to the large grains within the cast duplex stainless steels, relative to specimen dimensions. In addition, the fracture cross-section tended to be quite irregular instead of the near circular section one would expect to see with carbon or low alloy steels. These two characteristics make evaluation of r_f (the final gage section radius) and R (the radius of curvature of the necked region) very difficult, with attempts at consistent evaluation of average values made in all cases. These characteristics also are cause for questioning the applicability of the true stress-strain equations used, given their simplified assumptions on strain distribution and incompressibility.

4. FRACTURE TOUGHNESS TEST AND DATA ANALYSIS PROCEDURES

The fracture toughness data were evaluated using elastic-plastic fracture mechanics methodology, specifically the J integral and the J resistance or J-R curve. Applicable ASTM Standards E 813 (Standard Test Method for J_{Ic}, a Measure of Fracture Toughness) and E 1152 (Standard Test Method for Determining J-R Curves) were followed in all cases.

4.1 Test Specimen and Preparation

The fracture toughness tests were accomplished using 25.4-mm (1-in.) thick compact tension (CT) specimens of a 1T plan-size. The CT specimen design (Fig. 2) is similar to the ASTM E 399 specimen in overall dimensions, with an enlarged notch region consistent with ASTM E 813 and E 1152 to permit measurement of load-line displacement (see discussion in Section 4.3). For such measurements, razor blades are screwed onto the specimen along the load line.

After machining, fatigue precracks were introduced into the specimens via cycling at load levels within the linear elastic range. To facilitate crack initiation from the machined notch, the specimens were compressed to a load level of 12.9 kN (2.9 ksi) prior to fatigue cycling. Fatigue cycling was then over a load range from 12.9 kN (2.9 ksi) to 1.3 kN (0.3 ksi), with crack length monitored visually. The target final (surface) crack length to width (a/W) ratio was 0.5. At the end of precracking, K_{max} was ~ 22 MPa$\sqrt{m}$ (20 ksi$\sqrt{in.}$).

After precracking, all specimens were side grooved by 20% of the total specimen thickness B, 10% per side. The resultant net specimen thickness (B_N) was then equal to 0.8 B. Side grooving is used to promote uniform (straight) crack growth during testing and to give lower bound J-R curve levels. The straight crack growth improves the performance of the compliance method used for estimating crack growth during testing, and indicates a closer tendency towards generalized plane strain across the crack front.

4.2 Test Procedure

The J-R curve tests were performed using a servohydraulic test frame. The load cell used in all cases had a maximum load capacity of 111 kN (25 kips).

An analog trace of load vs. load-line displacement was made in each case. Load and displacement data were digitized using digital voltmeters and stored on floppy disks using a desktop computer. This system simplified post-test analysis and correction of the test data.

The test procedures used are in general conformance with ASTM E 813 and E 1152. Specifically, the single specimen compliance, or SSC, procedure was used. A complete description of this procedure, as used by MEA, is given in Reference 12.

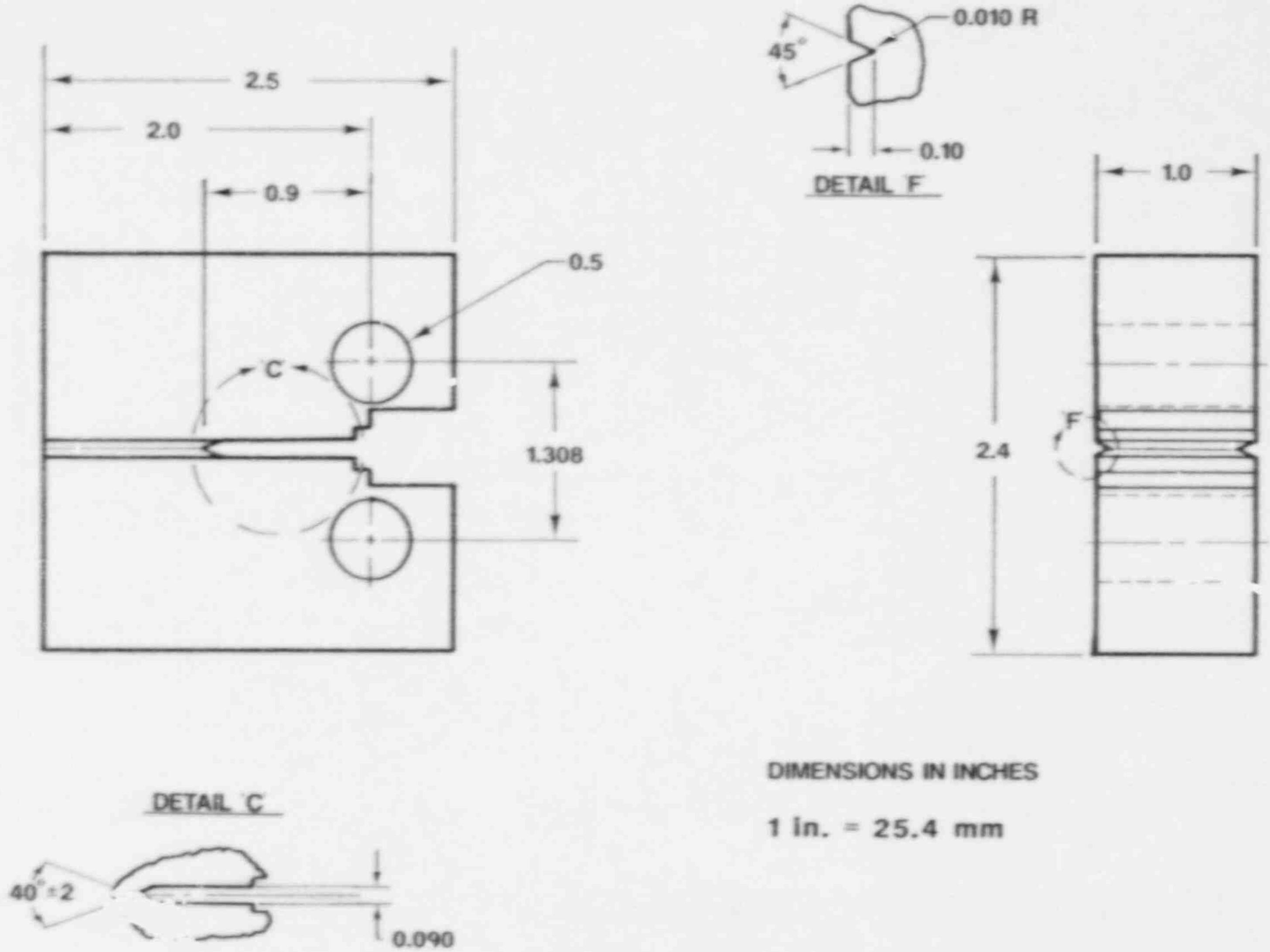

Fig. 2 The CT specimen design is a 1T-CT size, 25.4 mm (1 in.) thick. With this design, a standard loadline-mounted clip gage is used to measure displacement.

After each test, the specimen was heated in excess of 316°C to promote oxidation of the exposed fracture surface, i.e., to heat tint the surface. Once the specimen had returned to near ambient temperature, the specimen was fatigue cycled to failure (using a maximum load level no more than 80% of the final test load), exposing the fracture surface. The specimen initial (precrack) and final (test) crack lengths were measured directly from the fracture surface using an optical measurement system. This system consists of an X-Y micrometer slide assembly and a magnifying eyepiece. The crack lengths were evaluated using the 9/8 averaging technique, in which the two near surface measurements are averaged together, with the resultant value averaged with the other seven measurements.

4.3 Data Analysis Procedures

A detailed description of the data analysis procedures used are given in Appendix A. A brief summary is given here.

As mentioned previously, the compliance method has been used to determine crack length during the testing of each specimen. The Hudak-Saxena calibration equation (Ref. 13) is used to relate the measurements of compliance on the specimen load line to crack length. Both rotation (Ref. 14) and modulus corrections are made to the compliance data; these are described in detail in Appendix A.

The J-integral values reported here have been evaluated using the modified form of the J integral, J_M (Ref. 15), instead of the deformation theory J, J_D, as specified for use in ASTM Standards E 813-81 and E 1152. The severe validity criteria associated with J_D render J_D-R curve evaluations virtually useless for application to structural stability determinations, primarily due to limits on crack extension. Evaluation of J_D-R curves for different sizes of CT specimens have demonstrated specimen size dependence as well. Modified J is used here because it has been shown to be specimen size independent under greatly relaxed validity requirements, with much greater crack growth increments yielding acceptable results.

The J integral does have certain validity criteria associated with it, generally to ensure that a region of "J dominance" exists. The primary criteria for "J dominance" include:

$$\omega = \frac{b}{J}\frac{dJ}{da} >> 1 \tag{7}$$

$$\Delta a < (0.06 \text{ or } 0.1)\ b_o \tag{8}$$

$$J < \min(b,B)\ \sigma_f / (15, 20, \text{ or } 25) \tag{9}$$

The ω criteria (Eq. 7) is from Hutchison and Paris (Ref. 16), with a critical ω value of 5 normally suggested. The Δa limit of 0.06 was suggested by Shih (Ref. 17), while ASTM E 1152 uses a limit of 0.1. The J limits can be found variously in ASTM E 813-81 and E 1152, with E 813-81 specifying the factor of 25 for J_{Ic} validity and 15 for data used to determine J_{Ic}, whereas ASTM E 1152 specifies 20 as an upper limit on J evaluation.

A typical J-R curve is illustrated in Fig. 3. The J-R curve format is in accordance with that of ASTM E 813-81. The line emanating from the origin, called the blunting line, is given by $J = 2\sigma_f \Delta a$, where σ_f is the flow strength (the average of the 0.2% offset yield strength and the ultimate strength). The exclusion lines are constructed parallel to the blunting line, but offset by 0.15 mm (0.006 in.) and 1.5 mm (0.060 in.).

Tabulated values of J_{Ic} under a heading of "ASTM" are evaluated by ASTM E 813-81 procedures, whereby a straight line is fit to the test data between the 0.15-mm and 1.5-mm exclusion lines. This line is extrapolated back to the blunting line; the intersection is termed J_Q. J_{Ic} equals J_Q if various validity criteria are satisfied. In the present investigation, the overall (small) specimen sizes and the test materials (i.e., low strength and high toughness) preclude determination of J_{Ic} values valid per ASTM E 813.

In the power-law evaluation of the J-R curve data, an equation of the form $J = C\,\Delta a^n$ is fit to the data between the exclusion lines. (These values of C and n are given in the tabulated results.) The power law J_{Ic} (tabulated under a heading "MEA") is defined as the intersection of the power-law curve with the 0.15-mm exclusion line. Previous experience has shown that the power-law definition of J_{Ic} tends to give values nearly equivalent to the ASTM E 813-81 values for low alloy (ferritic) steels.

The tearing modulus, T_M, is used to characterize the tearing resistance of structural materials. T_M is given by:

$$T_M = \frac{E}{\sigma_f^2} \frac{dJ}{da} \tag{10}$$

where dJ/da is the slope of the J-R curve. Since the J-R curve generally conforms to a power law, the value of T_M changes (decreases) with increasing crack growth. For comparison purposes, average values of T_M, termed T_{avg}, typically are used. The "ASTM" T_{avg} value (as defined by MEA) uses the slope of the linear-fit curve as dJ/da; the "MEA" T_{avg} value is determined from a fit of the power law to a straight line, defining dJ/da as an average slope evaluated in a closed-form manner (see Appendix H of Ref. 12).

In the data tabulations, Δa_m represents the optically measured crack growth and $\Delta a_p - \Delta a_m$ represents the difference between the measured crack growth and that predicted by the unloading compliance method (Δa_p).

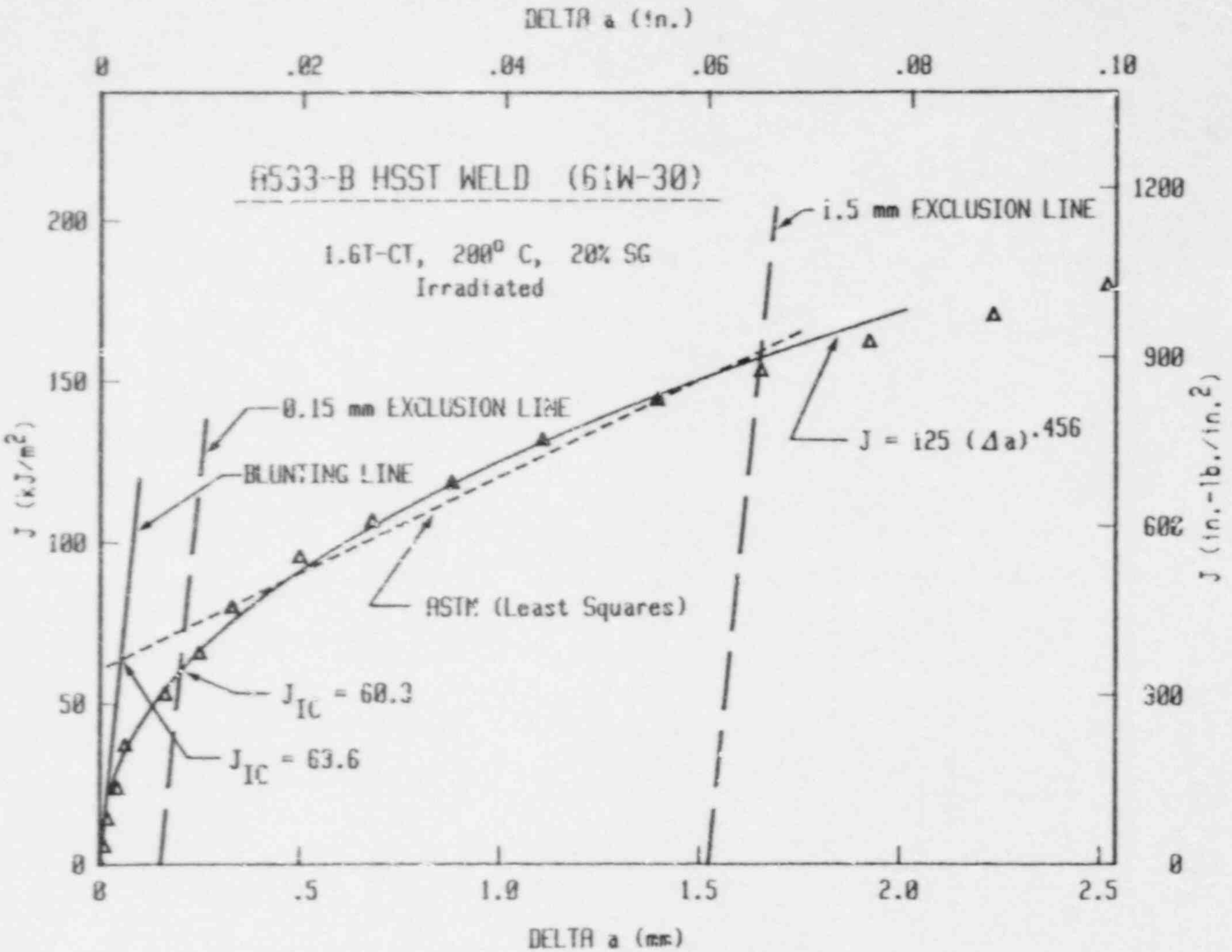

Fig. 3 Example of a typical J-R curve. The ASTM E 813-81 format is used in these cases.

5. RESULTS FOR COMMERCIAL HEATS

As described in Section 2, the commercial heats of cast stainless steel include two heats of centrifugally-cast pipe (Codes P1 and P2) and single heats from a static-cast pump impeller (Code I), a static-cast pump casing ring (Code C1) and a centrifugally cast ring (Code ZP18). The pump casing ring and the centrifugally cast ring heats were tested in the "unaged" condition only. Code C1 had the lowest ferrite content (2%), considerably lower than the 14.5% to 23.5% of the other four heats. In terms of C_v impact energy, average "upper shelf" energy levels (C_v USE) are summarized in Table 10. (These values are provided for reference purposes only to demonstrate thermal-aging effects and relative notch ductility levels.) In general, these materials demonstrate considerable variability at a single temperature. On the upper shelf, Charpy-V energy levels tend to be invariant with test temperatures, albeit considerable variability does occur.

For the CF8A grade material (Code ZP18), C_v data are summarized in Table 11 for four orientations at 25°C and 288°C. Figure 4 illustrates the variation of C_v energy with through-thickness location in the ring. No consistent trend is apparent for the midthickness or the surface yielding high or low values. The L-R and C-R orientation do give the same overall trend at 25°C and 288°C, although the L-R orientation indicates higher toughness when progressing from the outside diameter to the inside diameter and the C-R orientation indic lower toughness for the same through-thickness progression.

5.1 Tensile Data

In terms of tensile properties, the embrittlement of the cast stainless steels generally resulted in higher strength and lower ductility.

From average yield and ultimate strength levels at 25°C and 290°C (Table 12), the CF8A heat has the highest yield strength at 25°C and the highest ultimate strength at 290°C (Fig. 5). At both test temperatures, static cast CF8 Heat C1 has the lowest yield and generally the lowest ultimate strengths. The ambient temperature yield strength for this heat is even below the ASME specification of 205 MPa. In contrast, the centrifugally cast CF8 pipe (Code P1) has quite high strength levels. Likewise, the CF3 grades demonstrate no agreement, with static-cast Heat I yielding higher (average) strength levels than centrifugally cast Heat P2 in all cases. Increasing the test temperature from 25°C to 290°C results in lower strength levels in all cases. A slight orientation effect is evident for the CF8A heat only.

Table 10 Average Charpy "Upper Shelf" Energy Levels for Commercial Heats of Cast Stainless Steel

Heat	Grade	Aging Condition		Average Energy Value	Average Reduction
		Temp (°C)	Time (h)	(J/cm²)	(%)
ZP18	CF8A	Unaged		----	----
	(C-L)[a]			304	----
	(L-C)[a]			371	----
	(C-R)[a]			298	----
	(L-R)[a]			310	----
C1[b]	CF8	Unaged		93	----
I[b]	CF3	Unaged		180	----
		350	9980	152	16
P1[b]	CF8	Unaged		242	----
		350	9980	250	(3)[c]
		400	9980	133	45
P2[b]	CF3	Unaged		371	----
		350	3000	354	5
		350	9980	334	10
		400	9980	159	57

[a] Orientation per ASTM Standard E 399.
[b] Data from ANL.
[c] Average energy increased.

Table 11 Charpy-V Data for Code ZP18 (Centrifugally Cast Stainless Steel Ring, SA351-CF8A)

Test Temperature (°C)	Thickness Location	Absorbed Energy (J)			
		L-C[a]	C-L[a]	L-R[a]	C-R[a]
25	ID	270	221	---	221
	0.7T	241	255	270[b]	228
	0.4T	293	241	254[c]	244
	OD	340	249	247	250
288	ID	315	230	---	206
	0.7T	---	239	255[b]	240
	0.4T	309	---	230[c]	---
	OD	308	267	233	282

[a] Orientation per ASTM Standard E 399.
[b] 0.75T
[c] 0.5T

Table 12 Summary of Strength Data for Aged Cast Stainless Steels (Commercial Heats)

Heat ID	Orientation[a]	Aging Condition (°C/h)	25°C[b] Yield[c] (MPa)	25°C[b] Ultimate (MPa)	290°C[b] Yield[c] (MPa)	290°C[b] Ultimate (MPa)
ZP18	L	Unaged	267.8	558.1	154.2	438.7
(CF8A)	C	Unaged	305.1	618.2	150.9	457.9
C1 (CF8)	L	Unaged	192.4	520.0	123.5	359.3
I	L	Unaged	251.0	571.6	168.8	399.6
(CF3)		350/10000	+19%[d]	+11%	+11%	+5%
P1	L	Unaged	248.5	584.7	157.5	433.5
(CF8)		350/10000	+13%	+9%	+13%	+5%
		400/10000	+15%	+16%	+3%	+12%
	C	Unaged	245.3	582.2	152.7	423.2
		350/10000	+10%	+5%	+18%	+7%
		400/10000	+16%	+13%	+10%	+19%
P2	L	Unaged	211.5	549.3	141.0	396.0
(CF3)		350/3000	+18%	+8%	+14%	+5%
		350/10000	+25%	+11%	+9%	+6%
		400/10000	+12%	+12%	+4%	+9%
	C	Unaged	227.2	547.5	157.7	396.0
		350/3000	+11%	+10%	-3%	+1%
		350/10000	-----	-----	-1%	+1%
		450/10000	+3%	+10%	+2%	+13%

[a] Orientation: L = longitudinal (axial); C = circumferential
[b] Test temperature
[c] 0.2% offset yield strength
[d] Percentage change in strength (+ is increase, - is decrease).

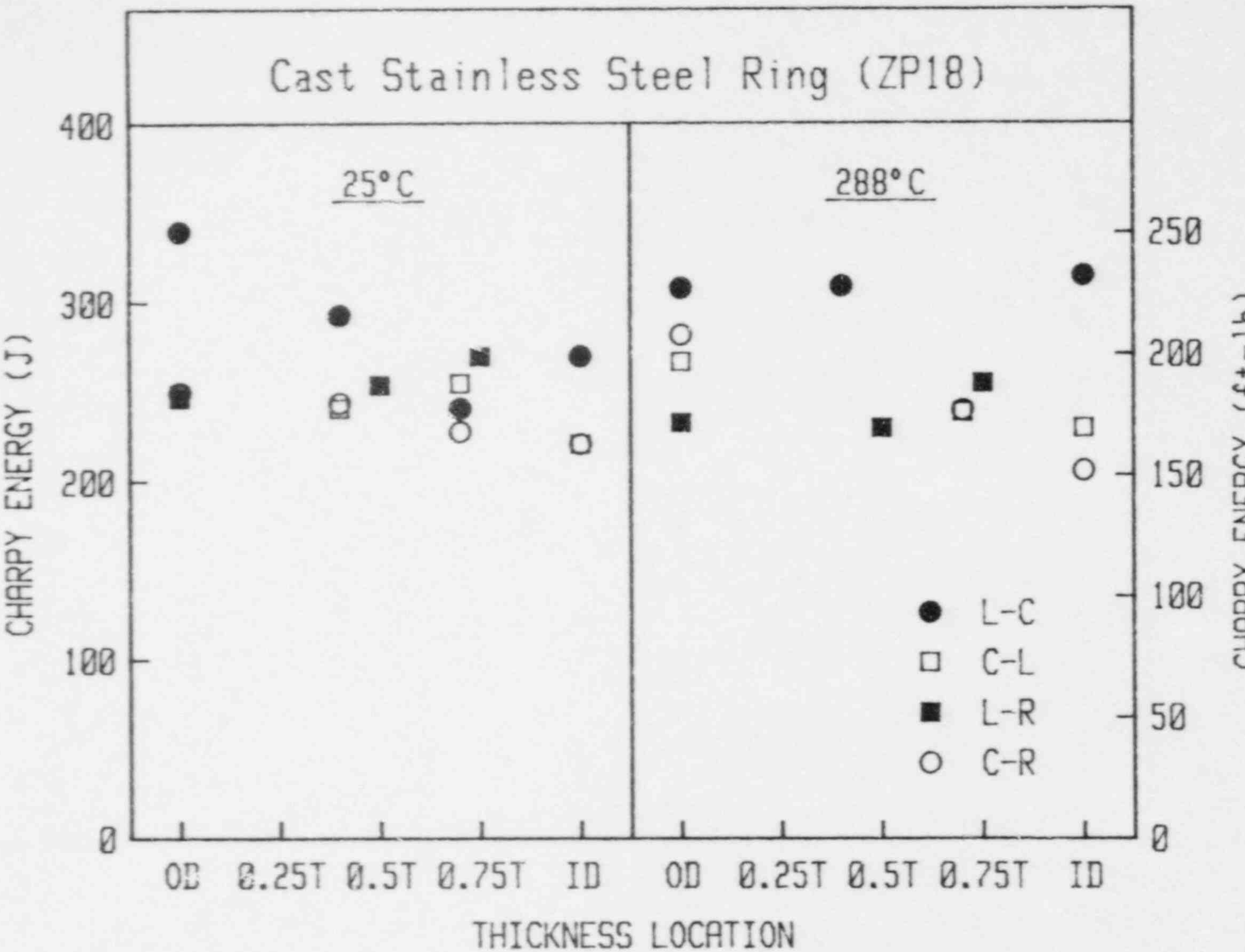

Fig. 4 Charpy-V data for Heat ZP18 demonstrate uniform energy levels at 25°C and 288°C. No consistent trend with thickness location is apparent for any of the four orientations.

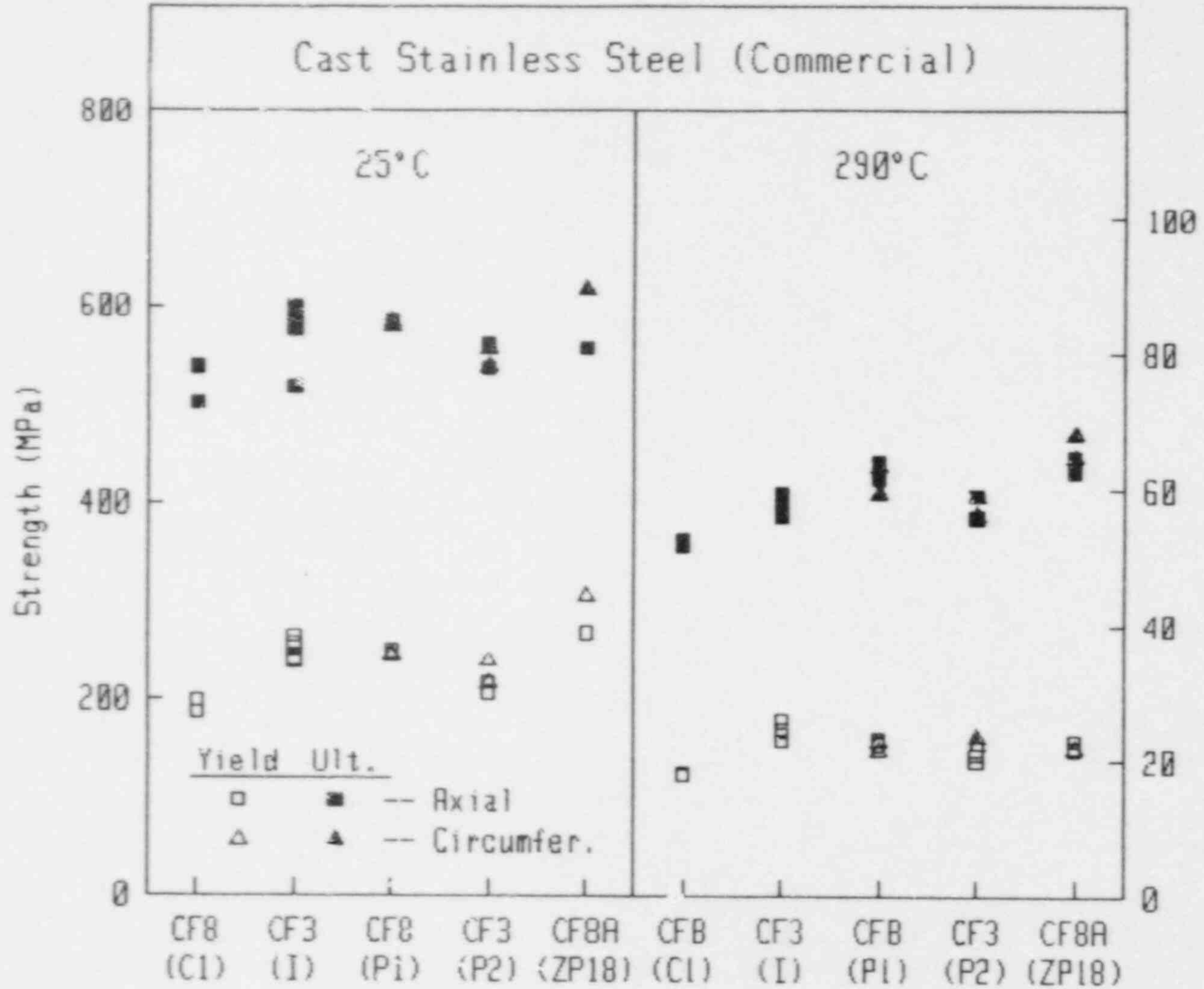

Fig. 5 Comparison of strength levels for the commercial heats in the as-received (unaged) condition. Increasing the test temperature reduces the strength in all cases. Heat C1 has the lowest strength at both temperatures, whereas Heat ZP18 has virtually the highest.

5.1.1 Heat ZP18 (CF8A)

For the CF8A grade material (Code ZP18), increasing the test temperature results in decreases in both yield and ultimate tensile strength (Fig. 6), as summarized in Table 13. Both orientations have similar strength levels, although the circumferential orientation has slightly higher strength in some cases. The absolute decreases in strength are the same for 0.2% offset yield and ultimate strength over the temperature interval of ~25°C to ~290°C. The largest percentage decrease is a 50% decrease in yield strength for the circumferential orientation.

5.1.2 Heat C1 (CF8)

For the pump casing ring (Code C1), increasing the test temperature (Table 14) resulted in significant decreases in both 0.2% offset yield (36%) and ultimate strengths (31%). Both elongation and reduction in area decreased significantly also. In comparison to the other commercial heats tested here, the yield and ultimate strengths for this heat are generally lower than for the other heats at both temperatures.

5.1.3 Heat I (CF3)

For the static-cast pump impeller (Code I), specimens aged at 350°C for 10000 h were tested in addition to "unaged" specimens (Table 15). While there is considerable variability in the results (Fig. 7), the thermal aging does result in increases in 0.2% yield and ultimate strengths at both test temperatures. In terms of overall average values, the percentage increase in 0.2% offset yield strength due to thermal aging is about twice that of ultimate strength; at ambient temperature, the percentage increases are about twice those at 290°C.

For the unaged material, increasing test temperature from 25°C to 290°C decreases the strength by 33% for 0.2% offset yield strength and 30% for ultimate strength. These percentage decreases are comparable to those exhibited by the pump casing ring (Heat C1). For the thermally-aged material, the decrease in yield strength (38%) and the decrease in ultimate strength (34%) due to increasing test temperature are slightly greater than those for the unaged material.

5.1.4 Heat P1 (CF8)

For the CF8 pipe material (Code P1), specimens aged for 10000 h at 350°C and 400°C were tested in addition to unaged specimens (Table 16), as illustrated in Fig. 8. For unaged material, both orientations exhibit similar yield and ultimate strength trends, although the longitudinal orientation gives slightly higher strengths in all cases.

As expected, the increases in yield and ultimate strength tend to be greater for material aged at 400°C as opposed to material aged at 350°C. The lone exception to this trend is for yield strength data at 290°C, where the strength for specimens aged at 350°C exceed that from specimens aged at 400°C by 8-9%. This anomalous behavior was found

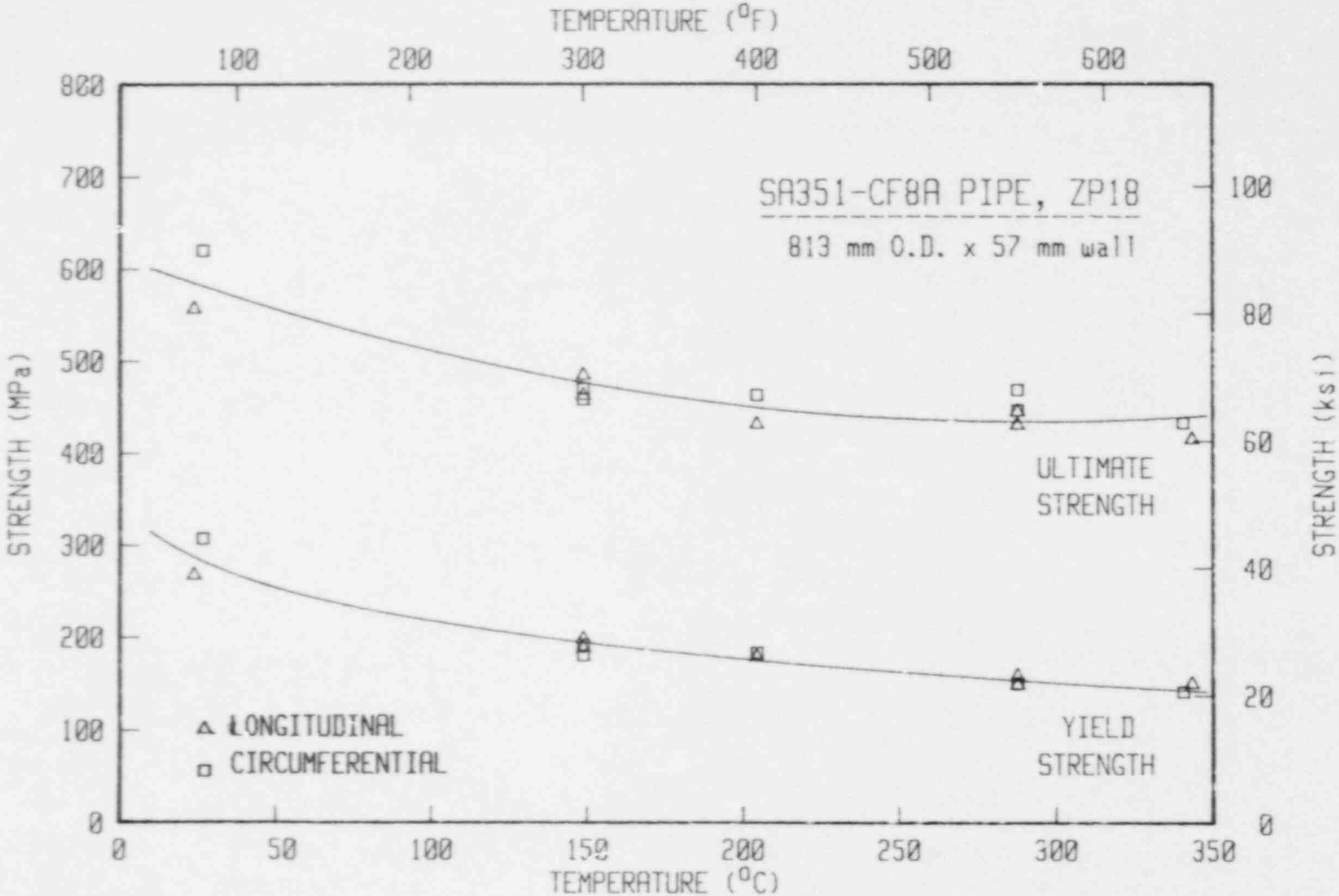

Fig. 6 Strength as a function of test temperature for grade CF8A (Heat ZP18). The two orientations exhibit similar trends of generally reduced strength with increasing test temperature.

Table 13 Tensile Results For Code ZP18 (Centrifugally Cast Stainless Steel Ring, SA351-CF8A)

Specimen Number	Orien-tation	Test Temp	True Stress-Strain		Engr Stress-Strain		Elonga-tion	Reduction in Area	Aging Condition	
			0.2% Yield	Fracture-Stress	0.2% Yield	Ultimate Stress			Temp	Time
		(°C)	(MPa)	(MPa)	(MPa)	(MPa)	(%)	(%)	(°C)	(h)
CF8A-6L	L	24	269.2	1747.1	267.8	558.1	40.7[a]	78.7	Unaged	
CF8A-7L	L	149	198.8	1142.9	198.2	472.6	70.6[b]	74.2	Unaged	
CF8A-8L	L	149	190.0	987.6	188.5	463.7	59.2[b]	72.2	Unaged	
CF8A-5L	L	204	178.6	650.8	178.1	425.8	42.8[a]	63.5	Unaged	
CF8A-2L	L	288	150.2	837.4	149.7	431.4	56.2[b]	66.4	Unaged	
CF8A-3L	L	288	159.2	853.0	158.7	446.0	c	66.6	Unaged	
CF8A-4L	L	343	151.0	560.6	150.5	419.8	40.7[a]	47.6	Unaged	
CF8A-6C	C	27	307.0	1622.3	305.1	618.2	56.1[a]	75.5	Unaged	
CF8A-1C	C	149	192.6	1177.9	191.9	470.4	c	64.0	Unaged	
CF8A-3C	C	149	181.1	1216.8	180.5	459.1	68.2[b]	79.3	Unaged	
CF8A-4C	C	204	182.8	851.5	181.7	466.4	48.5[a]	71.0	Unaged	
CF8A-8C	C	288	151.5	1031.2	151.0	469.1	55.0[b]	74.4	Unaged	
CF8A-7C	C	288	152.2	856.1	150.7	446.6	57.0[b]	72.8	Unaged	
CF8A-5C	C	343	142.4	758.4	142.0	433.5	54.1[a]	57.6	Unaged	

a In 18.6 mm (0.734 in.) b In 12.7 mm (0.5 in.) c Specimen broke outside of the gage marks

Table 14 Tensile Results For Code C1 (Static Cast Stainless Steel Pump-Casing Ring, SA351-CF8)

Specimen Number	Orientation	Test Temp	True Stress-Strain		Engr Stress-Strain		Elongation[a]	Reduction in Area	Aging Condition	
			0.2% Yield	Fracture-Stress	0.2% Yield	Ultimate Stress			Temp	Time
		(°C)	(MPa)	(MPa)	(MPa)	(MPa)	(%)	(%)	(°C)	(h)
C1A-1L	L	25	187.2	955.6	186.2	502.1	54.9	53.9	Unaged	
C1A-2L	L	25	199.3	775.6	198.6	537.8	49.0	41.6	Unaged	
C1A-3L	L	287	125.3	502.9	124.4	363.1	30.1	32.5	Unaged	
C1A-4L	L	287	123.0	495.6	122.6	355.6	37.7	47.5	Unaged	

[a] In 18.5 mm (0.727 in.)

Table 15 Tensile Results For Code I (Static Cast Stainless Steel Pump Impeller, SA351-CF3)

Specimen Number	Orientation	Test Temp	True Stress-Strain		Engr Stress-Strain		Elongation[a]	Reduction in Area	Aging Condition	
			0.2% Yield	Fracture-Stress	0.2% Yield	Ultimate Stress			Temp	Time
		(°C)	(MPa)	(MPa)	(MPa)	(MPa)	(%)	(%)	(°C)	(h)
I1-1L	L	25	265.6	1636.6	264.8	598.8	84.6	79.3	Unaged	
I1-2L	L	25	242.8	1698.4	242.1	583.4	78.4	79.5	Unaged	
I2-1L	L	25	251.7	1274.5	251.0	579.9	77.4	74.3	Unaged	
I2-2L	L	25	258.5	1671.7	257.7	578.1	75.0	80.2	Unaged	
I3C-1L	L	25	240.5	1274.8	239.7	517.6	66.2	69.5	Unaged	
I1-26L	L	25	282.3	1897.5	281.3	615.4	60.6	77.4	350	10000
I1-27L	L	25	304.4	1445.0	303.4	644.6	—[b]	62.2	350	10000
I2-19L	L	25	315.9	1296.9	314.7	642.0	72.0	68.4	350	10000
I2-3L	L	290	169.7	756.1	169.2	409.2	—[b]	58.9	Unaged	
I2-6L	L	290	179.1	837.8	178.5	402.4	39.4	64.6	Unaged	
I3C-2L	L	290	159.1	819.5	158.6	387.3	33.0	66.2	Unaged	
I1-28L	L	290	193.0	503.0	192.4	381.1	—[b]	36.0	350	10000
I1-29L	L	290	189.5	780.5	189.0	442.8	34.2	59.7	350	10000
I2-20L	L	290	179.7	756.0	179.1	437.8	39.0	51.6	350	10000

[a] In 12.7 mm (0.5 in.)

[b] Specimen broke outside gage length

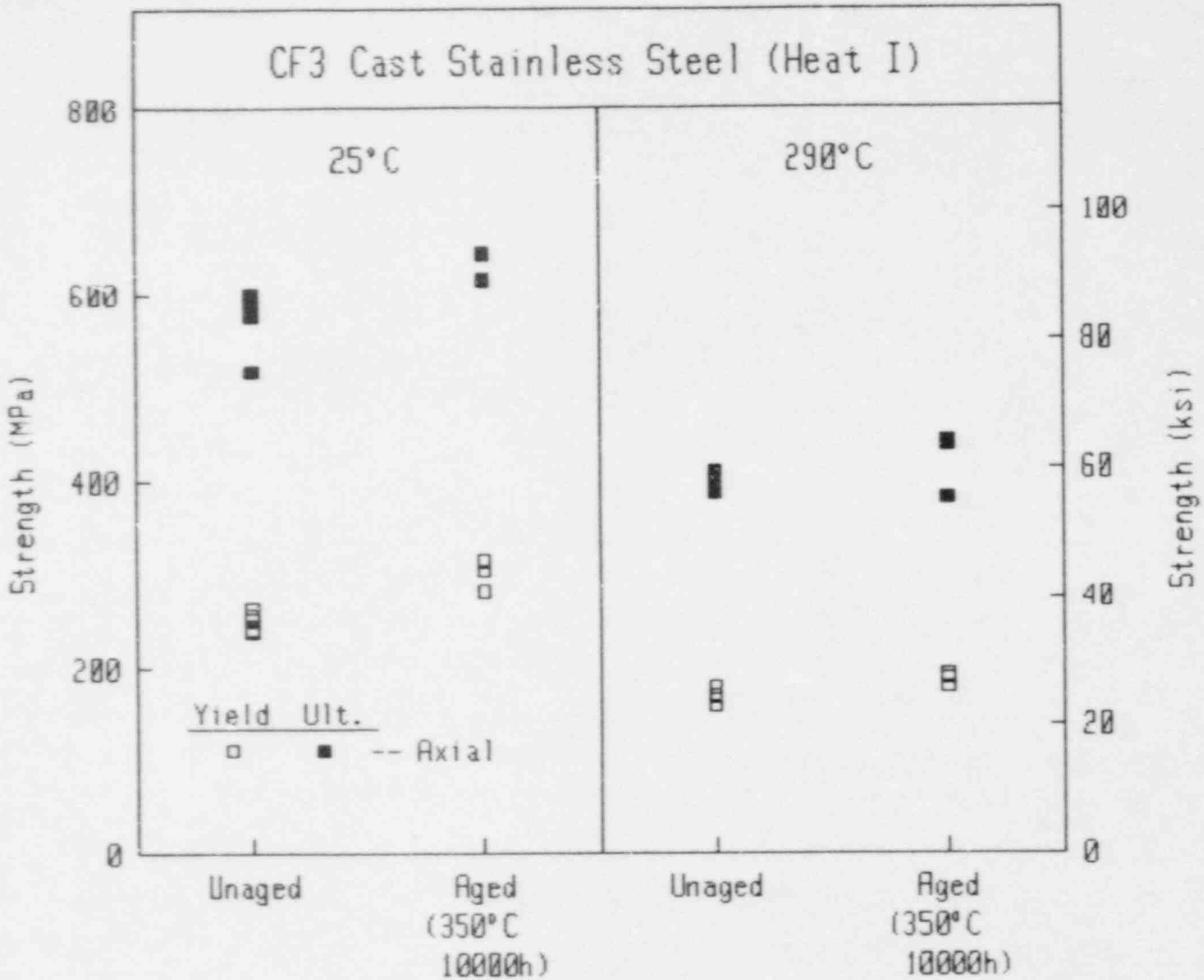

Fig. 7 Strength data for grade CF3 (Heat I). Thermal-aging results in higher strength in all cases, whereas increased test temperature results in lower strength in all cases.

Table 16 Tensile Results For Code P1 (Centrifugally Cast Stainless Steel Pipe, SA451-CF8)

Specimen Number	Orientation	Test Temp	True Stress-Strain		Engr Stress-Strain		Elongation[a]	Reduction in Area	Aging Condition	
			0.2% Yield	Fracture-Stress	0.2% Yield	Ultimate Stress			Temp	Time
		(°C)	(MPa)	(MPa)	(MPa)	(MPa)	(%)	(%)	(°C)	(h)
P11A-1L	L	23	——	1127.3	——	584.9	57.7[b]	64.0	Unaged	
P13A-1L	L	25	249.5	1579.5	248.5	584.5	62.4[b]	72.9	Unaged	
P12A-8L	L	25	291.4	1625.9	290.5	652.9	——[c]	75.2	350	10000
P12A-9L	L	25	272.2	2322.0	271.2	618.0	——[c]	80.2	350	10000
P13A-7L	L	25	287.2	1429.7	286.3	677.7	68.6	56.4	400	10000
P13T-1C	C	25	——	1221.5	244.7	584.5	56.5[b]	68.8	Unaged	
P13T-3C	C	25	246.8	1206.5	245.9	579.9	54.6[b]	65.9	Unaged	
P12T-6C	C	25	264.6	1781.6	263.4	608.7	87.2	76.1	350	10000
P12T-5C	C	25	277.9	1315.5	276.8	610.8	67.2	58.9	350	10000
P13T-7C	C	25	285.9	1351.7	285.0	660.0	46.8	55.8	400	10000
P11A-2L	L	289	160.4	497.0	159.9	442.7	35.5[b]	36.7	Unaged	
P13A-2L	L	290	155.7	850.8	155.0	424.4	43.0[b]	67.2	Unaged	
P12A-10L	L	290	174.2	919.6	173.7	451.3	43.4	62.8	350	10000
P12A-11L	L	290	181.7	823.2	180.7	457.7	42.4	55.8	350	10000
P13A-8L	L	290	163.4	881.0	162.8	485.6	35.6	51.0	400	10000
P13T-2C	C	290	149.0	642.2	148.5	408.8	33.3[b]	43.9	Unaged	
P14T-1C	C	287	157.8	622.3	157.0	437.5	32.6[b]	46.4	Unaged	
P12T-8C	C	290	181.7	981.5	180.2	454.2	——[c]	63.4	350	10000
P13T-8C	C	290	167.8	791.0	167.3	502.2	——[c]	49.6	400	10000

[a] In 12.7 mm (0.5 in.)
[b] In 18.5 mm (0.727 in.)
[c] Specimen broke outside gage length

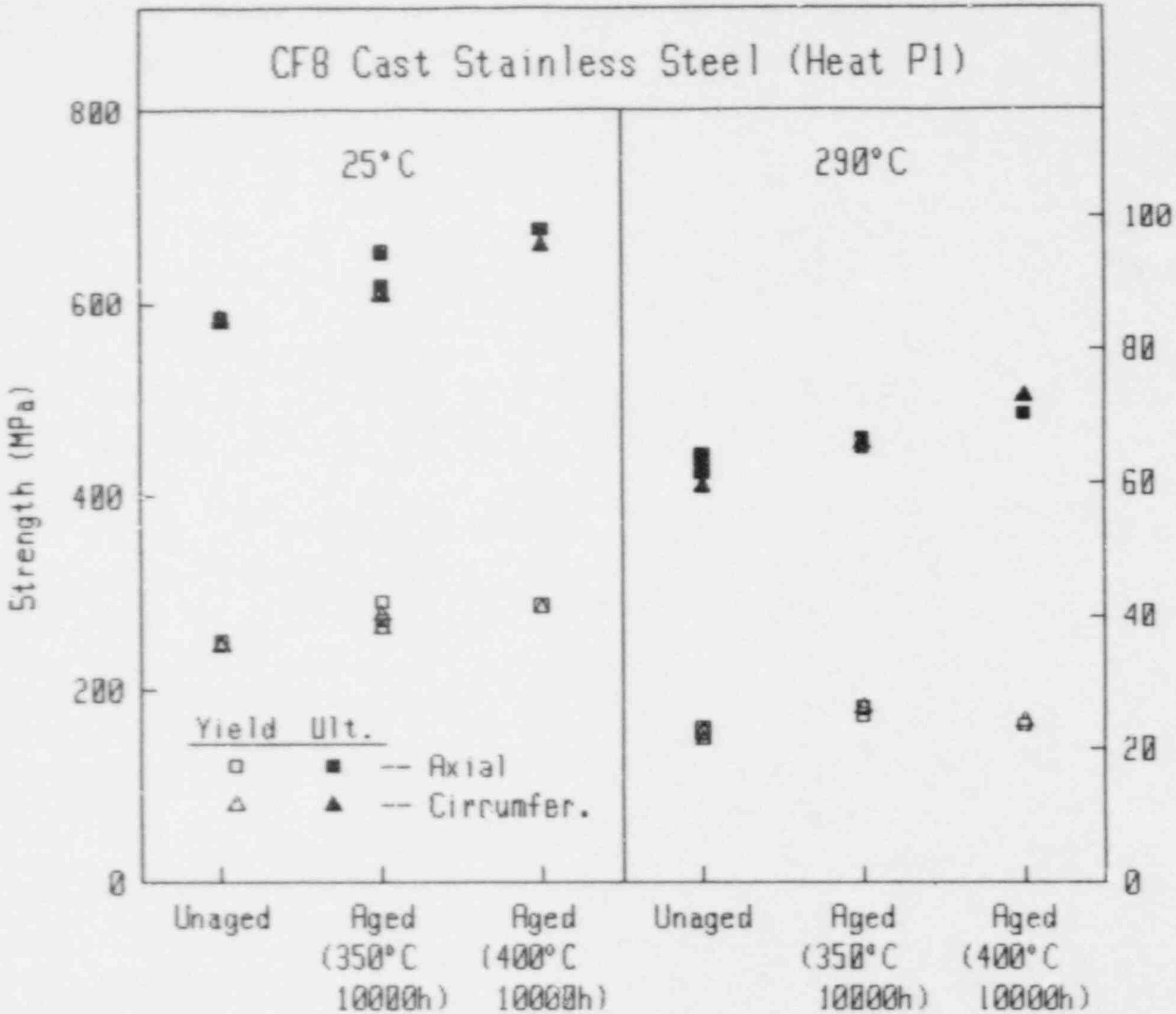

Fig. 8 Strength data for grade CF8 (Heat P1).

for both axial and circumferential-oriented specimens. In each case, the ultimate strengths are lower for the specimens aged at 350°C vs. those aged to 400°C, consistent with the trend found at ambient temperature.

Increasing the test temperature from 25°C to 290°C results in lower strength in all cases, similar to trends for the other heats described above.

5.1.5 Heat P2 (CF3)

For the CF3 pipe material (Code P2), specimens were aged for 3000 h and 10000 h at 350°C, and for 10000 h at 400°C (Table 17) as illustrated in Fig. 9. In this case, the unaged ultimate strength levels are in good agreement for the two orientations, whereas the circumferential orientation has higher yield strength (by ~ 16 MPa) at each test temperature.

For the axial orientation, the ultimate strength consistently increased with higher aging time and aging temperature. The yield strength tended to be unpredictable. At ambient temperature, the yield strength did increase in all cases, with the material aged at 350°C exhibiting a consistent trend (i.e., increased aging time gave greater strength increases). However, the material aged at 400°C gave lower yield strengths than either of the 350°C aging conditions. At 290°C, the yield strength increase is greatest for the material aged at the lowest temperature (350°C) for the least time (3000 h). Material aged at 400°C for 10000 h, which does give the highest ultimate strength increases, gives the lowest yield strength increase at both temperatures.

For the circumferential orientation of the CF3 pipe material (Code P2), the ultimate strength tends to increase consistently with aging time and aging temperature. At ambient temperature, the yield strength trends are consistent with those for the axial orientation, whereby aging at 350°C for 3000 h gives a smaller increase in strength then aging at 400°C for 10000 h. At 290°C, comparison of absolute yield strengths are consistent for the three aging conditions in terms of higher aging temperature and aging time exhibiting higher strength. However, the specimens aged at 350°C indicate small (< 4 MPa) decreases in yield strength as compared to the results for unaged material. The latter trend is inconsistent with that exhibited for the axial orientation.

Increasing the test temperature from 25°C to 290°C results in decreased strength levels, similar to the trends exhibited by the other heats.

5.2 J-R Curve Data

The J-R curve data described in this report frequently demonstrate two characteristics. The initial portion of many curves do not follow the ASTM "$2\sigma_f$" blunting line. As well, the crack growth prediction errors

Table 17 Tensile Results For Code P2 (Centrifugally Cast Stainless Steel Pipe, SA451-CF3)

Specimen Number	Orientation	Test Temp (°C)	True Stress-Strain 0.2% Yield (MPa)	True Stress-Strain Fracture-Stress (MPa)	Engr Stress-Strain 0.2% Yield (MPa)	Engr Stress-Strain Ultimate Stress (MPa)	Elongation[a] (%)	Reduction in Area (%)	Aging Condition Temp (°C)	Aging Condition Time (h)
P22A-1L	L	25	——	1094.5	206.4	561.7	73.7[b]	75.7	Unaged	
P23A-1L	L	25	217.5	887.3	216.7	536.9	62.4[b]	75.1	Unaged	
P23A-14L	L	25	250.1	2783.1	249.2	594.2	73.6	88.5	350	3000
P23A-26L	L	25	266.1	1830.2	265.2	608.5	76.6	78.8	350	10000
P24A-4L	L	25	237.0	2384.4	236.2	616.8	——[c]	78.0	400	10000
P21T-1C	C	25	217.2	1000.4	216.3	538.3	72.6[b]	59.9	Unaged	
P23T-1C	C	25	239.0	1568.5	238.1	556.8	106.0[d]	84.4	Unaged	
P22T-4C	C	25	255.2	2162.5	252.3	601.8	——[c]	85.3	350	3000
P24T-5C	C	25	234.3	1268.2	233.5	603.1	——[c]	68.8	400	10000
P22A-2L	L	288	138.7	755.6	137.9	406.8	47.2[b]	65.9	Unaged	
P23A-2L	L	287	——	538.7	144.0	385.1	39.9[b]	59.6	Unaged	
P23A-15L	L	290	161.4	900.5	161.0	415.4	——[c]	69.7	350	3000
P23A-27L	L	290	154.5	970.7	154.1	419.4	39.6	72.9	350	10000
P24A-5L	L	290	147.0	655.0	146.6	430.6	40.2	53.8	400	10000
P21T-2C	C	290	162.2	819.1	161.3	387.1	44.6[b]	72.2	Unaged	
P23T-2C	C	287	155.0	688.1	154.2	405.0	42.4[b]	65.9	Unaged	
P22T-5C	C	290	154.2	696.5	153.8	399.0	43.0	66.9	350	3000
P21T-8C	C	290	156.0	876.2	155.6	423.5	49.8	70.7	350	10000
P24T-6C	C	290	160.8	818.5	160.4	447.1	40.2	56.4	400	10000

[a] In 12.7 mm (0.5 in.)
[b] In 18.5 mm (0.727 in.)
[c] Specimen broke outside gage length
[d] In 16.6 mm (0.655 in.)

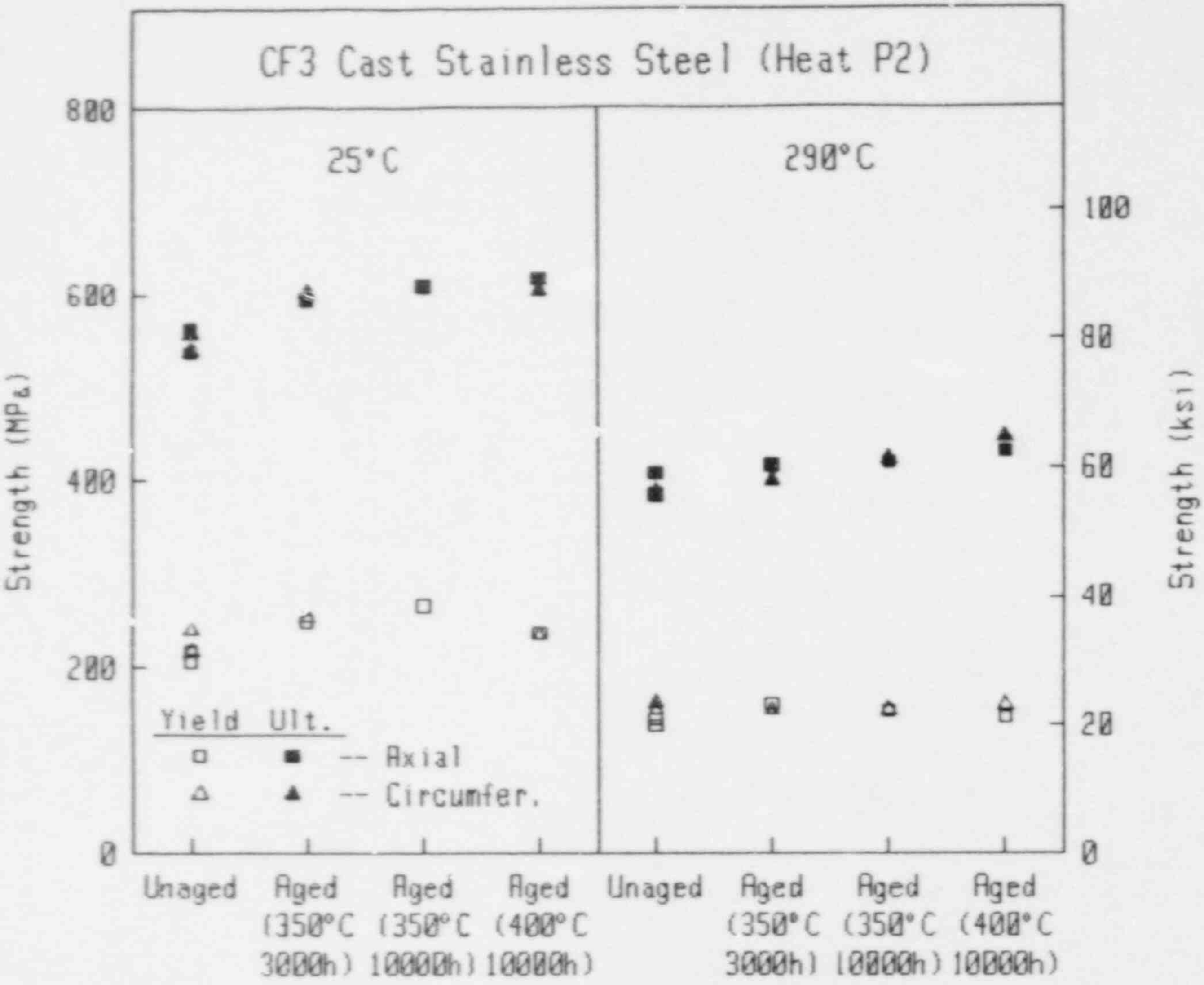

Fig. 9 Strength data for grade CF3 (Heat P2).

(Δa_p - Δa_m) tend to be quite large. Both of these topics are discussed in Section 7.1.

Thermal-aging generally results in reduced J levels and J-R curve slopes (dJ/da) in comparison to trends for "unaged" material. In terms of overall trends, the J-R curve toughness trends are qualitatively correlated with the C_v upper shelf energy, with high C_v USE levels corresponding to higher J-R curve toughness levels. Centrifugally-cast forms of the same grade yield higher toughness, for the CF8 and CF3 heats characterized. On balance, the CF3 grade has higher toughness than the CF8 or CF8A grades, with CF8 yielding the lowest toughness.

For the CF8 grades, the toughness of centrifugally-cast Heat P1 is much higher than that of static-cast Heat C1. As indicated in Fig. 10 for the L-C orientation at 25°C, the static cast material has lower J levels and J-R curve slopes at all crack growth increments. Each heat demonstrates considerable variability. The average J levels for the static cast heat are about a factor of 4 below the average levels for the centrifugally-cast heat. Similarly for the C-L orientation of the CF8 grade heats at 25°C (Fig. 11) the centrifugally-cast heat has J-R curve levels ~80% higher than those for the static cast heat. Lastly for the L-C orientation at 290°C (Fig. 12), the centrifugally cast heat has J levels ~80% higher than those for the static cast heat. The variability indicated at 25°C for the L-C orientation of Heat P1 is reflected at 290°C as well. At each temperature, the higher curve is from a specimen located at the outside diameter of the pipe, with the lower curve from a specimen located at the inside diameter of the pipe.

For the CF3 grade, centrifugally cast Heat P2 has higher J-R curve trends than does static cast Heat I. At 25°C for both the L-C (Fig. 13) and C-L (Fig. 14) orientations, Heat P2 has J levels about a factor of 2 higher than those for Heat I. At 290°C for the L-C orientation (Fig. 15), the J levels for Heat P2 are about a factor of 3 higher than those for Heat I.

All of the centrifugally cast heats were tested in the L-C and C-L orientations at 25°C and the L-C orientation at 290°C. For all three conditions, the CF3 grade (Heat P2) demonstrates the highest J-R curve levels. For the L-C orientation at 25°C (Fig. 16), grade CF8A demonstrates no significant variability, whereas grade CF8 has significantly higher toughness for the outside diameter as compared to the inside diameter of the pipe. As a result, the CF8A curves essentially bisect the CF8 curves in this case. For the C-L orientation at 25°C (Fig. 17), the CF8A grade demonstrates slightly higher toughness than the CF8 grade. In this case, the single specimen from the heat of CF8 is from the inside diameter portion of the pipe, which has been shown to give lower J-R curves than does the outside diameter. For the L-C orientation at 290°C (Fig. 18), the CF8 data lie below the CF8A data up to ~5 mm, at which point the higher of the CF8 curves (from the outside diameter) lies coincident with the CF8A curves. As at 25°C, a large difference in toughness is apparent between the inside and outside diameters of the CF8 pipe. For the CF3 pipe, some differences

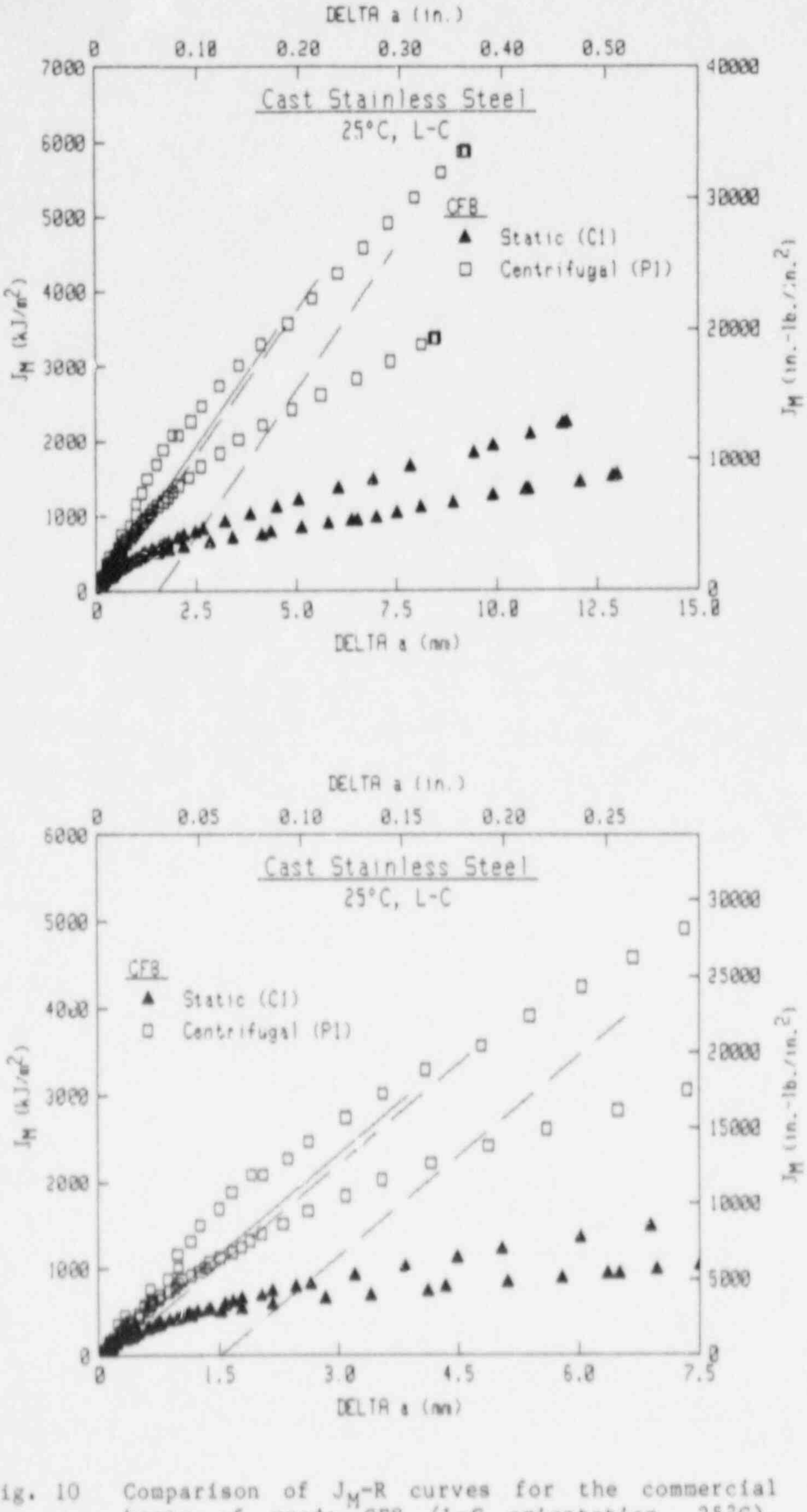

Fig. 10 Comparison of J_M-R curves for the commercial heats of grade CF8 (L-C orientation, 25°C). The centrifugally-cast heat has much higher toughness than the static-cast heat.

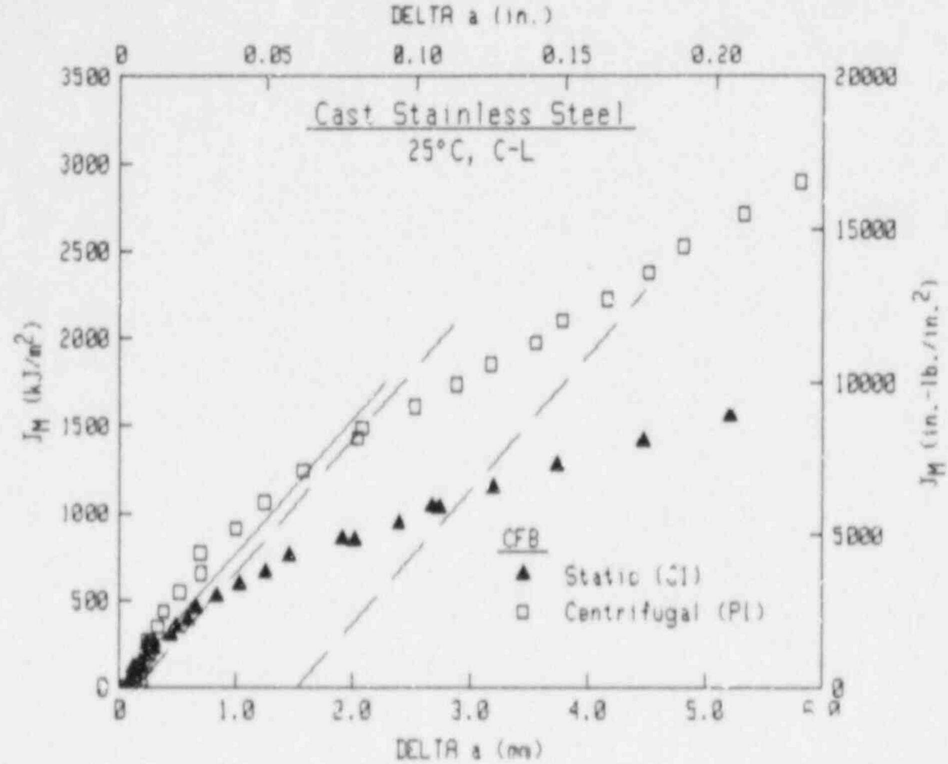

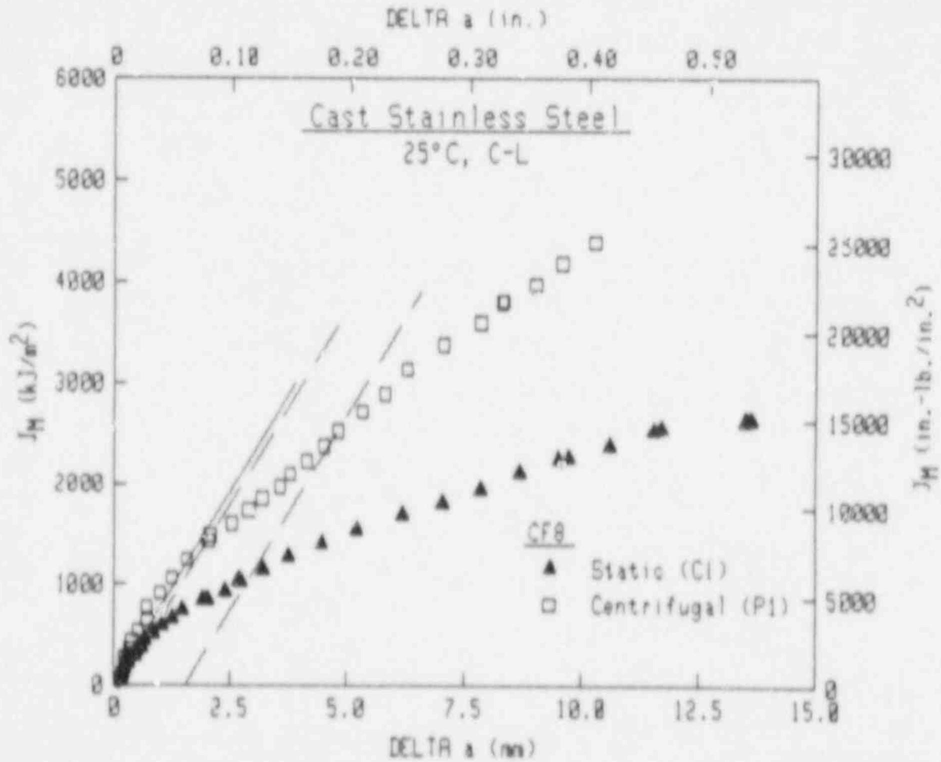

Fig. 11 Comparison of J_M-R curves for the commercial heats of grade CF8 (C-L orientation, 25°C). As for the L-C orientation, the centrifugally-cast heat has much higher toughness than the static-cast heat.

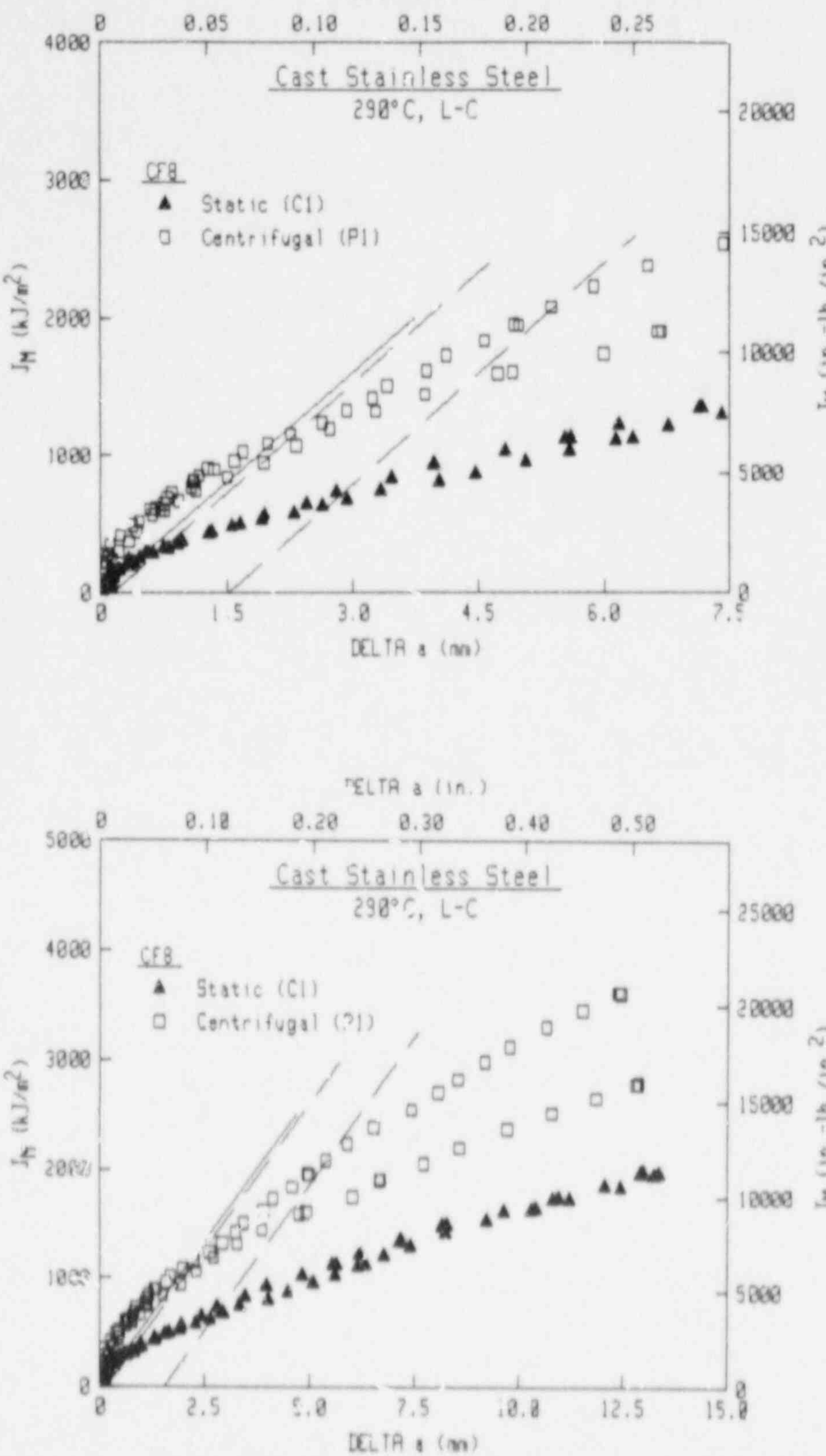

Fig. 12 Comparison of J_M-R curves for the commercial heats of grade CF8 (L-C orientation, 290°C). As at 25°C, the centrifugally-cast heat has much higher toughness than the static-cast heat.

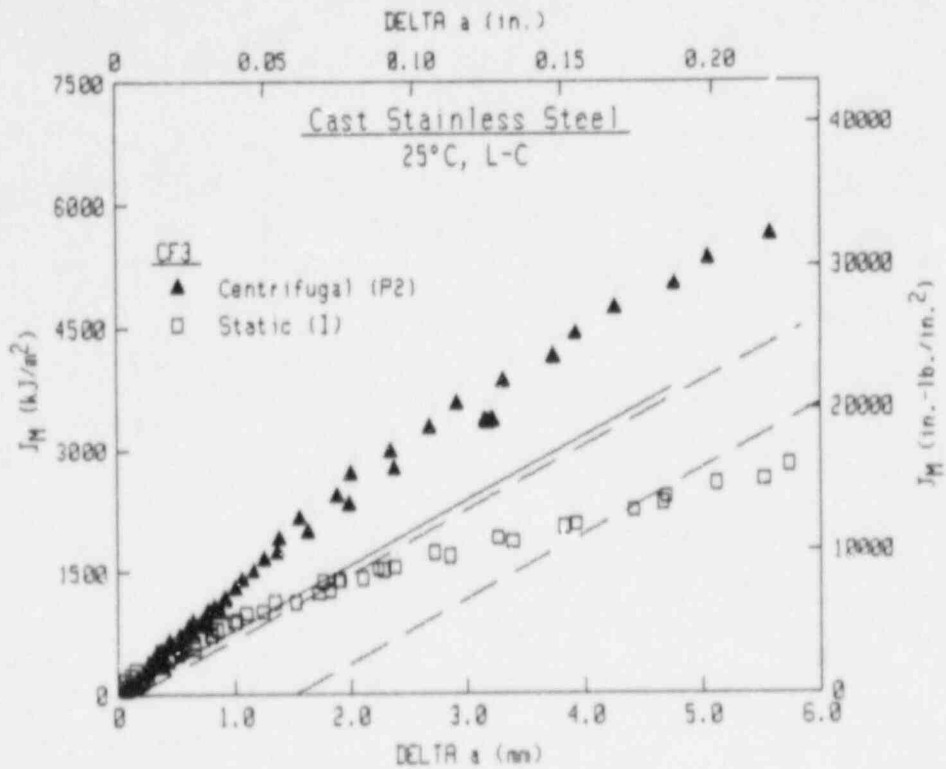

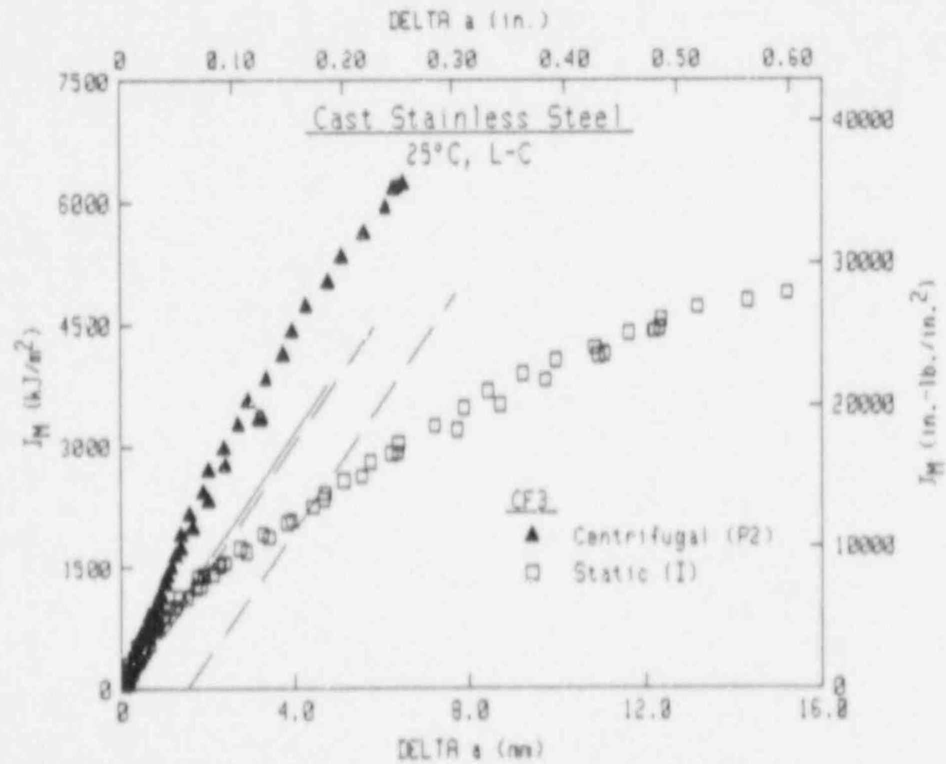

Fig. 13 Comparison of J_M-R curves for the commercial heats of grade CF3 (L-C orientation, 25°C).

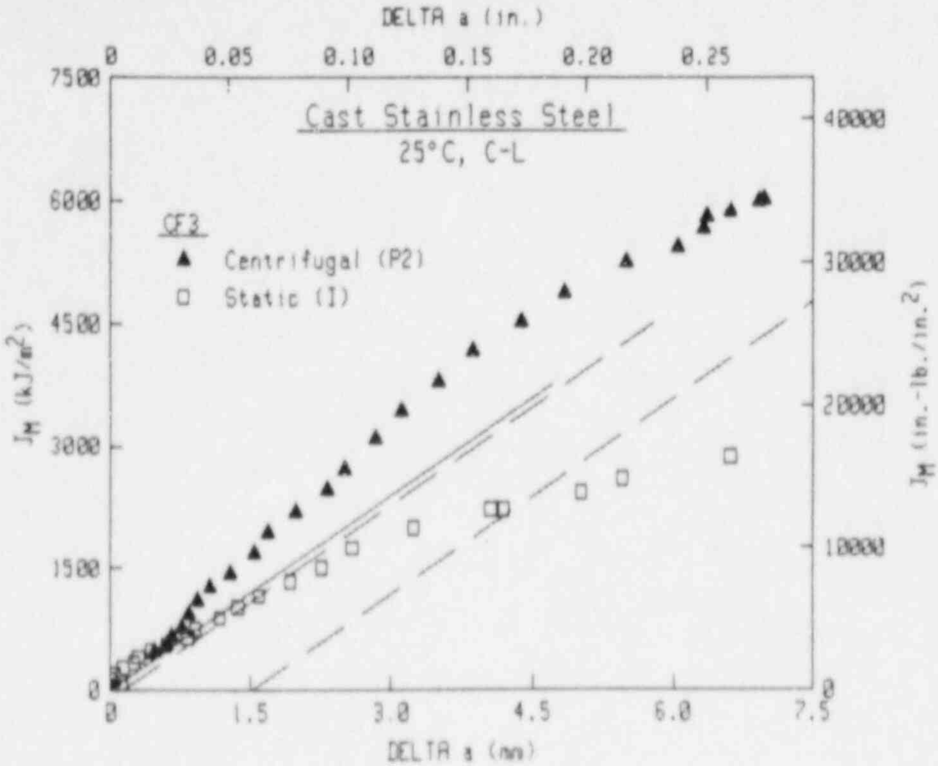

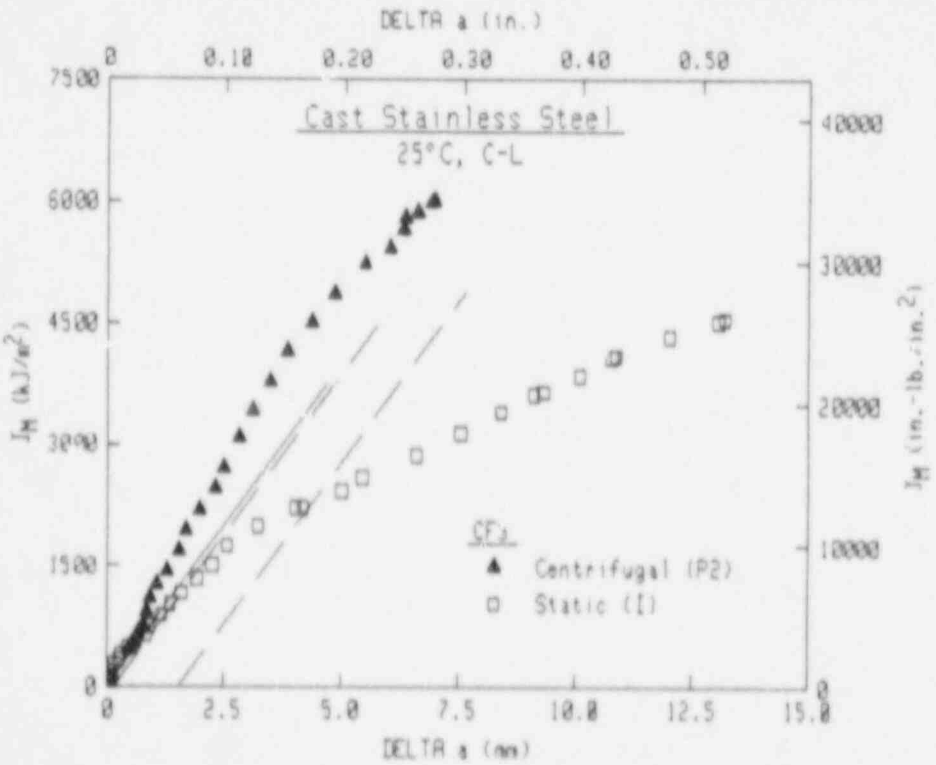

Fig. 14 Comparison of J_M-R curves for the commercial heats of grade CF3 (C-L orientation, 25°C). As for the C-L orientation, the centrifugally-cast heat has much higher toughness than the static-cast heat.

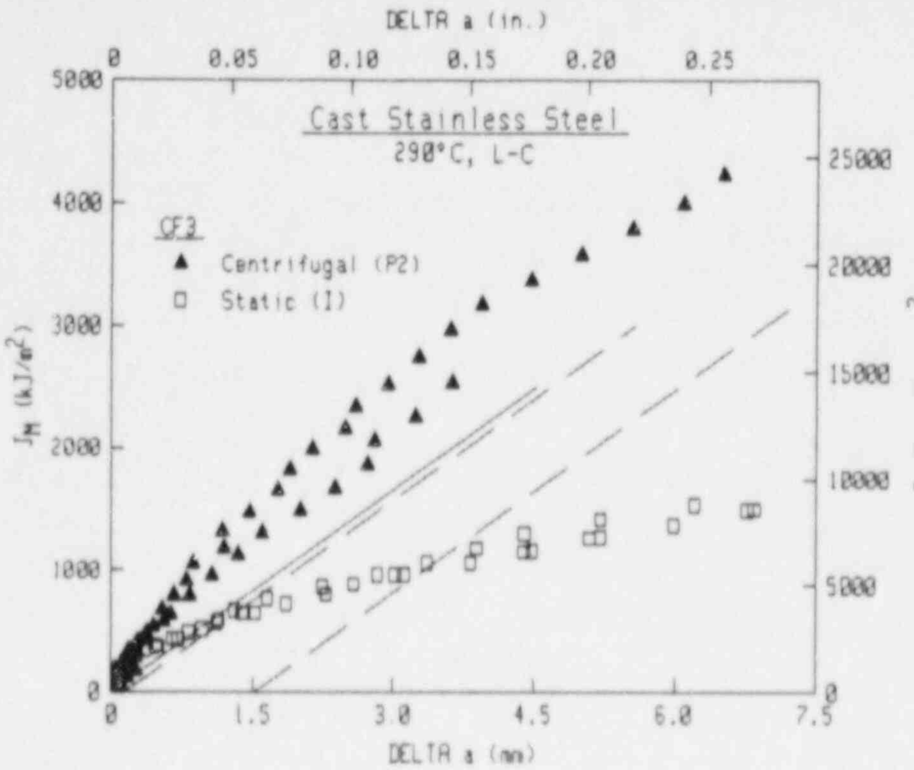

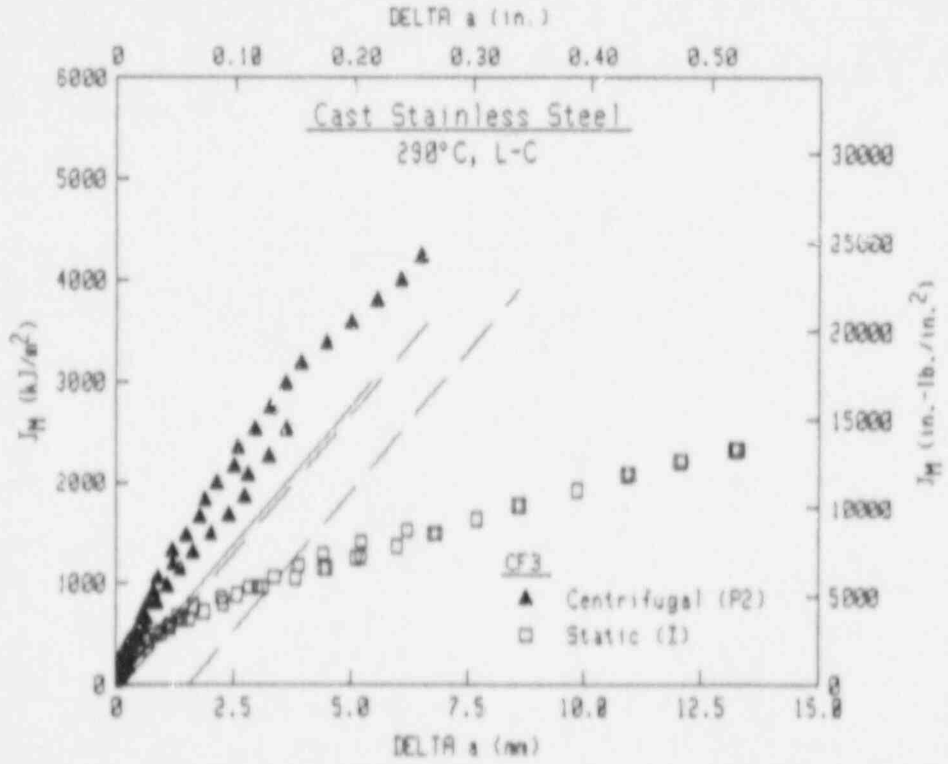

Fig. 15 Comparison of J_M-R curves for the commercial heats of grade CF3 (L-C orientation, 290°C). As at 25°C, the centrifugally-cast heat has much higher toughness than the static-cast heat.

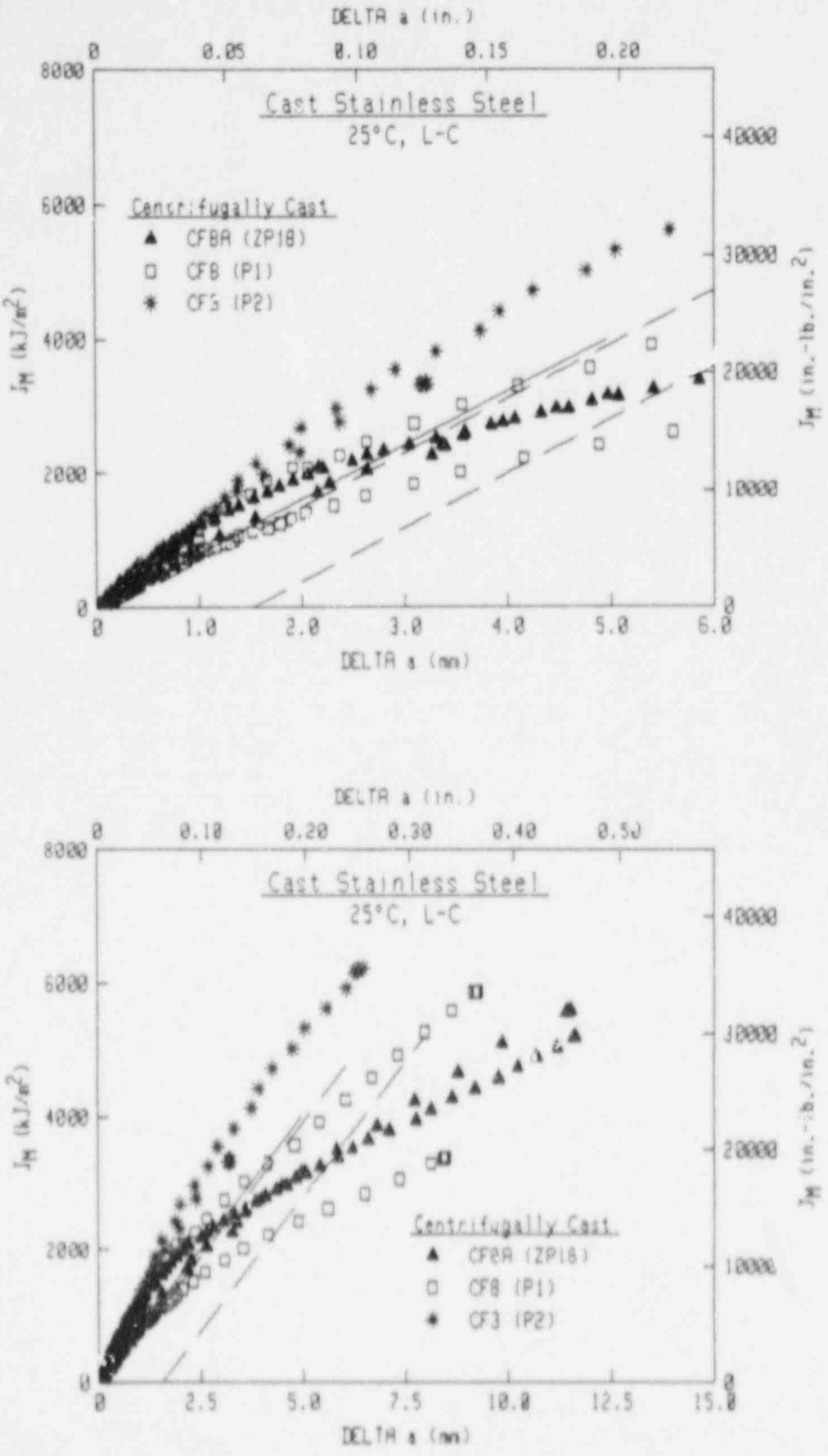

Fig. 16 For the centrifugally-cast commercial heats (L-C orientation, 25°C), the CF3 grade has the highest toughness levels. The CF8 grade has significant variability, with the average J_M-R curve levels consistent with those for the CF8A grade.

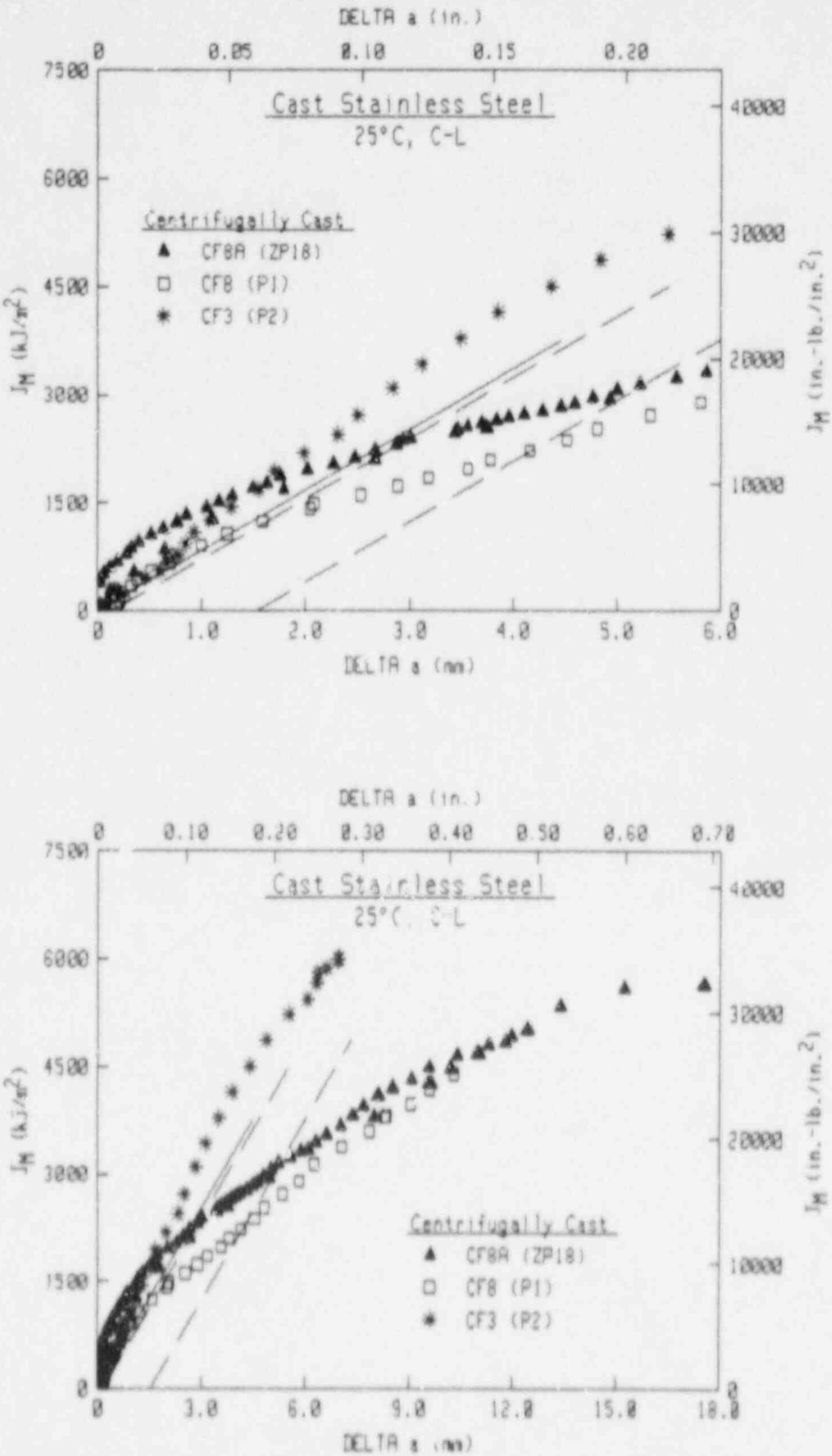

Fig. 17 For the centrifugally-cast commercial heats (C-L orientation, 25°C), the CF3 grade has the highest toughness levels. The CF8A grade has slightly higher toughness than the CF8 grade.

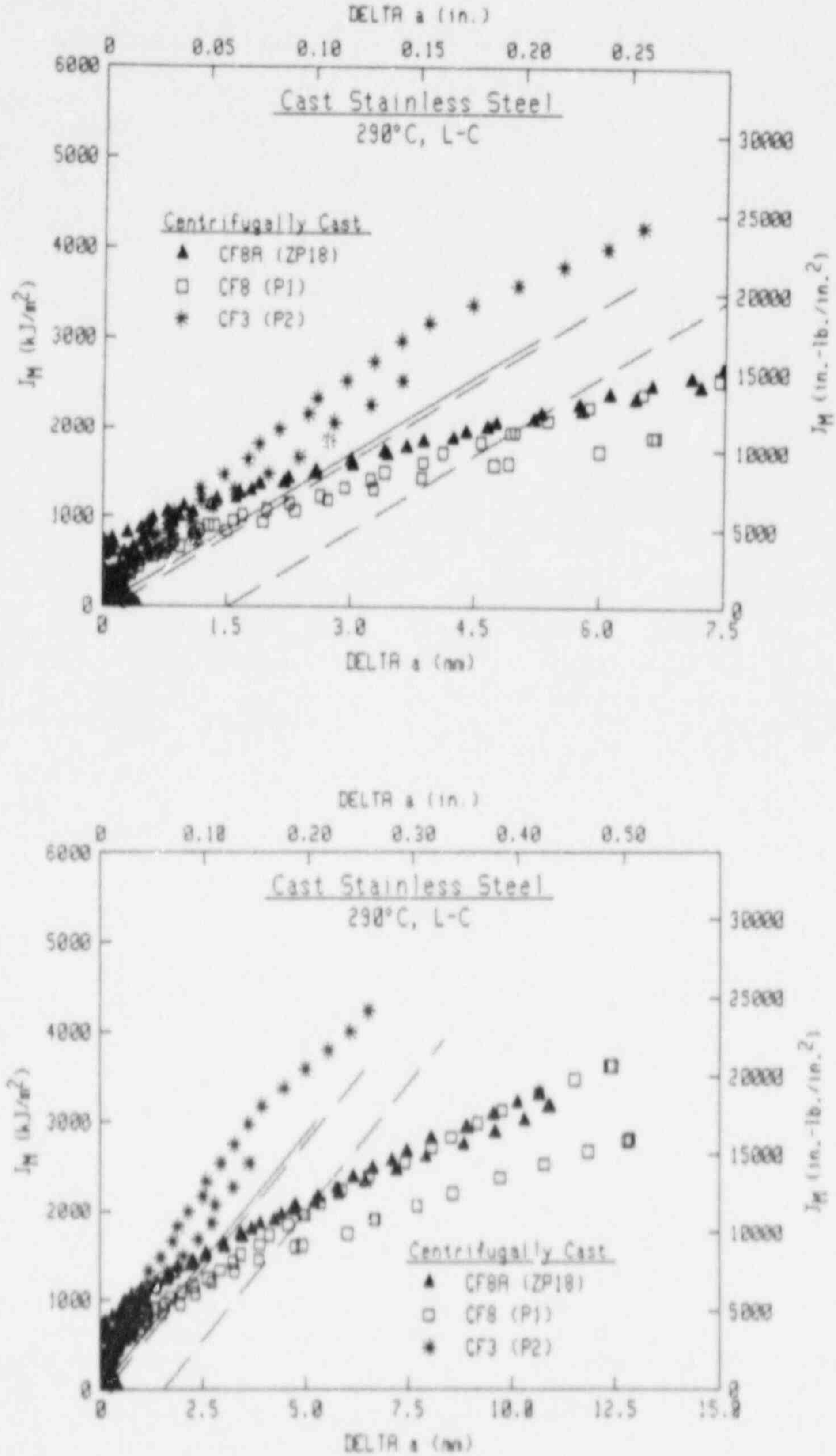

Fig. 18 As at 25°C for centrifugally-cast commercial heats, the CF3 grade has the highest toughness for the L-C orientation at 290°C. The CF8A grade has slightly higher toughness than the CF8 grade.

are apparent between the inside and outside diameter at both 25°C and 290°C, although in each case one test was terminated after < 4 mm of crack growth. In contrast to the results for the CF8 pipe, the inside diameter of the CF3 pipe has (slightly) higher toughness than the outside diameter.

Similarly for the heats of static cast stainless steel, the heat of CF3 has higher toughness than the heat of CF8, at both 25°C (Fig. 19) and 290°C (Fig. 20) for the L-C orientation and at 25°C for the C-L orientation (Fig. 21). The differences are more pronounced at 25°C than at 290°C. Within heat variability is significant only for the CF8 grade at 25°C.

5.2.1 Heat ZP18 (CF8A)

J-R curve results for Heat ZP18 are summarized in Table 18. As indicated, four different crack plane and growth orientations were characterized for this heat, with the L-C and C-L orientations tested at ambient temperature and 149°C, and all four orientations tested at 288°C. In terms of initiation toughness levels (J_{Ic}), the L-R and C-R orientations demonstrate lower toughness than the L-C and C-L orientations at 288°C (Fig. 22). Overall the J levels for the L-R and C-R orientations tend to lie below those for the L-C and C-L orientations, although J-R curve slopes (and hence tearing modulus values) tend to be lower for the latter. In terms of structural performance for this material, part-through cracks in the longitudinal (L) or circumferential (C) orientations would tend to progress through-thickness in preference to propagating lengthwise. The close agreement between the L-C and C-L orientations and (separately) the C-R and L-R orientations is remarkable, in the sense that the curves are colinear.

In a tearing instability format (i.e., J-T format), the higher J levels of the L-C and C-L orientation are apparent in comparison to the C-R and L-R orientations (Fig. 23).

As at 288°C, the L-C and C-L orientations yield consistent J-R curve trends at 25°C (Fig. 24) and 149°C (Fig. 25).

In contrast to the C_v data which demonstrated invariance with test temperature, increasing the test temperature results in decreased J-R curve levels for both orientations (Fig. 26 and 27). The slopes of the J-R curves are also reduced with higher test temperature (Fig. 28). However, comparisons of J-T curves (Fig. 29) for the three temperatures indicate higher toughness at 149°C than at 25°C or 288°C. The latter trend is reflected in the T_{avg} values, where increased test temperature can even give higher T_{avg} values. The contradictory nature of these comparisons is primarily due to the flow strength term in the tearing modulus formulation. As indicated in Section 5.1, these cast stainless steels demonstrate large strength decreases with higher test temperatures, particularly on a percentage basis. For the axial orientation (applicable to the L-C and L-R orientations for J-R curves), the flow strength decreases by 29% from 25°C to 288°C. With the flow strength squared term in the tearing modulus formulation, J-R curves at 25°C and 288°C could have the same

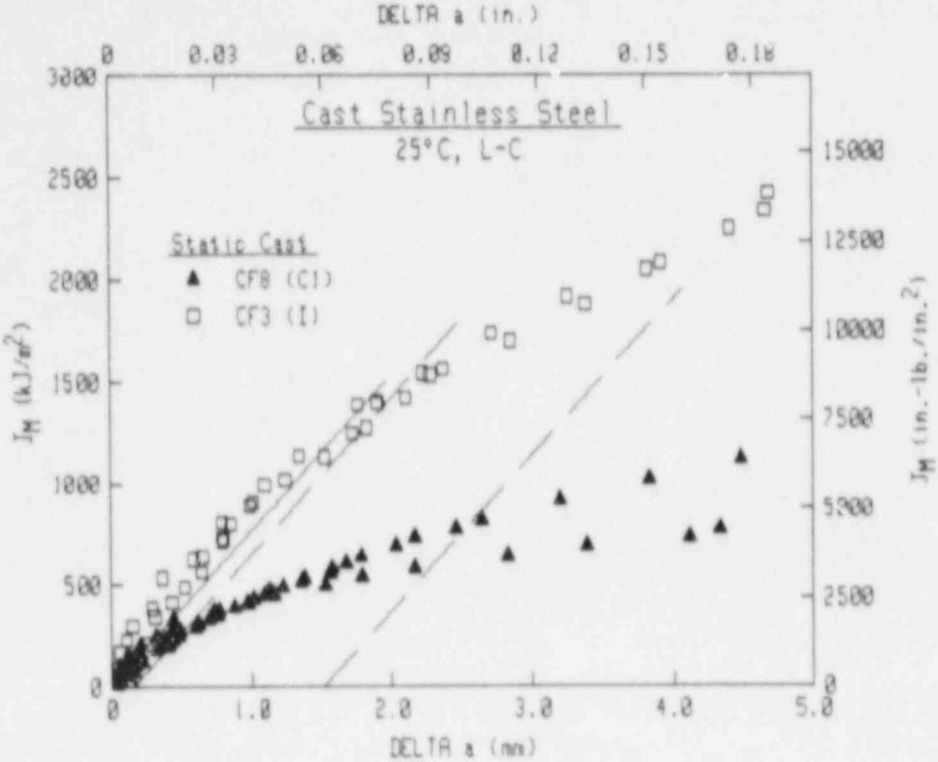

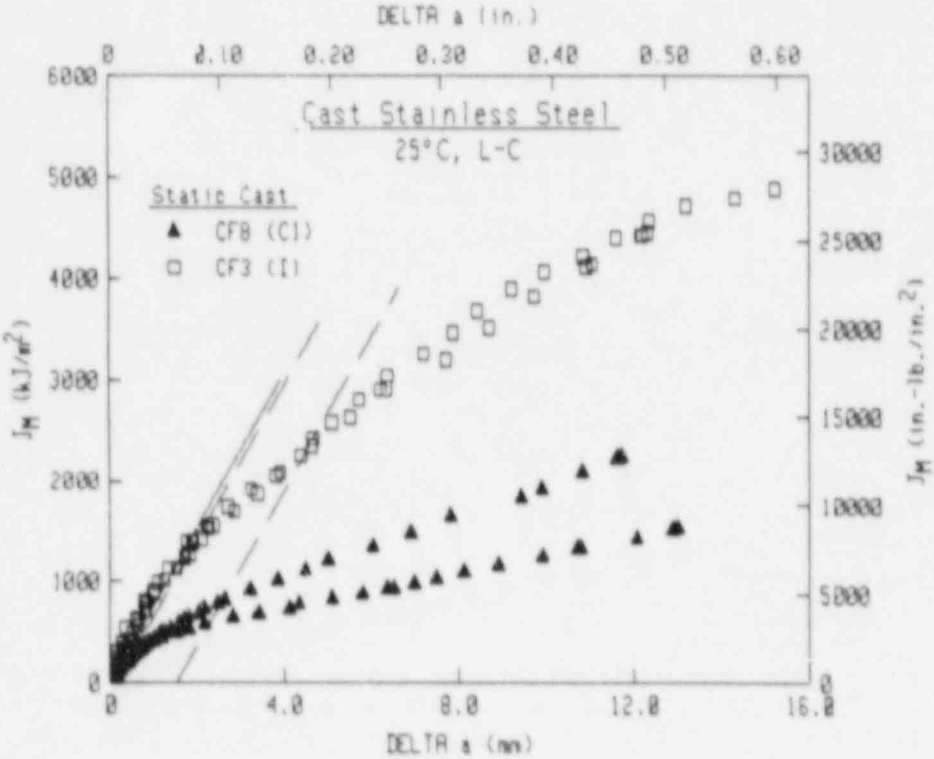

Fig. 19 For the static-cast commercial heats (L-C orientation, 25°C), the CF3 grade has much higher toughness than the CF8 grade. This trend is consistent with that for the centrifugally-cast heats.

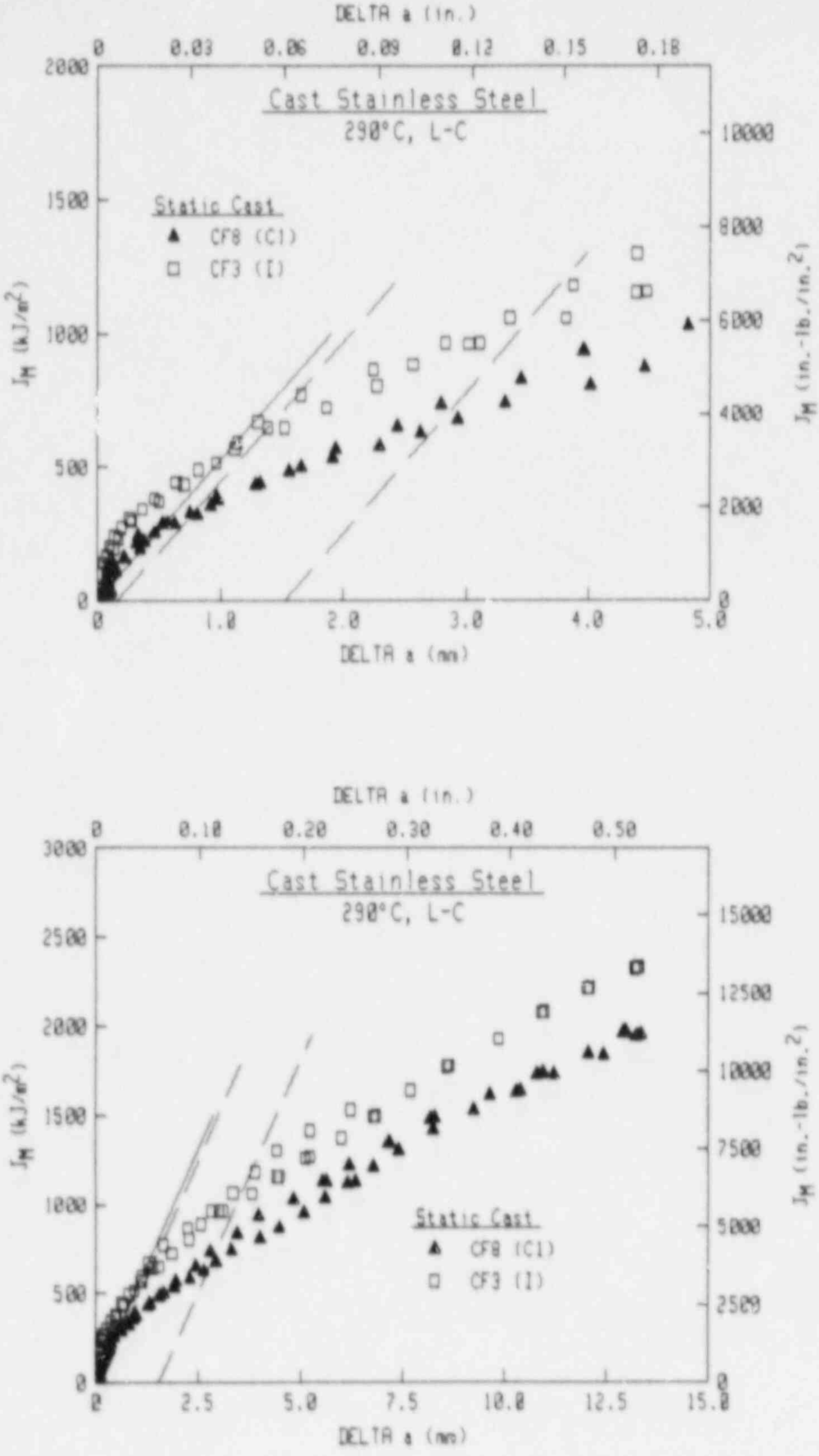

Fig. 20 For the static-cast commercial heats (L-C orientation, 290°C), the CF3 grade has higher toughness than the CF8 grade. This trend is consistent with all other comparisons for commercial heats of cast stainless steel.

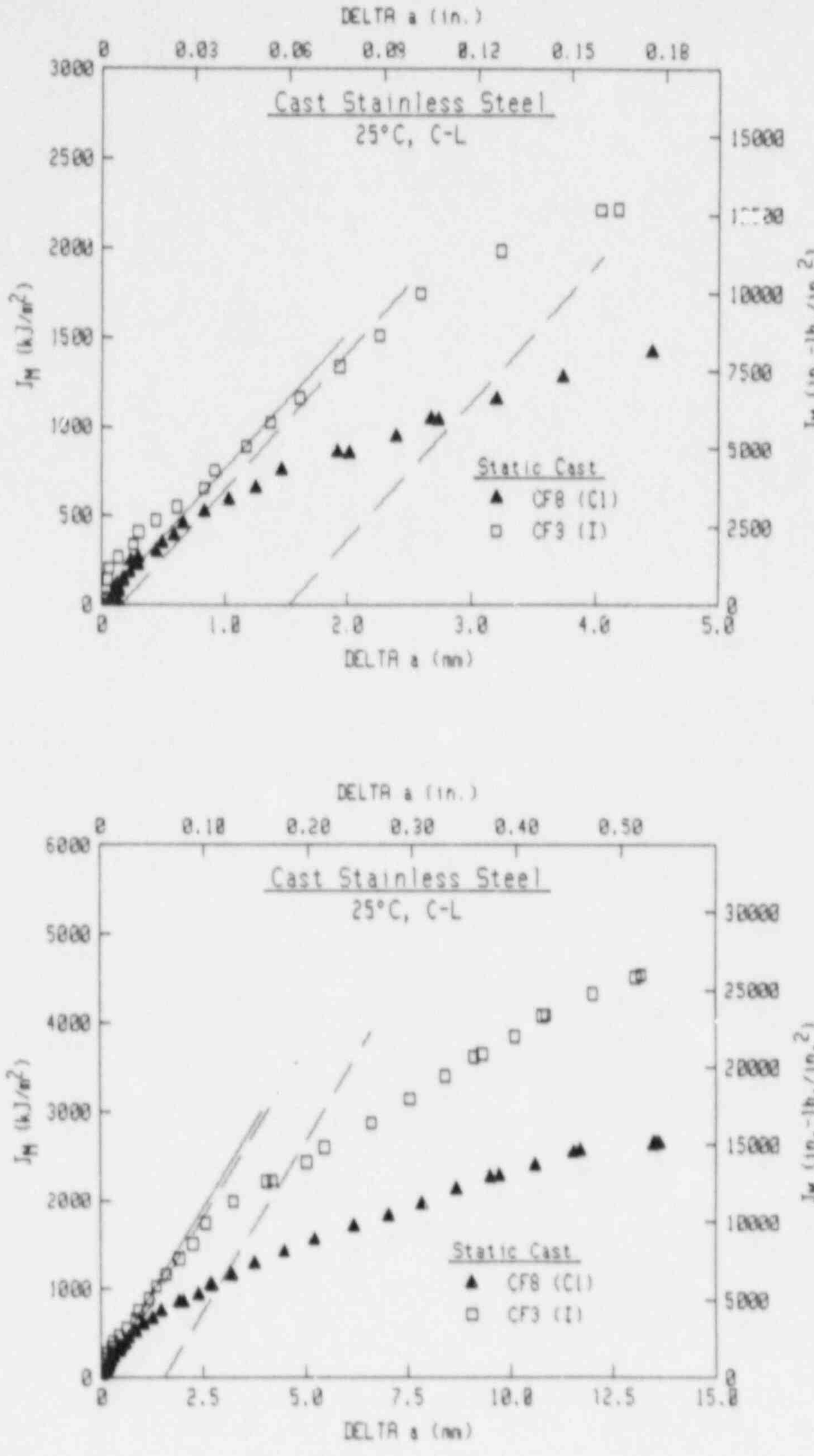

Fig. 21 For the static-cast commercial heats (C-L orientation, 25°C), the CF3 grade has much higher toughness than the CF8 grade, consistent with the trend for the L-C orientation.

Table 18 J-R Curve Results for Code ZP18 (Cast Stainless Steel, SA351-CF8A)

Specimen Number	Orientation	Test Temp	$(a/W)_i$	Δa_m	$\Delta a_p - \Delta a_m$	J_{Ic}		T_{avg}		C	n	σ_f	Aging Condition	
						MEA	ASTM	MEA	ASTM				Temp	Time
		(°C)		(mm)	(mm)	(kJ/m²)	(kJ/m²)			(kJ/m²)		(MPa)	(°C)	(h)
CF8A-2LC	L-C	24	0.525	13.22	-1.80	2109.8	1838.6	544	604	1085.3	0.6672	413.0	Unaged	
CF8A-4LC	L-C	25	0.540	13.33	-1.72	2461.6	2367.6	411	428	1387.8	0.5041	413.0	Unaged	
CF8A-3LC	L-C	148	0.544	10.97	-1.75	2384.7	2316.8	525	493	1199.[illegible]	0.5188	330.8	Unaged	
CF8A-5LC	L-C	288	0.547	12.17	-1.52	1632.7	1554.8	467	519	1008.3	0.4479	293.8	Unaged	
CF8A-6LC	L-C	288	0.536	12.80	-1.91	1542.4	1483.4	512	538	931.6	0.4933	293.8	Unaged	
CF8A-4CL	C-L	25	0.535	12.93	-0.99	2165.2	2159.9	331	313	1401.7	0.4748	461.7	Unaged	
CF8A-5CL	C-L	24	0.538	19.97	-2.47	1893.0	1858.5	382	379	1220.8	0.5551	461.7	Unaged	
CF8A-3CL	C-L	148	0.544	7.75	-1.67	2386.0	2237.7	526	581	1202.9	0.5110	325.5	Unaged	
CF8A-2CL	C-L	288	0.537	13.08	-2.05	1565.1	1464.1	398	464	1045.4	0.4026	304.4	Unaged	
CF8A-6CL	C-L	288	0.538	13.18	-1.61	1527.7	1500.8	382	360	1043.5	0.3892	304.4	Unaged	
CF8A-2LR	L-R	288	0.578	10.44	-1.51	974.0	834.6	626	691	682.1	0.5998	293.8	Unaged	
CF8A-2CR	C-R	288	0.581	11.94	-1.82	949.8	902.5	477	492	716.3	0.5238	304.4	Unaged	

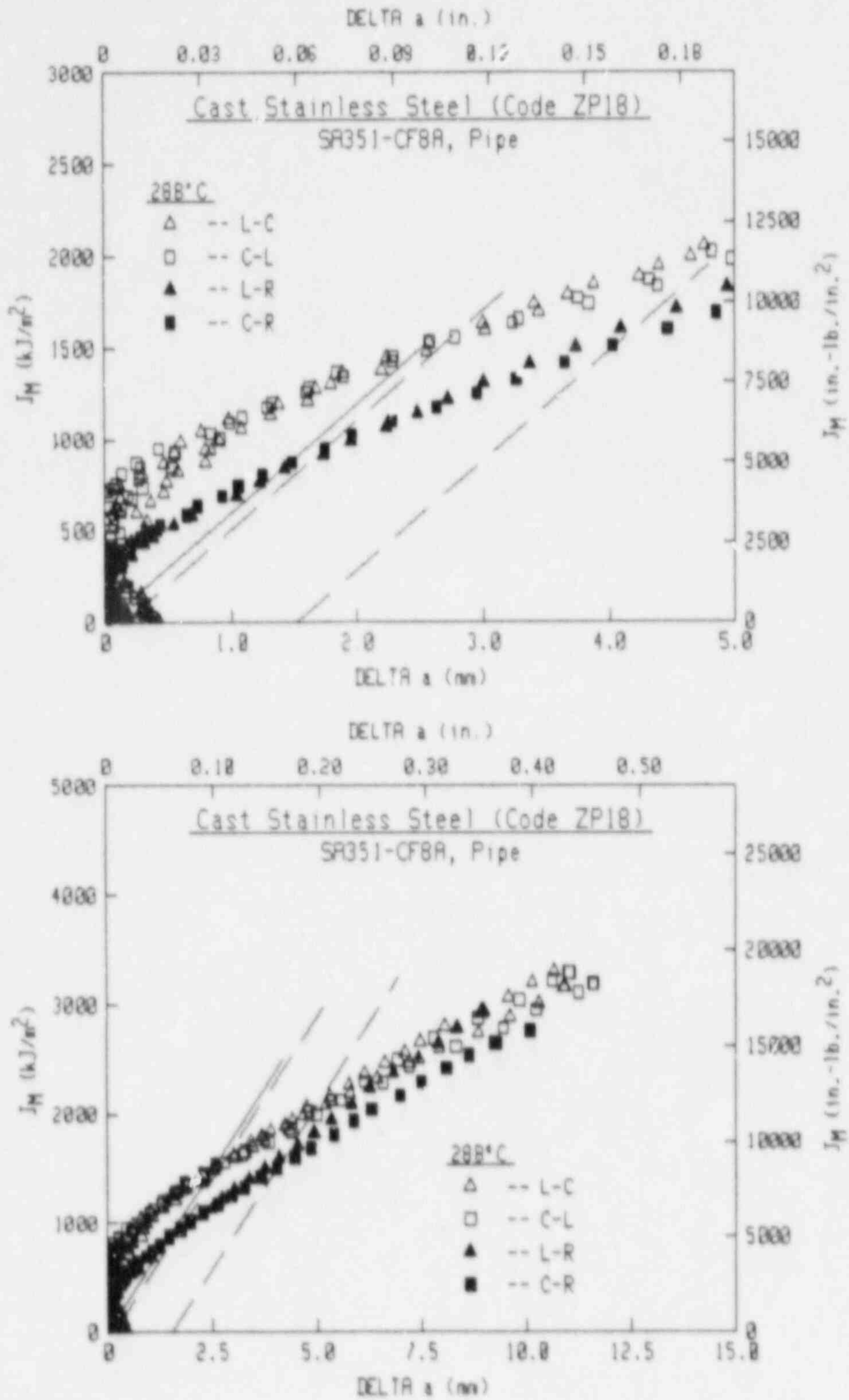

Fig. 22 For Heat ZP18 (grade CF8A) at 288°C, the L-C and C-L orientations demonstrate higher toughness than the L-R and C-R orientations.

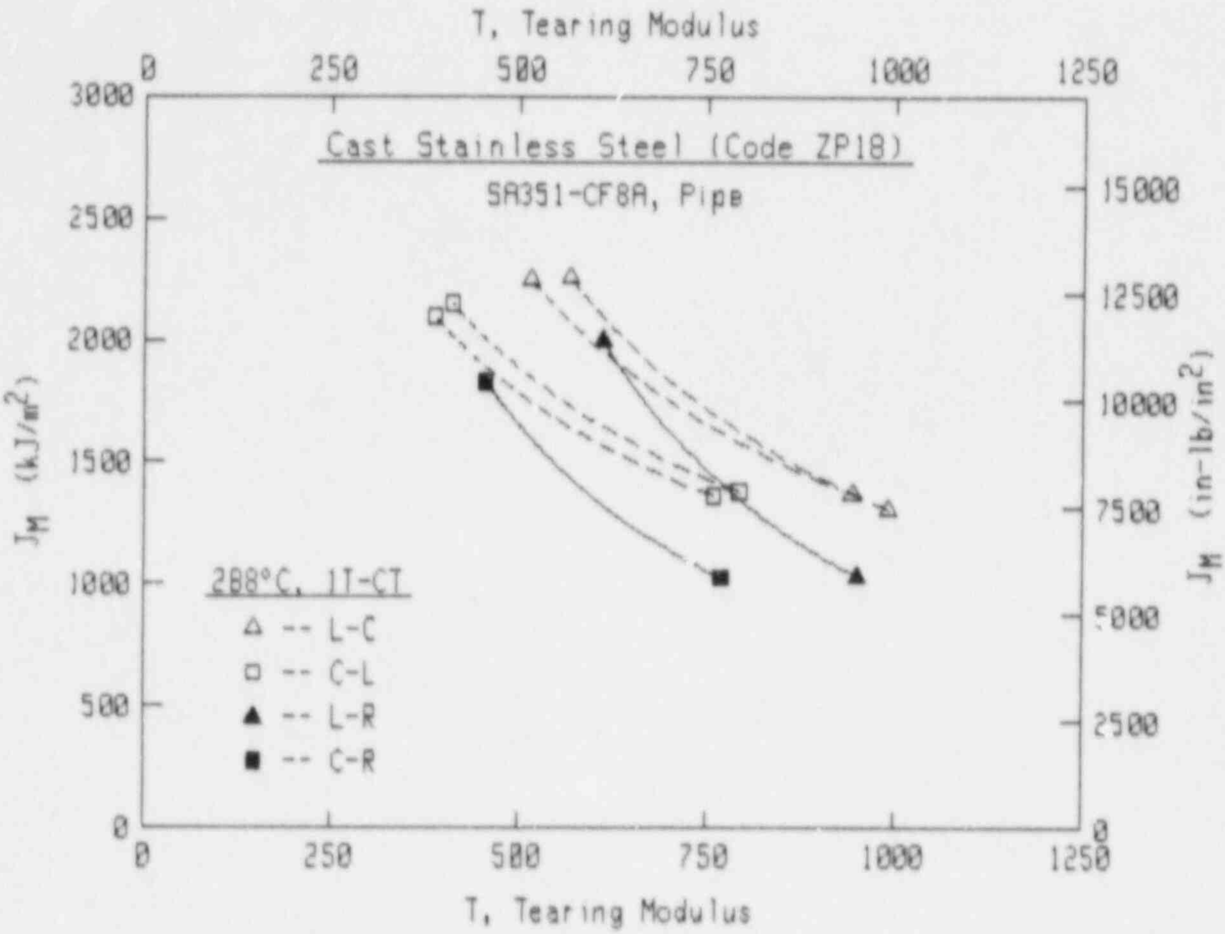

Fig. 23 For Heat ZP18 (grade CF8A) at 288°C, J-T curves for the L-C and C-L orientations have higher J levels and similar slopes to those for the L-R and C-R orientations.

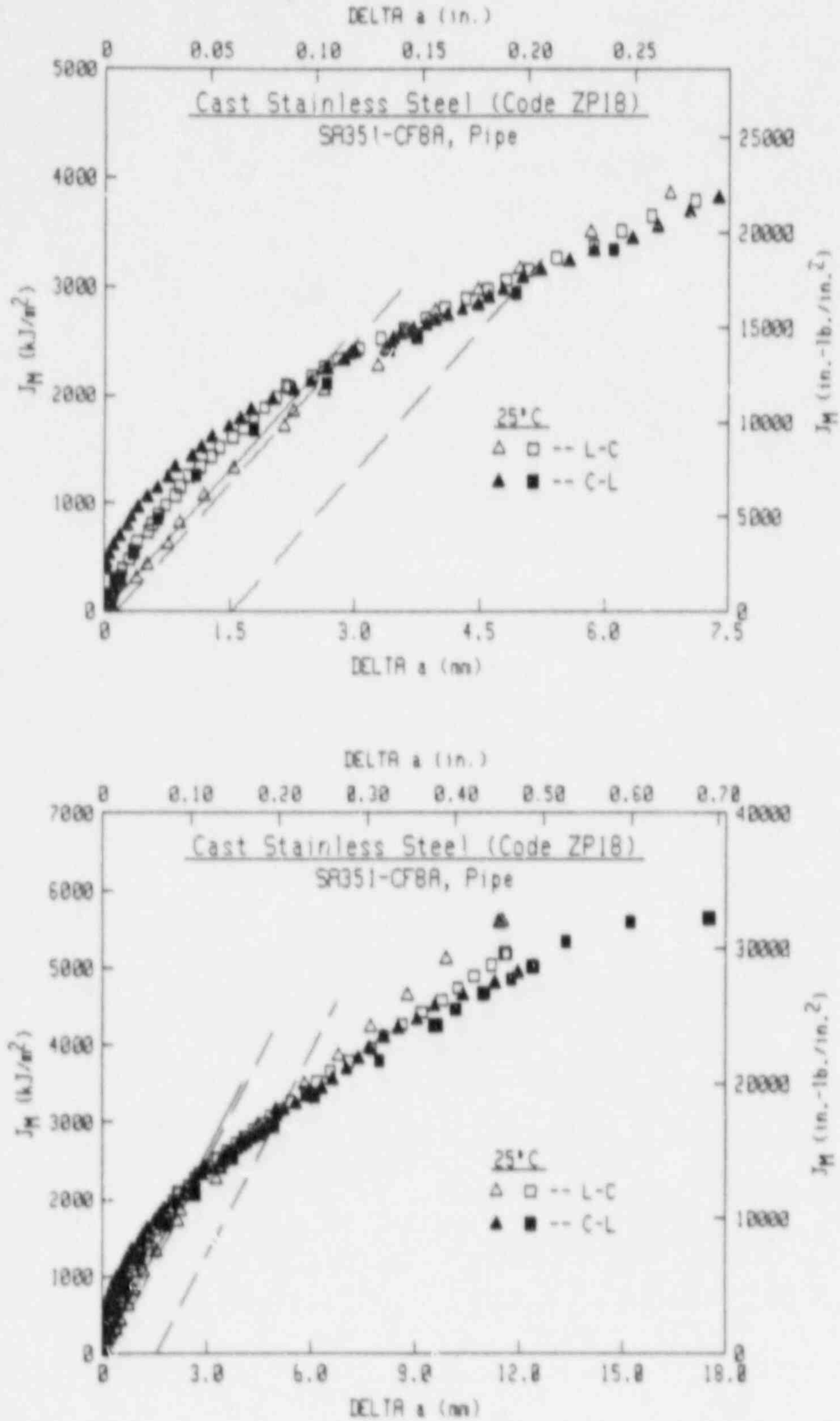

Fig. 24 At 25°C for Heat ZP18, J_M-R curves for the L-C and C-L orientations are in good agreement.

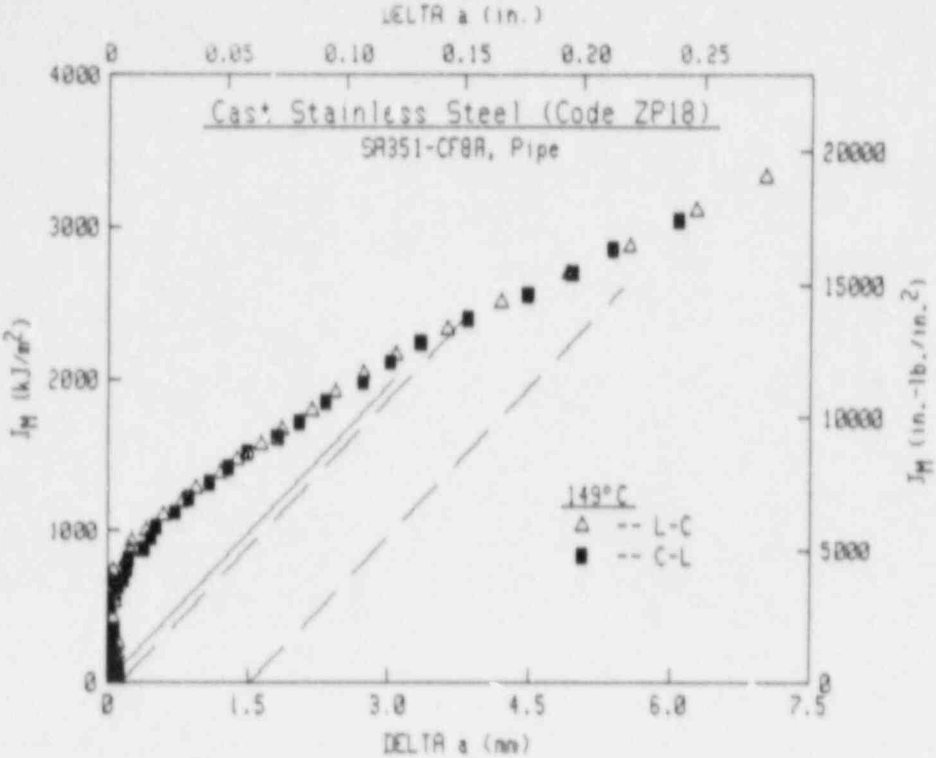

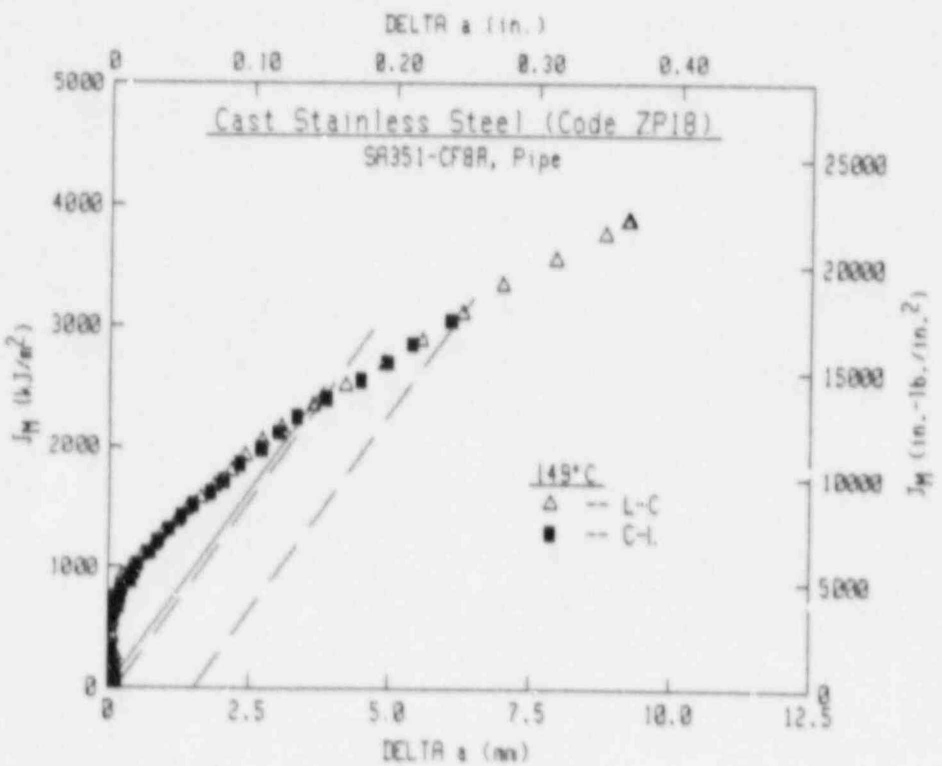

Fig. 25 As at the other temperatures, the J_M-R curves for the L-C and C-L orientations are in good agreement at 149°C for Heat ZP18.

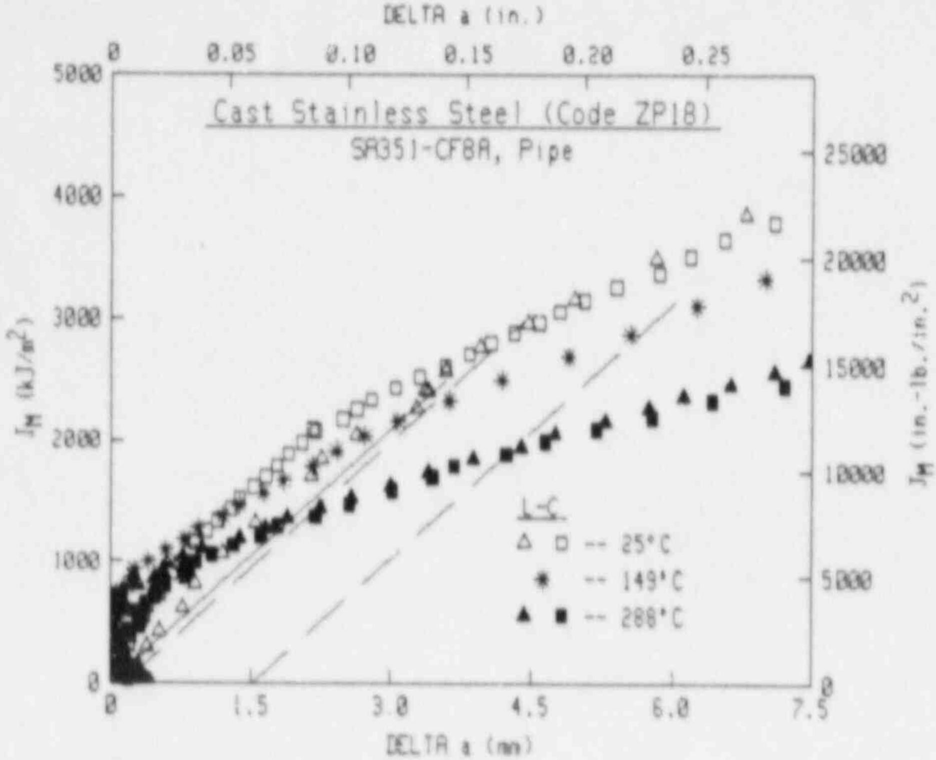

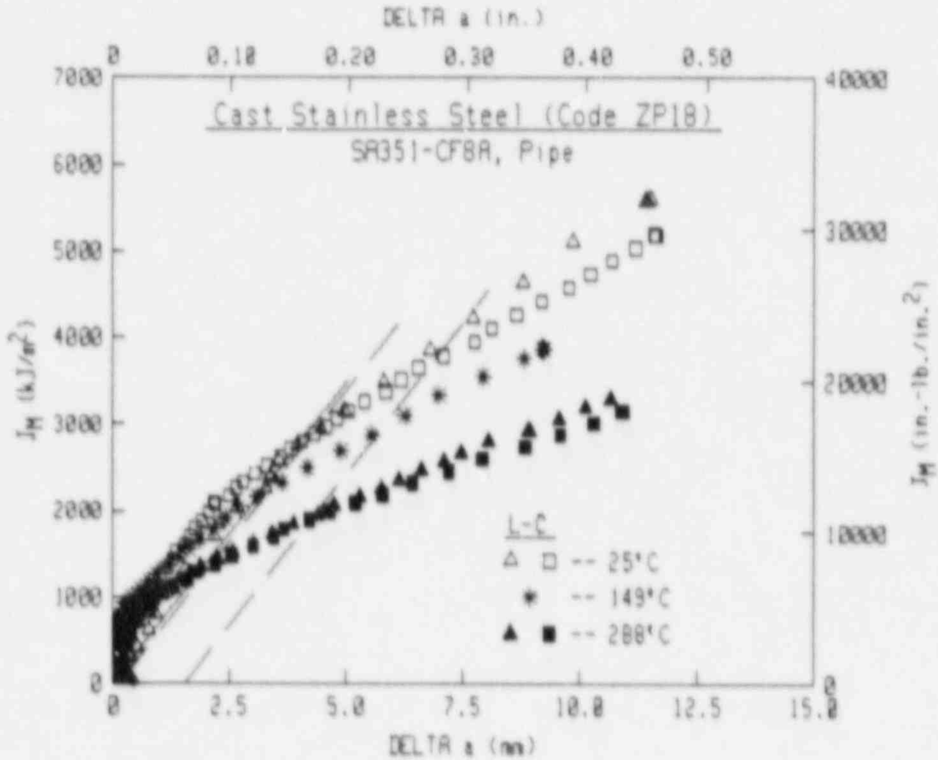

Fig. 26 For the L-C orientation of Heat ZP18 (grade CF8A), increasing the test temperature results in lower J_M-R curve levels.

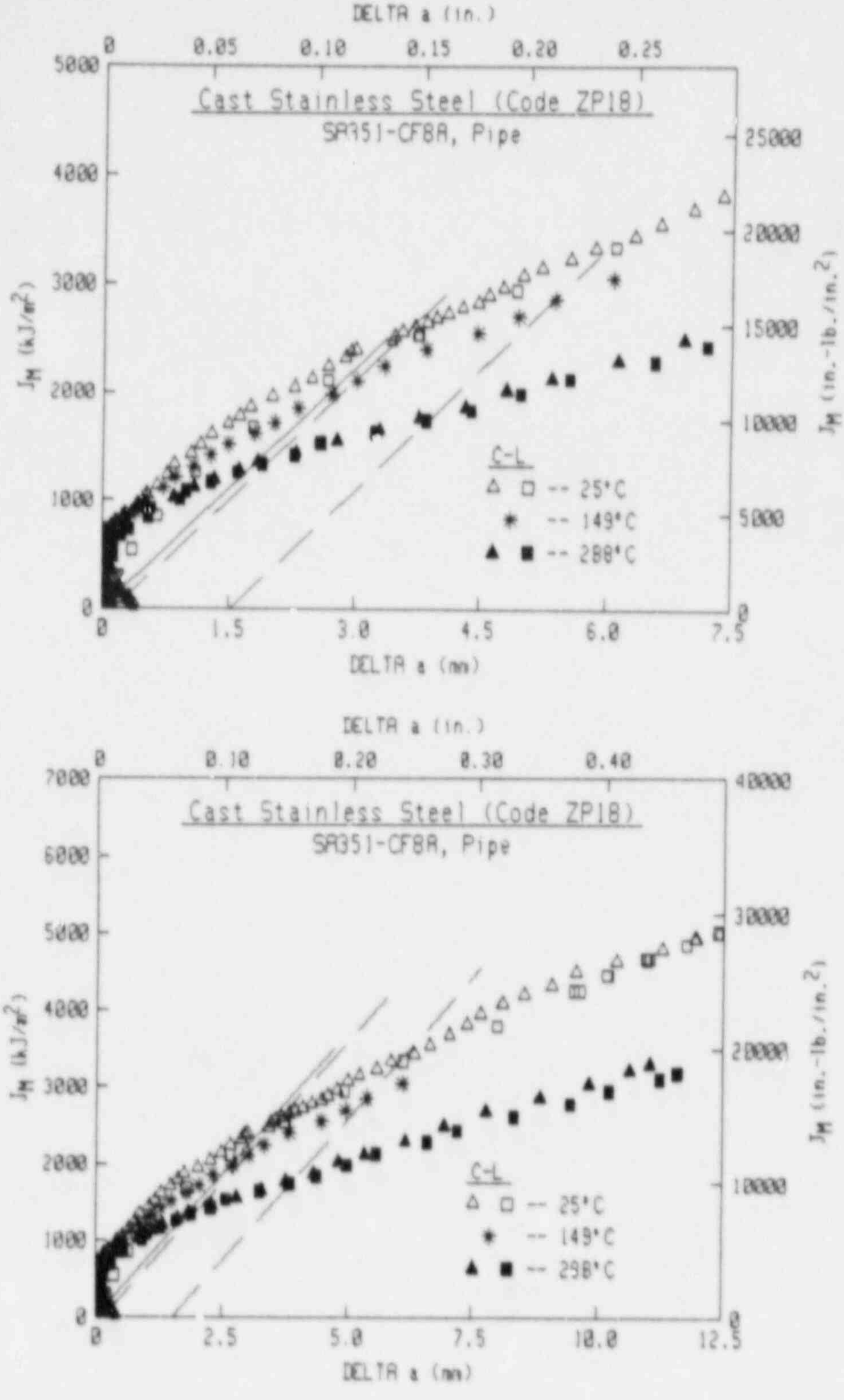

Fig. 27 As with the L-C orientation, the C-L orientation of Heat ZP18 (grade CF8A) demonstrates lower J_M-R curve levels with increasing test temperature.

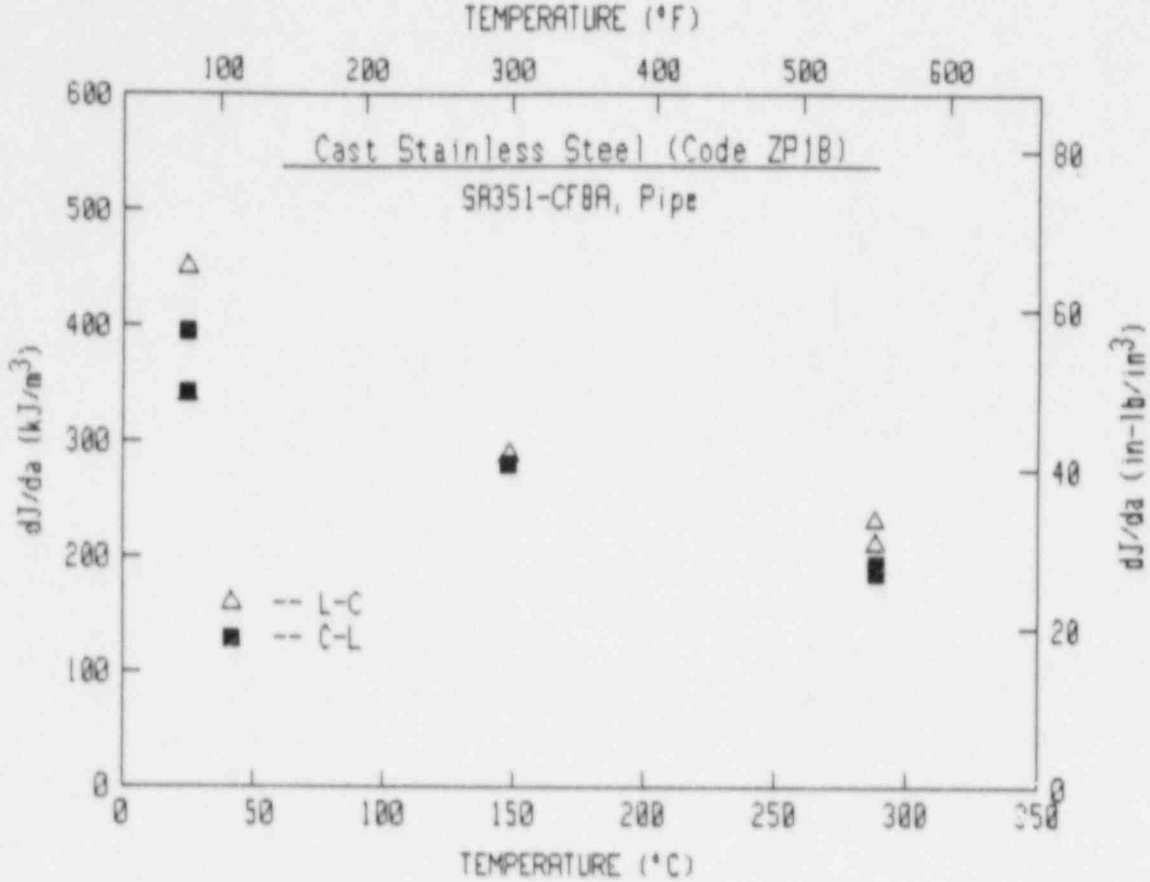

Fig. 28 For Heat ZP18, both the L-C and C-L orientations indicate reduced tearing resistance, in the form of dJ/da, with higher test temperature.

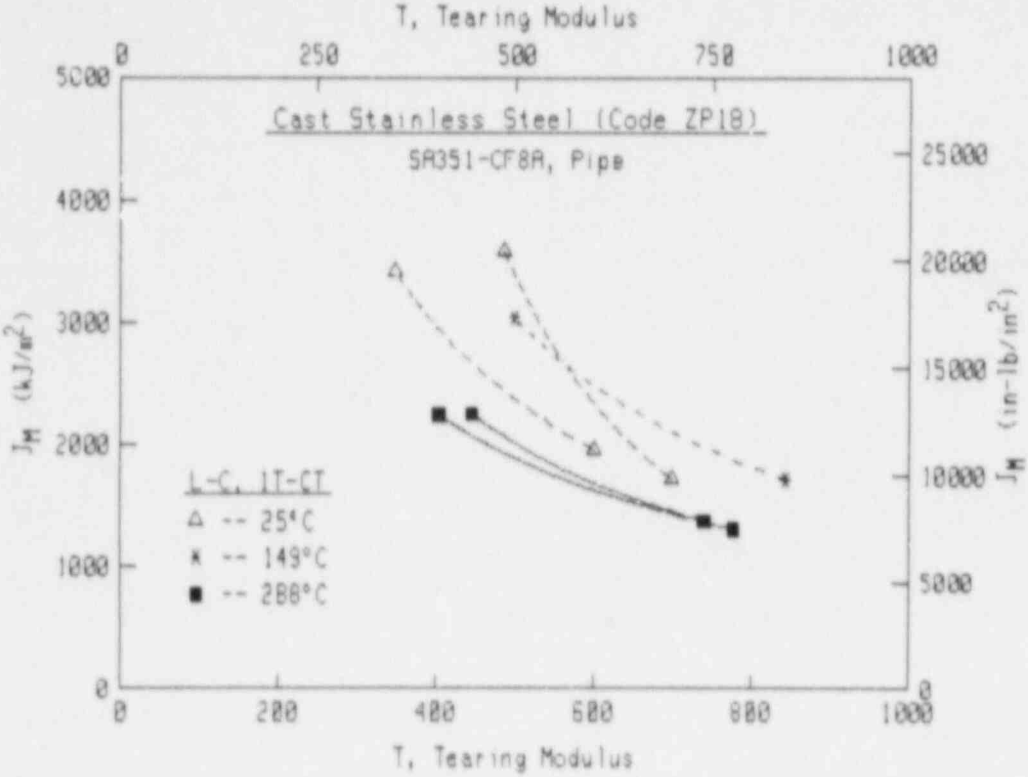

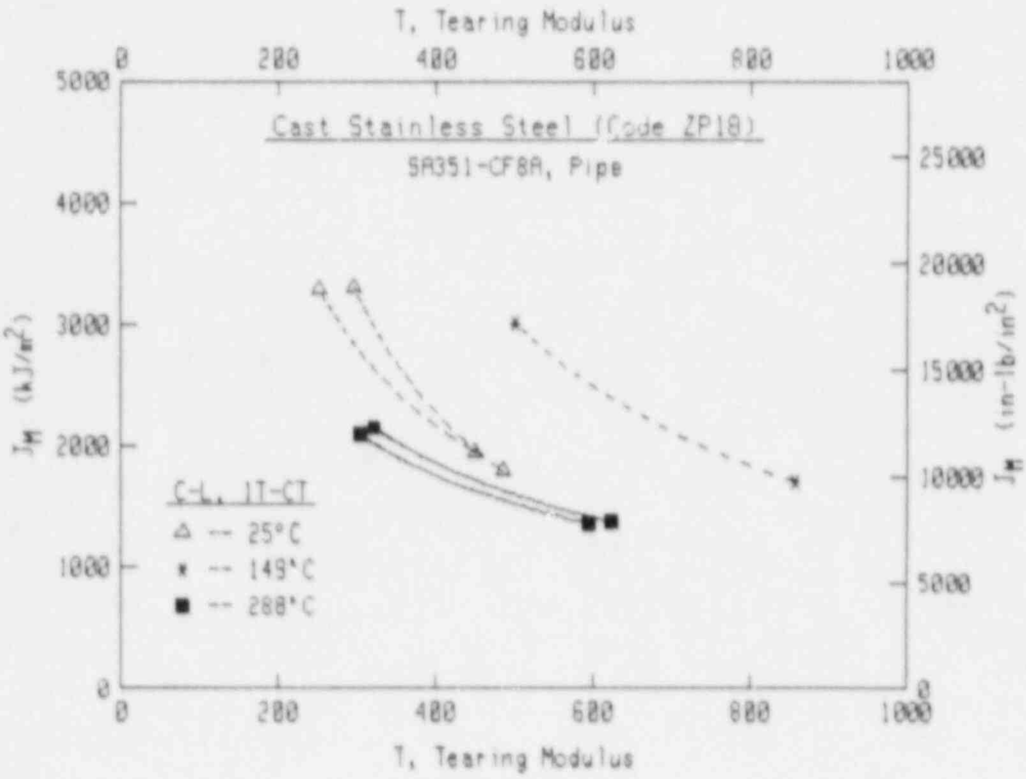

Fig. 29 In contrast to the dJ/da levels illustrated in Fig. 28, J-T curves for the C-L and L-C orientations of Heat ZP18 indicate higher tearing resistance at 149°C and lower tearing resistance at 288°C.

tearing modulus despite the J-R curve at 288°C exhibiting a slope which was a factor of two below that for the curve at 25°C. Therefore, comparison of trends using tearing modulus or J-T comparisons can be misleading in terms of evaluating the relative effect of increased test temperature on the fracture resistance of such materials. This concept is most applicable to low strength materials such as cast stainless steels due to the large percentage decreases in strength with increasing test temperature. As an example, ferritic reactor pressure vessel (RPV) steels have significantly higher strength levels which are not decreased as significantly as those for the cast stainless steels, rendering flow strength effects on tearing modulus much less significant for RPV steels.

5.2.2 Heat C1 (CF8)

J-R curve results for Heat C1 are summarized in Table 19. In contrast to results for the CF8A ring, this CF8 ring demonstrates an orientation effect, whereby the C-L orientation has higher toughness than the L-C orientation (Fig. 30). Significant variability is indicated for the two tests from the L-C orientation, in particular at large crack growth increments (> 2 mm). The higher of the two curves is relatively close to the single curve for the C-L orientation.

Likewise, higher temperature does not result in significant changes in J-R curve level (Fig. 31). As illustrated, the data at 290°C essentially bisect the two curves at 25°C. The data at 290°C also demonstrate little variability, in particular in comparison to the data at 25°C.

5.2.3 Heat I (CF3)

J-R curve results for Heat I are summarized in Table 20. In general, results from duplicate tests are in good agreement, indicative of little variability for this heat. In this case the L-C and C-L orientations demonstrate close agreement of J-R curves at 25°C (Fig. 32), consistent with trends for Heat ZP18 (CF8A). The duplicate tests of the L-C orientation are virtually colinear up to ~5 mm of crack growth.

The effect of temperature on the J-R curves for unaged material (Fig. 33) is similar to that for Heat ZP18 (CF8A). In this case the J-R curve levels are reduced by a factor of ~2 at 290°C in comparison to results at 25°C. Comparison of the load-deflection curves for these tests (Fig. 34) indicates lower maximum loads at 288°C and (somewhat) lower deflection at maximum load. Similarily, the Δa-deflection curves (Fig. 35) indicate greater crack growth at 288°C and crack initiation at a lower deflection. The combination of these two trends results in the J-R curve differences illustrated in Fig. 33.

With thermal-aging at 350°C for 10000 h, the J-R curve trends are reduced in all cases for this heat with the magnitude of the reduction similar to those for the C_v USE trends (15% reduction). At 25°C, both the L-C (Fig. 36) and the C-L (Fig. 37) orientations indicate ~20% decreases in J level after thermal-aging. Similar decreases are evident for this heat at 290°C for the L-C orientation (Fig. 38).

Table 19 J-R Curve Results for Code C1 (Static Cast Stainless Steel Pump - Casing Ring, SA351-CF8)

Specimen Number	Orien-tation	Test Temp (°C)	$(a/W)_i$	Δa_m (mm)	$\Delta a_p-\Delta a_m$ (mm)	J_{Ic} MEA (kJ/m^2)	J_{Ic} ASTM (kJ/m^2)	T_{avg} MEA	T_{avg} ASTM	C (kJ/m^2)	n	σ_f (MPa)	Aging Condition Temp (°C)	Aging Condition Time (h)
C1B1LC	L-C	25	0.526	14.45	-1.58	356.1	340.4	223	239	422.7	0.4018	356.2	Unaged	
C1B2LC	L-C	23	0.537	12.65	-1.05	285.6	258.1	409	417	426.3	0.6773	356.2	Unaged	
C1B3CL	C-L	25	0.531	15.20	-1.73	568.2	545.2	409	414	584.9	0.5721	356.2	Unaged	
C1B4LC	L-C	288	0.529	14.44	-1.55	352.7	304.0	586	641	380.2	0.6047	241.4	Unaged	
C1B5LC	L-C	290	0.529	14.94	-1.73	350.8	359.8	508	474	376.0	0.5413	241.4	Unaged	

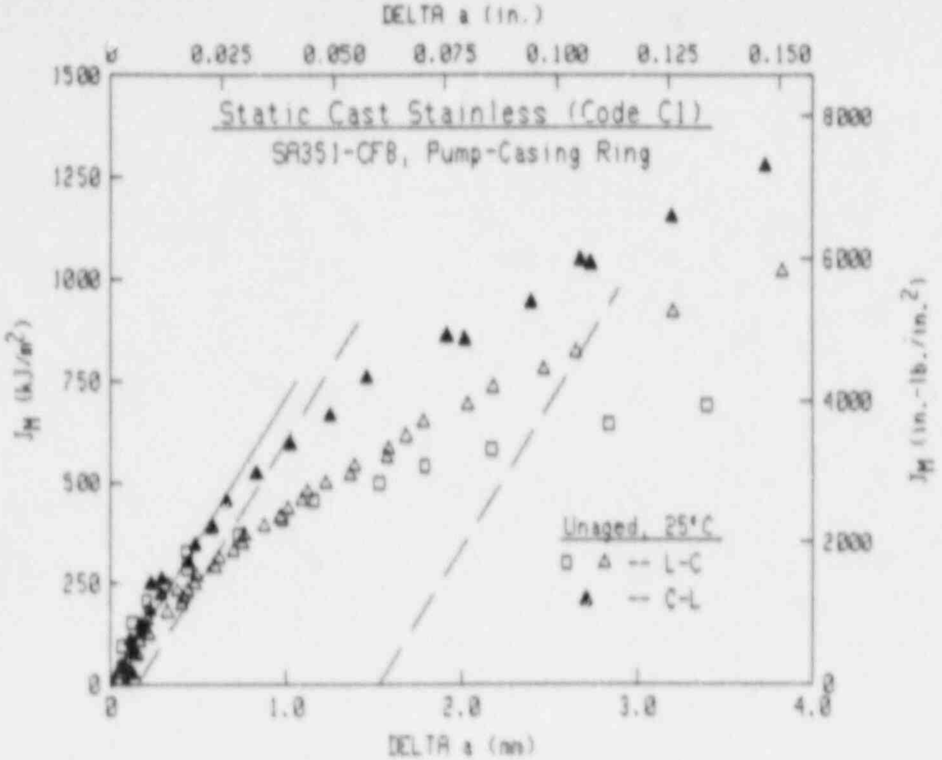

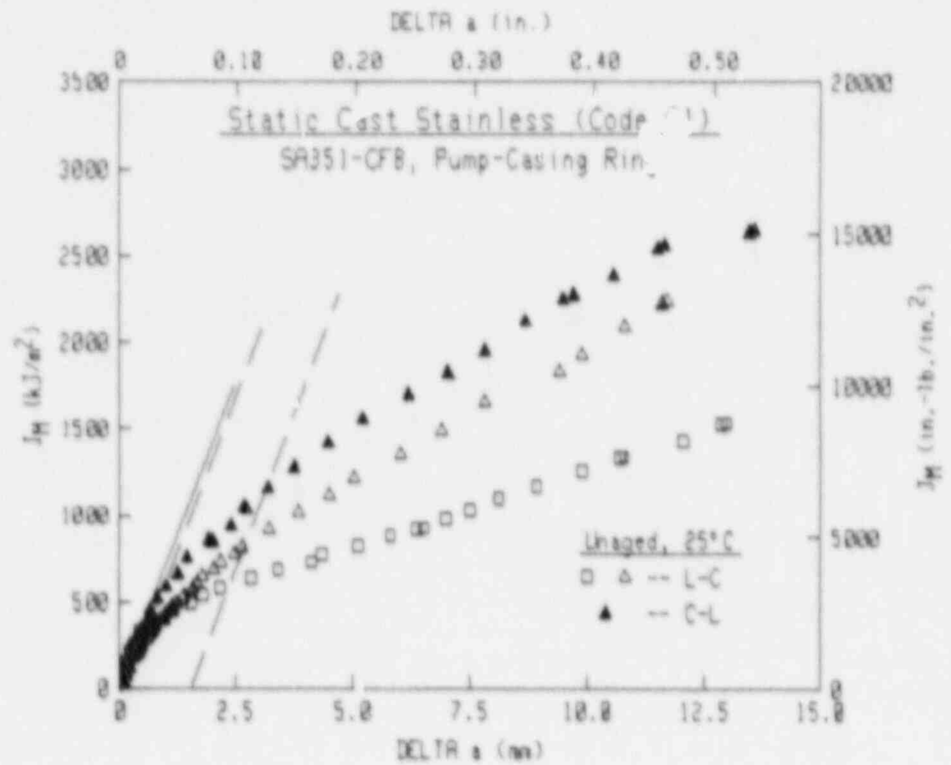

Fig. 30 In contrast to results for Heat ZP18 (grade CF8A), Heat C1 (grade CF8) demonstrates an orientation bias at 25°C, whereby the C-L orientation exhibits higher toughness than the L-C orientation.

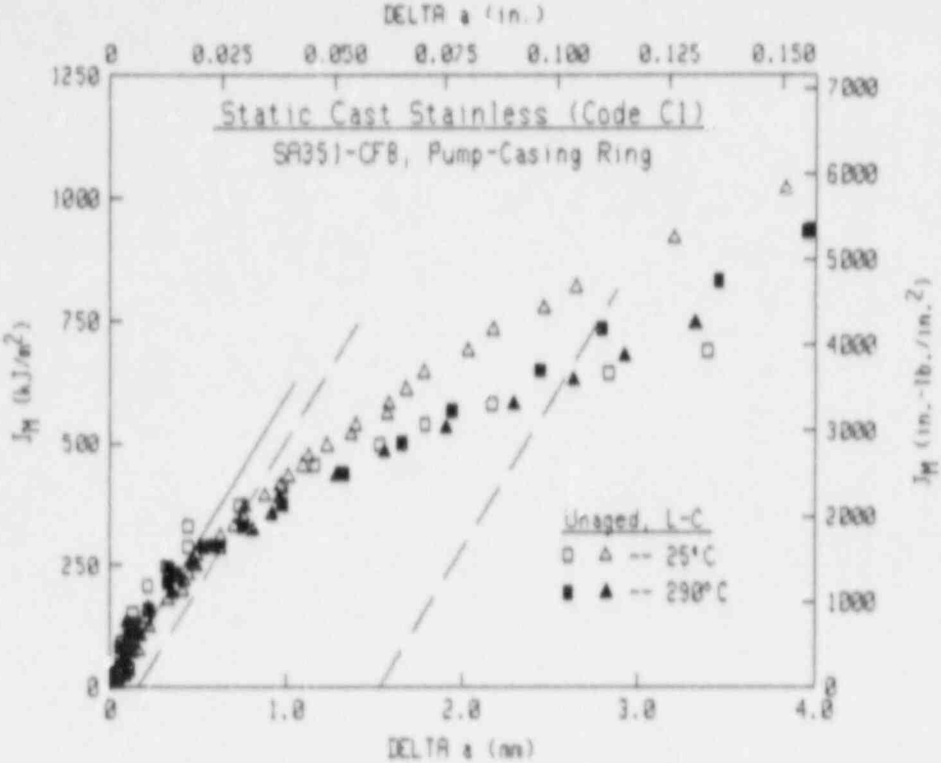

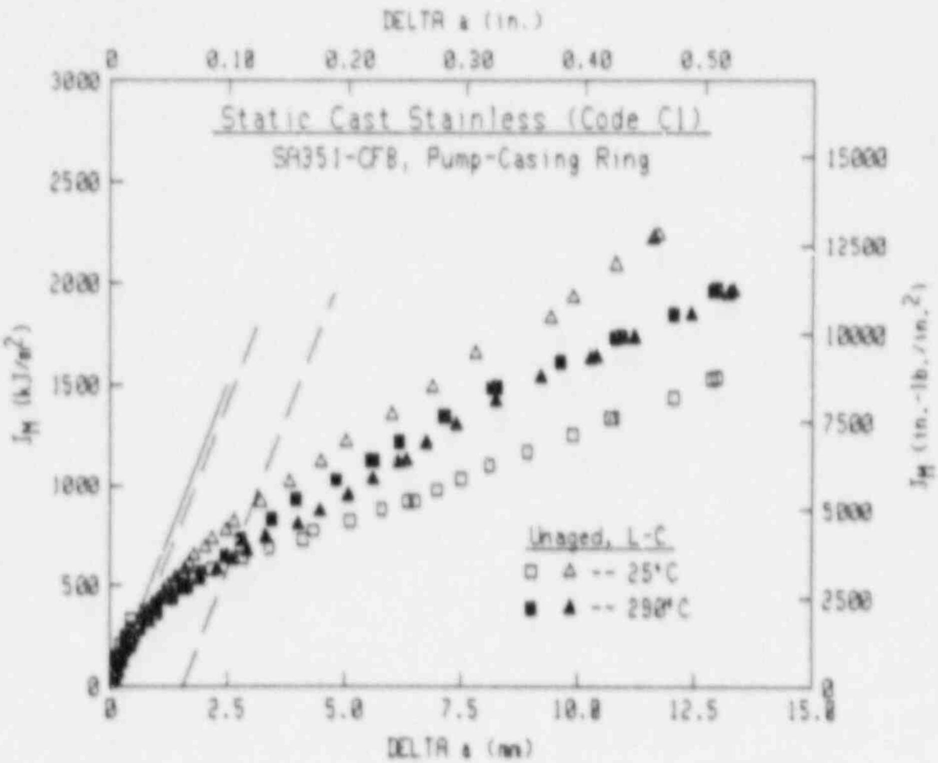

Fig. 31 Based on average trends for Heat C1 (grade CF8), no significant effect of test temperature is apparent. In this case, data at 25°C demonstrate significant variability whereas data at 290°C demonstrate good agreement.

Table 20 J-R Curve Results for Code I (Static Cast Stainless Steel Pump Impeller, SA351-CF3)

Specimen Number	Orientation	Test Temp	$(a/W)_I$	Δa_m	$\Delta a_p - \Delta a_m$	J_{Ic}		T_{avg}		C	n	σ_f	Aging Condition	
						MEA	ASTM	MEA	ASTM				Temp	Time
		(°C)		(mm)	(mm)	(kJ/m^2)	(kJ/m^2)			(kJ/m^2)		(MPa)	(°C)	(h)
I11LC	L-C	25	0.538	13.77	+1.43	1268.0	1167.6	450	473	920.1	0.6075	411.2	Unaged	
I21LC	L-C	25	0.534	13.66	-1.48	1239.3	1308.5	462	396	903.1	0.6241	411.2	Unaged	
I14LC	L-C	25	0.535	14.04	-1.18	702.3	685.3	290	291	741.6	0.5470	466.8	350	10000
I23LC	L-C	25	0.544	14.17	-1.24	647.4	559.1	354	399	721.7	0.6510	466.8	350	10000
I13CL	C-L	25	0.530	12.90	-0.16	1153.6	1255.6	524	466	846.4	0.7003	411.2	Unaged	
I16CL	C-L	25	0.527	14.72	-2.03	728.1	701.8	322	315	758.5	0.5887	466.8	350	10000
I1-2LC	L-C	288	0.525	14.85	-1.65	579.8	552.5	453	468	533.8	0.5181	284.2	Unaged	
I2-2LC	L-C	288	0.532	7.24	-1.03	683.7	693.7	450	403	587.9	0.4954	284.2	Unaged	
I1-5LC	L-C	288	0.541	13.62	-1.17	354.8	312.1	352	379	415.2	0.5151	303.7	350	10000
I2-4LC	L-C	288	0.538	13.91	-1.26	388.3	368.9	405	412	442.6	0.5618	303.7	350	10000

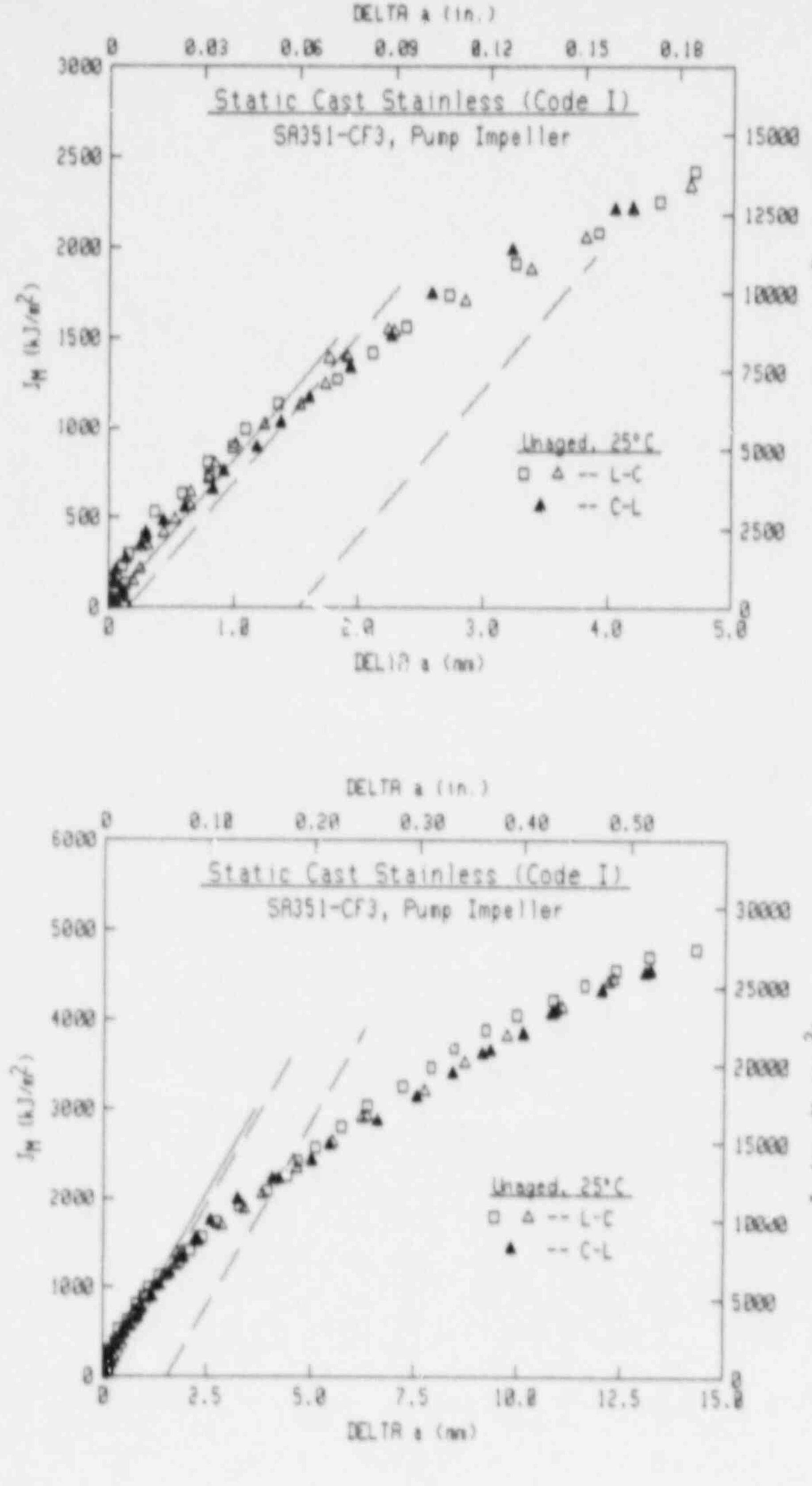

Fig. 32 For Heat I (grade CF3) at 25°C, the L-C and C-L orientations demonstrate good agreement of J_M-R curve trends.

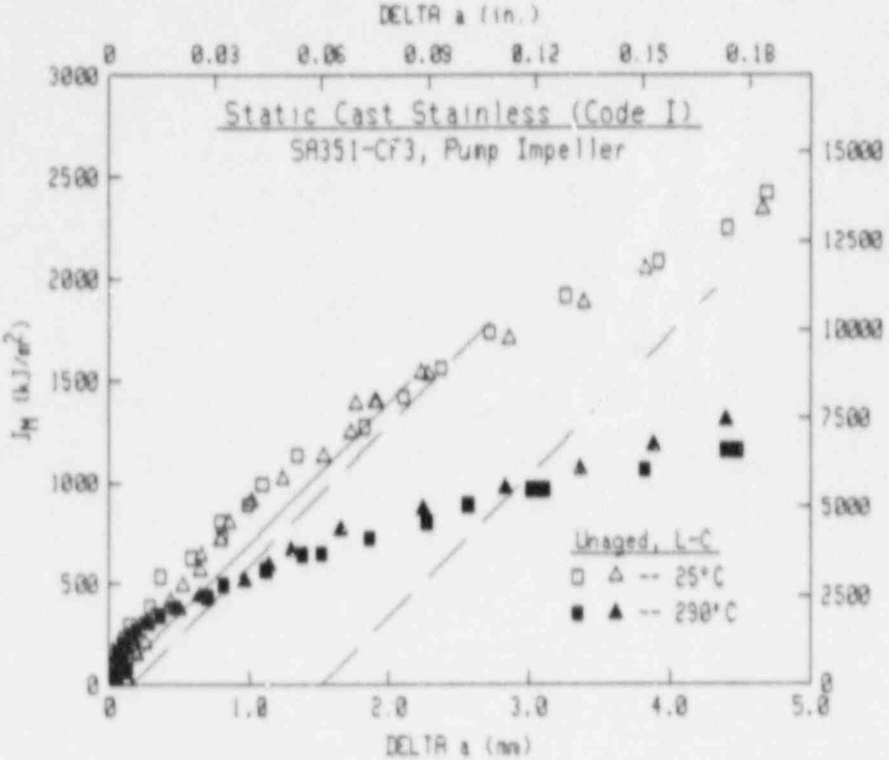

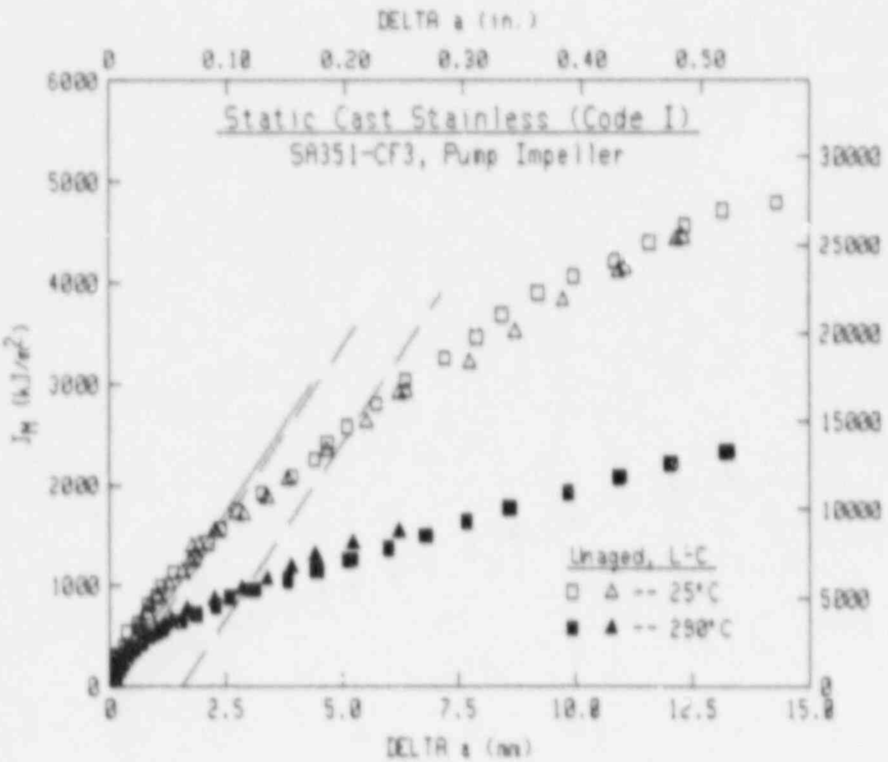

Fig. 33 For the L-C orientation of Heat I (grade CF3), increas[illegible] he test temperature results in a ~50% redu[illegible] in J_M-R curve levels.

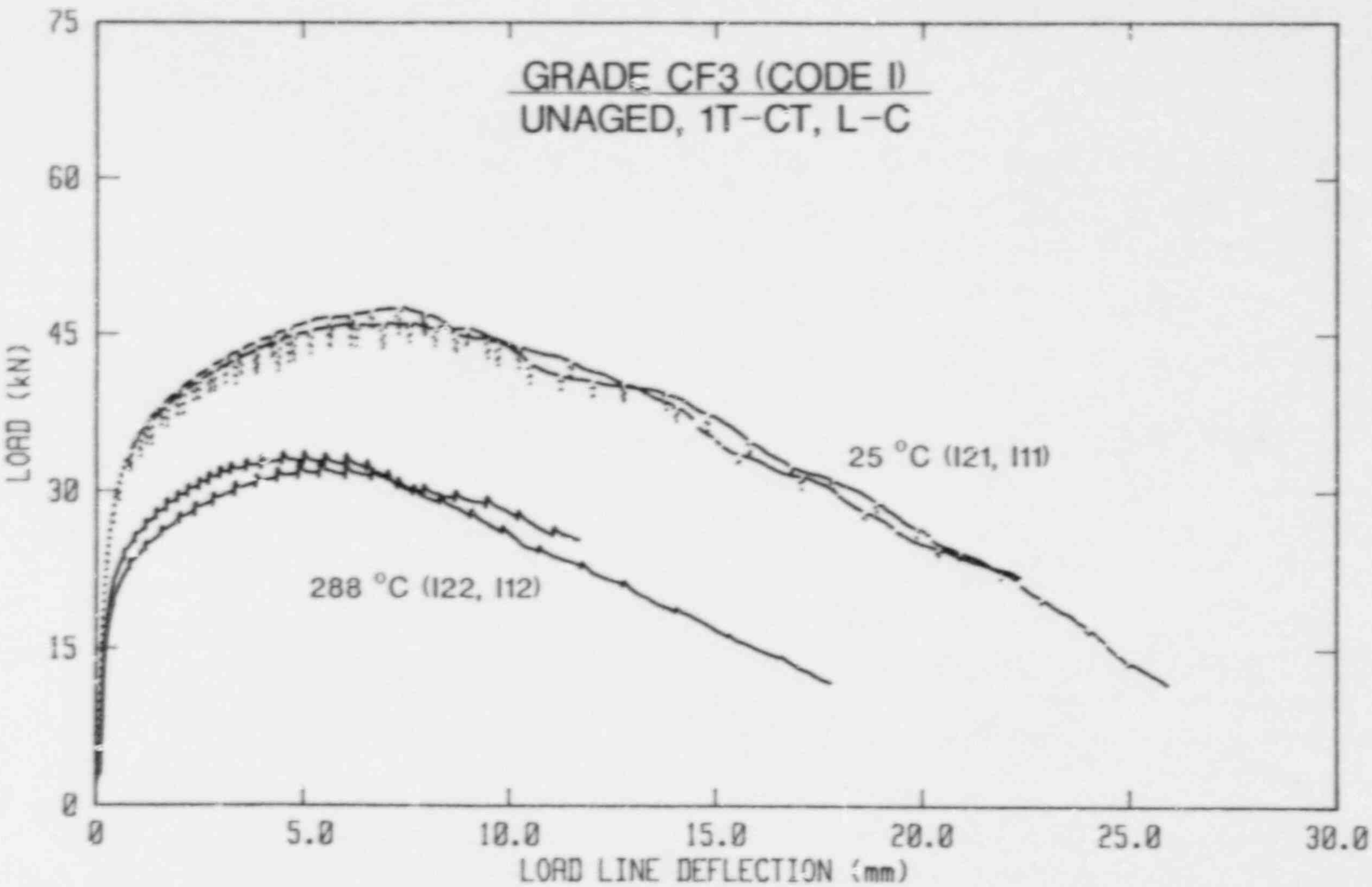

Fig. 34 Load-deflection curves for the Heat I J-R curves illustrated in Fig. 33. Higher test temperature results in much lower maximum load levels.

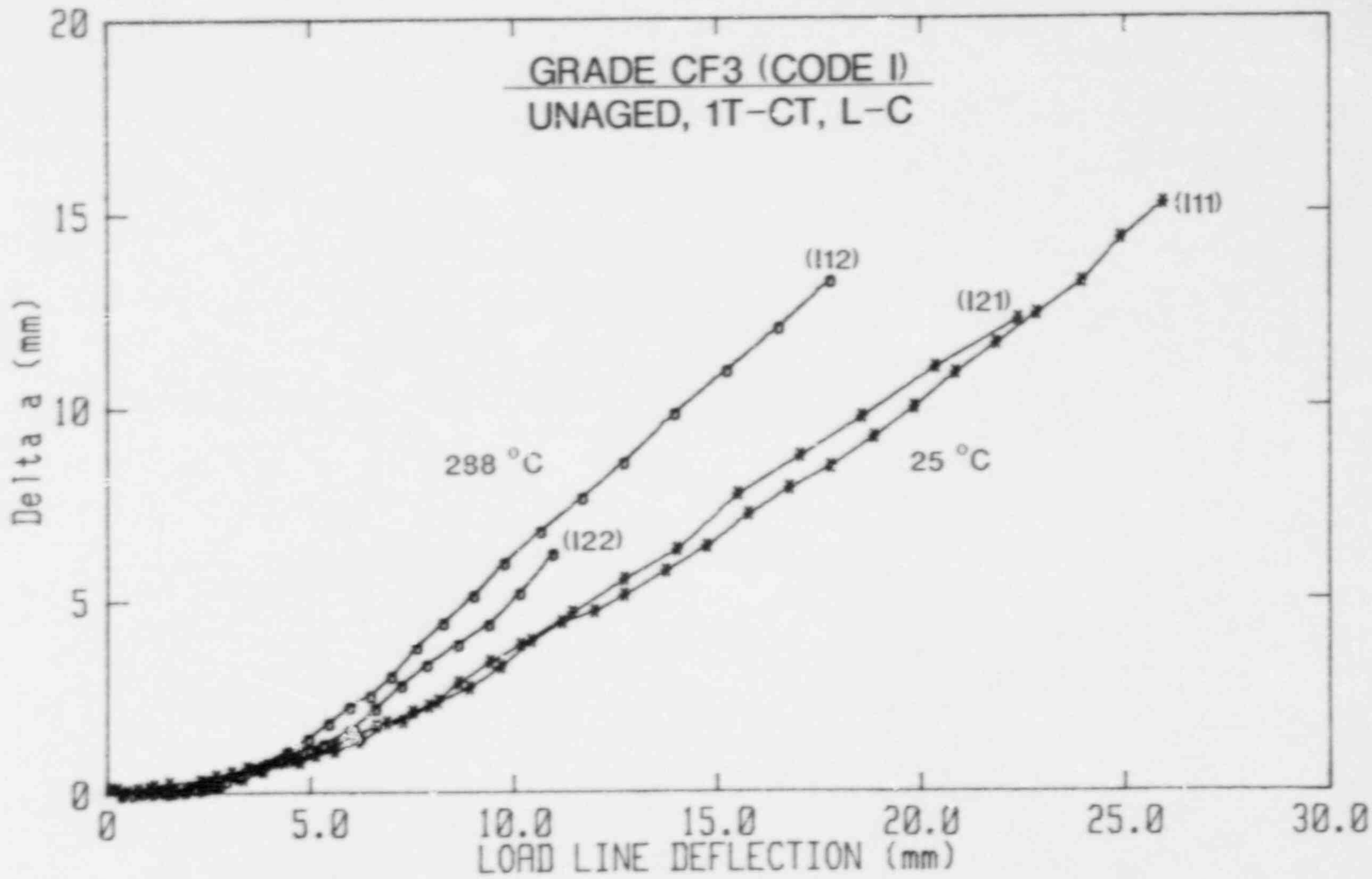

Fig. 35 Crack growth (Δa)-deflection curves for the same tests as in Fig. 34. Higher test temperature results in more crack growth at lower deflection.

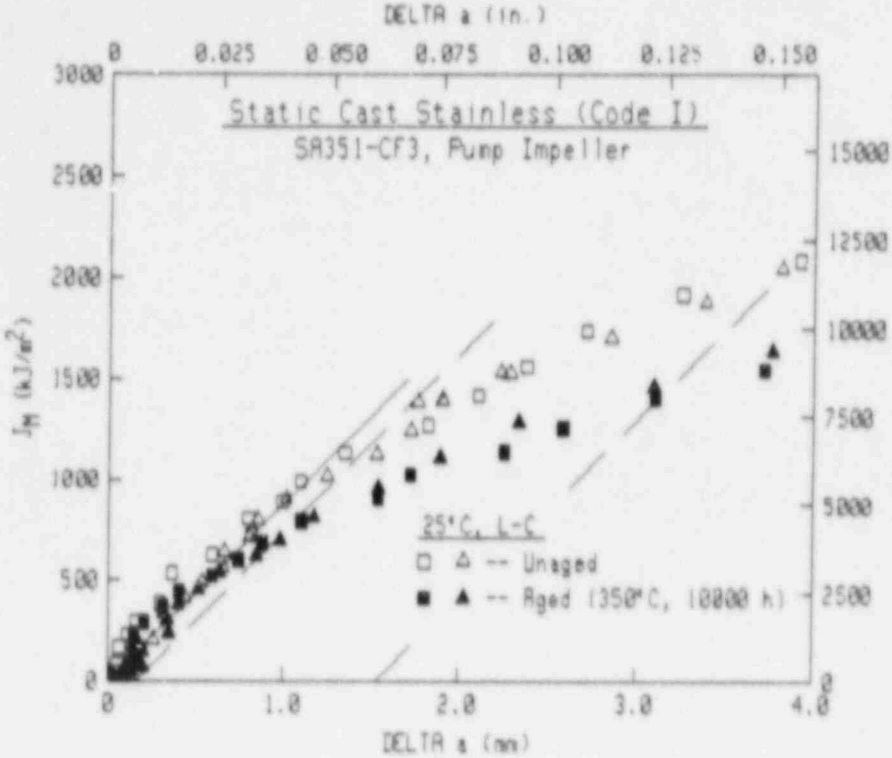

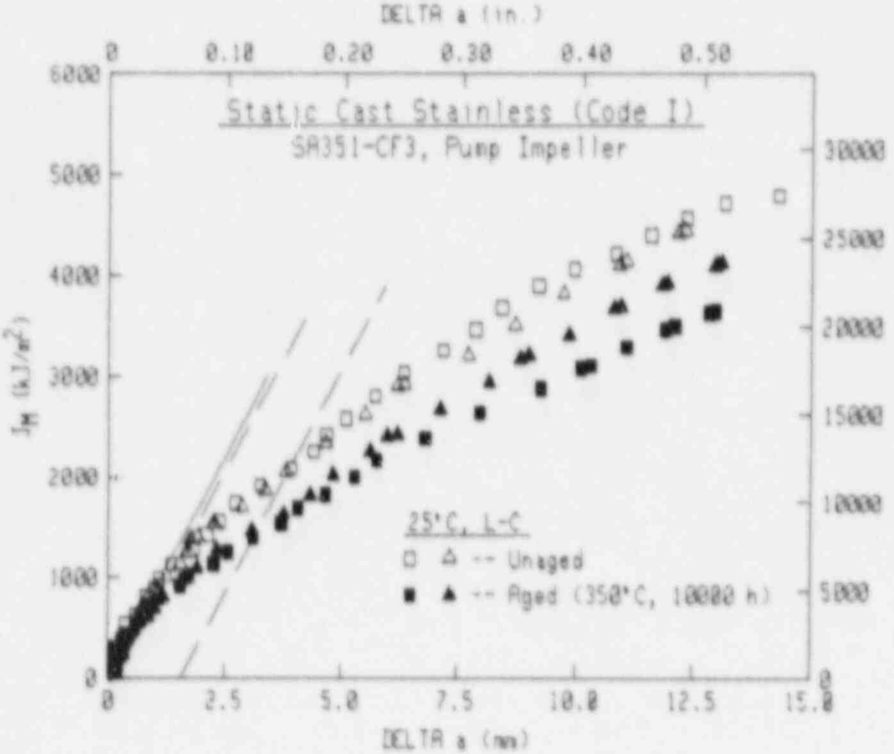

Fig. 36 For the L-C orientation of Heat I (grade CF3) at 25°C, thermal-aging at 350°C for 10000 h results in some reduction in J_M-R curve trends.

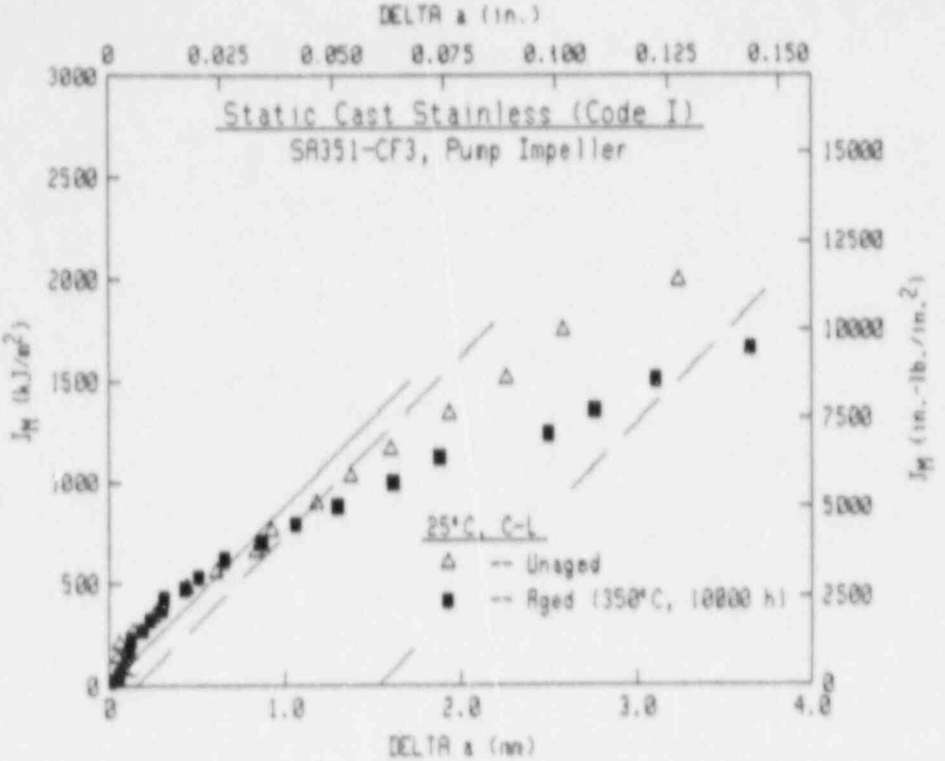

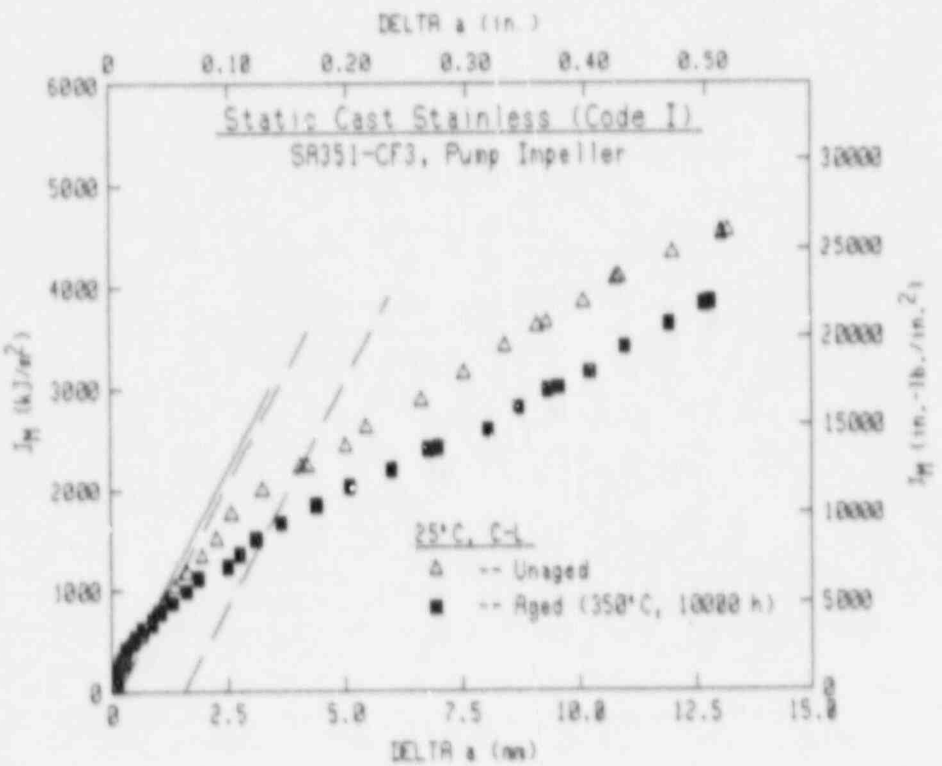

Fig. 37 For the C-L orientation of Heat I (grade CF3) at 25°C, the reduction in J_M-R curve levels due to thermal-aging at 350°C for 10000 h is consistent with that exhibited by the L-C orientation (Fig. 36).

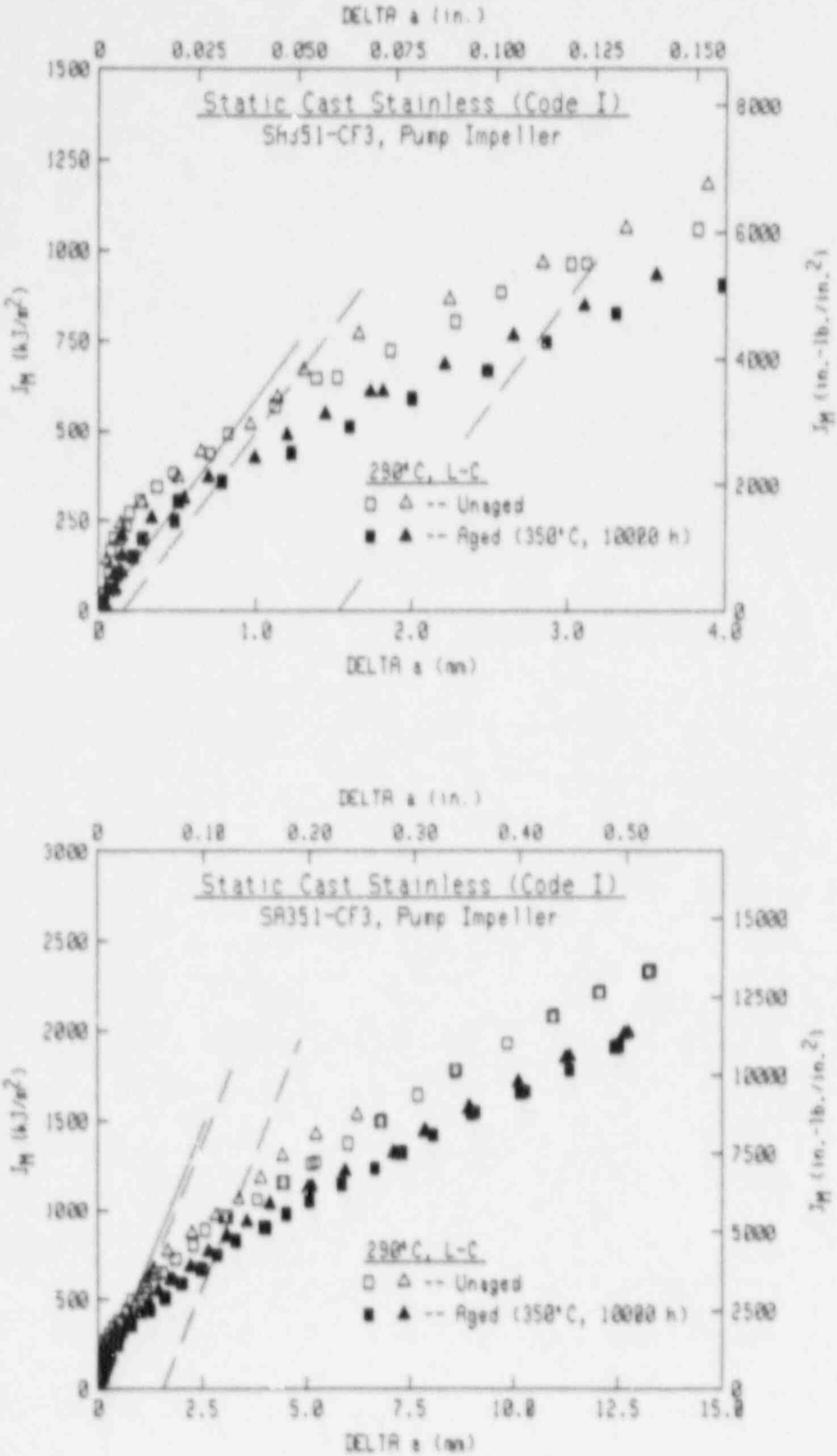

Fig. 38 For the L-C orientation of Heat I (grade CF3) at 290°C, thermal-aging results in a small reduction in J_M-R curve trends.

As with unaged material, increasing the test temperature to 290°C from 25°C for the aged condition results in a reduction in J-R curve level by a factor of ~2 (Fig. 39). Overall, the J level is reduced by a factor of ~2.5 for the aged condition at 290°C as opposed to the unaged condition at 25°C. For this heat, consideration of the service temperature is more significant than the effect of thermal-aging.

5.2.4 Heat P1 (CF8)

J-R curve results for this heat are summarized in Table 21. As mentioned previously for this heat, a large difference in J-R curve trends for unaged material was found for this heat based upon material location in the original pipe. In particular, material from the outside diameter (O.D.) gave significantly higher toughness than did material from the inside diameter (I.D.) Only the measured ferrite content was much larger for the outside diameter (27.6% vs. 19.5%), as the chemical compositions for the two locations were similar in other respects. An illustration of this effect is given in Fig. 40 at 25°C. The higher of the curves for the L-C orientation is from the outside diameter, whereas the lower L-C curve and the lone C-L curve is for the inside diameter of the pipe. The latter curves demonstrate good agreement for nominally the same starting material location. For the unaged condition, higher test temperature results in ~40% reduction in J level for the inside diameter material and ~50% reduction in J level for the outside diameter material (Fig. 41). As a result, the difference in J-R curves based on diameter are slightly less pronounced at 290°C than at 25°C.

The J-R curves for the L-C orientation at 25°C indicate a substantial effect of diameter location. For the load-deflection curves (Fig. 42), the specimen from the outside diameter of the pipe has only a slightly higher maximum load, but a deflection at maximum load which is much greater than that for the specimen from the inside diameter of the pipe.

In terms of thermal-aging effects, the J-R curve levels for aged material are below those of unaged material. For aging at 350°C for 1000 h, the C_v levels are similar to those for unaged material. Likewise, the J-R curve trends for the aged condition are similar in magnitude to those for the unaged condition. For the L-C orientation at 25°C, two data sets for material aged at 350°C for 10000 h demonstrate good agreement with one another (Fig. 43). This result is unexpected since one aged specimen is from the O.D. portion of the pipe (the solid triangles on the plot) whereas the other aged specimen is from the pipe I.D. (the solid squares). As well, the data from the aged I.D. specimen are consistent with data from the unaged I.D. specimen. Given the measured ferrite differences between the pipe I.D. and O.D. locations, the (apparently) higher embrittlement demonstrated by the material from the O.D. is not surprising. The absence of embrittlement indicated for the I.D. material may result from inherent toughness variability in the virgin material (i.e., the unaged I.D. specimen may be from a slightly lower toughness region of the pipe) combined with compositional variability (i.e., the aged I.D. specimen may be from a region less susceptible to thermal-aging

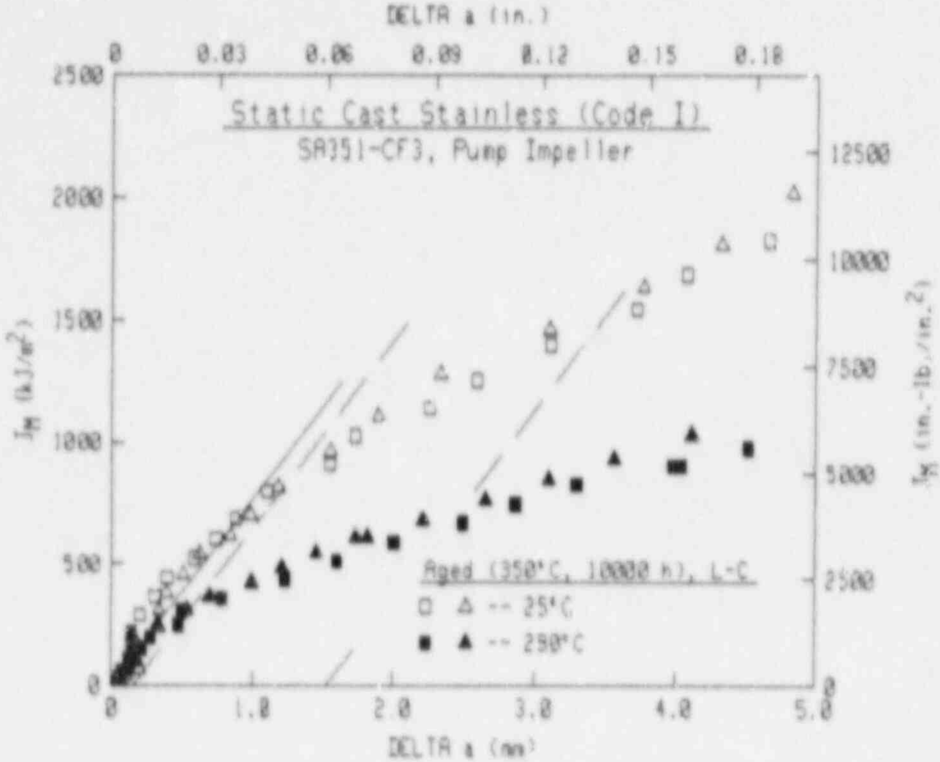

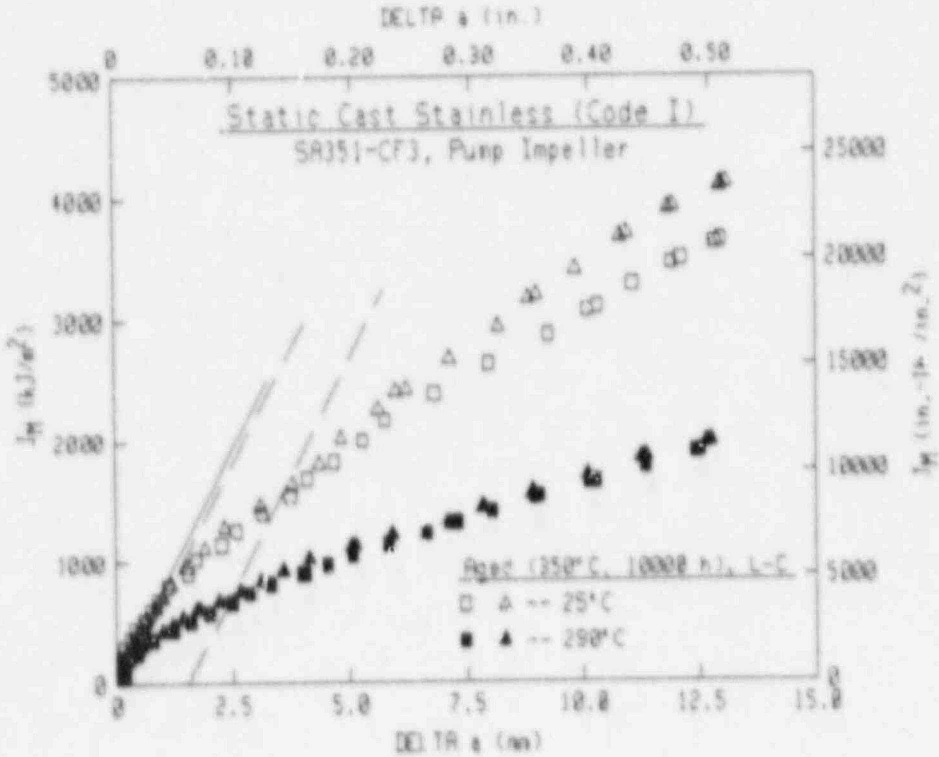

Fig. 39 As with unaged material for Heat I (grade CF3), higher test temperature for material thermally-aged at 350°C for 10000 h results in ~50% reduction in J_M-R curve levels.

Table 21 J-R Curve Results for Code P1 (Centrifugally Cast Stainless Steel Pipe, SA451-CF8)

Specimen Number	Orien-tation	Test Temp	$(a/W)_i$	Δa_m	$\Delta a_p-\Delta a_m$	J_{Ic}		T_{avg}		C	n	σ_f	Aging Condition	
						MEA	ASTM	MEA	ASTM				Temp	Time
		(°C)		(mm)	(mm)	(kJ/m^2)	(kJ/m^2)			(kJ/m^2)		(MPa)	(°C)	(h)
P1B1LC	L-C	23	0.524	9.07	-0.65	1138.6	1073.6	484	492	861.4	0.6660	416.5	Unaged	
P1T1LC	L-C	25	0.537	10.42	-1.17	3169.4	2850.9	602	634	1202.3	0.7043	416.5	Unaged	
P1B6LC	L-C	25	0.523	3.07	+0.81	1288.6	1219.0	332	359	1021.8	0.5218	458.1	350	10000
P1T6LC	L-C	25	0.525	13.79	-1.21	1181.9	1115.8	383	391	948.3	0.5999	458.1	350	10000
P1B5LC	L-C	25	0.535	14.13	-1.78	285.4	224.9	218	258	459.1	0.5932	481.8	400	10000
P1T4LC	L-C	25	0.558	12.22	-0.47	222.8	190.9	182	199	384.2	0.5689	481.8	400	10000
P1B3CL	C-L	23	0.526	12.53	-2.26	1307.3	1243.3	435	442	944.6	0.5909	413.8	Unaged	
P1T8CL	C-L	25	0.519	13.07	-0.83	[illegible]	202.2	397	470	609.8	0.7190	439.8	350	10000
P1B2LC	L-C	288	0.522	14.84	-2.05	886.6	831.2	529	561	668.0	0.5638	295.8	Unaged	
P1T2LC	L-C	288	0.533	14.45	-2.08	1131.3	924.1	568	667	745.7	0.5744	295.8	Unaged	
P1B7LC	L-C	288	0.527	9.63	-2.44	538.3	523.5	404	396	536.8	0.5366	315.8	350	10000
P1T7LC	L-C	288	[illegible]	14.10	-1.74	831.4	777.9	453	465	[illegible]	0.5354	315.8	350	10000
P1T5LC	L-C	288	0.513	13.47	-0.99	416.5	422.1	350	330	469.8	0.5261	324.2	400	10000

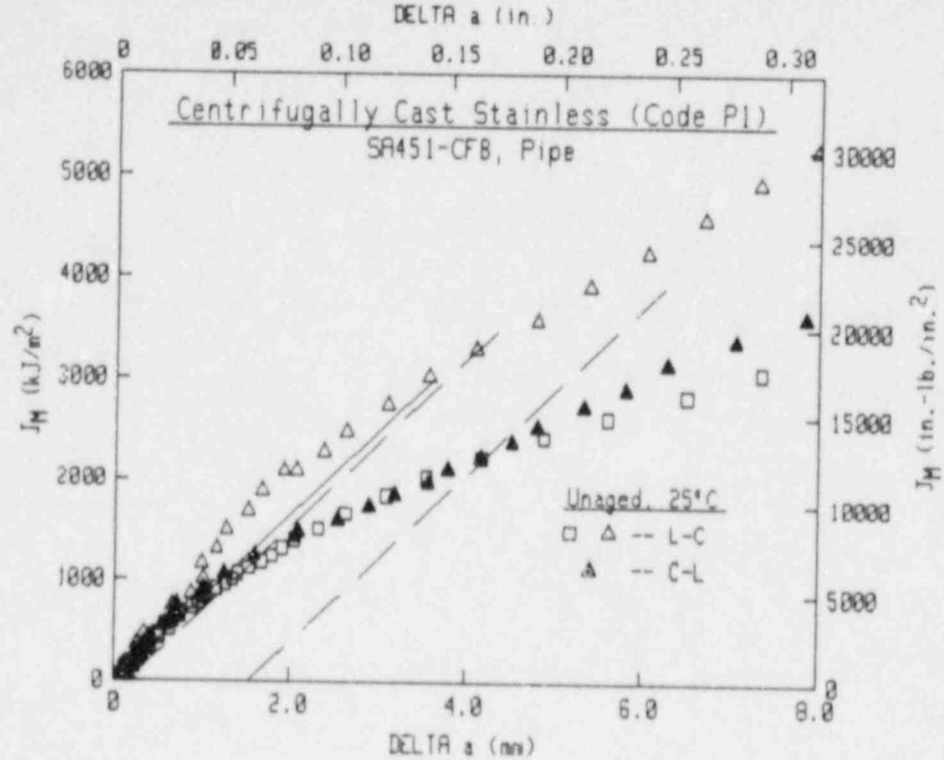

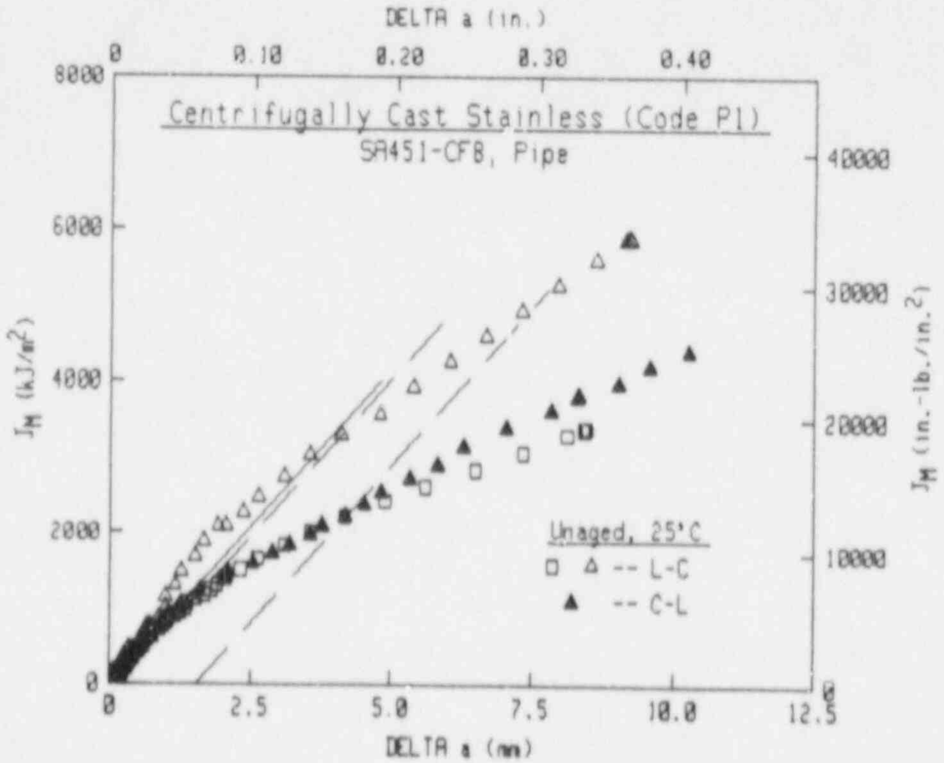

Fig. 40 For Heat P1 (grade CF8) at 25°C, the L-C orientation has substantial variability, whereby the pipe outside diameter (open triangles) demonstrates higher toughness than the pipe inside diameter (open squares). The lone curve for the C-L orientation, from the pipe inside diameter, is consistent with the L-C data from the pipe inside diameter.

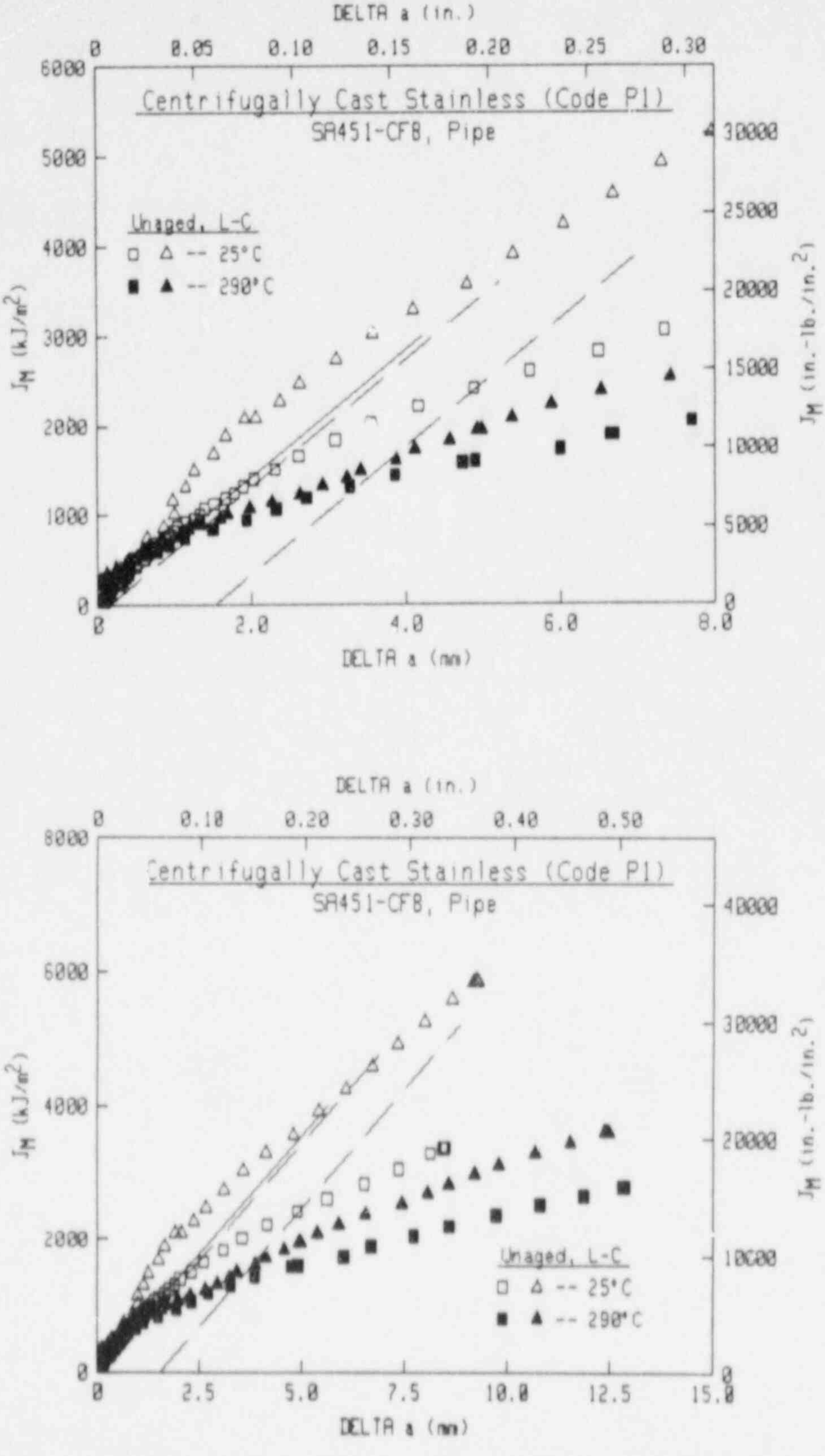

Fig. 41 For the L-C orientation of Heat P1 (grade CF8), increasing the test temperature results in reduced J_M-R curve levels. As at 25°C, the highest curve at 290°C is for material from the pipe outside diameter, although the differences are less than those at 25°C.

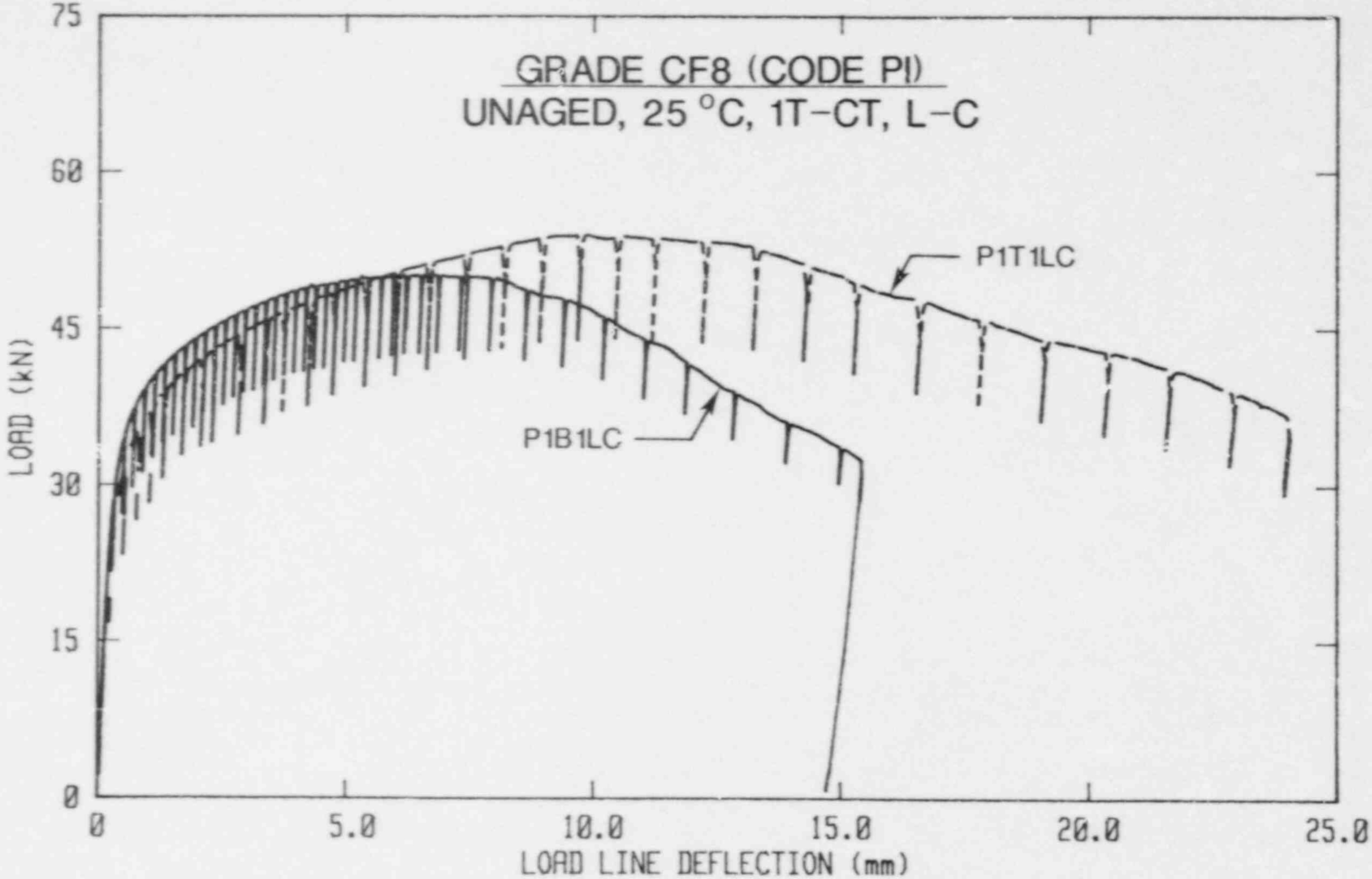

Fig. 42 Load-deflection curves for the J-R curves at 25°C in Fig. 40. The large differences in J-R curve levels are easily understood based upon the differences illustrated here.

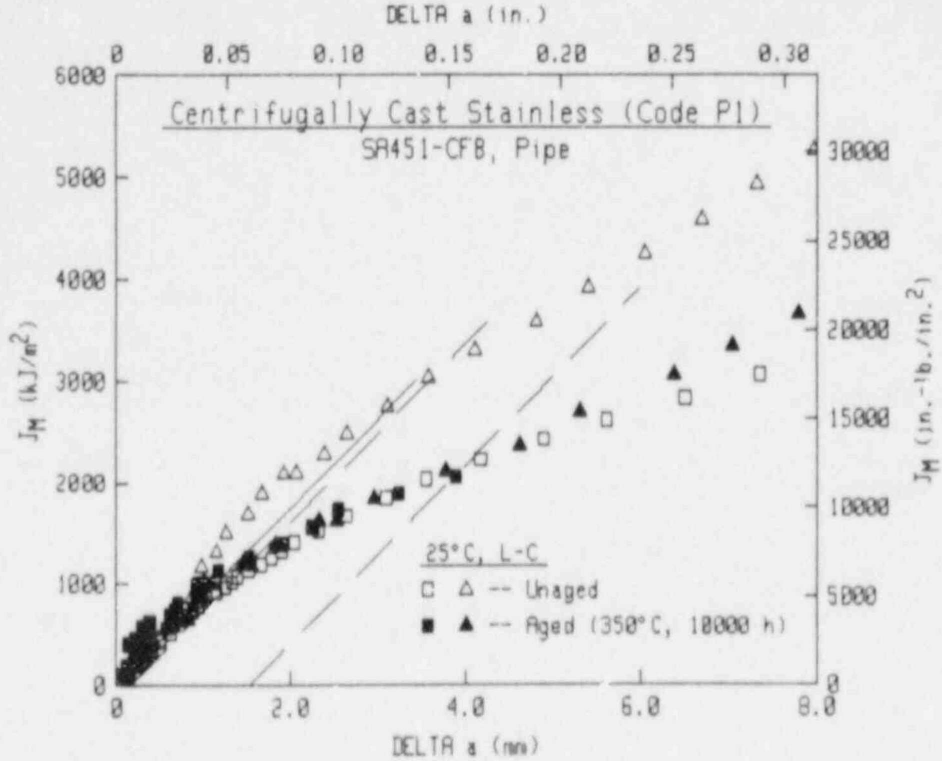

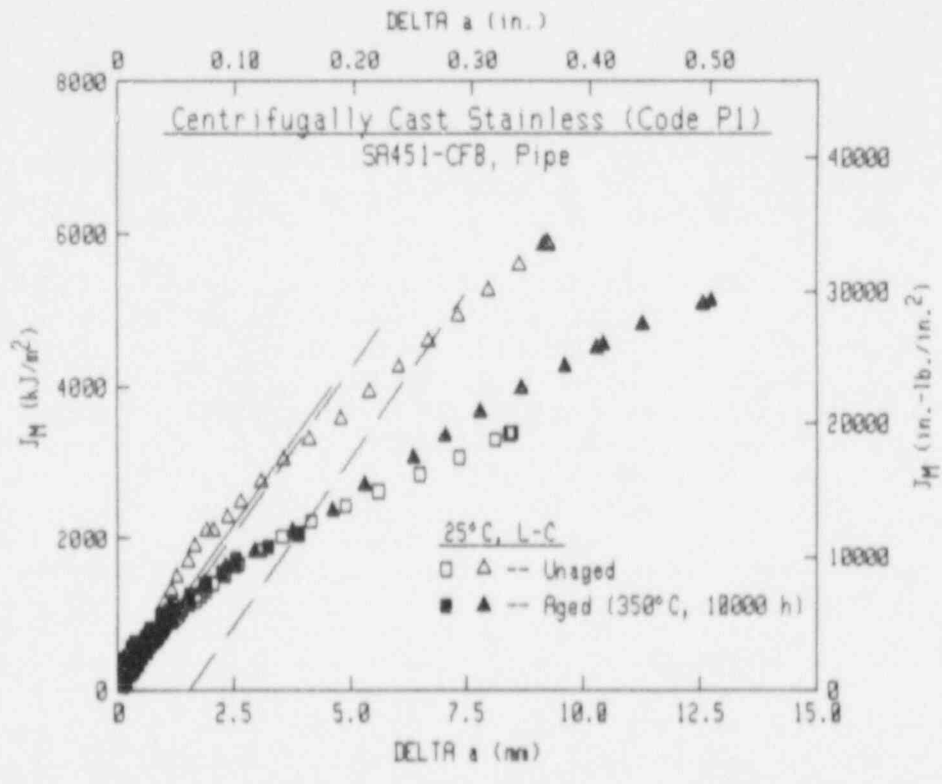

Fig. 43 For the L-C orientation of Heat P1 (grade CF8), both data sets for material thermally-aged at 350°C for 10000 h are consistent with the lower curve for unaged material. For the aged condition, specimens from the pipe inside and outside diameter were tested. Data for the latter end at ~ 4 mm of Δa, with all data for each aged specimen consistent up to that point.

effects, possibly with a low local ferrite content). Overall then, either moderate embrittlement (data from the O.D.) or no embrittlement (data from the I.D.) results for this heat at 25°C for aging at 350°C for 10000 h.

For the L-C orientation at a test temperature of 290°C (Fig. 44), overall trends after aging at 350°C for 10000 h are similar to those found at 25°C. At 290°C, the data from an aged O.D. specimen does exceed that for an aged I.D. specimen, in similar proportion to that exhibited by data from unaged specimens. As at 25°C, the aged O.D. specimen yields J-R curve trends similar to those for the unaged I.D. specimen. The overall decrease in J level is ~20% for each diameter location.

Thermal-aging at 400°C for 10000 h results in much higher embrittlement than aging at 350°C for 10000 h, as indicated by C_V data (45% reduction) and J-R curve data. In this case, toughness reductions are much larger than reductions in C_V data. At 25°C (Fig. 45), J-R curve data from an aged O.D. specimen is even below that from an aged I.D. specimen. For the O.D. location, the J level decreases by a factor of 4 or 5. For the I.D. location, the J level decreases by a factor of 2. In terms of the load-deflection trends for these specimens (Fig. 46), the aged specimen demonstrated lower maximum loads and, more significantly, much lower deflections at maximum load. In terms of Δa-deflection curves (Fig. 47), the aged specimens exhibit crack growth initiation much before the unaged specimens and a steeper overall trend of crack growth as a function of deflection. From a structural standpoint, these two trends indicate crack growth initiation at lower loads for the aged condition, lower load carrying capacity, and far less deflection "capacity" at maximum load.

At 290°C only an O.D. specimen was aged at 400°C for 10000 h. As illustrated in Fig. 48, the J levels for this aged specimen are ~40% below those for the unaged O.D. specimen.

For material aged at 350°C for 10000 h, comparison of data at 25°C and 290°C (Fig. 49) is consistent with that for unaged material. In this case, the two sets at 25°C indicate no significant bias based upon diameter location, whereas at 290°C the O.D. specimen yields lower J levels. At 25°C, the C-L orientation gives lower J levels at crack growth initiation than the L-C orientation (Fig. 50), but similar tearing resistance.

For material aged at 400°C for 10000 h, the curve at 290°C is consistent with the higher curve at 25°C (Fig. 51). In this case, the higher of the curves at 25°C is from the I.D. Therefore, the two curves from O.D. material indicate a moderate elevation in toughness with increasing test temperature. This trend is unexpected from any other results for this heat or the other heats of cast stainless steel.

As expected, higher aging temperature results in greater embrittlement. At 25°C, specimens aged at 400°C exhibit J levels ~60-70% below those for specimens aged at 350°C (Fig. 52). At 290°C (Fig. 53), only

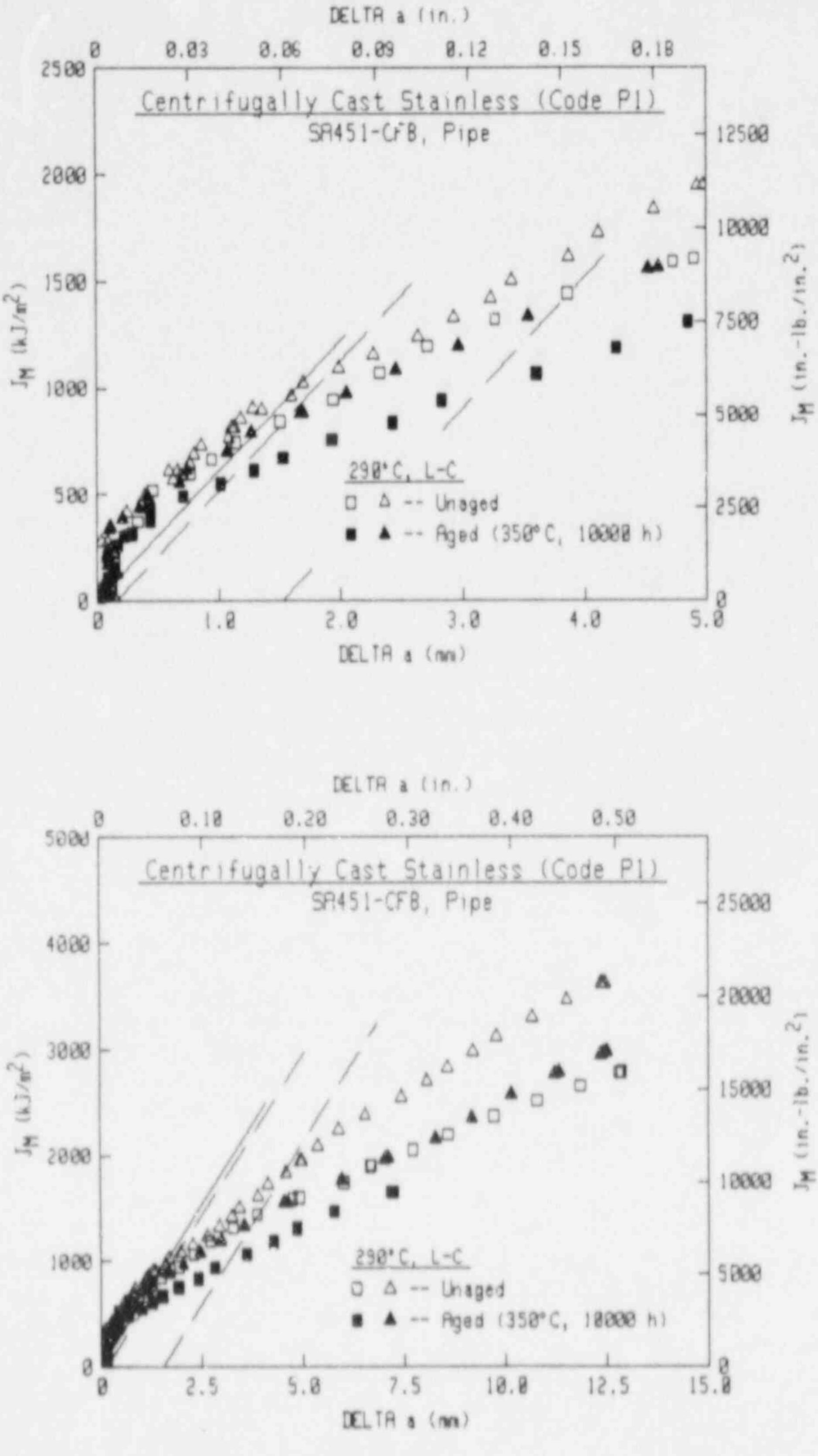

Fig. 44 For the L-C orientation of Heat P1 (grade CF8) tested at 290°C, two specimens thermally-aged at 350°C for 10000 h demonstrate the diameter location bias observed for unaged specimens.

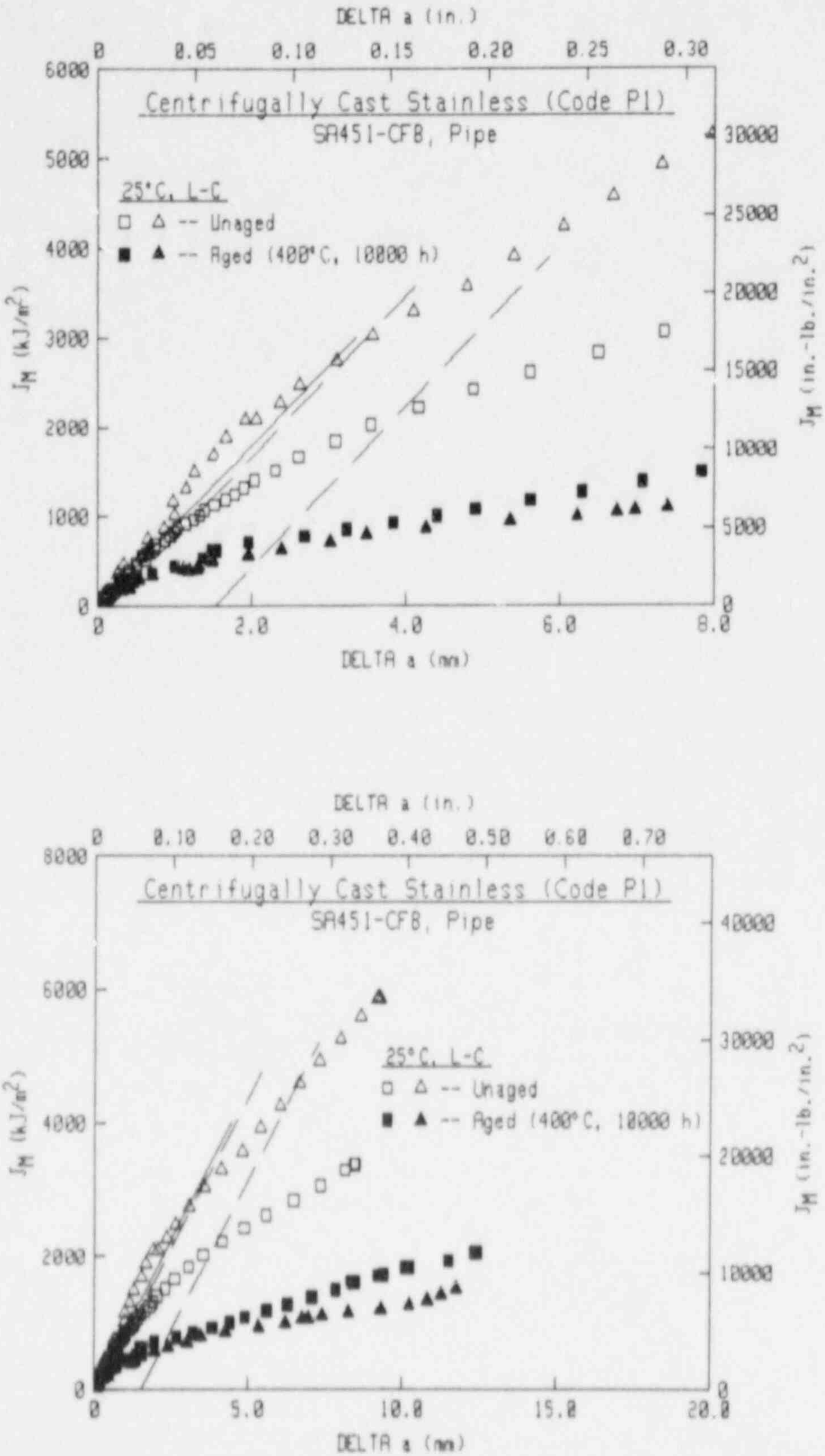

Fig. 45 With thermal-aging at 400°C for 10000 h, large reductions in J_M-R curve level are apparent for the L-C orientation of Heat P1 (grade CF8) at 25°C.

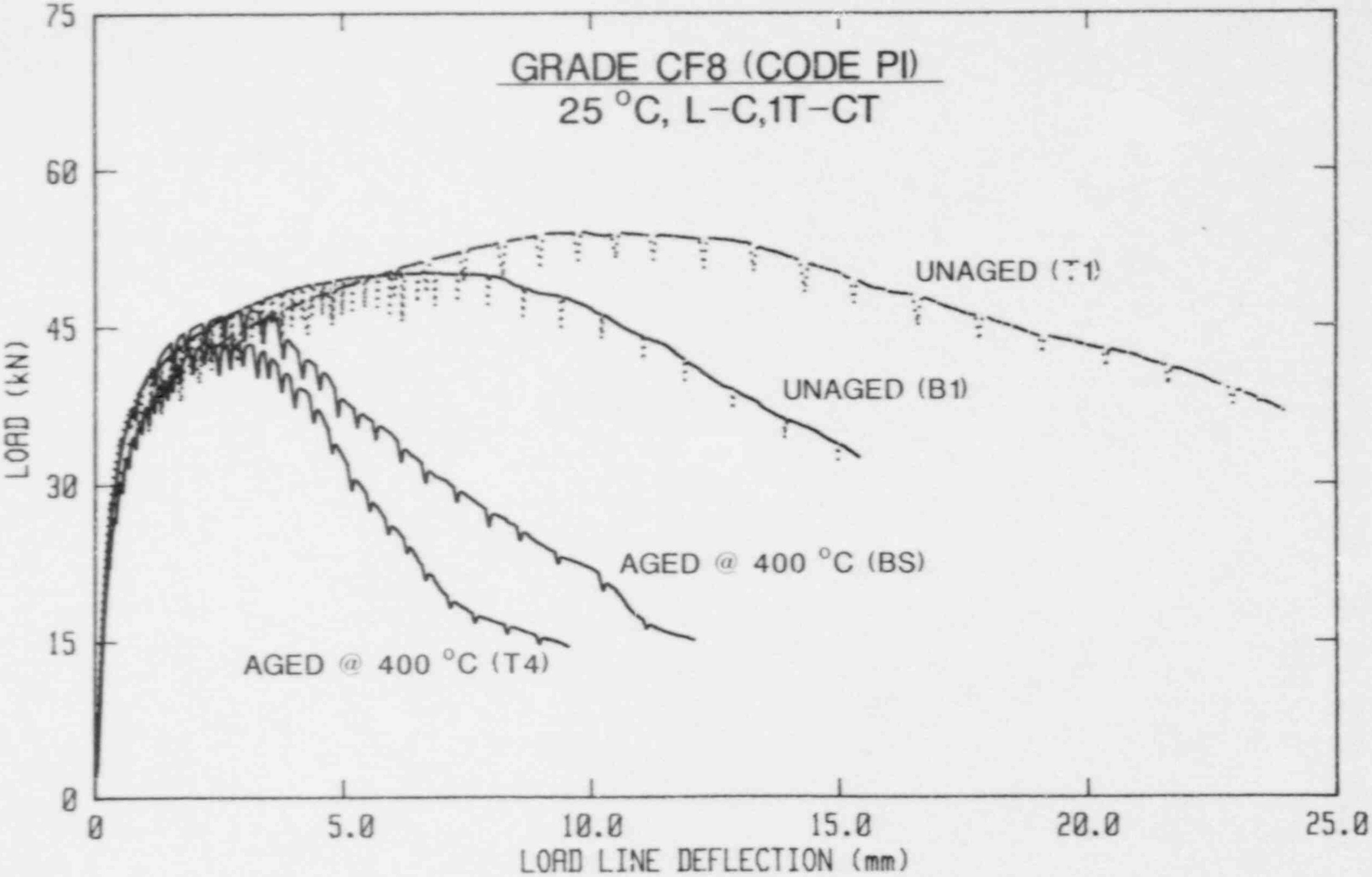

Fig. 46 Load-deflection curves for the J-R curves illustrated in Fig. 45. Data for the aged condition exhibit much lower deflection at maximum load and poor load retention thereafter.

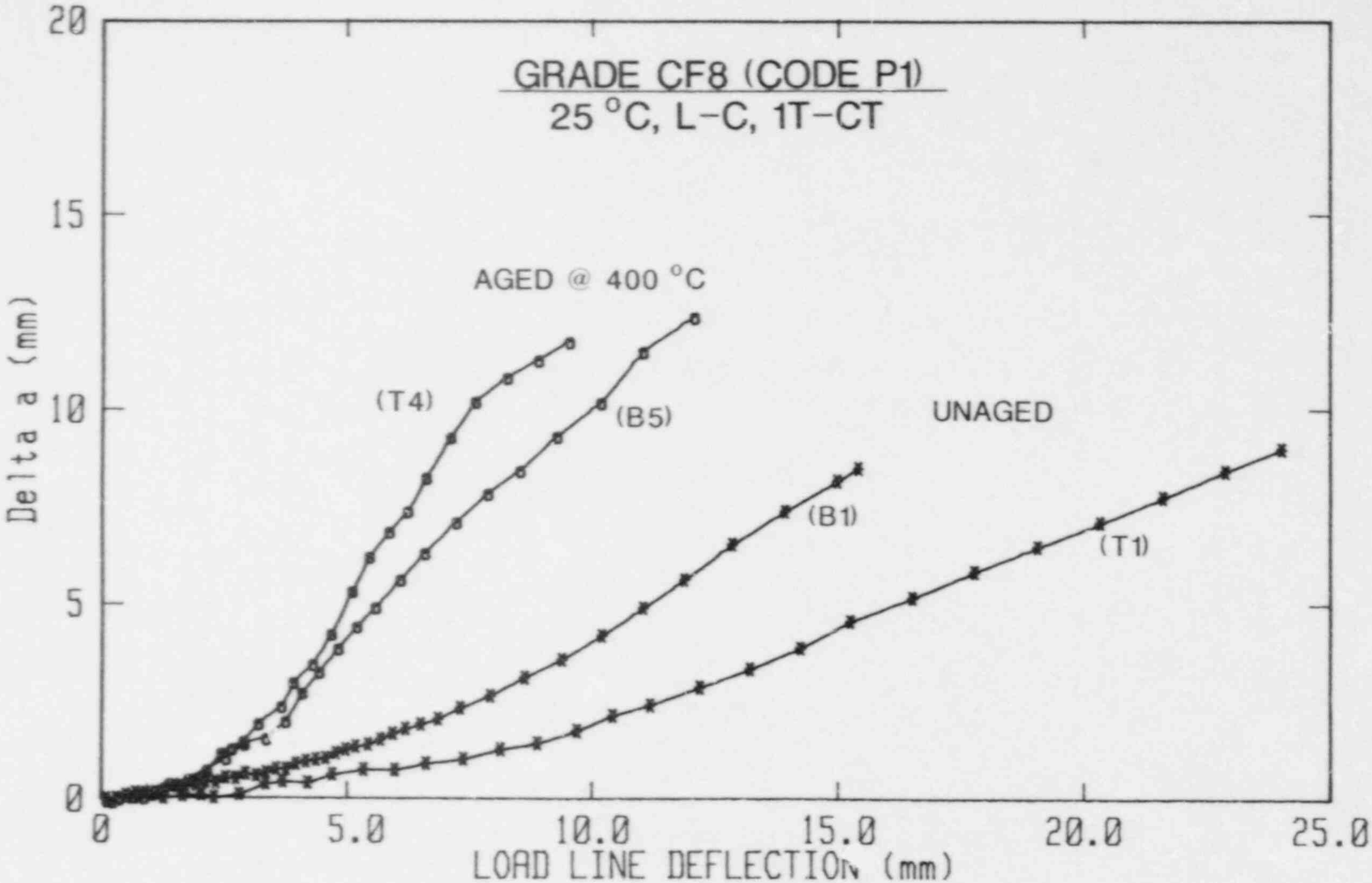

Fig. 47 Crack growth (Δa)-deflection curves for those tests illustrated in Fig. 45. The aged condition exhibits greater crack growth at lower deflection.

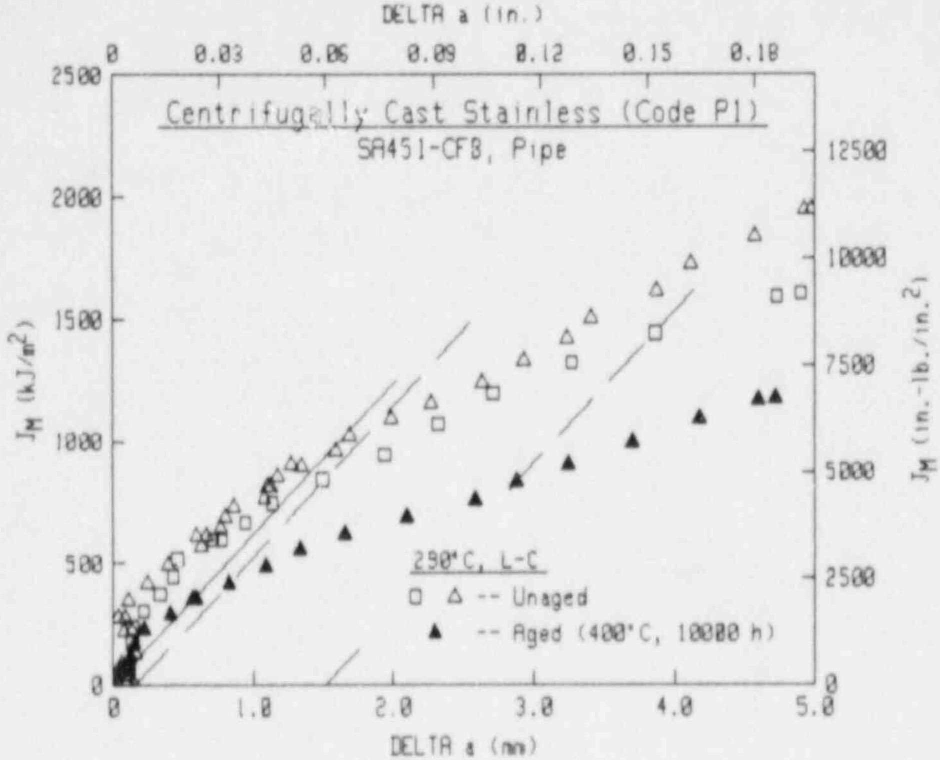

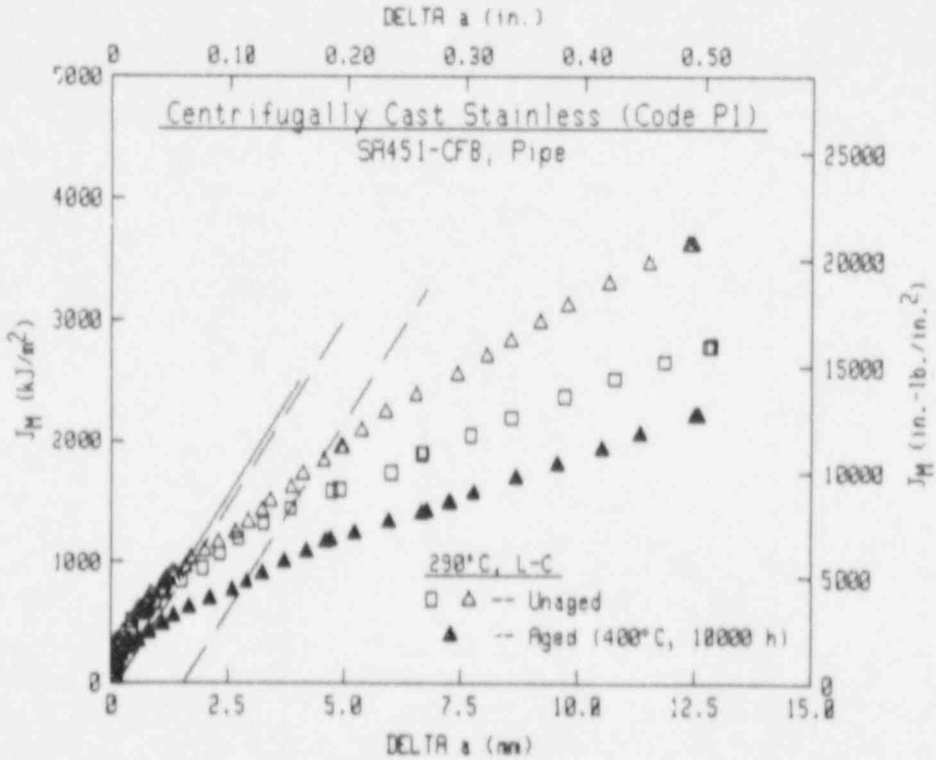

Fig. 48 At a test temperature of 290°C, thermal aging at 400°C for 10000 h results in a moderate reduction of toughness for the L-C orientation of Heat P1 (grade CF8).

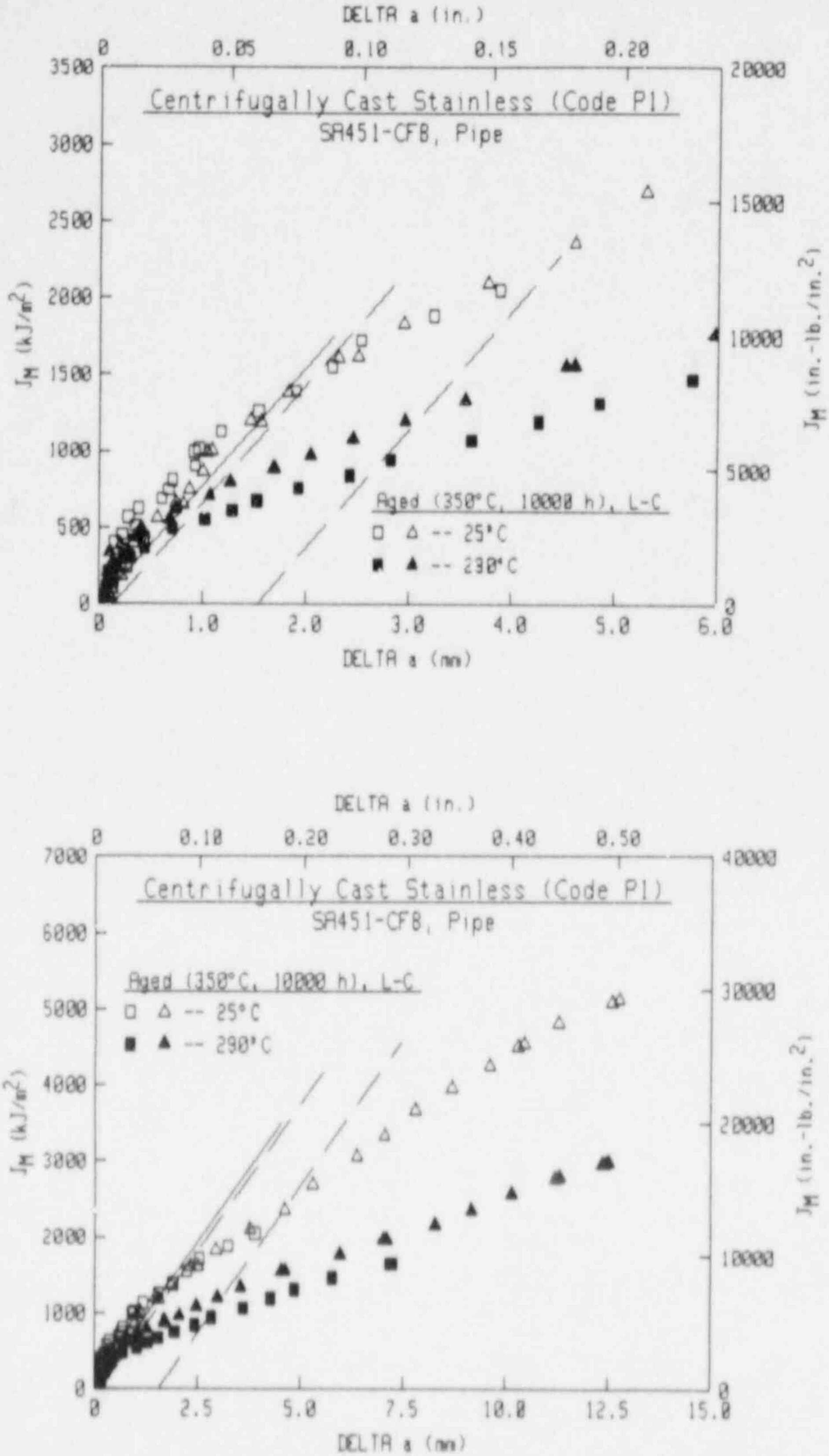

Fig. 49 After thermal-aging at 350°C for 10000 h, increasing the test temperature results in lower J_M-R curves for the L-C orientation of Heat P1 (grade CF8).

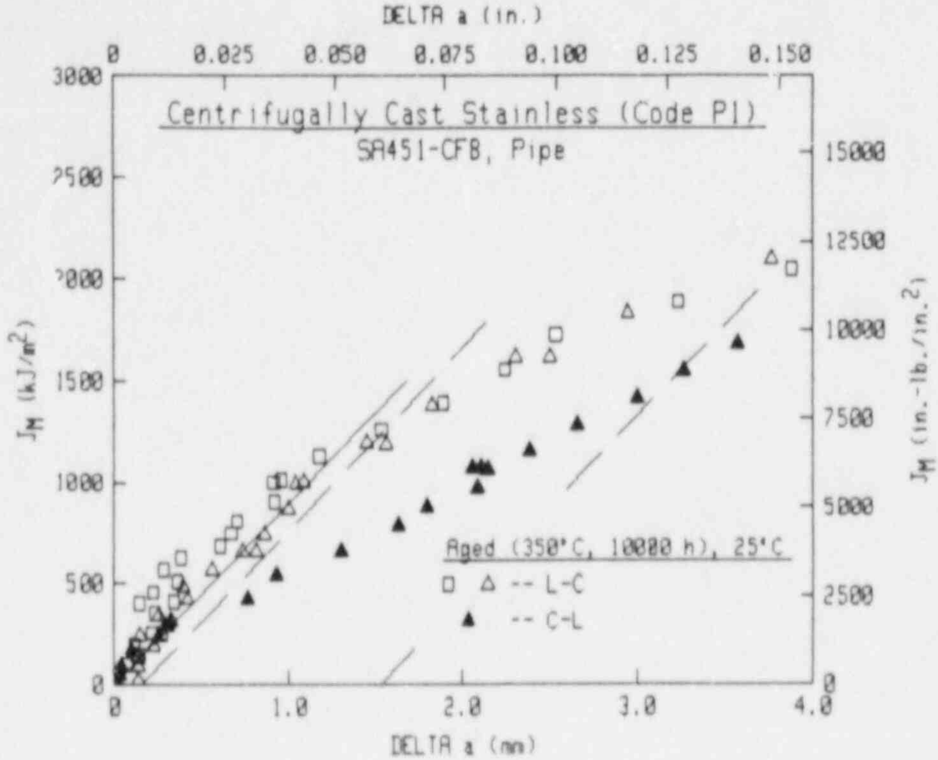

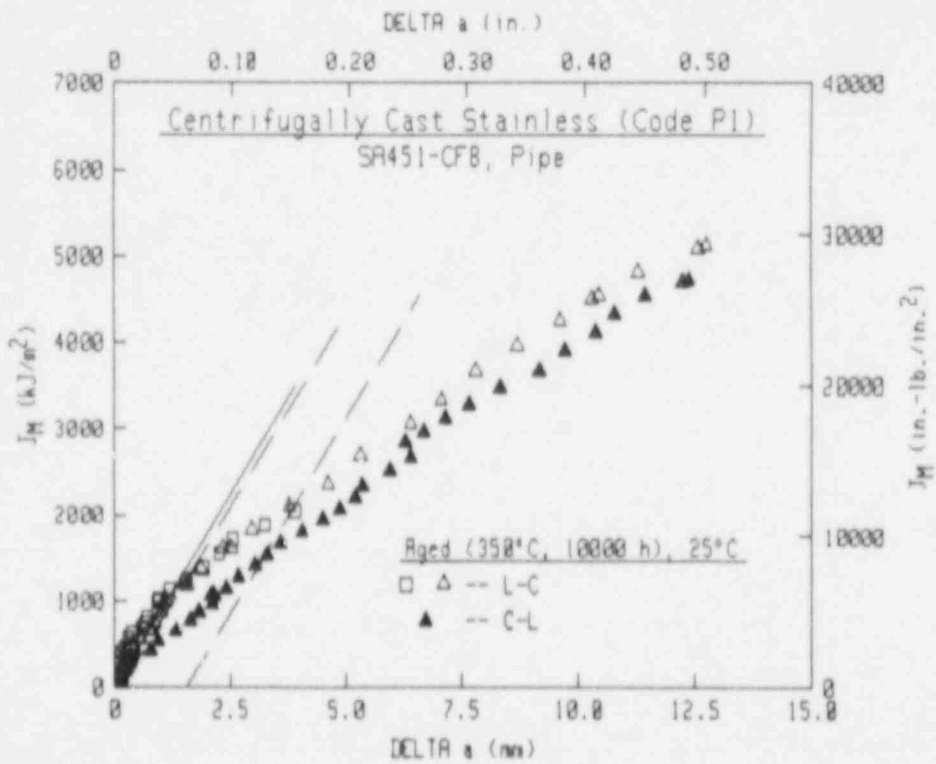

Fig. 50 After thermal aging at 350°C for 10000 h, the C-L orientation of Heat P1 (grade CF8) exhibits lower J levels at crack growth initiation than does the L-C orientation, but similar tearing resistance.

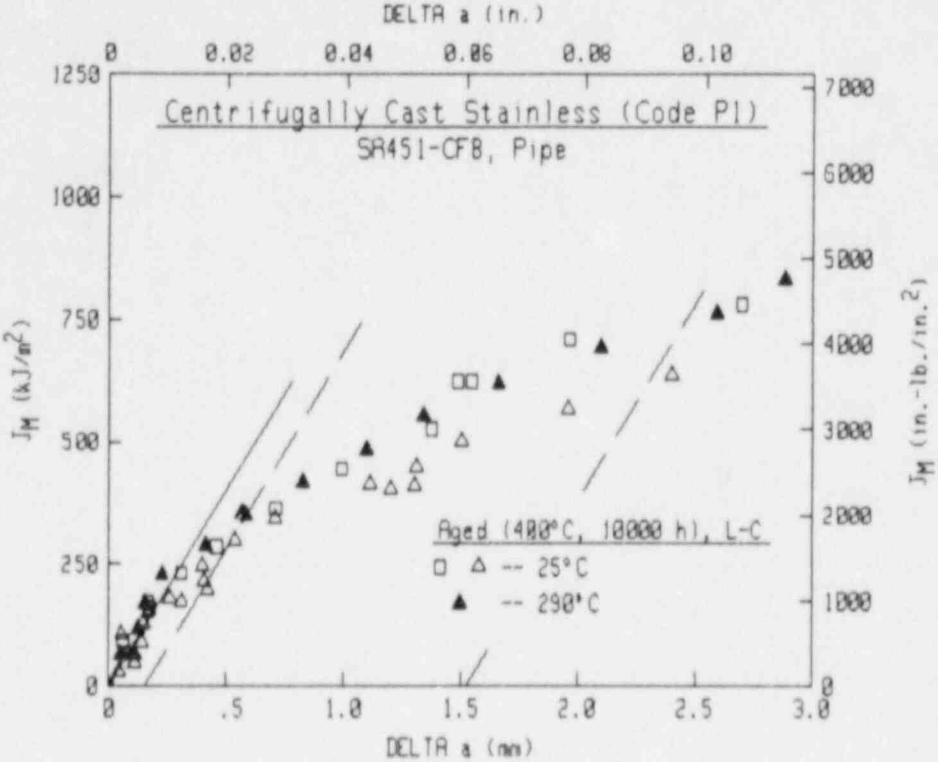

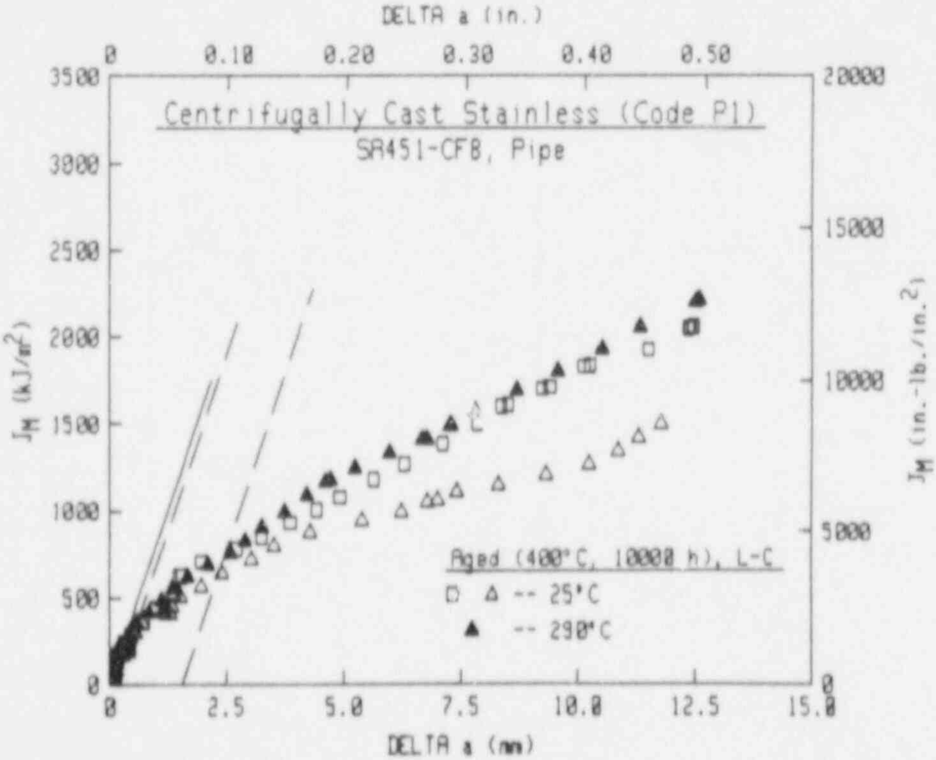

Fig. 51 After thermal-aging at 400°C for 10000 h, increasing the test temperature results in some increase in J_M-R curve levels for the L-C orientation of Heat P1 (grade CF8).

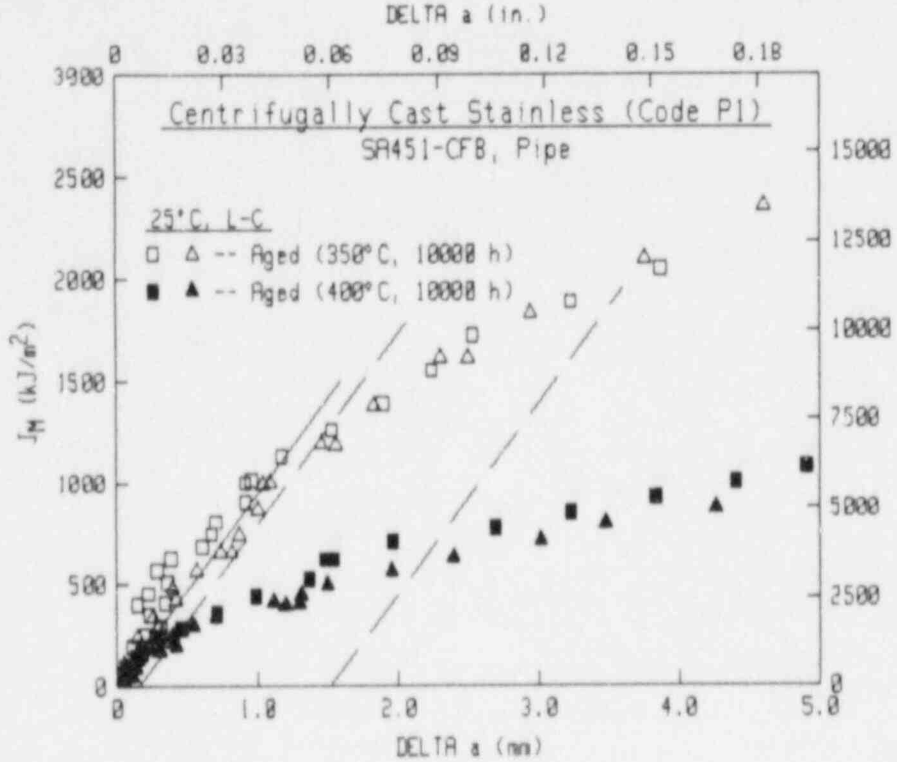

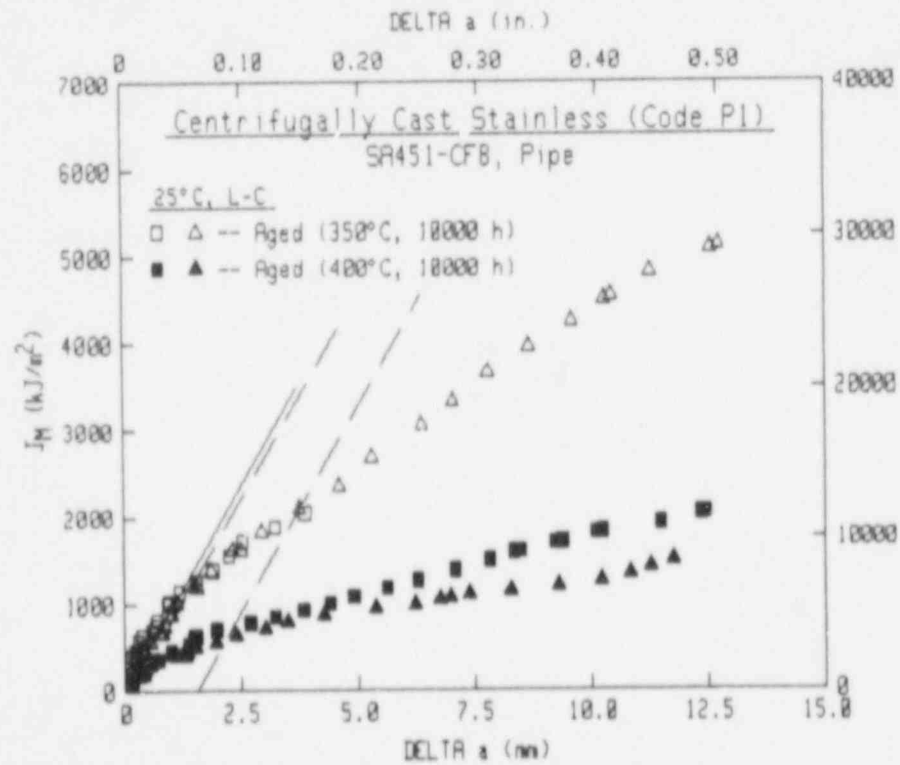

Fig. 52 For the L-C orientation of Heat P1 (grade CF8) at 25°C, higher thermal-aging temperature (400°C vs. 350°C) results in significant (~65%) decreases in J_M-R curve levels.

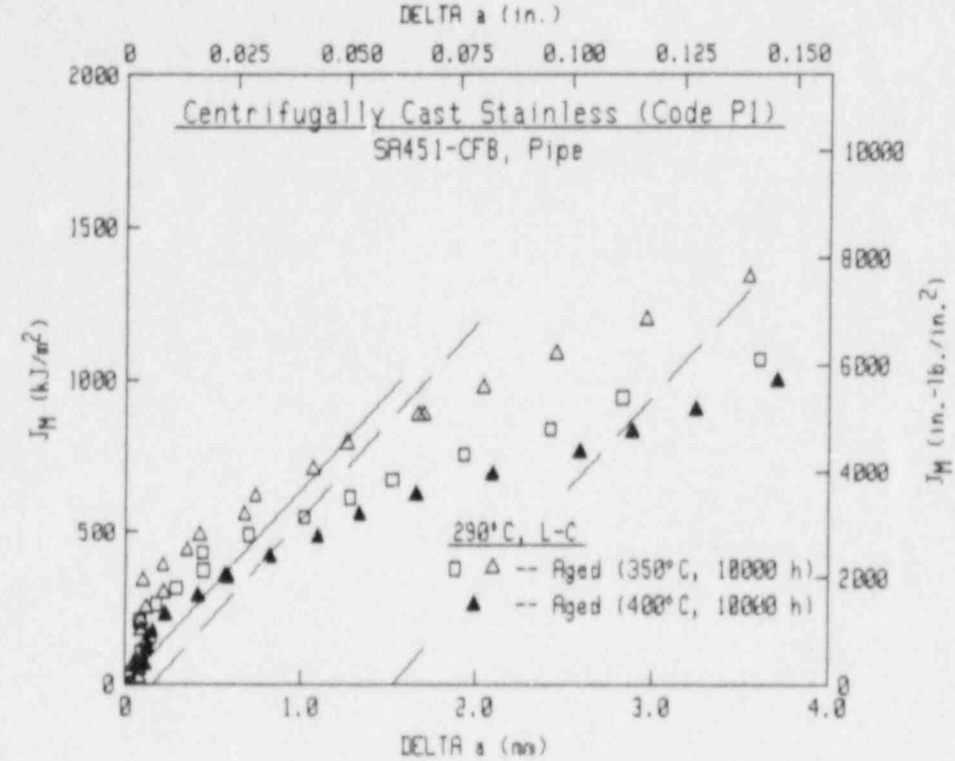

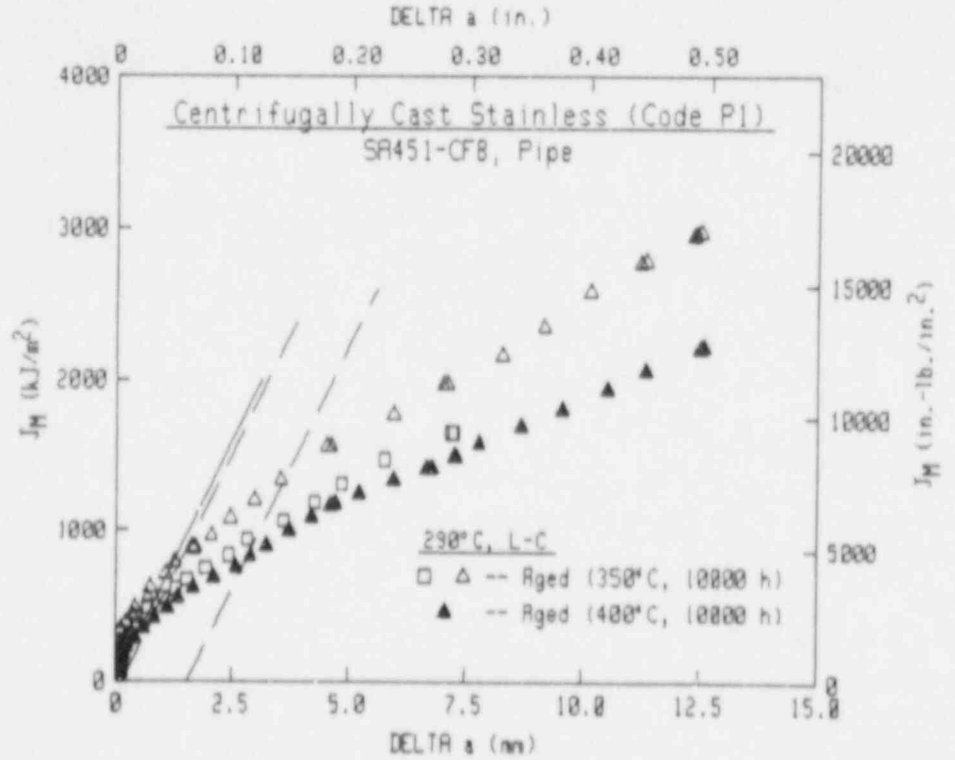

Fig. 53 At a test temperature of 290°C, higher thermal-aging temperature results in only a small decrease in J_M-R curve levels.

small differences in J levels are evident for specimens aged at the two temperatures. In this case, the specimen aged at 400°C is from the pipe O.D.; data from this specimen are just below those for an I.D. specimen aged at 350°C, and ~30% below that for an O.D. specimen aged at 350°C.

5.2.5 Heat P2 (CF3)

J-R curve results for this heat are summarized in Table 22. For the unaged material of this heat, no J-R curve data cross the ASTM E 813 blunting line, in spite of the large crack advance obvious in the J-R curves and on the fracture surfaces. As illustrated at 25°C (Fig. 54), both the L-C and C-L orientation yield similar J-R curve trends.

With increasing test temperature for the L-C orientation (Fig. 55), the J levels are ~30% lower for data from 290°C tests as compared to data from 25°C tests. Some differences are apparent here based upon location in the original pipe, as the I.D. location yields slightly higher J-R curves at each temperature in this case. This is in contrast to Heat P1, where the O.D. location gave higher J-R curve levels.

With aging at 350°C for 3000 h, no significant effect on J-R curve levels are apparent at 25°C (Fig. 56) or 290°C (Fig. 57) consistent with the small reduction in C_v level for this aging condition (~ 5%). At 25°C, O.D. and I.D. specimens were tested in the unaged and the aged condition. In each case, the only apparent change in J level is a small increase. At 290°C, data from the aged specimen, from the pipe O.D., is slightly higher than that from the unaged specimen from the pipe O.D..

With aging at 350°C for 10000 h, J-R curve data at 25°C are consistent with that from unaged specimens up to ~3.5 mm, with some reduction in toughness thereafter (Fig. 58). In this case, both aged specimens are from the pipe O.D., whereas the higher curve for unaged material is from the pipe I.D. and data from the O.D. terminates at ~3 mm of Δa; if the latter curve extended to higher Δa increments, no significant embrittlement may have been evident. Similarly at 290°C (Fig. 59), the data for an aged specimen (from the pipe O.D.) are consistent with that for an unaged specimen from the pipe O.D., but ~15% below that for an unaged specimen from the pipe I.D. Overall, no significant effect of 350°C aging for 10000 h can be discerned for this heat, generally consistent with the reduction in C_v level of 10% for this aging condition.

In contrast to results after aging at 350°C, aging at 400°C for 10000 h results in significant toughness reduction at both test temperatures as indicated by C_v data as well (57% reduction). At 25°C (Fig. 60), both the I.D. and O.D. specimens exhibit J levels reduced by ~40% after thermal-aging. Data from aged specimens demonstrate good agreement between the pipe I.D. and O.D. in this case. At 290°C (Fig. 61), toughness reductions are on the order of 25-35% for the aged O.D. specimen (no aged I.D. specimen was tested). The lower

Table 22 J-R Curve Results for Code P2 (Centrifugally Cast Stainless Steel Pipe, SA451-CF3)

Specimen Number	Orien-tation	Test Temp	$(a/W)_i$	Δa_n	$\Delta a_p-\Delta a_m$	J_{Ic}		T_{avg}		C	n	σ_f	Aging Condition	
						MEA	ASTM	MEA	ASTM				Temp	Time
		(°C)		(mm)	(mm)	(kJ/m²)	(kJ/m²)			(kJ/m²)		(MPa)	(°C)	(h)
P2B1LC	L-C	23	0.541	7.18	-0.93	—	—	—	—	1638.8	0.7194	381.0	Unaged	
P2T1LC	L-C	22	0.539	2.92	+0.26	—	—	—	—	1333.6	0.7984	381.0	Unaged	
P2B3CL	C-L	23	0.538	7.95	-1.03	—	—	—	—	1839.0	0.6124	387.4	Unaged	
P2T6LC	L-C	25	0.719	4.17	-0.86	—	—	—	—	1471.6	0.6988	421.7	350	3000
P2B7LC	L-C	25	0.537	6.45	-0.47	—	—	—	—	1914.0	0.6749	421.7	350	3000
P2T8LC	L-C	25	0.531	10.76	-1.24	4562.1	4430.0	435	450	1885.8	0.5251	436.8	350	10000
P2T10LC	L-C	25	0.531	8.39	+0.14	4793.5	4723.1	468	460	1818.9	0.5600	436.8	350	10000
P2B6LC	L-C	23	0.527	13.04	-1.31	1446.6	1515.0	572	529	910.2	0.7532	426.4	400	10000
P2T4LC	L-C	23	0.528	12.18	-0.92	1755.7	1639.3	544	556	1002.9	0.7051	426.4	400	10000
P2B2LC	L-C	288	0.531	7.97	-1.46	—	—	—	—	1299.3	0.6308	268.5	Unaged	
P2T2LC	L-C	288	0.534	3.98	-0.36	—	—	—	—	900.8	0.7695	268.5	Unaged	
P2T7LC	L-C	288	0.525	9.50	-1.14	3834.7	3703.7	602	665	1456.1	0.5048	288.2	350	3000
P2T9LC	L-C	290	0.529	10.47	-2.03	3627.2	3445.3	767	769	1100.0	0.6385	286.8	350	10000
P2T5LC	L-C	288	0.515	13.63	-1.78	1771.4	1718.6	681	679	859.0	0.6184	288.6	400	10000

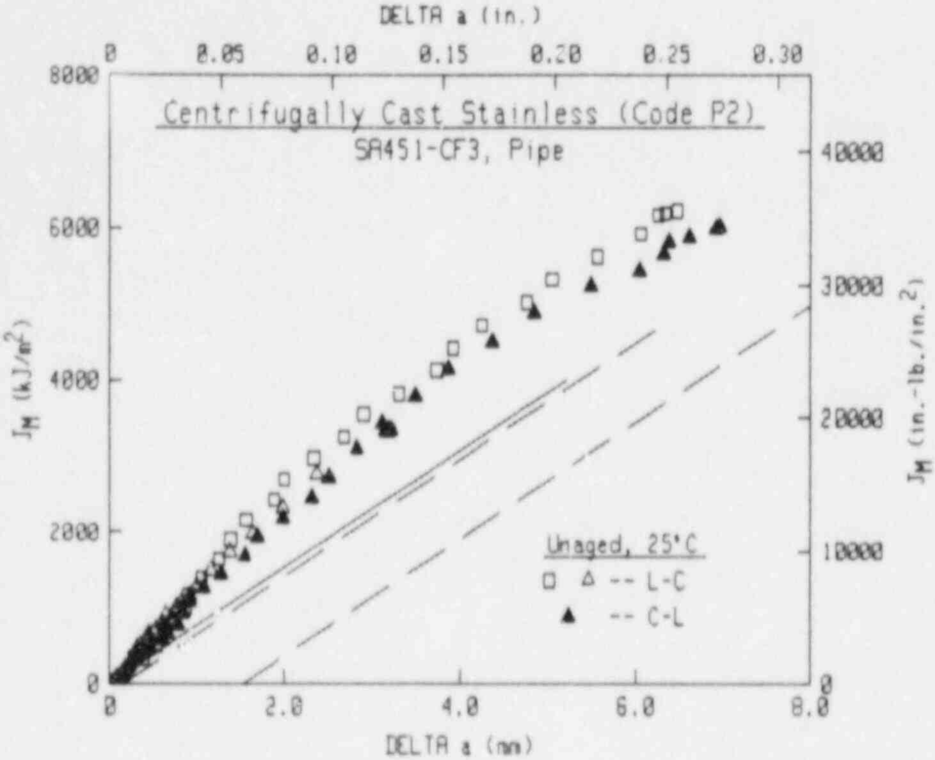

Fig. 54 As with three of the other four commercial heats, Heat P2 (grade CF3) demonstrates orientation independance for the L-C and C-L orientations at 25°C.

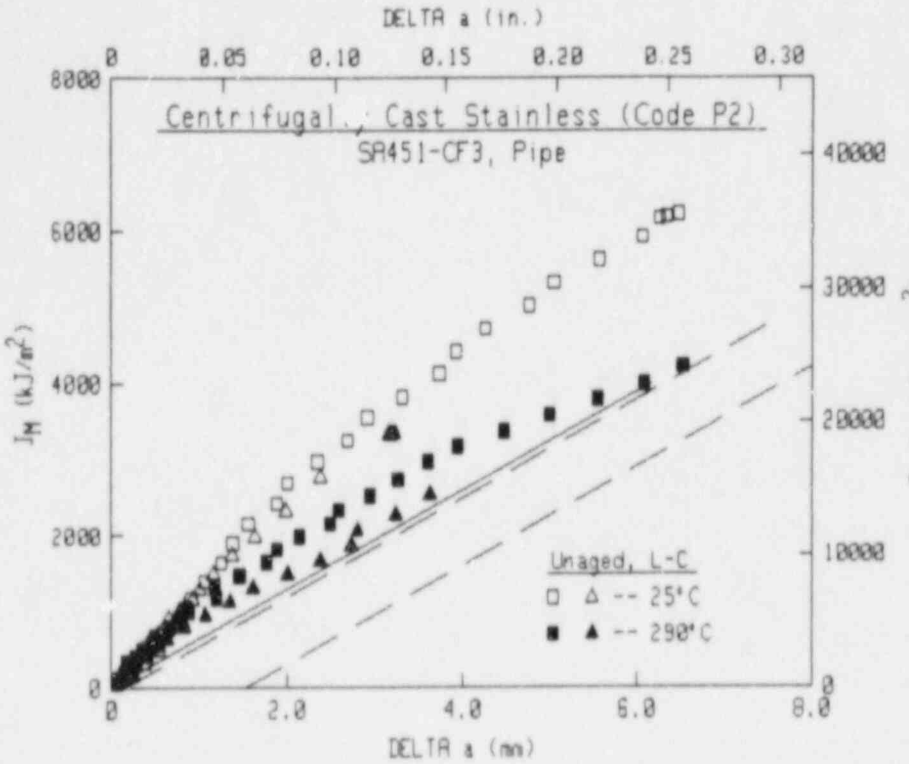

Fig. 55 As with the other commercial heats, increasing the test temperature results in lower J_M-R curve trends for the L-C orientation of Heat P2 (grade CF3).

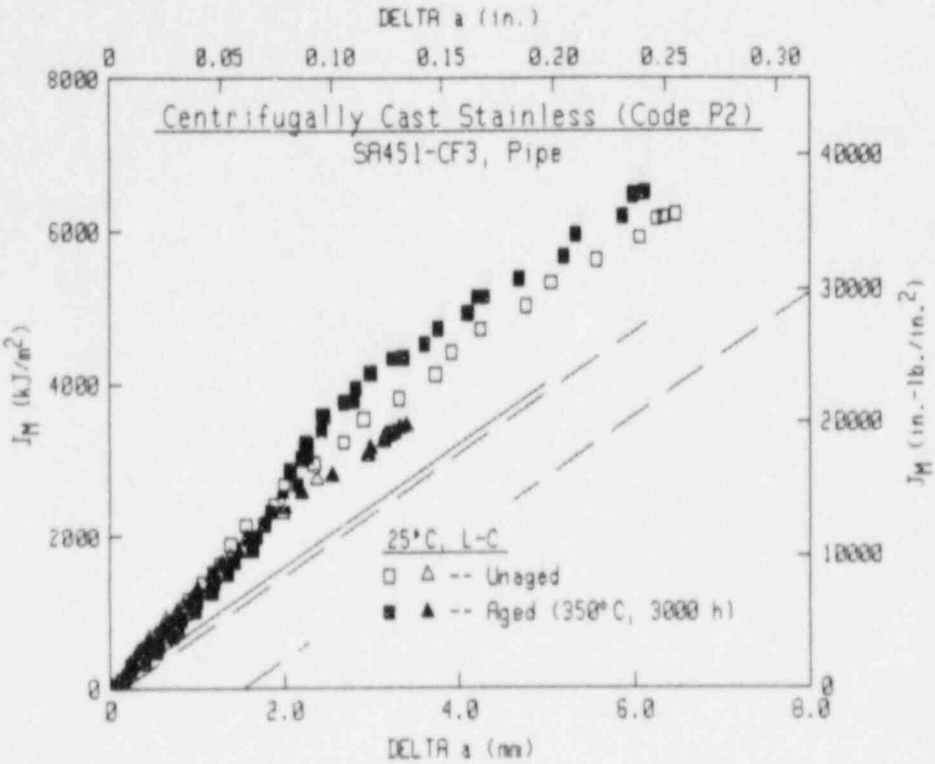

Fig. 56 For Heat P2 (grade CF3) at 25°C, thermal-aging at 350°C for 3000 h does not change the J_M-R curve levels from those for the unaged condition.

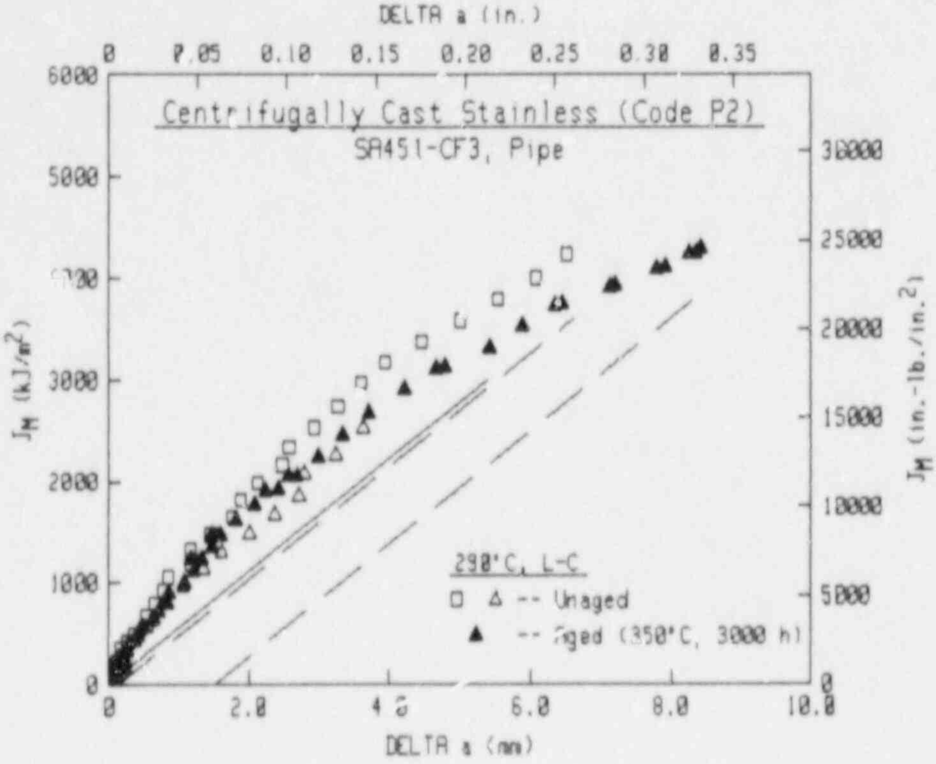

Fig. 57 For Heat P2 (grade CF3) at 290°C, thermal-aging at 350°C for 3000 h does not significantly change the J_M-R curve levels from those for the unaged condition.

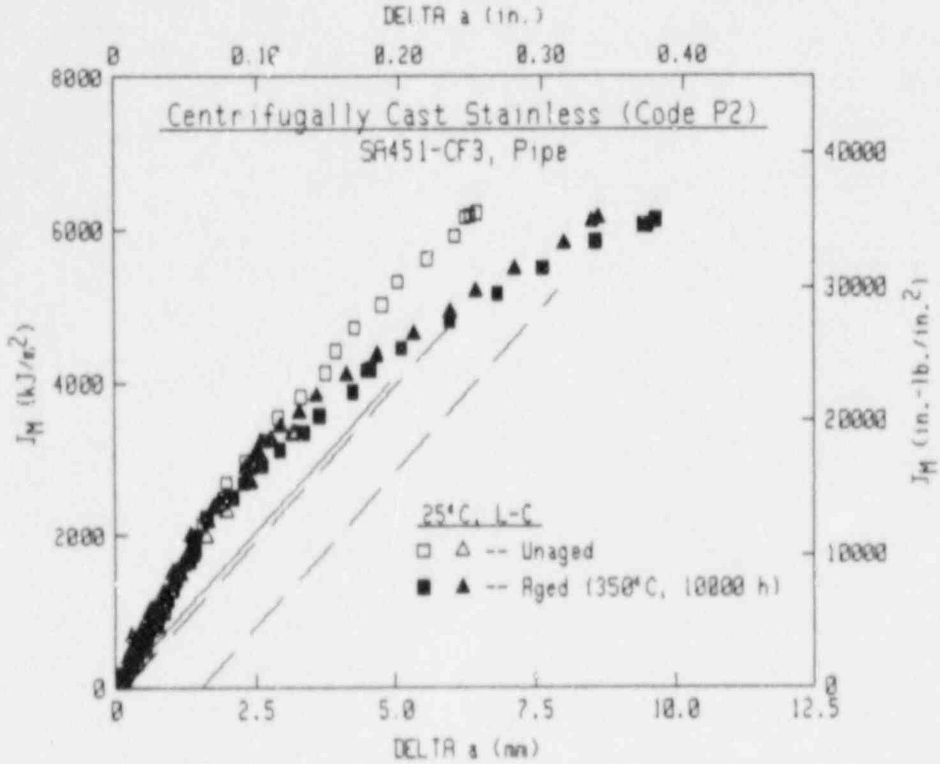

Fig. 58 For Heat P2 (grade CF3) at 25°C, thermal-aging for 10000 h at 350°C results in minimal reductions in J_M-R curve levels from those for the unaged condition.

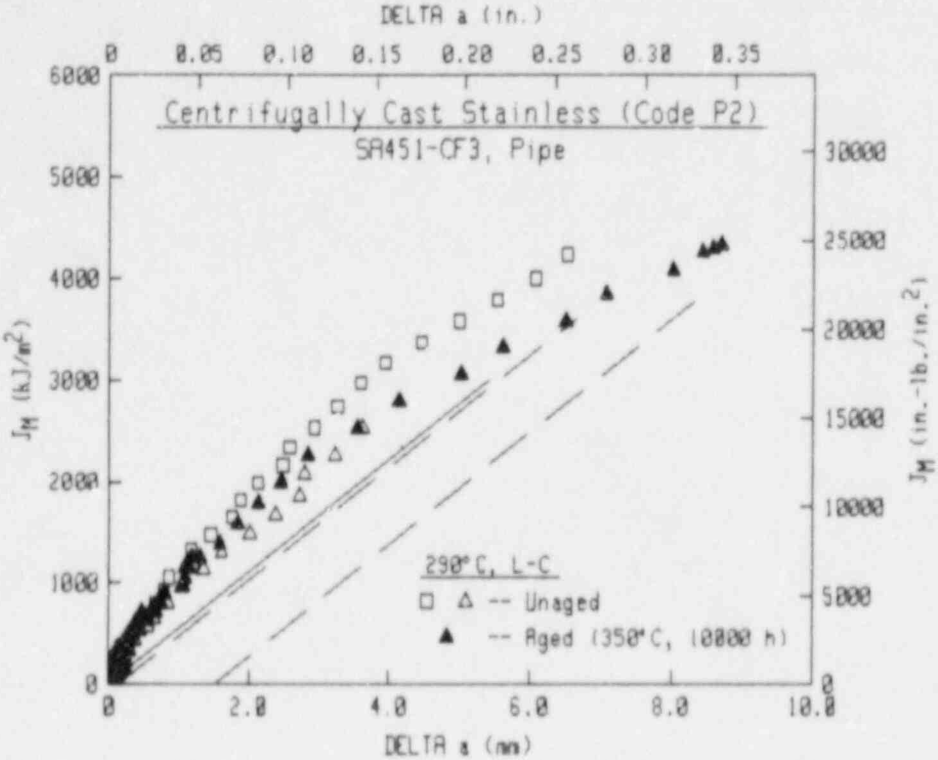

Fig. 59 For Heat P2 (grade CF3) at 290°C, thermal-aging for 10000 h at 350°C results in minimal reductions in J_M-R curve levels from those for the unaged condition.

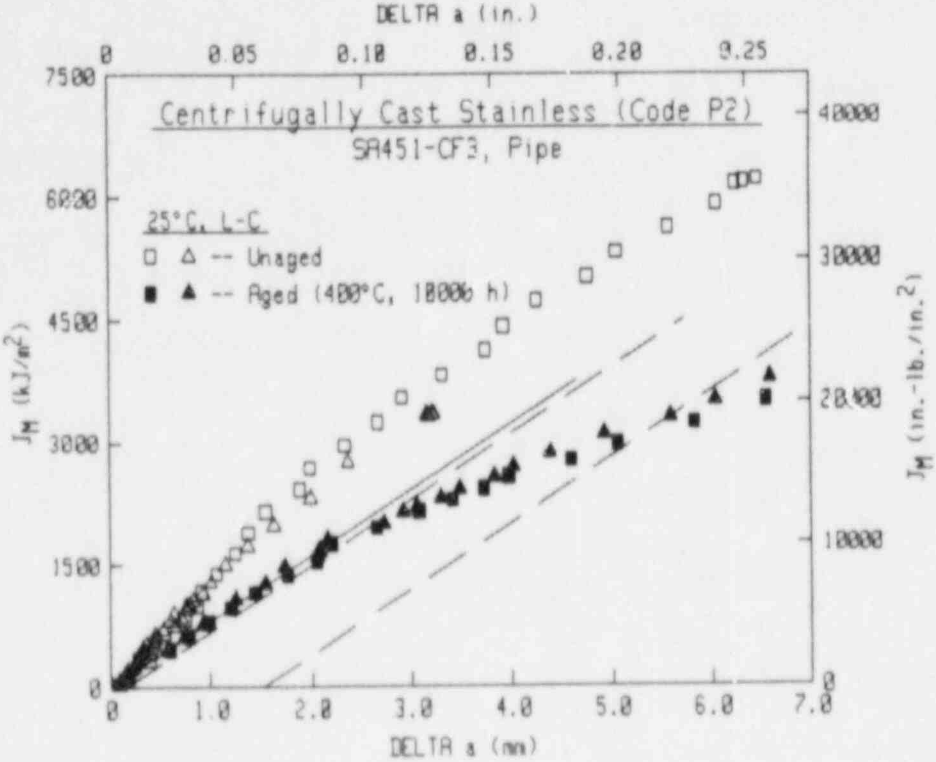

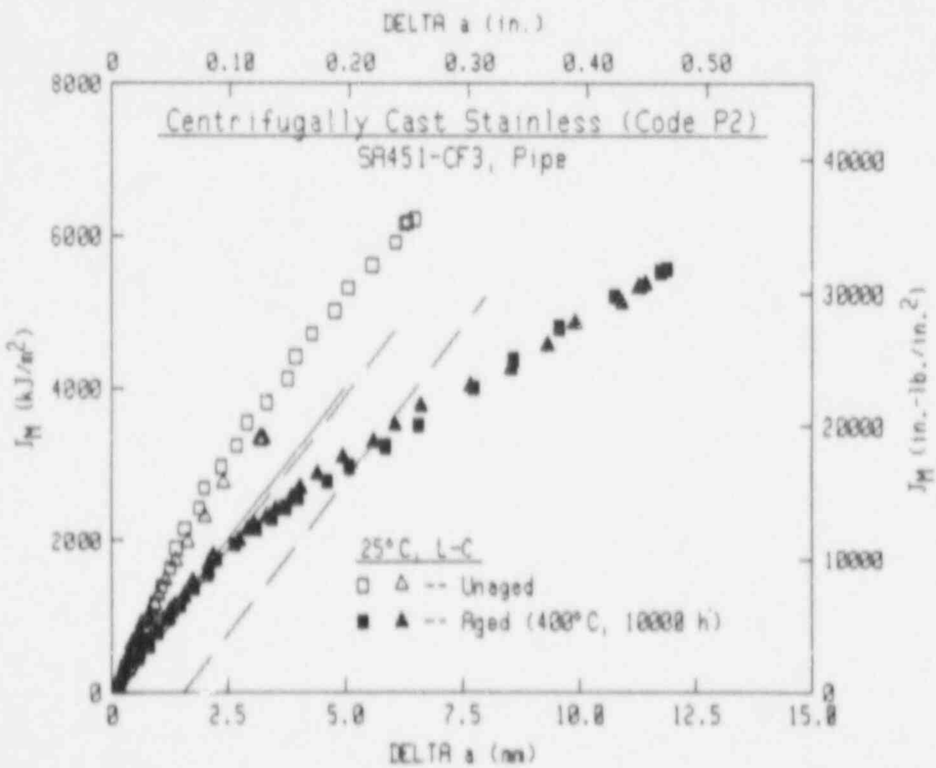

Fig. 60 For Heat P2 (grade CF3) at 25°C, thermal-aging at 400°C for 10000 h results in significant toughness reductions in comparison to trends for the unaged condition.

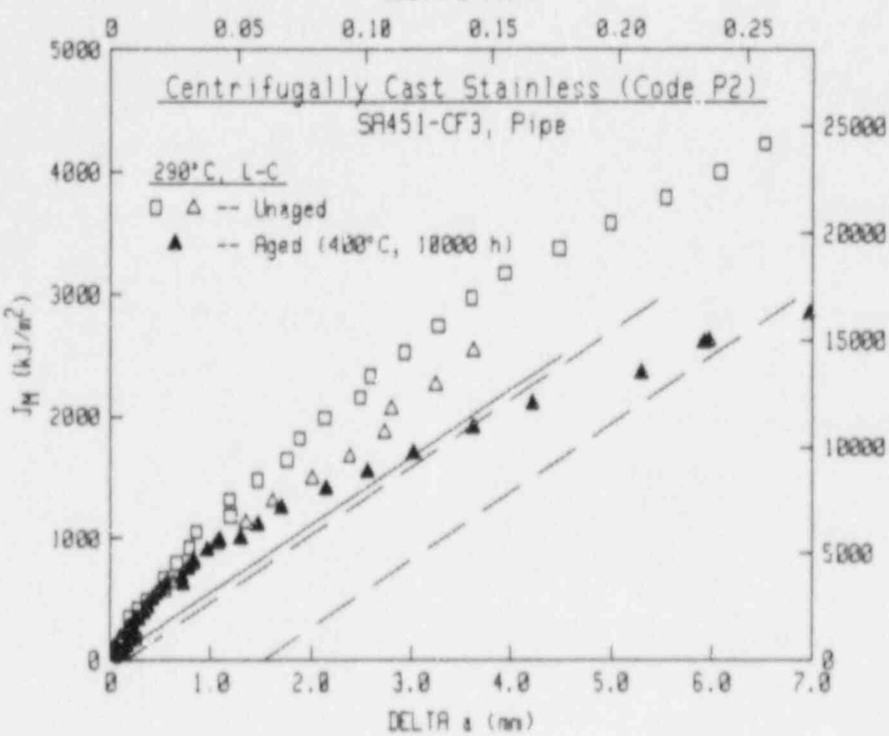

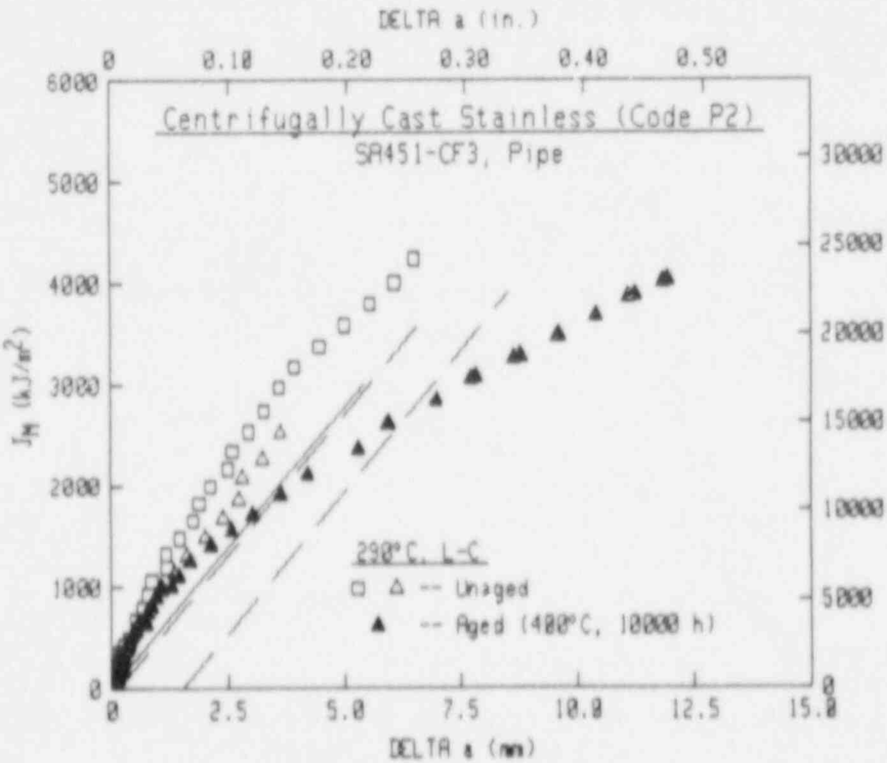

Fig. 61 For Heat P2 (grade CF3) at 290°C, thermal-aging at 400°C for 10000 h results in moderate toughness reductions in comparison to trends for the unaged condition.

reduction is referenced to data from an O.D. unaged specimen and the higher reduction is referenced to data from an I.D. unaged specimen.

For the aged specimens, increasing the test temperature results in reduced J-R curve trends in all three cases. Referencing the data at 290°C to data from the pipe O.D. (since all 290°C tests were with O.D. specimens), reductions in J level range from ~25-30% for aging at 350°C for 3000 h (Fig. 62), ~30% for aging at 350°C for 10000 h (Fig. 63), and ~25% for aging at 400°C for 10000 h (Fig. 64).

Comparison of data for the three aging conditions indicates the large degradation in J levels due to aging at 400°C. At 25°C (Fig. 65), data for aging at 350°C (from O.D. specimens) indicates no significant degradation with increased aging time from 3000 h to 10000 h. (The higher curve from material aged at 350°C for 3000 h is from the pipe I.D.). Aging at 400°C results in J level reduction of ~30-40% from that for aging at 350°C. At a test temperature of 290°C (Fig. 66), data from specimens aged at 350°C for 3000 h and 10000 h are consistent with one another (both specimens are from the pipe O.D.). Aging at 400°C for 10000 h results in toughness reduced by ~25-30% from that for aging at 350°C.

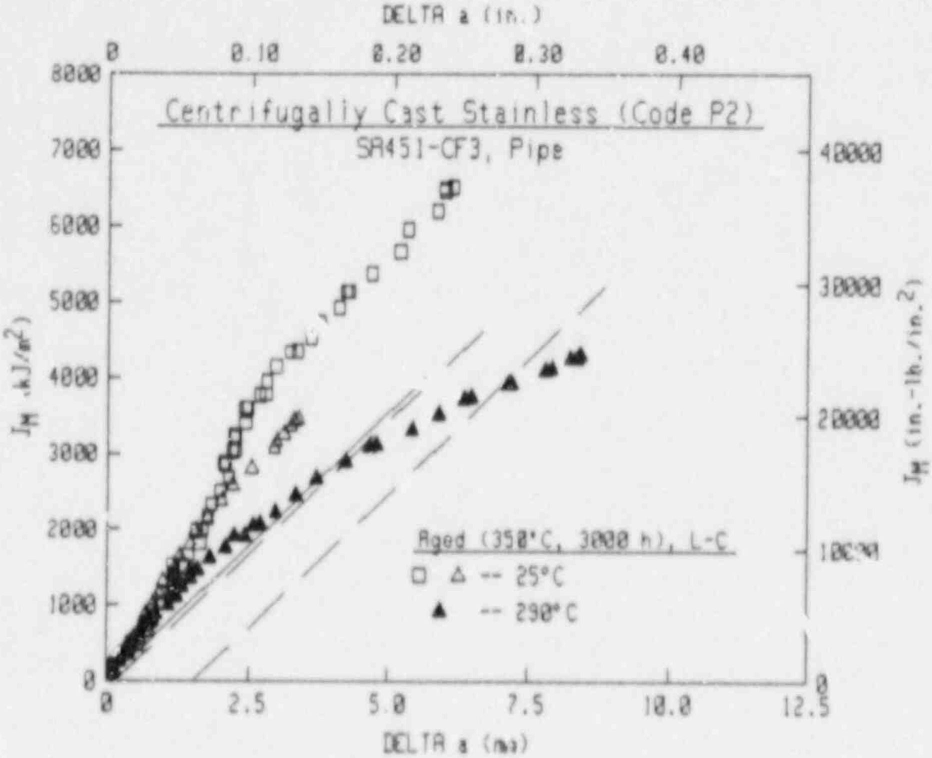

Fig. 62 After thermal-aging of Heat P2 (grade CF3), at 350°C for 3000 h increasing the test temperature results in reduced J_M-R curve levels.

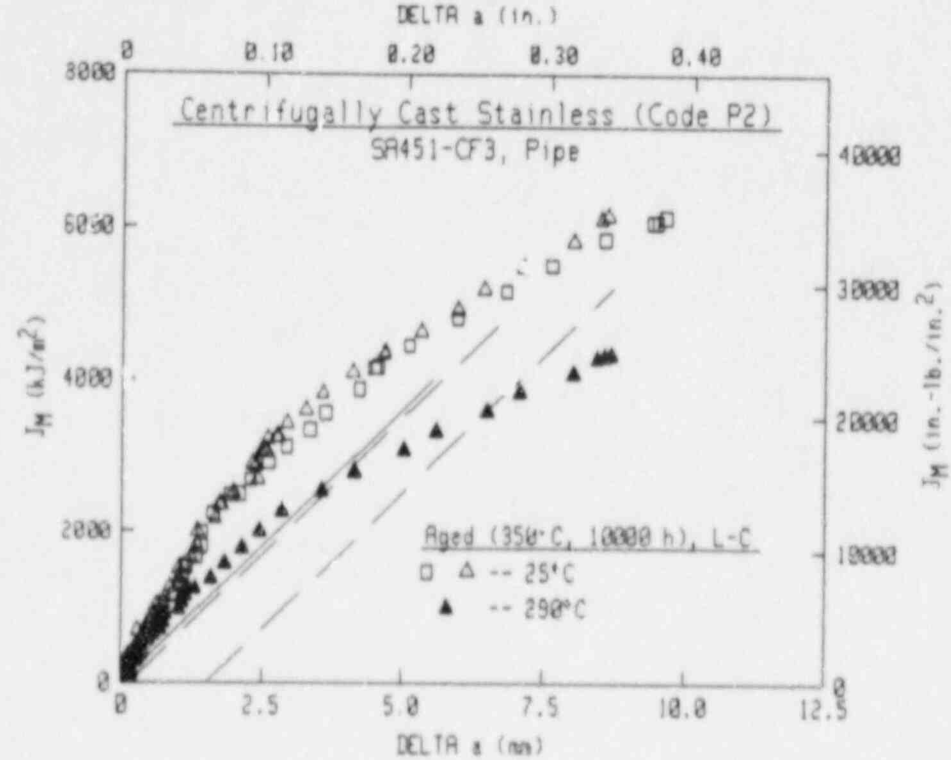

Fig. 63 Increasing the test temperature results in reduced J_M-R curve levels for Heat P2 (grade CF3) after thermal-aging at 350°C for 10000 h.

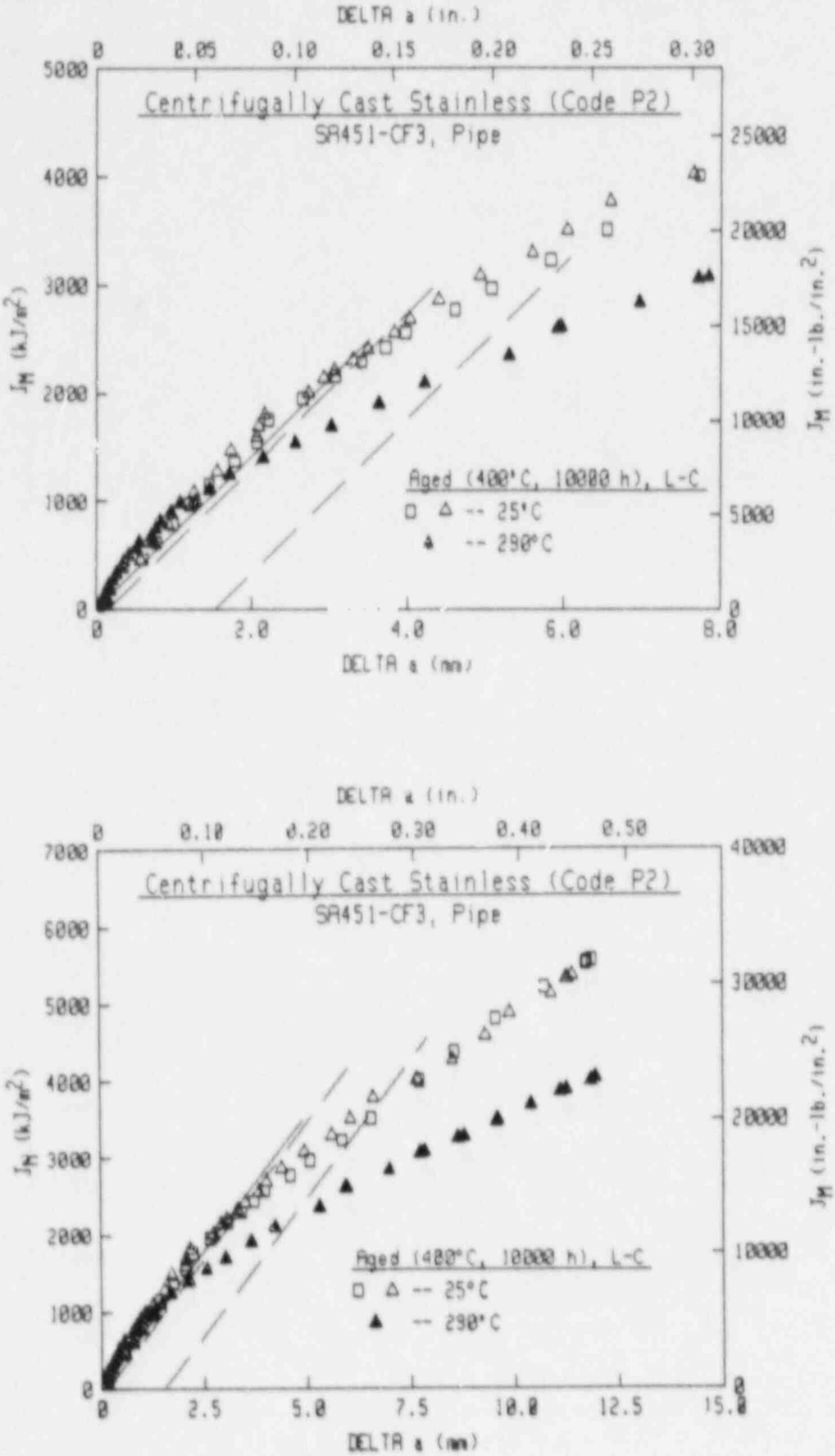

Fig. 64 After thermal-aging of Heat P2 (grade CF3) at 400°C for 10000 h, increasing the test temperature results in decreased J_M-R curve levels.

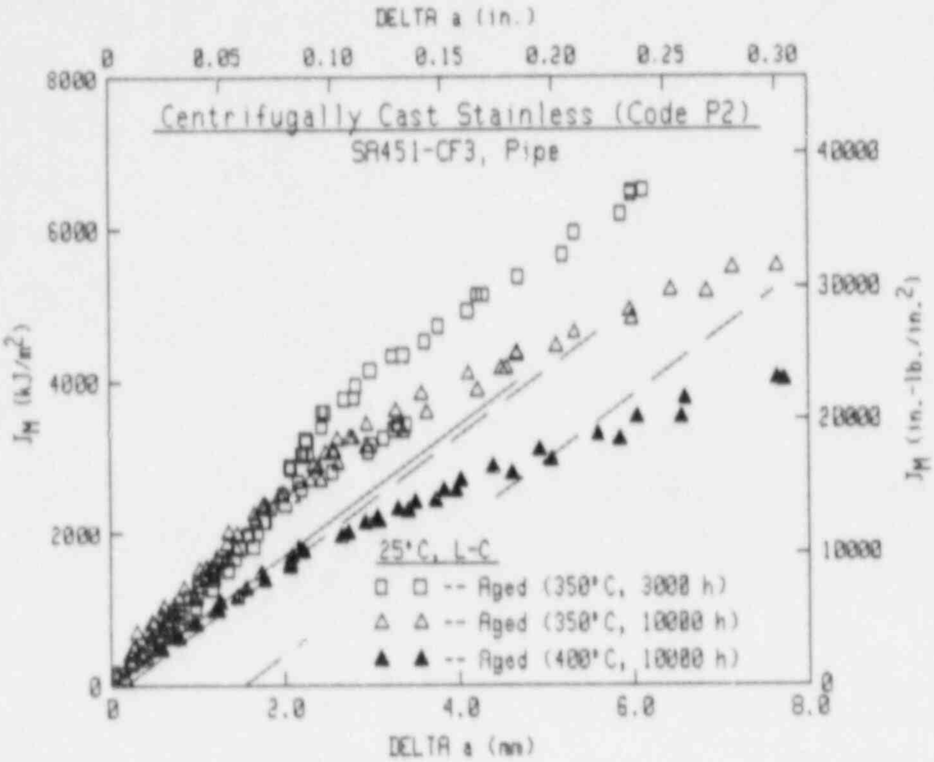

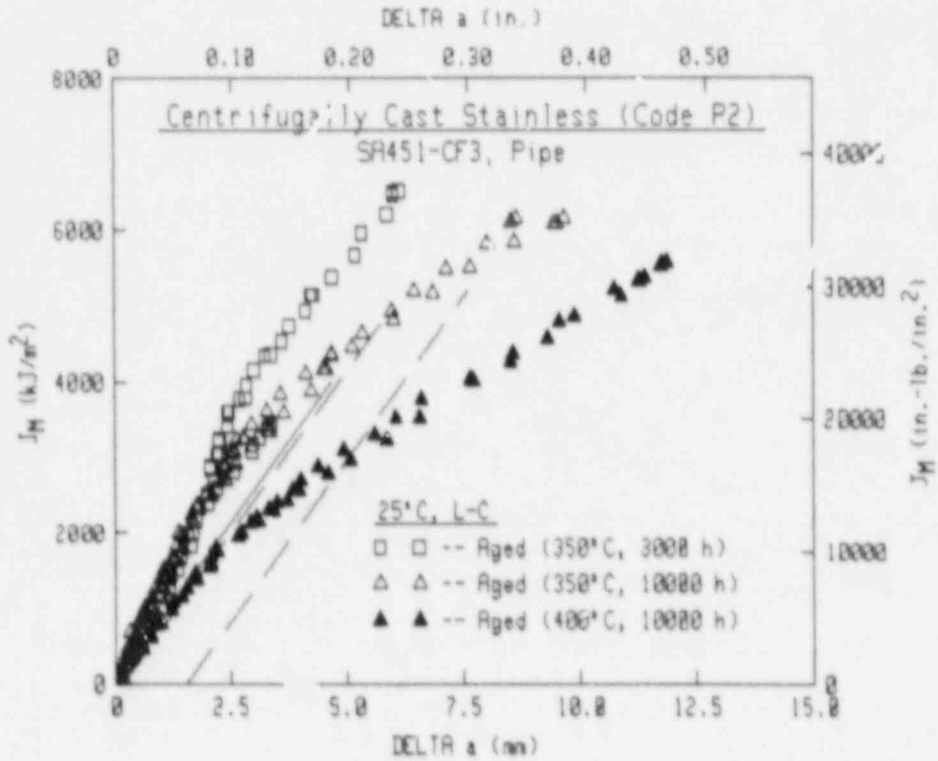

Fig. 65 At a test temperature of 25°C for Heat P2 (grade CF3), thermal-aging at 350°C for 3000 h or for 10000 h results in only small toughness reductions for the longer aging time, whereas aging at 400°C for 10000 h results in large reductions.

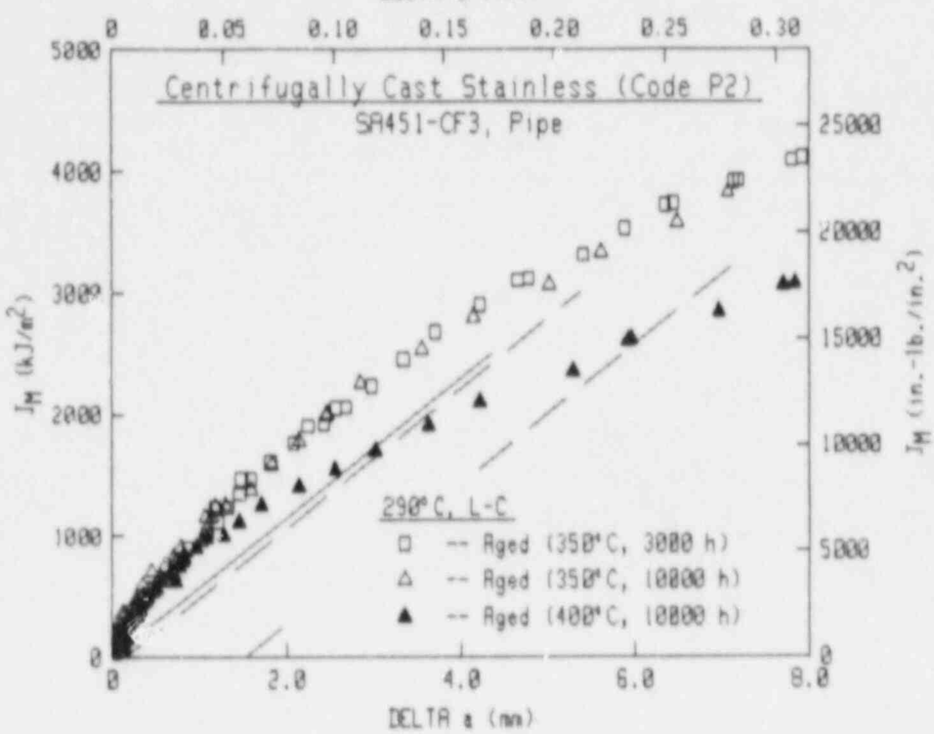

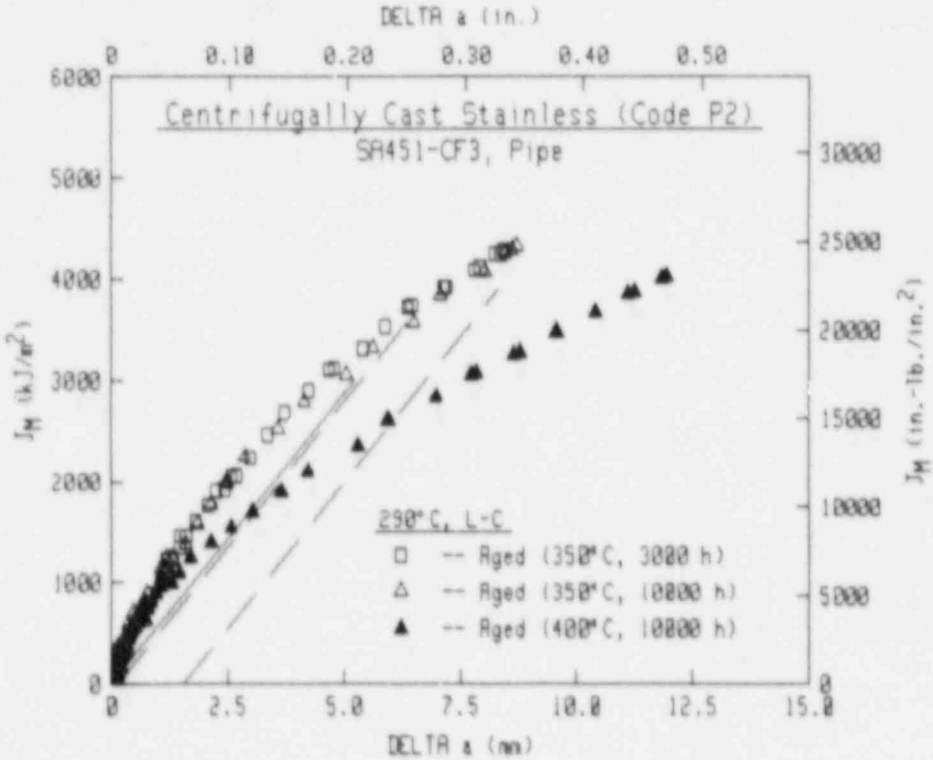

Fig. 66 At a tect temperature of 290°C for Heat P2 (grade CF3), thermal-aging at 350°C for 3000 h and for 10000 h results in similar J_M-R curve trends. Thermal-aging at 400°C for 10000 h results in significant reductions in J_M-R curve levels from those for thermal-aging at 350°C.

6. RESULTS FOR EXPERIMENTAL HEATS

As described in Section 2, the experimental heats of cast stainless steel were cast as slabs. Three grades are represented, including CF8 (Heat 68), CF3 (Heat 69) and CF8M (Heat 70). For each heat, specimens were aged for 3000 h at 350°C, 400°C, and 450°C. Heats 68 and 69 were tested at 25°C and 290°C, whereas Heat 70 was tested at 25°C only. Average "upper shelf" Charpy energy values (for reference purposes only) are summarized in Table 23.

Table 23 Average Charpy "Upper Shelf" Energy Levels for Experimental Heats of Cast Stainless Steel

Heat	Grade	Aging Condition		Average Energy Value	Average Reduction
		Temp (°C)	Time (h)	(J/cm²)	(%)
68	CF8	Unaged		265	....
		350	2570	167	37
		400	2570	[illegible]	40
		450	2570	125	53
69	CF3	Unaged		277	....
		350	2570	198	29
		400	2570	147	47
		450	2570	132	52
70	CF8M	Unaged		193	....
		350	2570	170	12
		400	2570	136	30
		450	2570	93	52

6.1 Tensile Data

Average strength results for the experimental heats are summarized in Table 24 and Fig. 67. For the unaged condition, Heat 69 generally has the highest strength levels. At 25°C, Heat 68 has the highest yield strength, but the lowest ultimate strength.

For Heats 68 and 69, increasing the test temperature from 25°C to 290°C results in decreases in strength ranging from 23% to 45%. Decreases in ultimate strength (an average of 27.5%) tend to be less than those for yield strength (an average of 39.0%) on a percentage basis, but greater on an absolute basis.

Table 24 Summary of Strength Data for Aged Cast Stainless Steels (Experimental Heats)

Heat ID	Aging Condition (°C/h)	25°C[a] Yield (MPa)	25°C[a] Ultimate (MPa)	290°C[a] Yield (MPa)	290°C[a] Ultimate (MPa)
68	Unaged	276.8	523.6	159.6	404.8
	350/3000	+4%	+15%	+16%	+12%
	400/3000	+6%	+23%	+1%	+14%
	450/3000	+7%	+23%	+13%	+21%
69	Unaged	276.1	594.8	183.9	419.0
	350/3000	+7%	+8%	-6%	+8%
	400/3000	+0%	+11%	-11%	+6%
	450/3000	-3%	+14%	-4%	+14%
70[c]	Unaged	264.0	535.2	-----	-----
	350/3000	-0%	+3%	-----	-----
	400/3000	+1%	+10%	-----	-----
	450/3000	-7%	+15%	-----	-----

[a] Test temperature [b] 0.2% offset yield strength [c] Data from ANL

6.1.1 Heat 68 (CF8)

For Heat 68 (Table 25), thermal-aging increases the yield and ultimate strength in all cases (Fig. 68). Additionally, higher aging temperature generally results in higher strength at both temperatures, with only the yield strength at 290°C not following this trend. For the latter, aging at 350°C gives the greatest increase in strength, whereas aging at 400°C results in negligible strength increase.

With increasing test temperature, all four conditions of this heat give similar decreases in strength. Yield strength decreases by an average of 40.6% (35.8% to 44.8%) and ultimate strength decreases an average of 24.6% (22.7% to 28.0%).

6.1.2 Heat 69 (CF3)

For Heat 69 (Table 26 and Fig. 69), thermal-aging results in higher ultimate strength in all cases, whereas yield strength increases only at 25°C for two aging conditions (350°C and 400°C aging). Ultimate strength tends to be "well-behaved," with higher aging temperature tending to result in higher strength. In fact, the percentage increases in ultimate strength are the same at 25°C and 290°C for aging at 350°C and 450°C. For aging at 400°C, the increase in

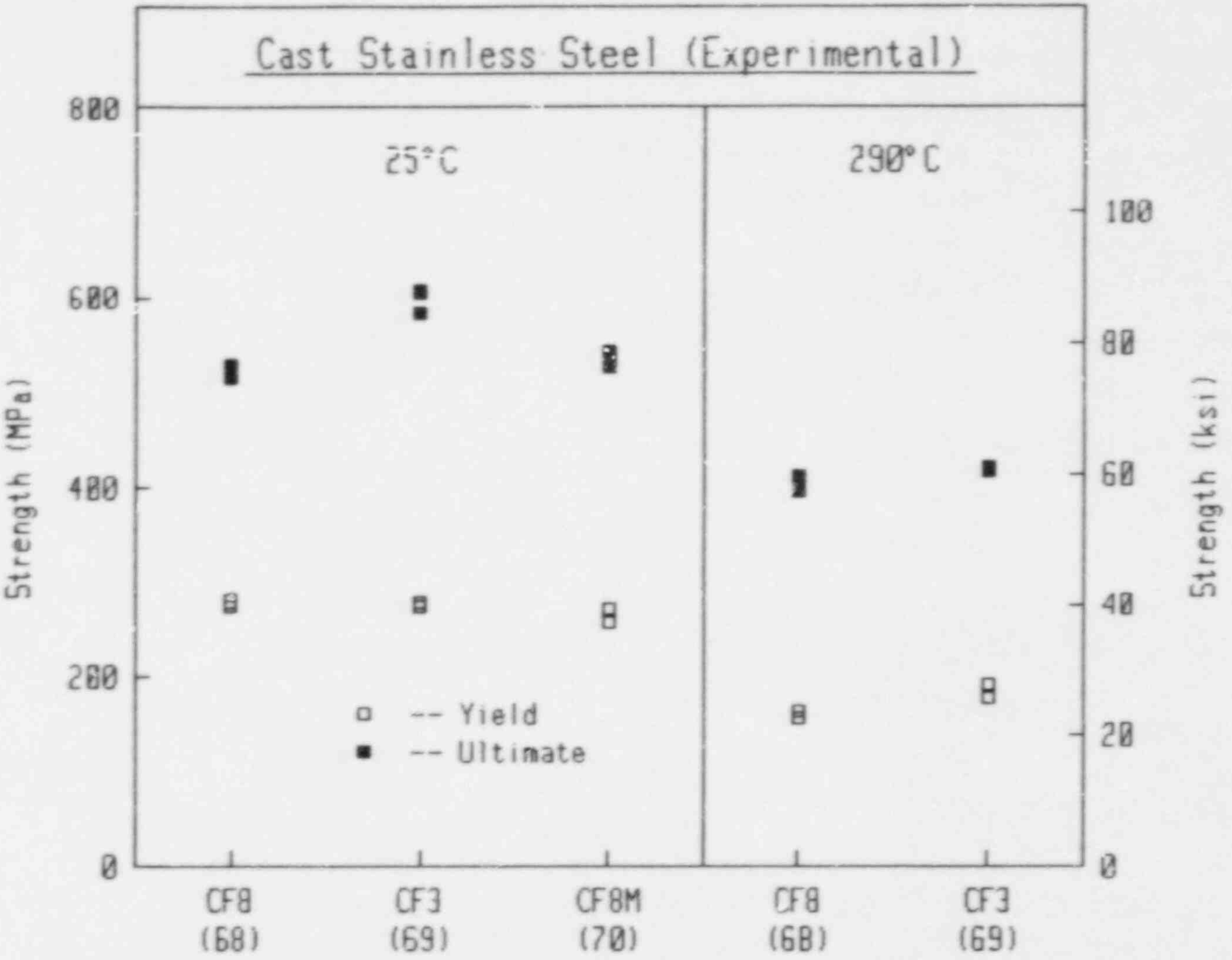

Fig. 67 Comparison of strength levels for the experimental heats in the as-received (unaged) condition. All three heats exhibit similar yield strength levels at 25°C, with grade CF3 exhibiting the highest ultimate strength levels.

Table 25 Tensile Results For Code 68 (Cast Stainless Steel Slab, SA351-CF8)

Specimen Number	Test Temp	True Stress-Strain		Engr Stress-Strain		Elongation[a]	Reduction in Area	Aging Condition	
		0.2% Yield	Fracture-Stress	0.2% Yield	Ultimate Stress			Temp	Time
	(°C)	(MPa)	(MPa)	(MPa)	(MPa)	(%)	(%)	(°C)	(h)
683-40	25	275.0	996.8	274.1	530.0	45.4	53.4	Unaged	
683-41	25	280.3	811.3	279.4	517.2	36.4	49.2	Unaged	
682-25	25	285.2	1647.2	281.5	601.6	64.1	75.2	350	3000
682-26	25	295.8	1620.7	294.8	599.4	62.0	73.5	350	3000
682-16	25	295.2	1534.6	294.1	657.8	75.0	64.0	400	3000
682-17	25	290.7	1313.0	289.8	629.5	——[b]	64.6	400	3000
681-4	25	293.8	1030.9	291.3	653.1	41.5	38.7	450	3000
681-5	25	310.5	1447.0	309.4	632.9	——[b]	68.7	450	3000
683-42	288	163.2	815.4	162.7	397.3	29.2	57.8	Unaged	
684-40	288	156.9	792.0	156.4	412.3	37.9	60.6	Unaged	
682-27	288	185.7	826.2	185.1	452.4	41.7	57.8	350	3000
682-18	288	161.8	711.3	161.3	463.1	32.1	47.1	400	3000
681-6	288	170.2	700.4	169.7	486.8	——[b]	36.8	450	3000
682-9	288	194.5	769.0	191.6	503.8	35.5	42.6	450	3000

[a] In 20.3 mm to 20.5 mm (0.8 in. to 0.808 in.)
[b] Specimen broke outside gage length

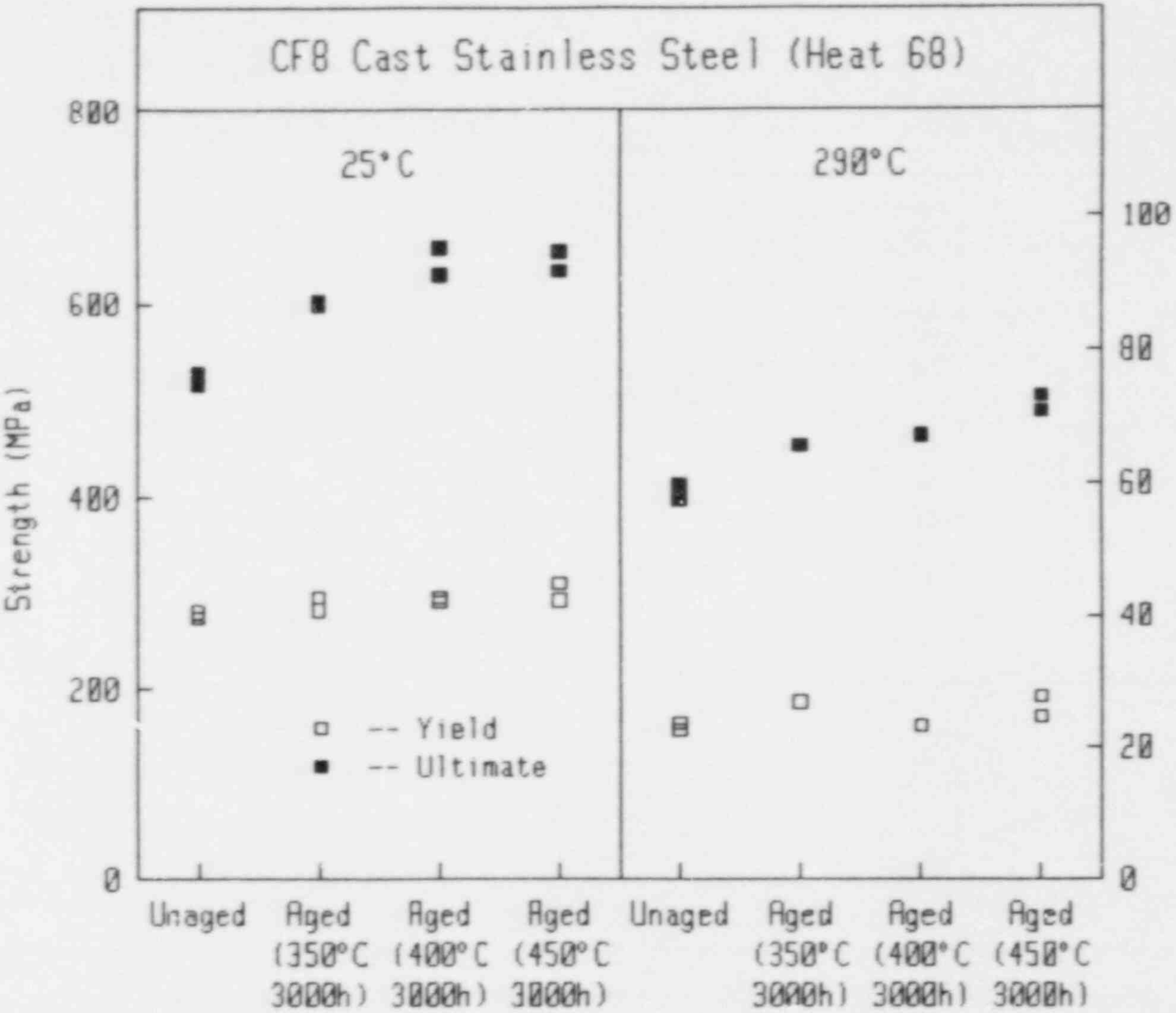

Fig. 68 Strength data for grade CF8 (Heat 68). Increasing the test temperature results in lower strength in all cases. Whereas ultimate strength exhibits larger increases due to thermal-aging, yield strength exhibits minimal increases.

Table 26 Tensile Results For Code 69 (Cast Stainless Steel Slab, SA351-CF3)

Specimen Number	Test Temp	True Stress-Strain		Engr Stress-Strain		Elongation[a]	Reduction in Area	Aging Condition	
		0.2% Yield	Fracture-Stress	0.2% Yield	Ultimate Stress			Temp	Time
	(°C)	(MPa)	(MPa)	(MPa)	(MPa)	(%)	(%)	(°C)	(h)
693-40	25	279.9	1070.1	278.8	606.0	57.1	48.9	Unaged	
693-41	25	274.3	1093.4	273.4	583.6	54.1	54.4	Unaged	
692-25	25	286.5	1483.2	285.4	633.4	67.7	76.2	350	3000
692-26	25	303.7	1364.3	302.6	648.2	62.5	72.4	350	3000
692-16	25	254.5	1358.9	253.6	638.8	52.4	72.4	400	3000
692-17	25	301.9	1309.9	300.9	683.2	44.3	60.6	400	3000
691-4	25	272.2	1476.9	271.3	692.2	36.5	71.4	450	3000
691-5	25	263.9	1528.1	263.1	664.6	56.6	73.2	450	3000
693-42	288	191.4	908.2	190.8	420.9	35.9	63.4	Unaged	
694-40	288	177.5	809.0	177.0	417.0	33.6	59.7	Unaged	
692-27	288	175.5	752.6	173.1	451.2	32.3	53.8	350	3000
692-18	288	164.2	556.4	163.9	444.8	21.8	33.2	400	3000
691-6	288	178.2	683.6	177.7	479.7	28.5	44.9	450	3000
692-9	288	176.3	793.4	175.7	477.1	27.4	51.0	450	3000

[a] In 20.3 mm to 20.6 mm (0.798 in. to 0.810 in.)

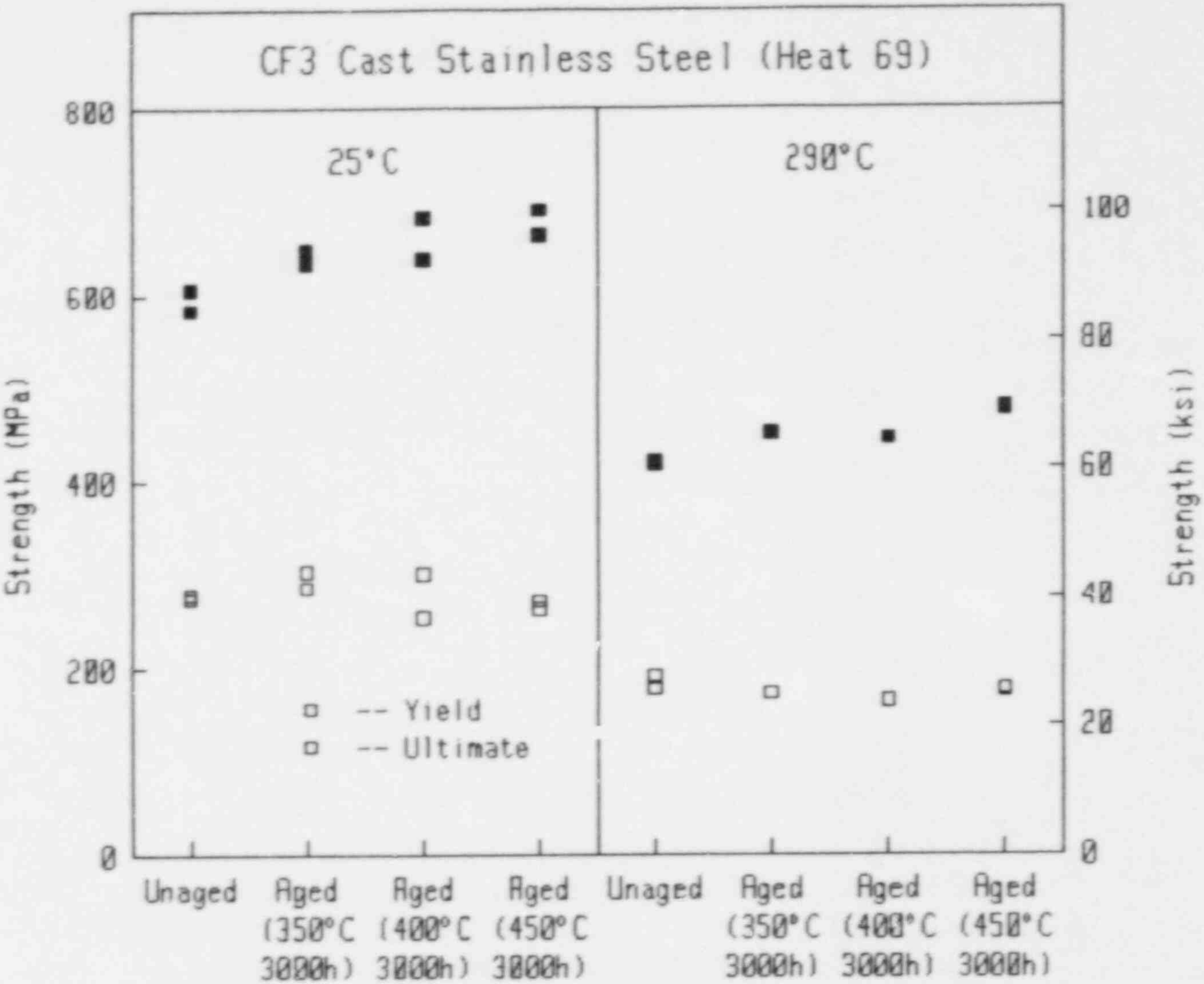

Fig. 69 Strength data for grade CF3 (Heat 69). Yield strength tends to decrease in some cases after thermal-aging.

ultimate strength at 290°C is much lower than that at 25°C, and also lower than that for aging at 350°C.

In contrast to the trends for ultimate strength and for Heat 68, the yield strength results do not describe an expected trend or even a consistent trend. At 25°C, thermal-aging at 350°C gives a moderate increase in yield strength (+7%), whereas thermal-aging at 400°C gives no substantial change in yield strength (+1.2 MPa or 0.4%) and thermal-aging at 450°C gives a small decrease in yield strength (-3%). For this case, increasing the thermal-aging temperature gives successive decreases in yield strength, exactly contrary to the expected trend.

At 290°C, all three thermal-aging conditions result in decreases in yield strength. In this case, thermal-aging at 400°C results in the lowest yield strength (highest percentage decrease), whereas thermal-aging at 450°C results in the highest yield strength of the aged conditions (lowest percentage decrease).

With increasing test temperature, strength levels are decreased substantially for all four conditions. Percentage decreases in yield strength (~ 37% on average) are greater than those for ultimate strength (~ 30% on average), but absolute decreases are greater for ultimate strength.

6.1.3 Heat 70 (CF8M)

Tensile tests of Heat 70 were performed (at 25°C only) by ANL. Whereas, values reported in Table 24 are average values (from duplicate tests), individual values are reported in Table 27 and illustrated in Fig. 70. As with the other experimental heats, ultimate strength is "well-behaved," as thermal-aging increases ultimate strength in all three cases, and higher aging temperature results in higher strength. Aging at 400°C results in the highest yield strength (~ 268 MPa), a small increase from the strength of unaged material, whereas aging at 450°C results in a moderate decrease in strength (~ 19 MPa or 7%). Thermal-aging at 350°C results in essentially no change in yield strength.

6.2 J-R Curve Data

In contrast to results for the experimental heats, the commercial heats of grades CF8 (Heat 68) and CF3 (Heat 69) yield similar J_M-R curve trends at 25°C (Fig. 71) and 290°C (Fig. 72), although the CF8 grade does have slightly higher toughness than the CF3 grade at 25°C. Overall, the CF8M grade (Heat 70) has the highest toughness at 25°C (no tests of this heat were made at 290°C).

Table 27 Tensile Results[a] for Code 70 (Cast Stainless Steel Slab, SA 351-CF8M)

Test Temperature (°C)	Engineering Stress-Strain 0.2% Yield (MPa)	Ultimate (MPa)	Aging Condition Temp (°C)	Time (h)
25	271.2	542.4	Unaged	
25	256.8	528.0	Unaged	
25	273.1	570.1	350	3000
25	253.9	536.5	350	3000
25	265.6	598.3	400	3000
25	270.1	578.9	400	3000
25	240.2	619.7	450	3000
25	249.1	615.6	450	3000

[a] Data from ANL tests

6.2.1 Heat 68 (CF8)

J_M-R curve results for Heat 68 are summarized in Table 28. This heat demonstrated an unusual trend in the unaged condition (Fig. 73). Specifically, data of 290°C (from one test) are not much lower than data at 25°C, and actually are higher than the 25°C data at less than ~ 4 mm of Δa. The curve shape is flatter for the 290°C data, with J levels lower than those for 25°C tests at Δa greater than 10 mm. The curve shape difference is apparent in a J-dJ/da comparison (Fig. 74).

For this heat, thermal-aging at 350°C for 3000 h results in higher toughness (J_M-R curve levels) at 25°C as compared to the unaged condition (Fig. 75). In contrast, C_v data indicate a large reduction in level (37%) due to this aging condition. Comparison of the load-deflection curves (Fig. 76) illustrates the higher load-carrying capacity and greater deflection at maximum load for the aged specimen. As illustrated, the J levels are increased by a factor of ~ 2. At 290° (Fig. 77), a moderate reduction (~ 15%) in J level occurs for the thermally aged specimen, with the curve shapes for the two data sets quite similar.

With thermal-aging at 400°C for 3000 h, the J_M-R curve at 25°C is elevated over that for the unaged condition (Fig. 78). In contrast, C_v data indicate a large reduction in level (40%) due to this aging condition. This elevation is apparent at all Δa intervals, with ~ 20% increase at the end of the data for the aged specimens. At 290°C (Fig. 79), a substantial reduction (~ 25%) in J level is exhibited by the thermally aged condition in comparison to trends for unaged

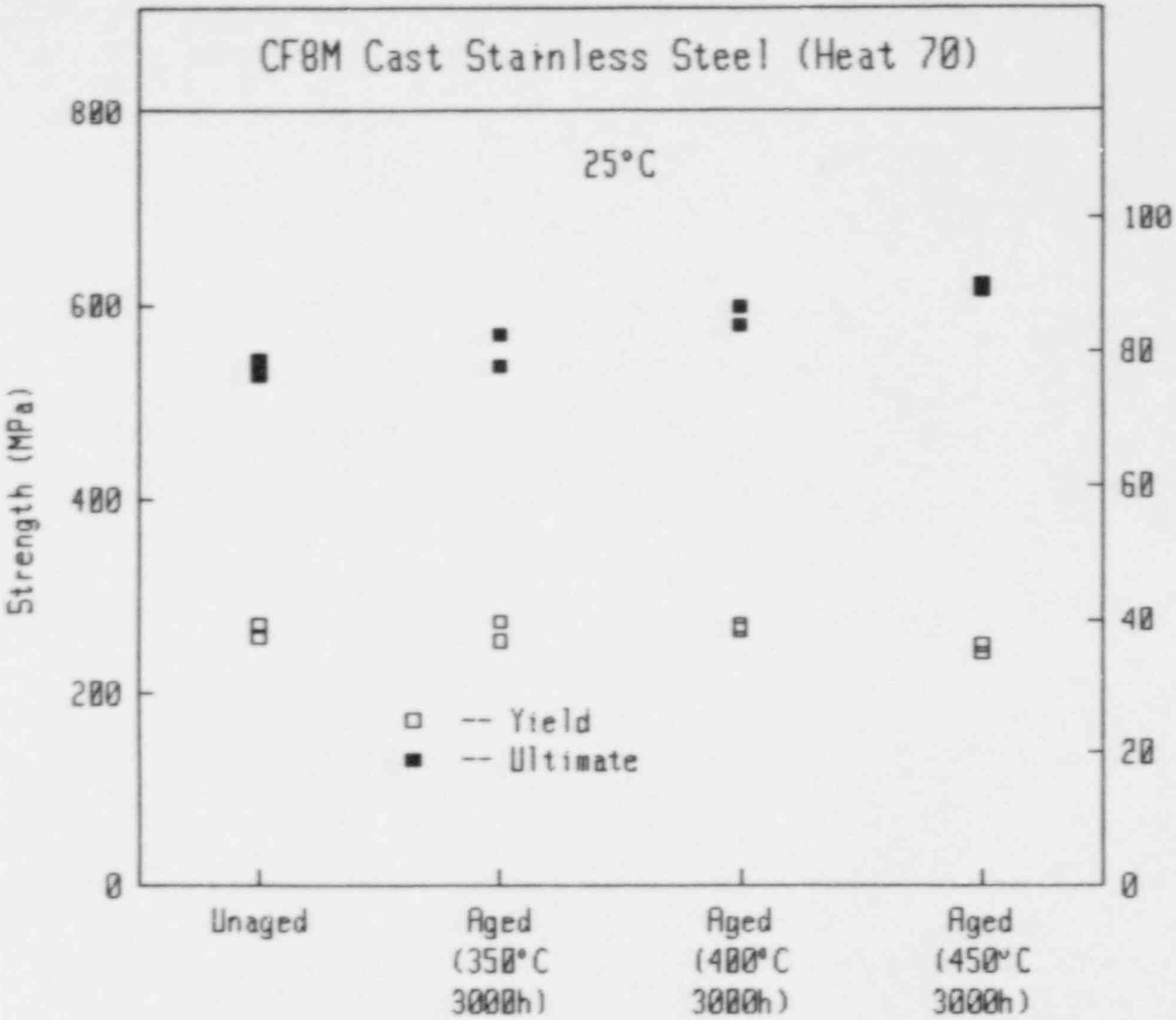

Fig. 70 Strength data for grade CF8M (Heat 70). Thermal aging results in higher ultimate strength and no change in yield strength.

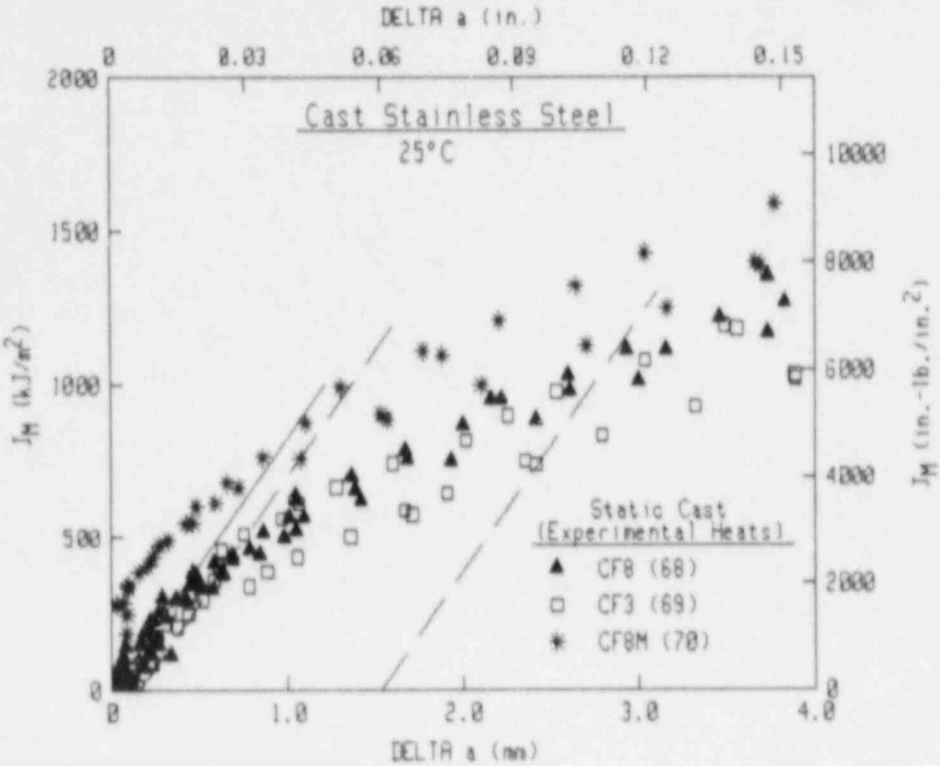

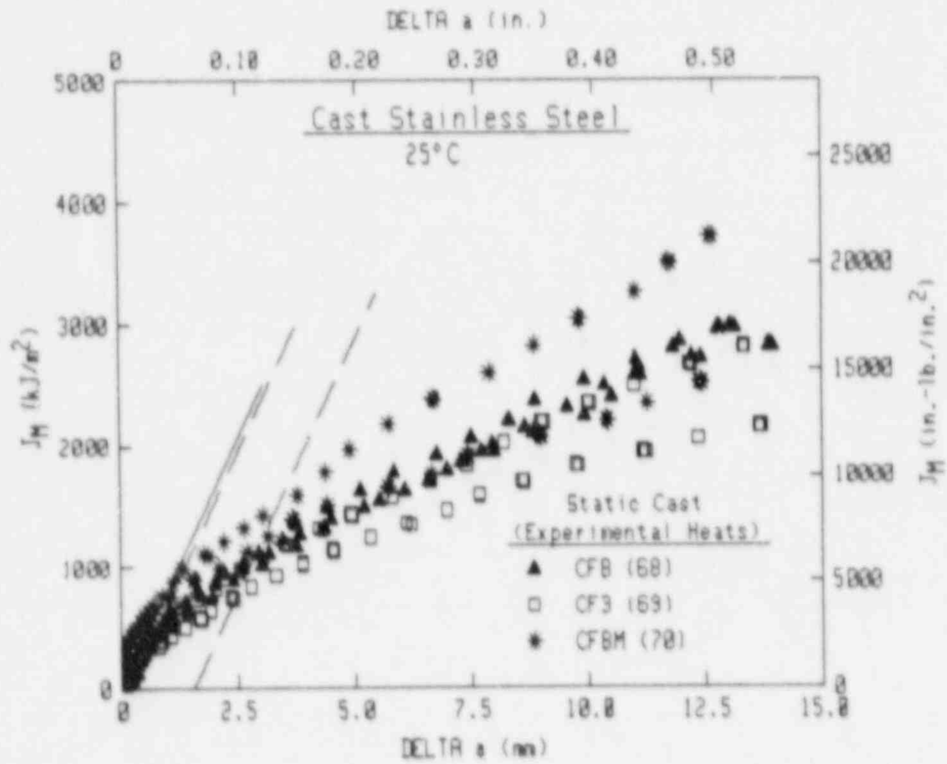

Fig. 71 For the experimental heats at 25°C in the unaged condition, grade CF8M demonstrates the highest toughness whereas grade CF3 demonstrates the lowest toughness.

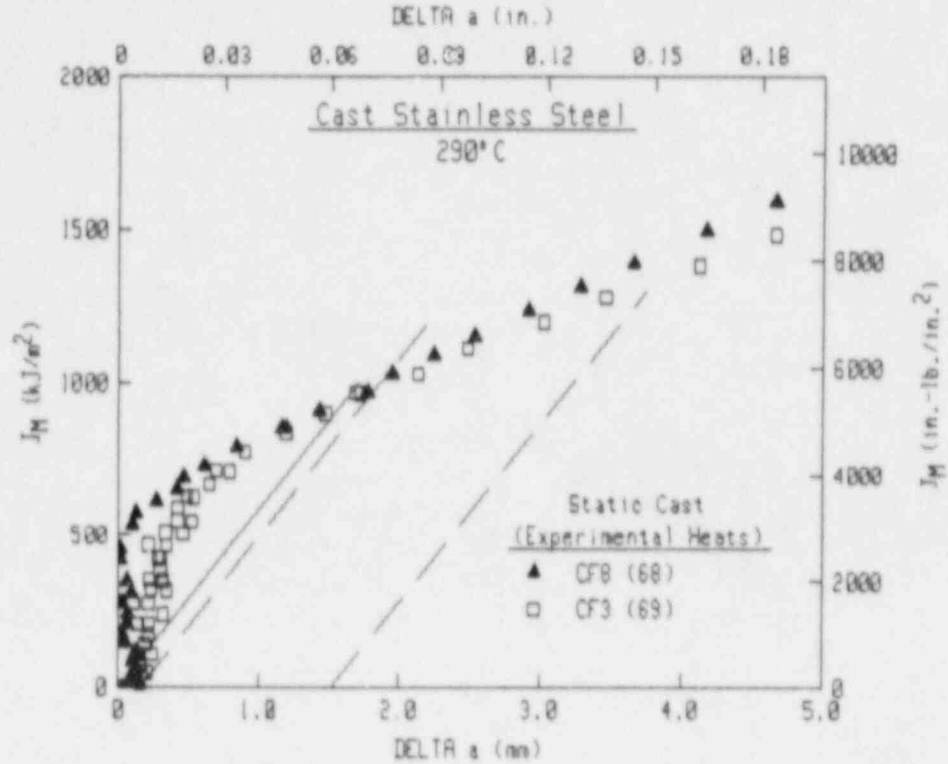

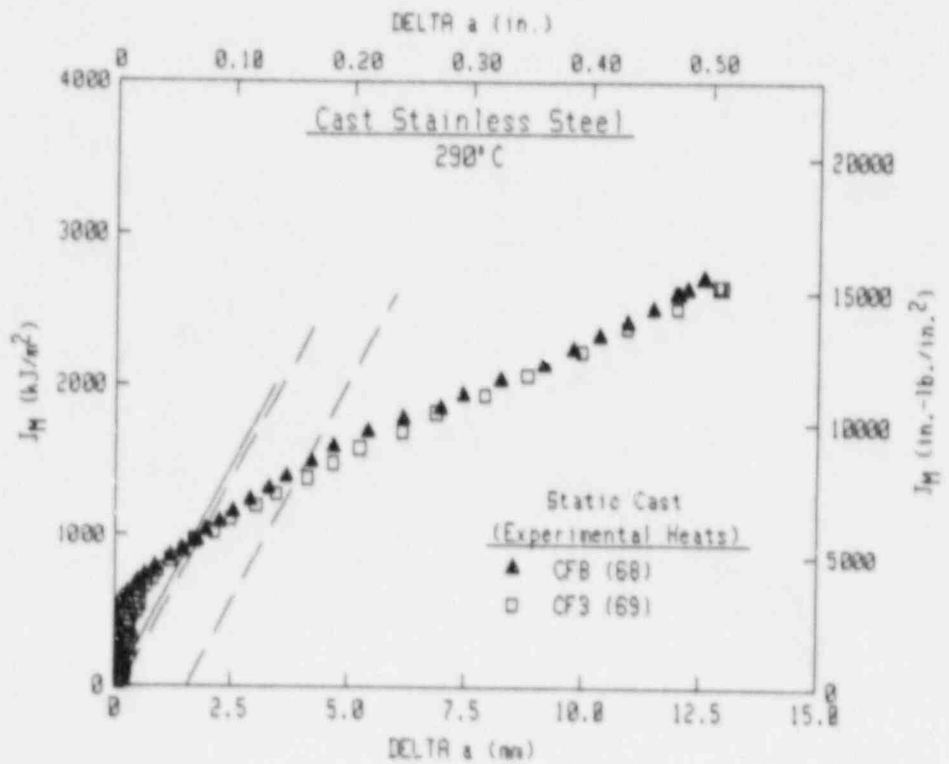

Fig. 72 For the experimental heats at 290°C in the unaged condition, grades CF8 and CF3 exhibit similar J_M-R curve trends.

Table 28 J-R Curve Results for Code 68 (Cast Stainless Steel Slab, SA351-CF3)

Specimen Number	Test Temp (°C)	$(a/W)_i$	Δa_m (mm)	$\Delta a_p - \Delta a_m$ (mm)	J_{Ic} MEA (kJ/m^2)	J_{Ic} ASTM (kJ/m^2)	T_{avg} MEA	T_{avg} ASTM	C (kJ/m^2)	n	σ_f (MPa)	Aging Condition Temp (°C)	Aging Condition Time (h)
683-5B	25	0.527	14.68	-1.64	483.2	410.1	383	406	576.8	0.6348	400.2	Unaged	
683-5T	25	0.519	16.29	-2.41	386.3	325.9	338	362	510.2	0.6133	400.2	Unaged	
683-3V	25	0.523	15.00	-2.19	452.7	393.8	356	382	554.1	0.6110	400.2	Unaged	
681-4B	25	0.543	11.65	-1.43	1635.1	1512.5	450	465	1057.8	0.6311	444.3	350	3000
681-3B	25	0.548	12.13	-1.40	546.2	510.7	318	321	661.4	0.6261	467.8	400	3000
681-4T	25	0.531	14.52	-1.60	361.4	334.8	196	207	492.7	0.4966	471.7	450	3000
681-5B	25	0.540	[a]	[a]	410.6	426.2	238	228	550.5	0.5521	471.7	450	3000
683-7T	290	0.536	14.50	-1.92	1016.1	986.8	503	512	727.3	0.4991	282.2	Unaged	
681-6T	290	0.544	15.28	-1.88	737.6	723.4	339	338	656.6	0.4307	318.8	350	3000
681-5T	290	0.550	14.66	-1.97	451.1	450.6	336	336	480.7	0.4777	312.2	400	3000
681-3T	290	0.529	13.77	-1.08	447.9	446.4	263	246	489.0	0.4278	338.5	450	3000

[a] Cannot be determined

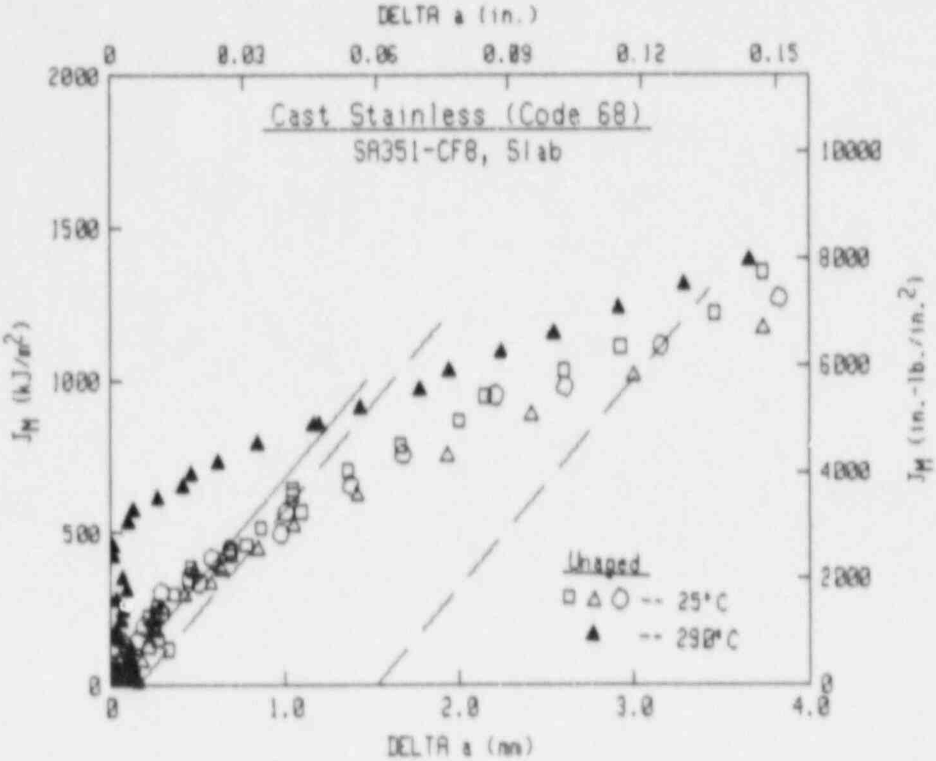

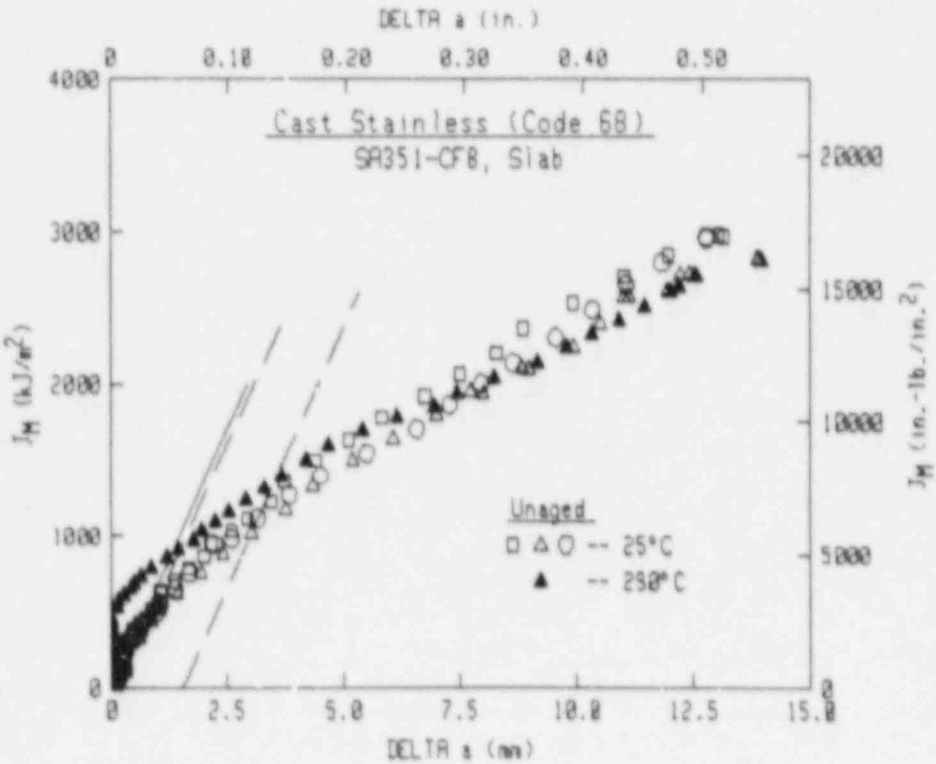

Fig. 73 For the unaged condition of Heat 68 (grade CF8), data at 290°C are similar to data at 25°C.

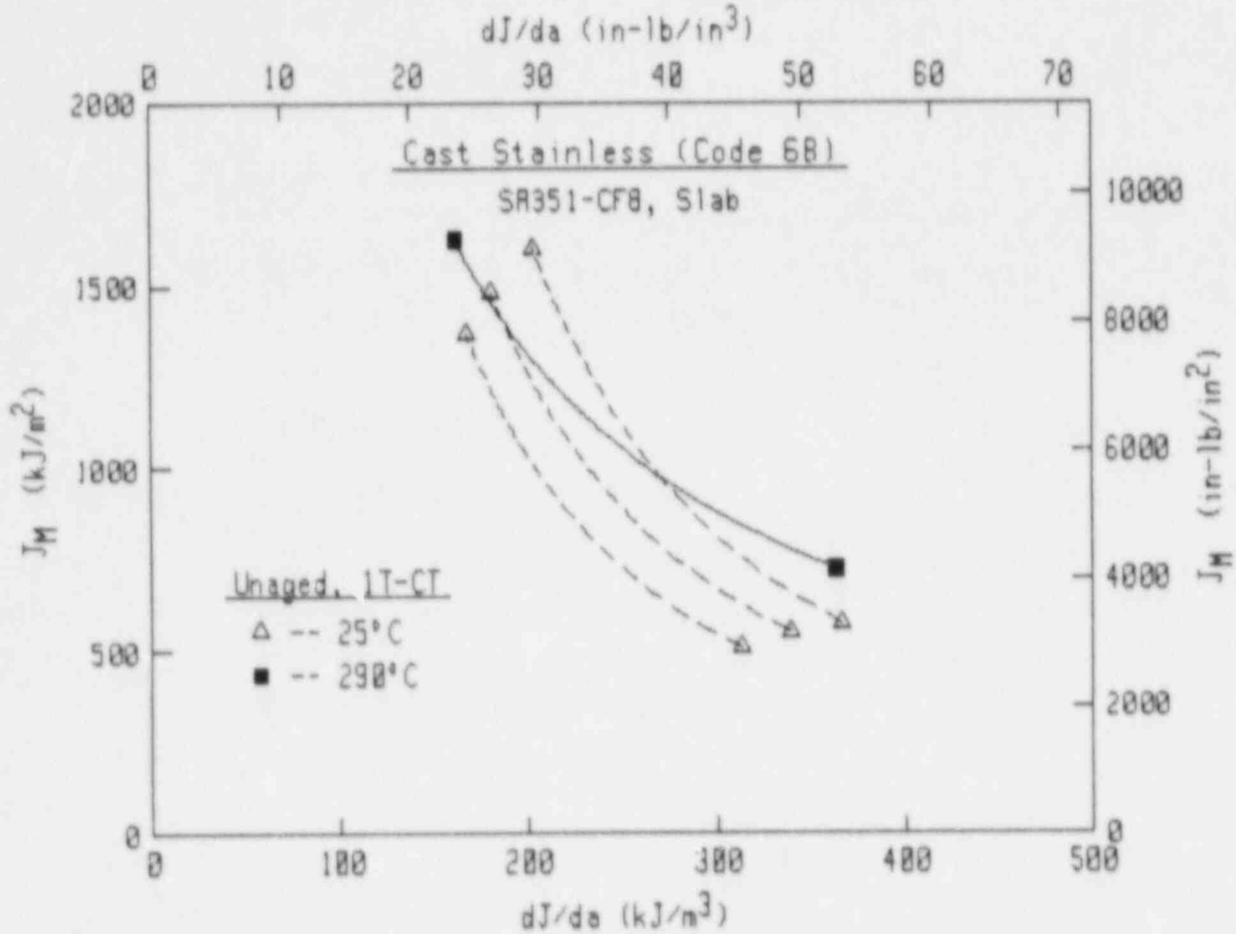

Fig. 74 For Heat 68 in the unaged condition, increasing the test temperature results in higher toughness at small crack growth intervals (lower right portion of the curve) and lower toughness at large crack growth intervals (upper left portion of the curve).

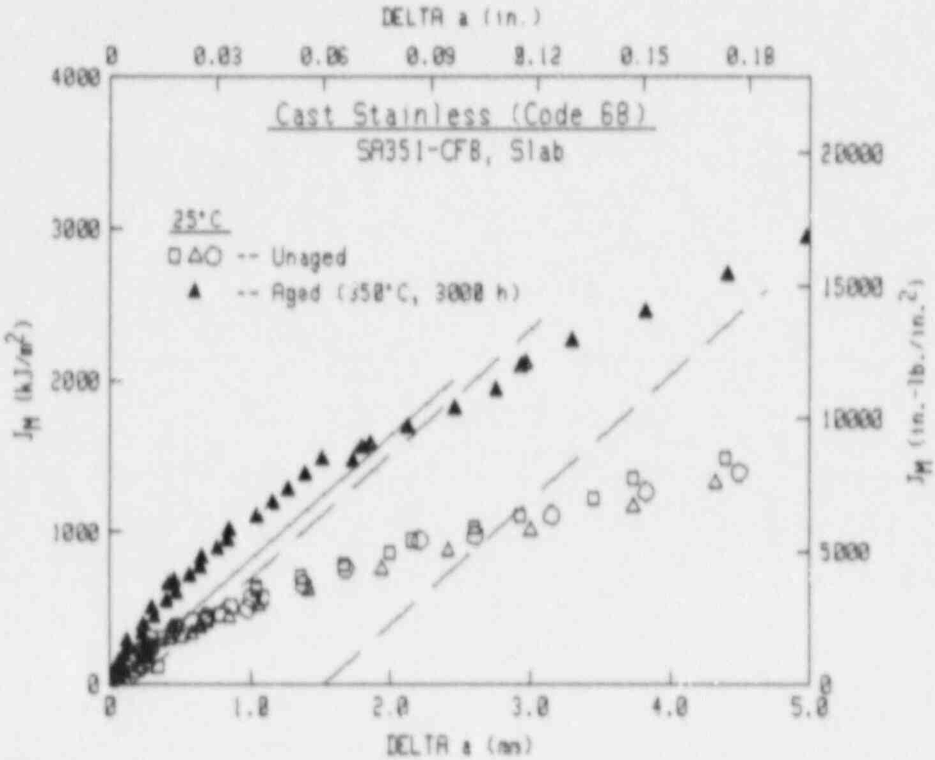

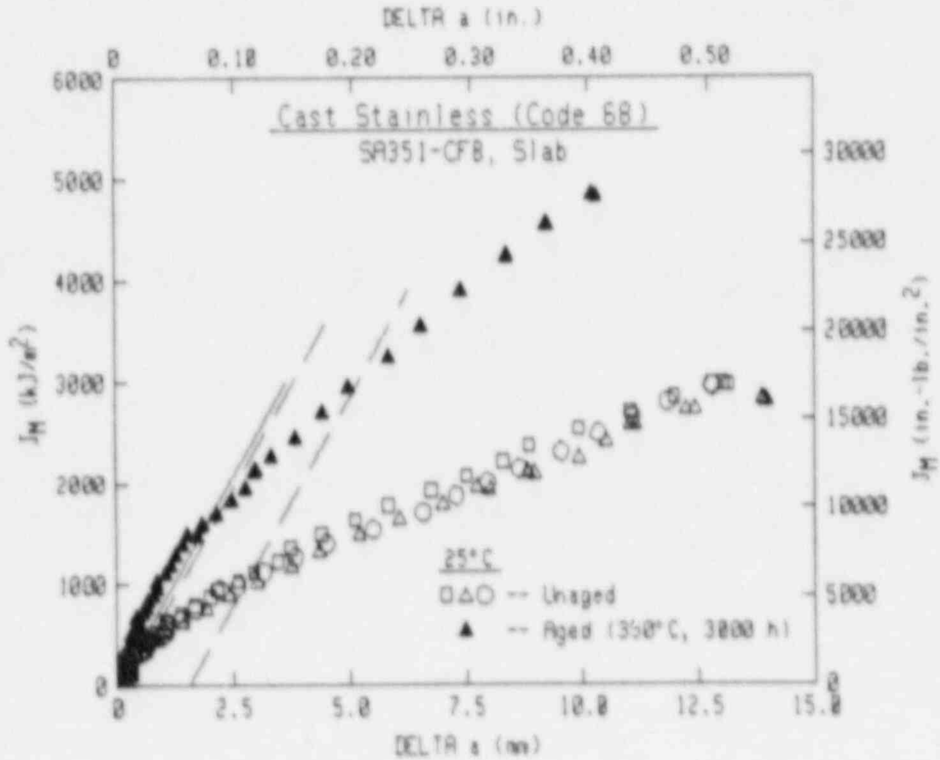

Fig. 75 For Heat 68 (grade CF8) at 25°C, thermal-aging at 350°C for 3000 h results in substantial increases in J level, by a factor of ~ 2.

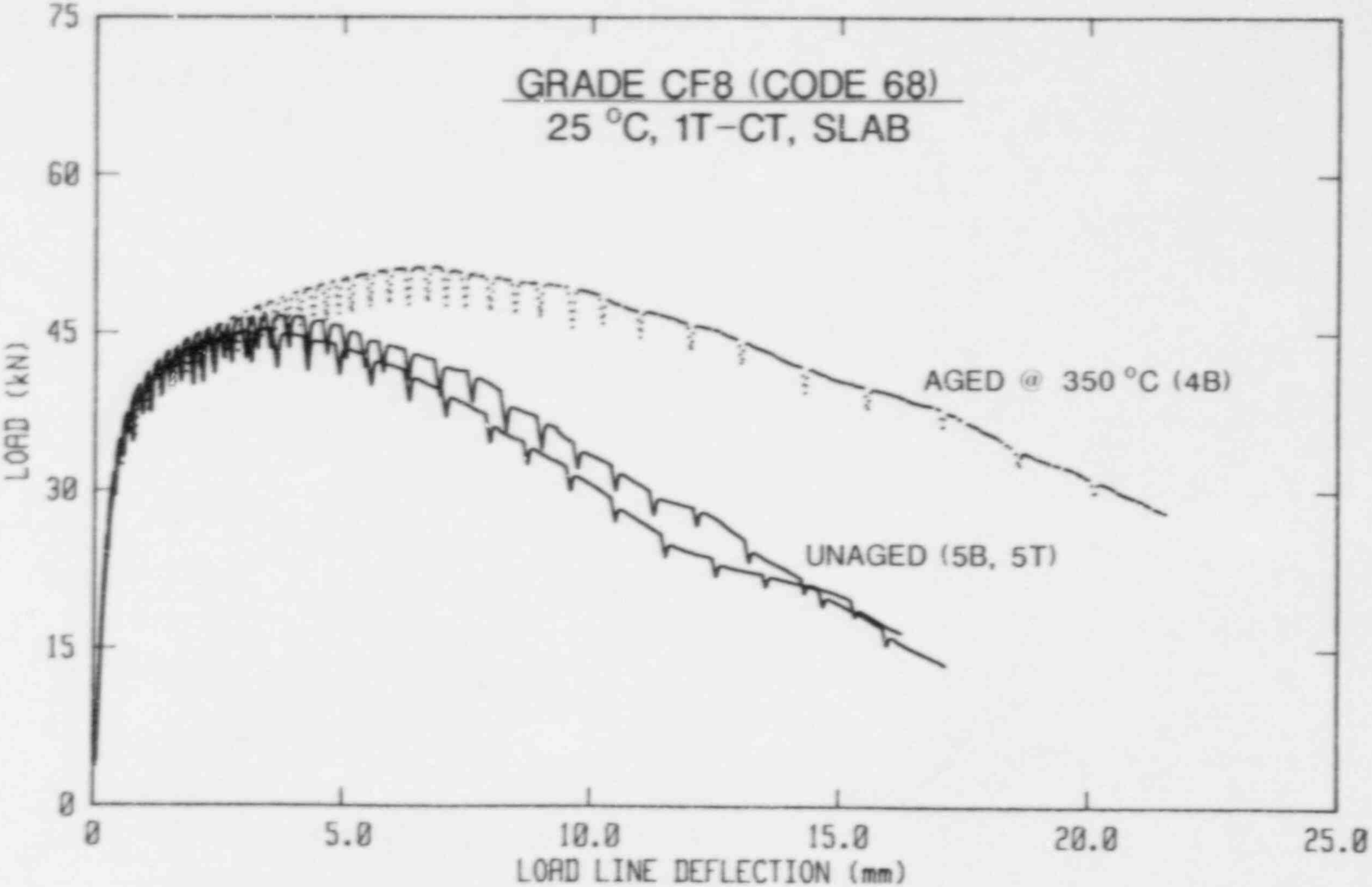

Fig. 76 Load-deflection curves for the J-R curves illustrated in Fig. 75. In this case, the aged condition exhibits higher maximum load levels and higher deflection levels at maximum load.

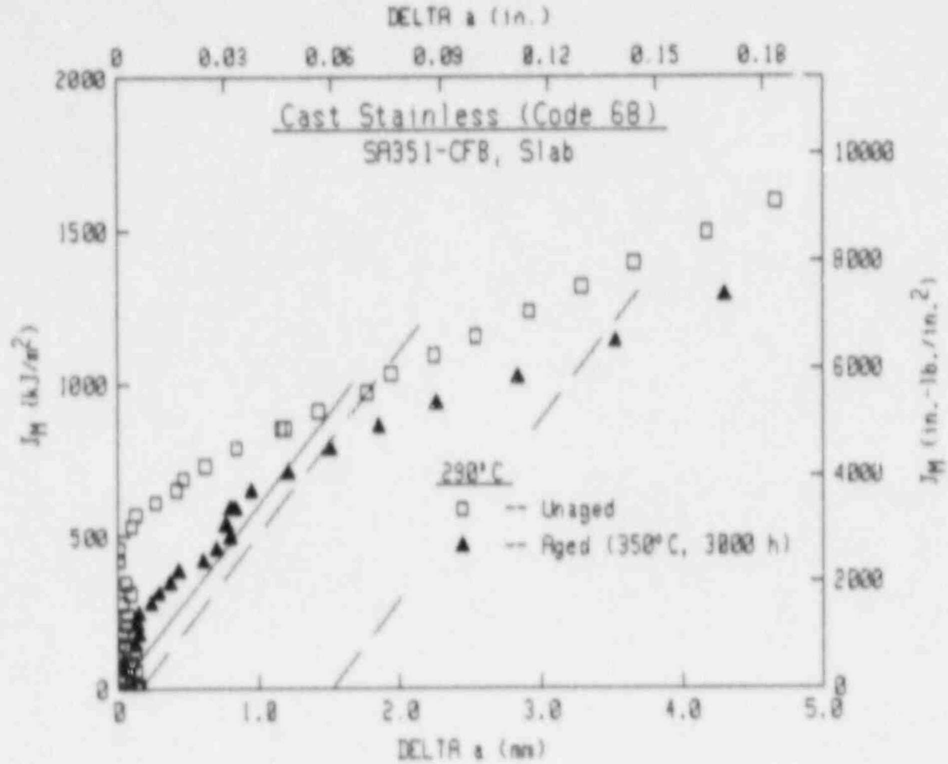

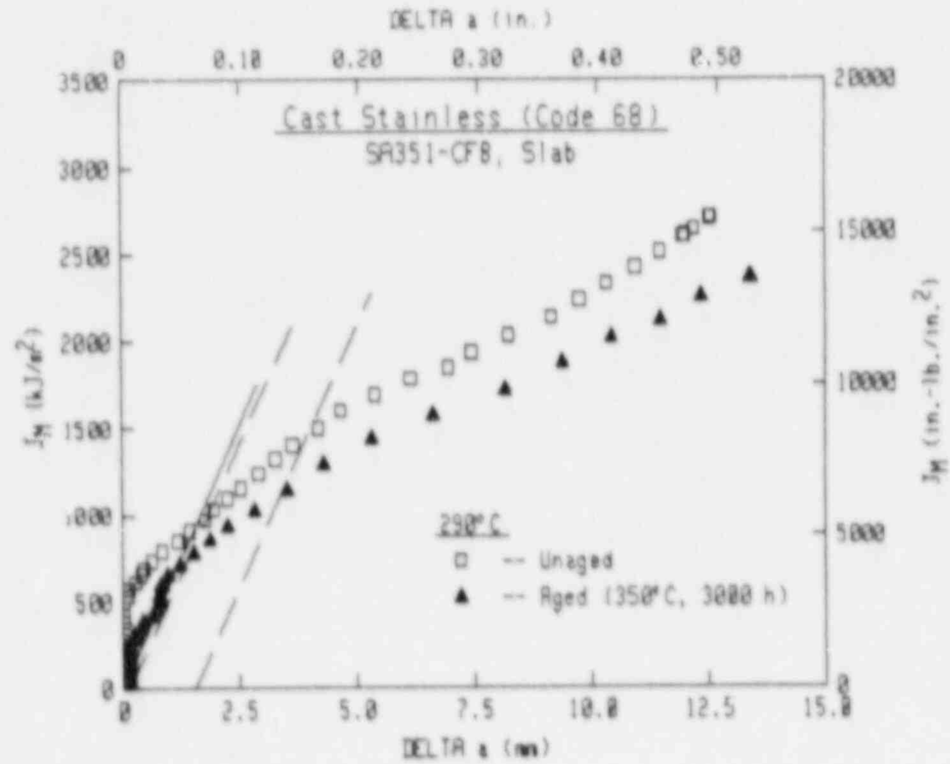

Fig. 77 For Heat 68 (grade CF8) at 290°C, thermal-aging at 350°C for 3000 h results in a small decrease in J levels.

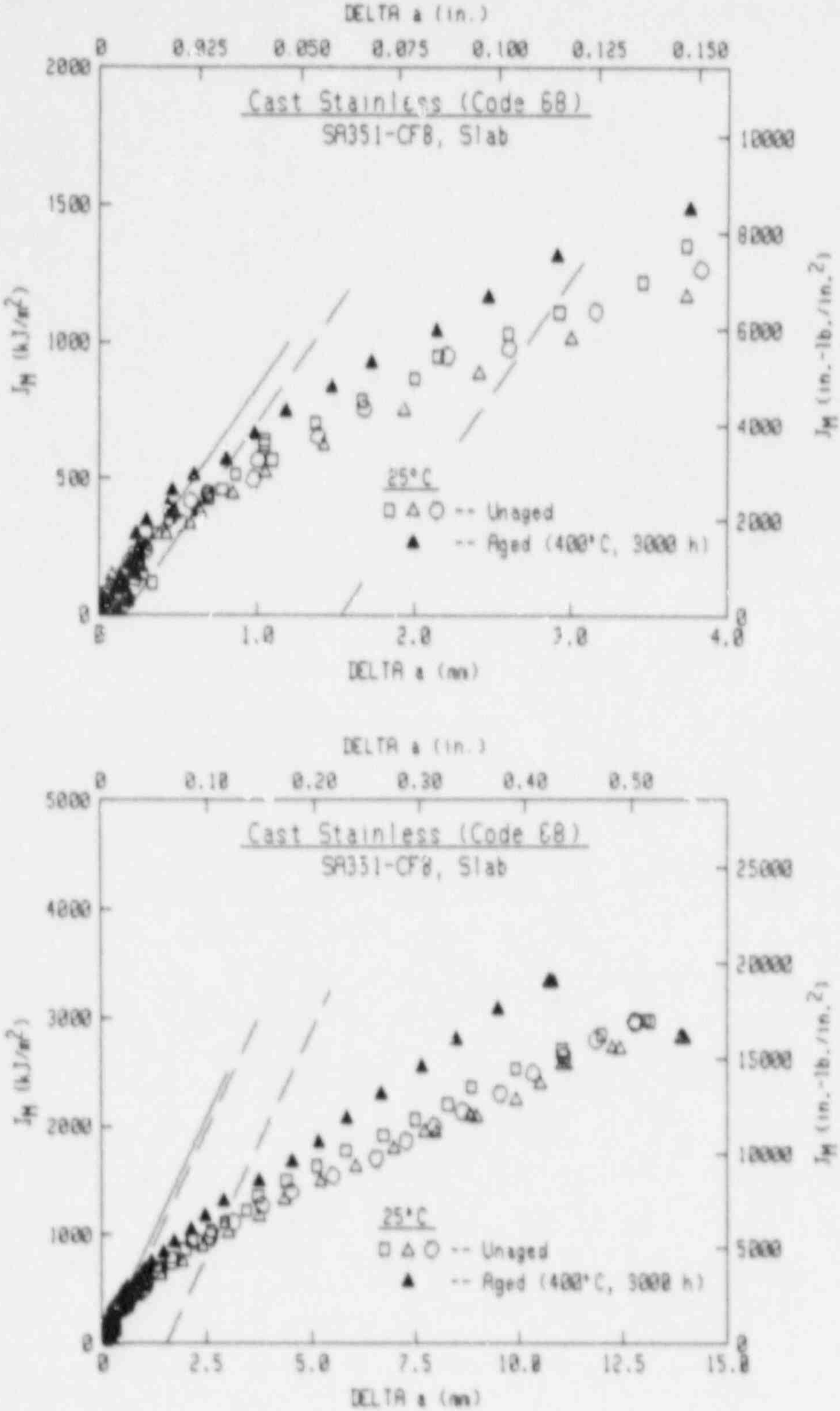

Fig. 78 For Heat 68 (grade CF8) at 25°C, thermal-aging at 400°C for 3000 h results in higher toughness in comparison to data for unaged material.

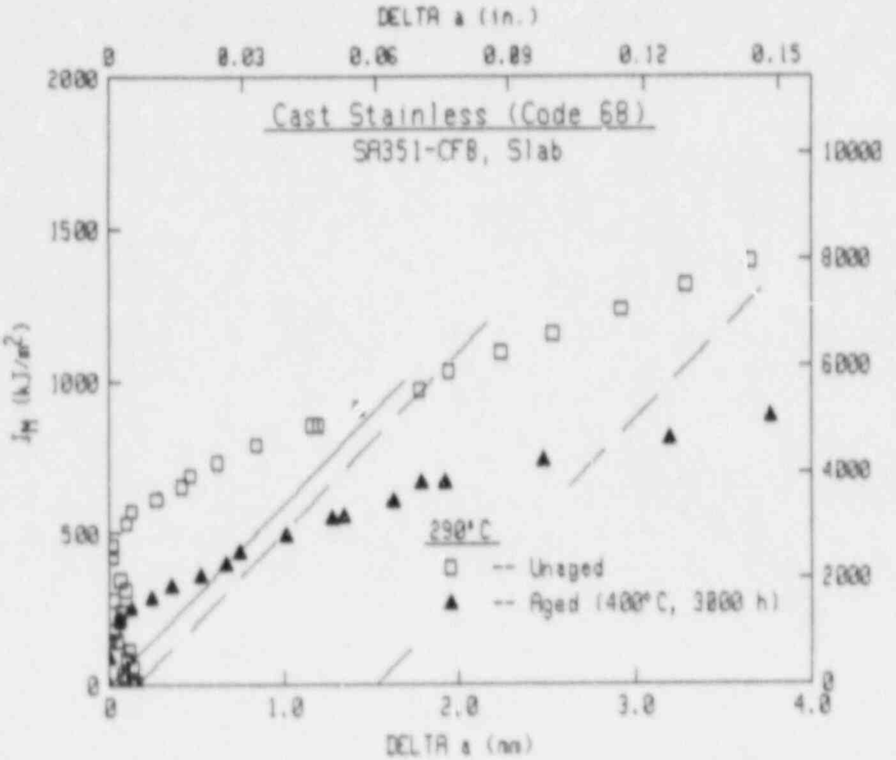

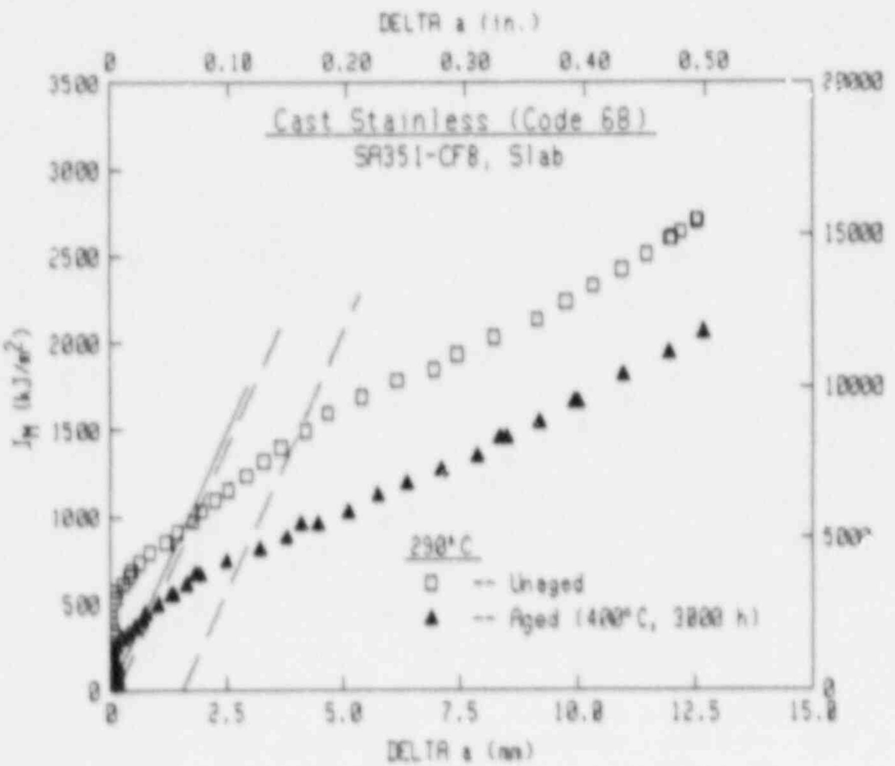

Fig. 79 For Heat 68 (grade CF8) at 290°C, thermal-aging at 400°C for 3000 h results in significantly lower toughness.

material. In this case, an almost constant difference in J level exists after ~ 3-4 mm of Δa.

With thermal-aging at 450°C for 3000 h, some reduction in J_M-R curve level is apparent at 25°C (Fig. 80), much less than the 53% reduction indicated from C_V data. The lower curve in this case (from specimen 681-4T) suffered a large load drop (~ 50%) after ~ 5 mm (0.2 in.) of stable crack growth (Fig. 81), with a crack jump of ~ 4 mm (0.16 in.) due to the event. The fracture surface for this specimen (Fig. 82) has a large faceted area in the center, typical of a low toughness fracture. This surface is in contrast to that for an unaged specimen tested at this same temperature. The other aged specimen tested at 25°C (specimen 681-5B) likewise suffered several small drops of ~ 5% in load. These load drops do not have a discernible effect on the J_M-R curve levels and likewise are not evident on the fracture surface.

At a test temperature of 290°C, J_M-R curve data for a thermal-aging condition of 450°C for 3000 h demonstrate significant reduction in toughness from the unaged condition (Fig. 83). In this case, the reductions in J level are fairly constant at ~ 40% for the entire range of Δa.

For the three aging conditions, higher test temperature results in lower J levels in all cases (Figs. 84 to 86). On a percentage basis, the reduction in J level is greatest for the 350°C aging condition and lowest for the 450°C aging condition. This result is in contrast to the trend demonstrated by unaged material (Fig. 73), where data at 290°C were higher than those at 25°C.

Direct comparison of data for the three aging conditions indicates that higher aging temperature results in reduced J_M-R curve levels. At a test temperature of 25°C (Fig. 87), a large reduction in J level occurs between aging at 350°C and aging at 400°C, with a smaller (additional) reduction evident with aging at 450°C (excluding the post-load-drop data). At a test temperature of 290°C (Fig. 88), data for aging at 400°C and 450°C tend to lie close together, whereas data for aging at 350°C are up to ~ 30% higher.

6.2.2 Heat 69 (CF3)

J_M-R curve results for this heat are summarized in Table 29.

As with Heat 68 (Fig. 73), data for the unaged condition of Heat 69 demonstrate higher toughness (or at least no reduction in toughness) at 290°C as compared to data at 25°C (Fig. 89). In this case, a large degree of variability is apparent for the data at 25°C, with the top of the cast slab yielding the higher of the two J_M-R curves at this temperature. The data at 290°C are likewise from the top of the cast slab.

Aging at 350°C for 3000 h results in elevated toughness from the unaged condition for this heat at 25°C (Fig. 90), in contrast to the reduced C_V levels (29% reduction) for this aging condition. The aged

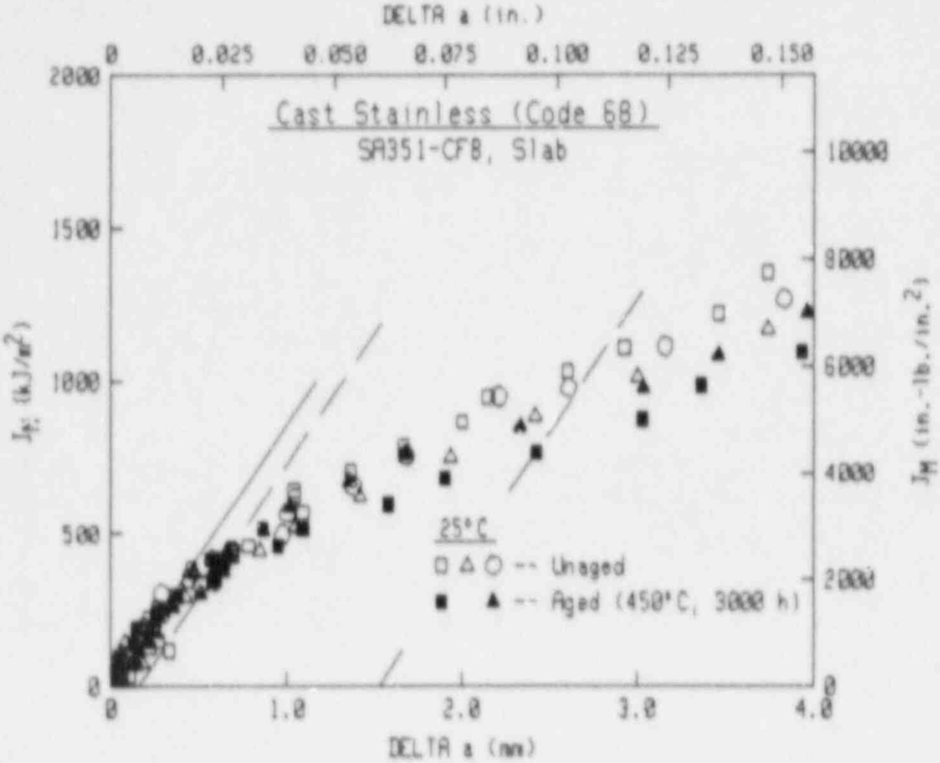

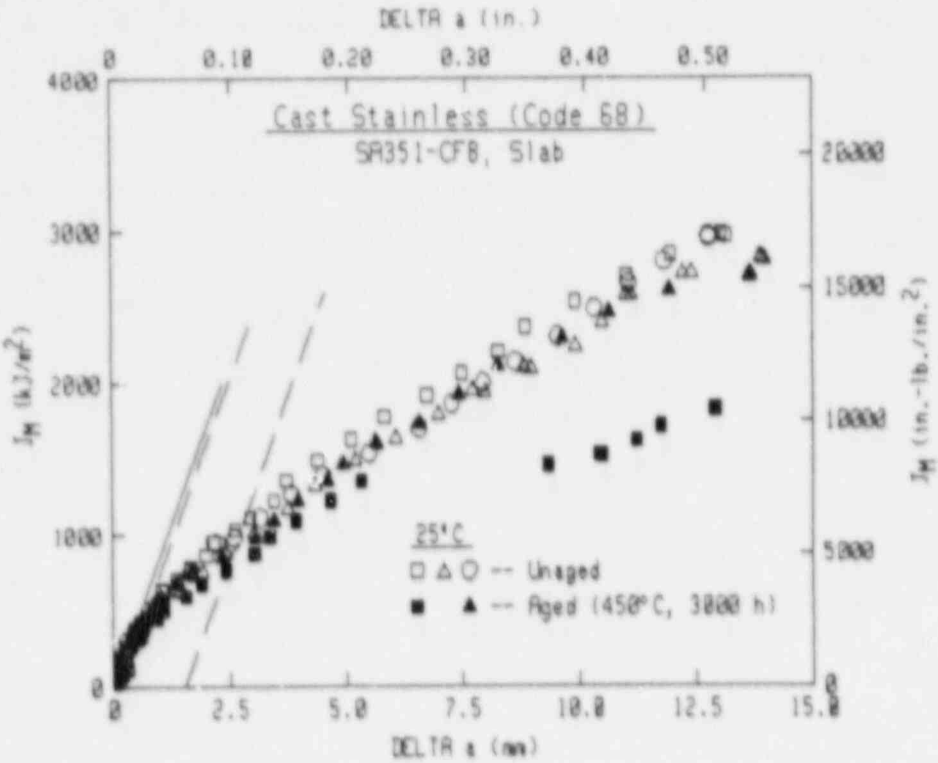

Fig. 80 For Heat 68 (grade CF8) at 25°C, thermal-aging at 450°C for 3000 h results in only a small decrease in toughness. For the lowest curve for aged material, a large load drop resulted in a crack jump of ~ 4 mm.

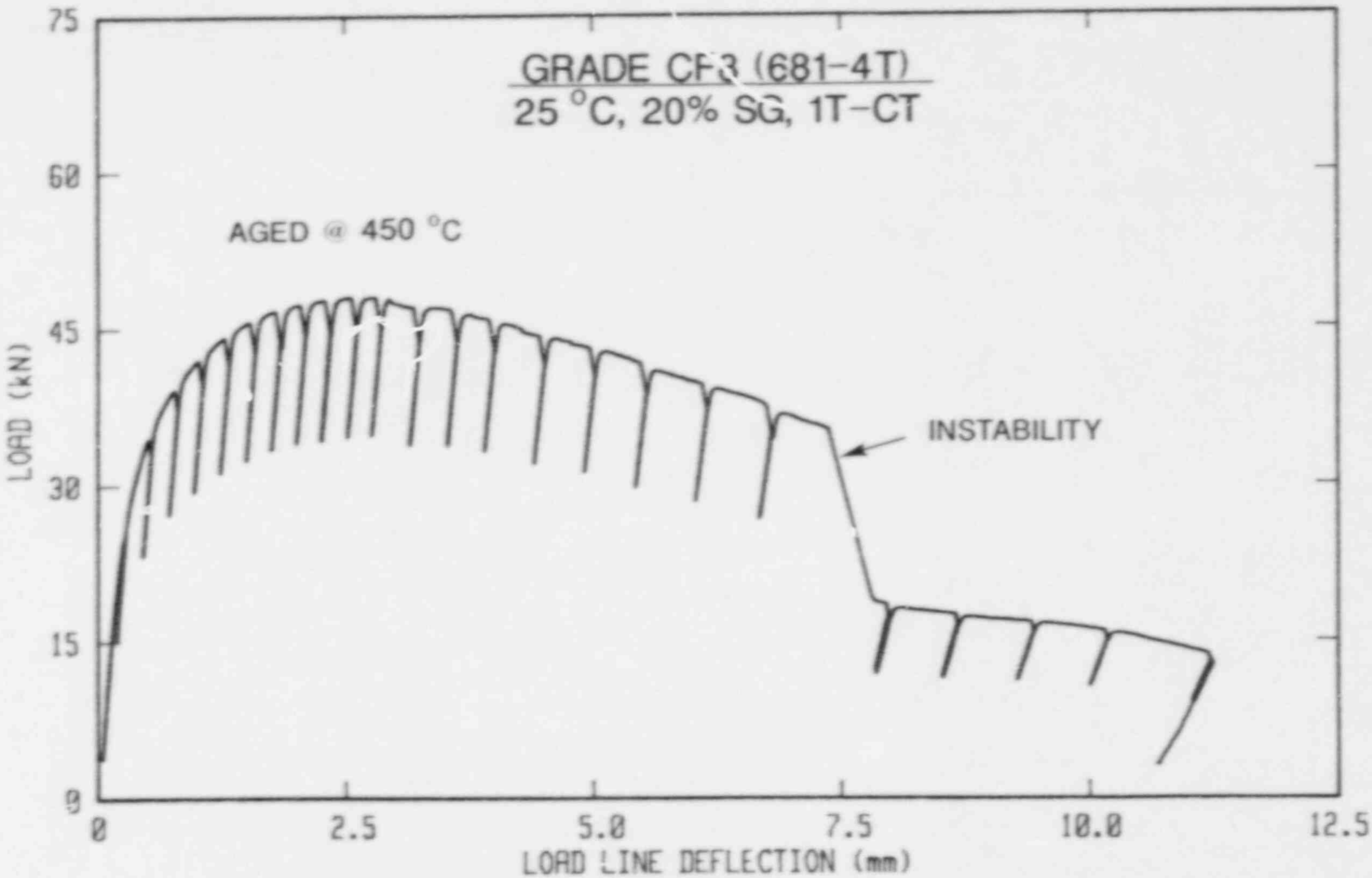

Fig. 81 The load-deflection curve for specimen 681-4T, thermally-aged at 450°C for 3000 h and tested at 25°C. The instability illustrated results in a crack jump of ~ 4 mm (0.16 in.)

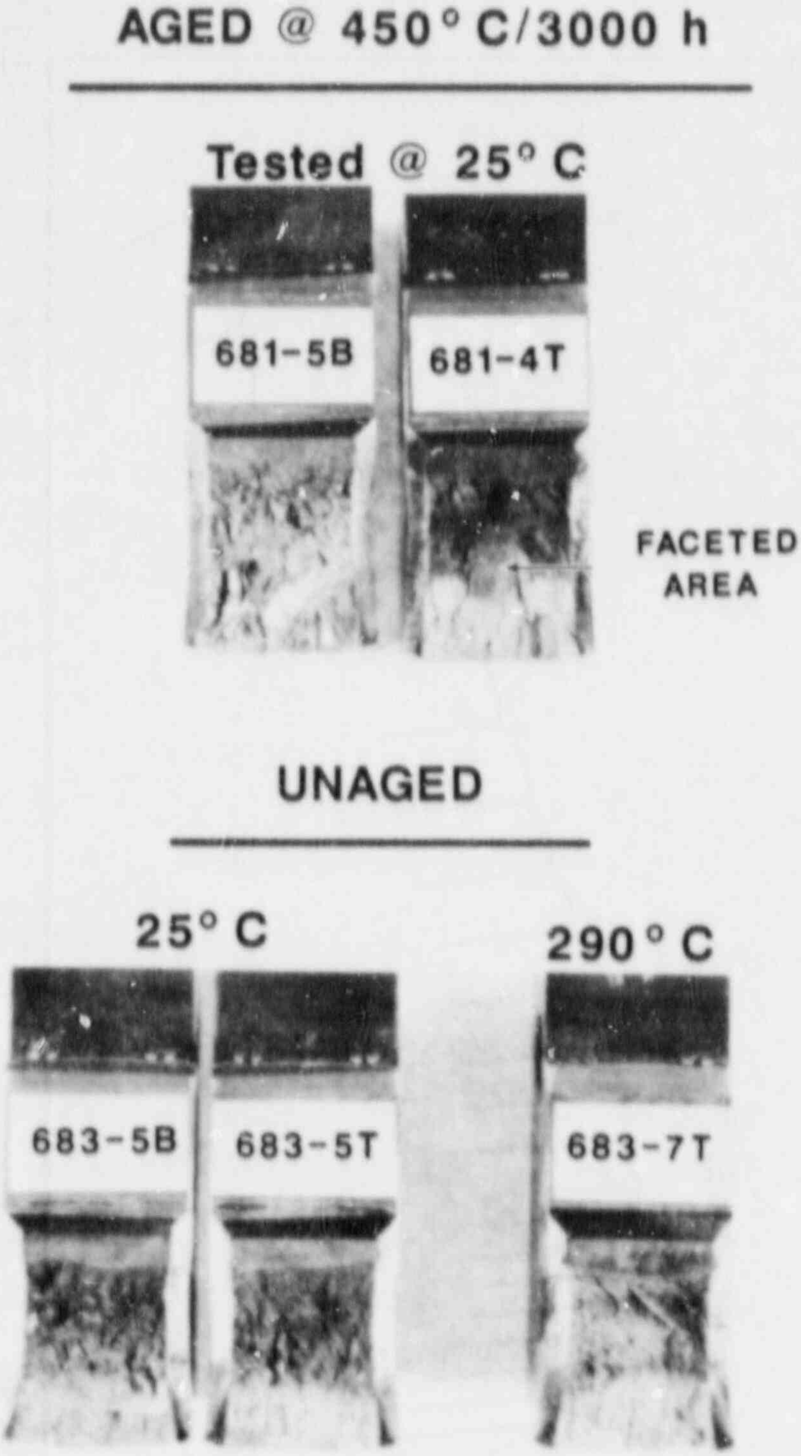

Fig. 82 The fracture surface for specimen 681-4T, as compared to those for other specimens, exhibits a faceted appearance not obvious on the other specimens.

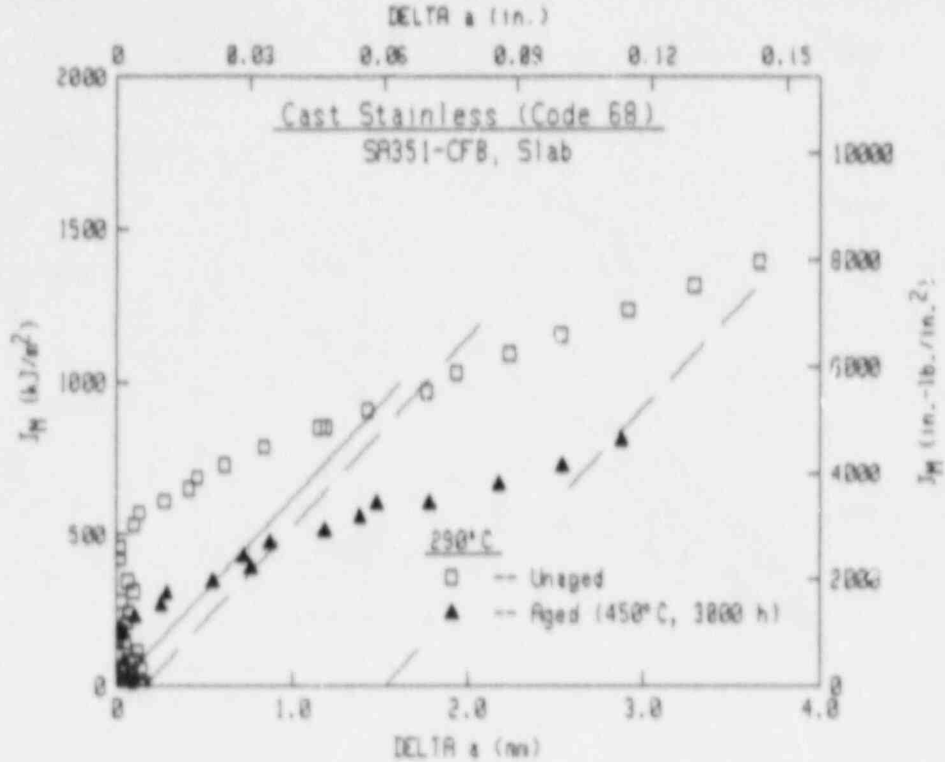

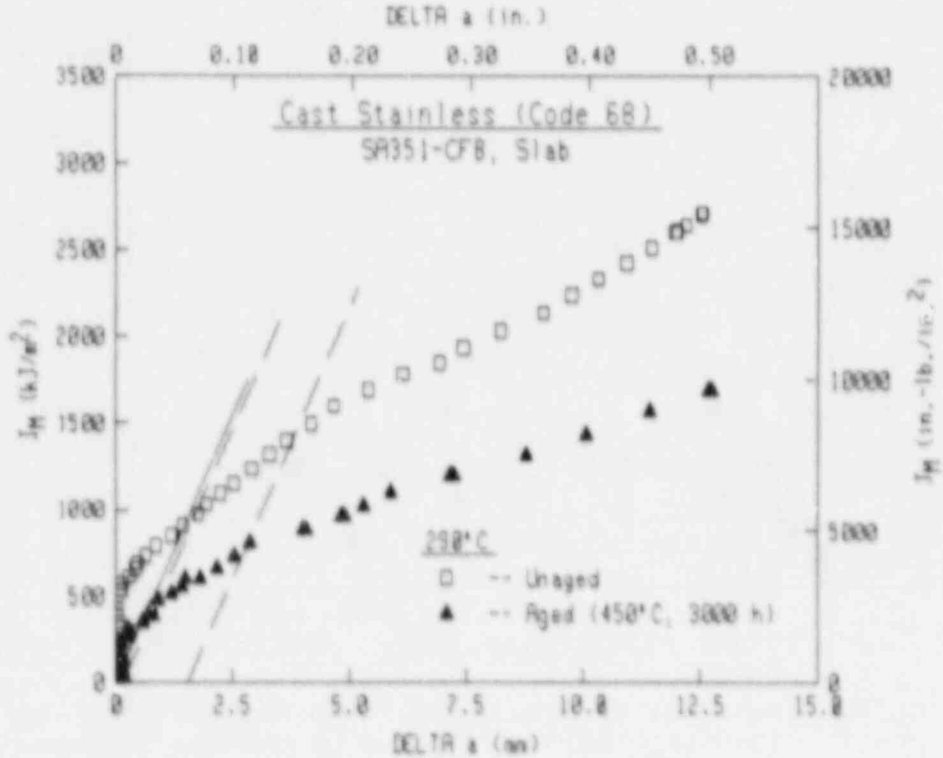

Fig. 83 For Heat 68 (grade CF8) at 290°C, thermal-aging at 450°C for 3000 h results in toughness reductions of ~ 40% in J level.

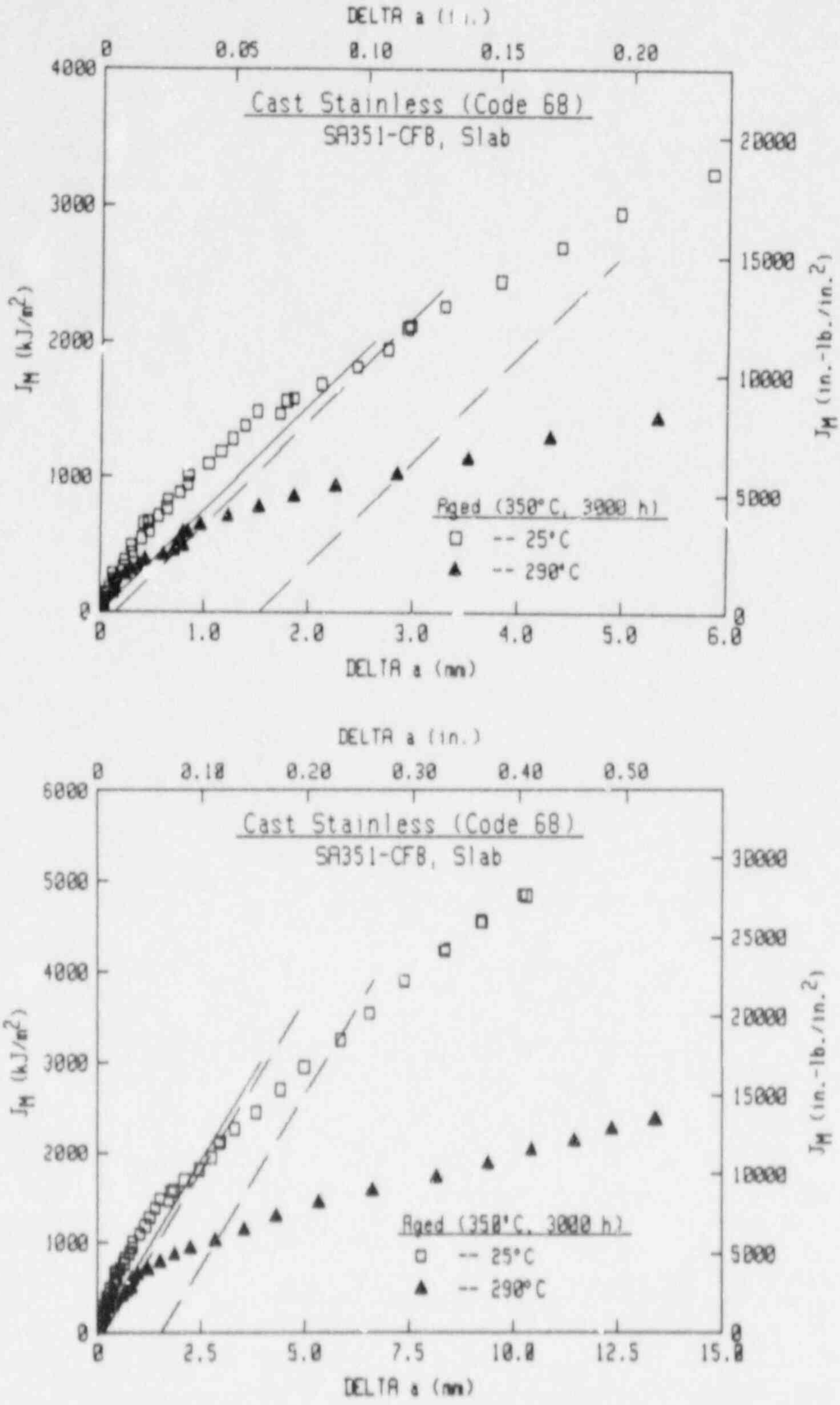

Fig. 84 For Heat 68 (grade CF8) with thermal-aging at 350°C for 3000 h, increasing the test temperature from 25°C to 290°C results in J-level reductions of ~ 50%.

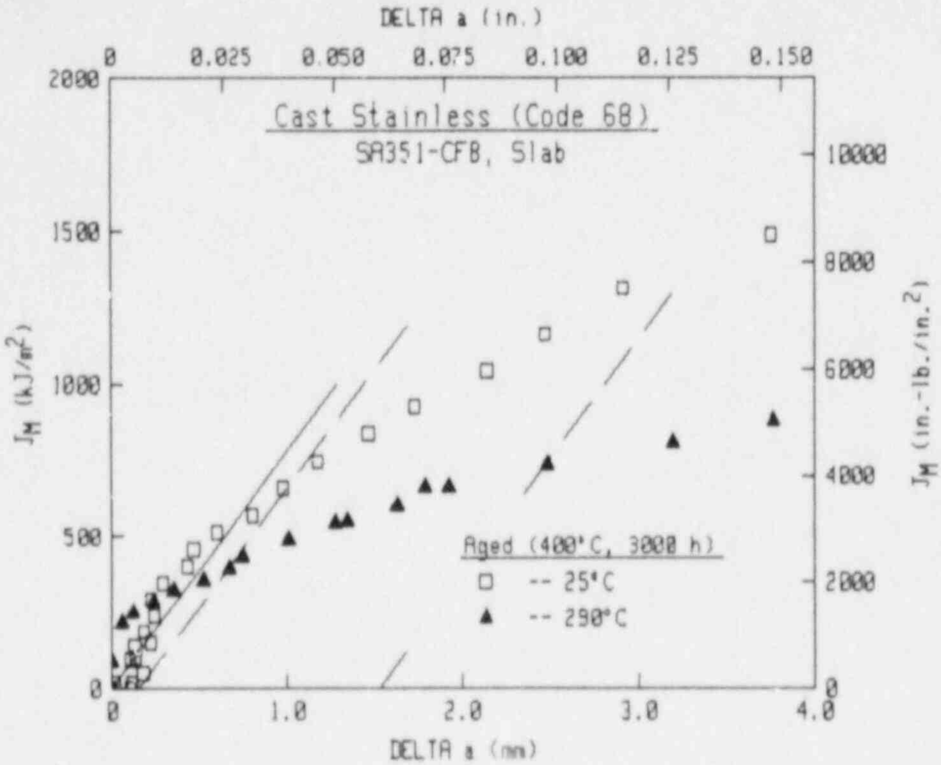

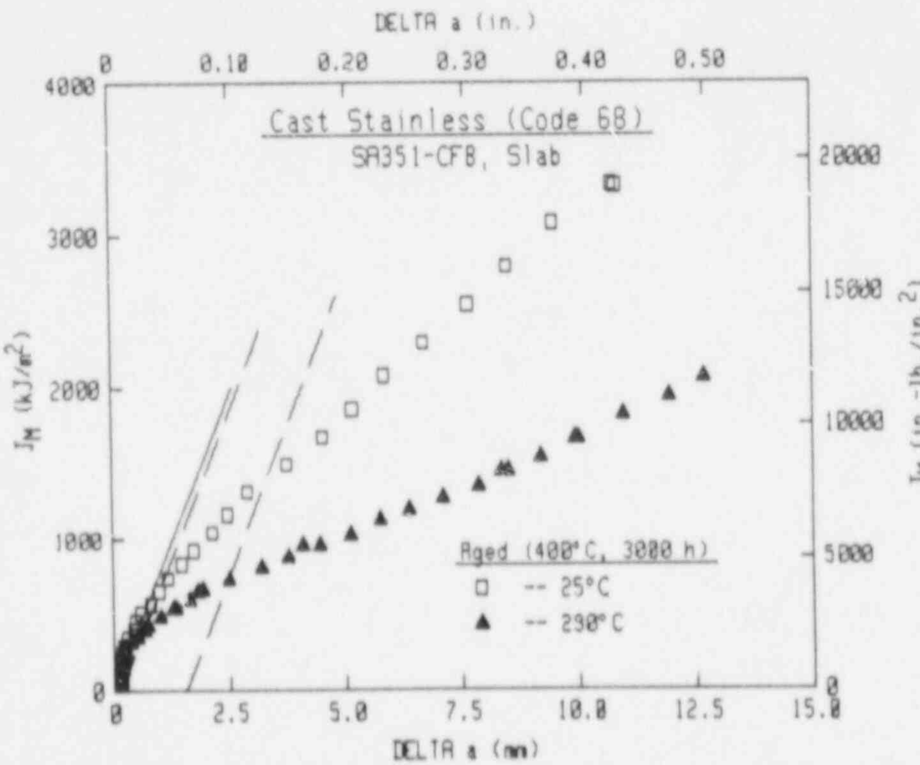

Fig. 85 For Heat 68 (grade CF8) with thermal-aging at 400°C for 3000 h, increasing the test temperature from 25°C to 290°C results in J levels reduced by ~ 40%.

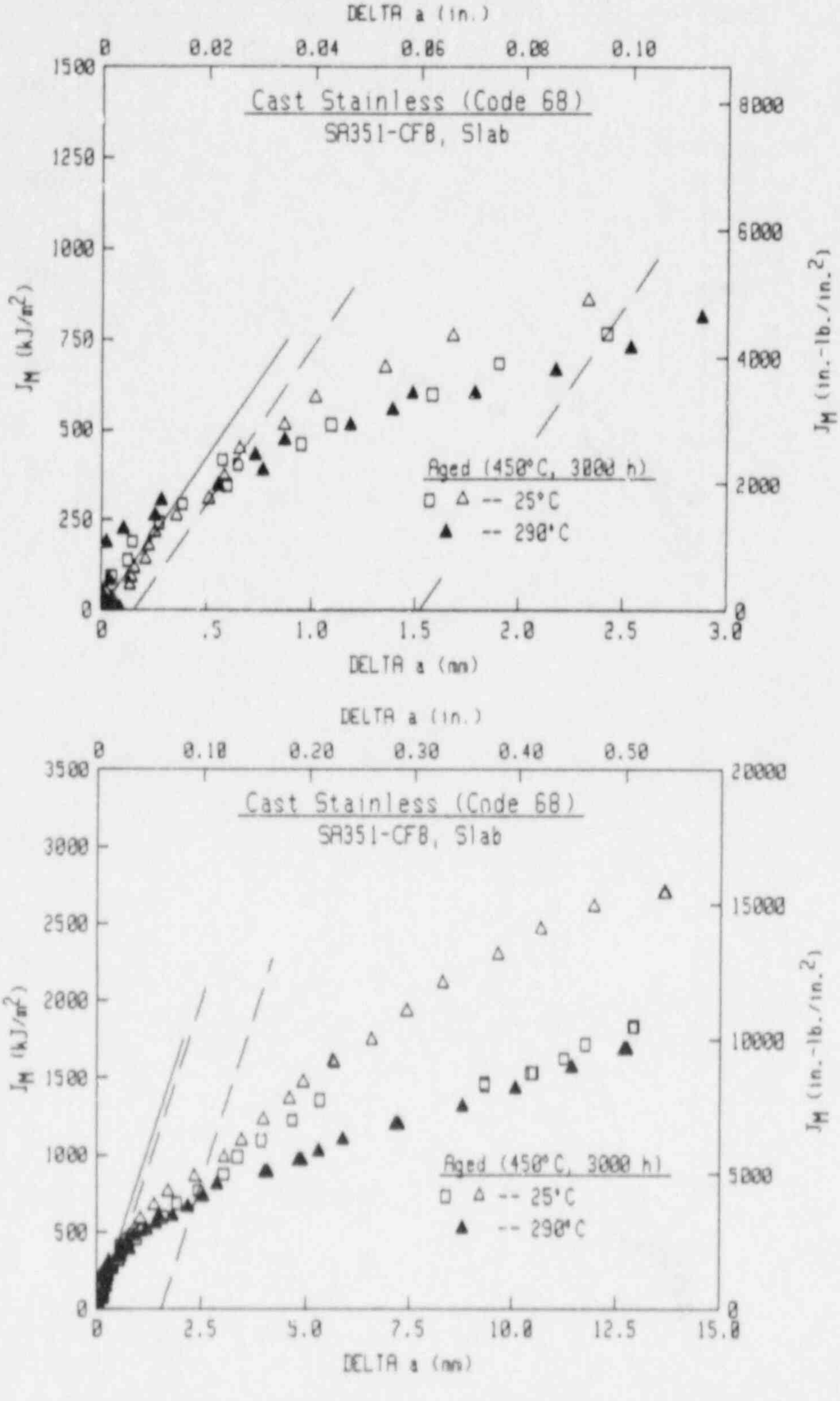

Fig. 86 For Heat 68 (grade CF8) with thermal-aging at 450°C for 3000 h, increasing the test temperature from 25°C to 290°C results in reduced J levels.

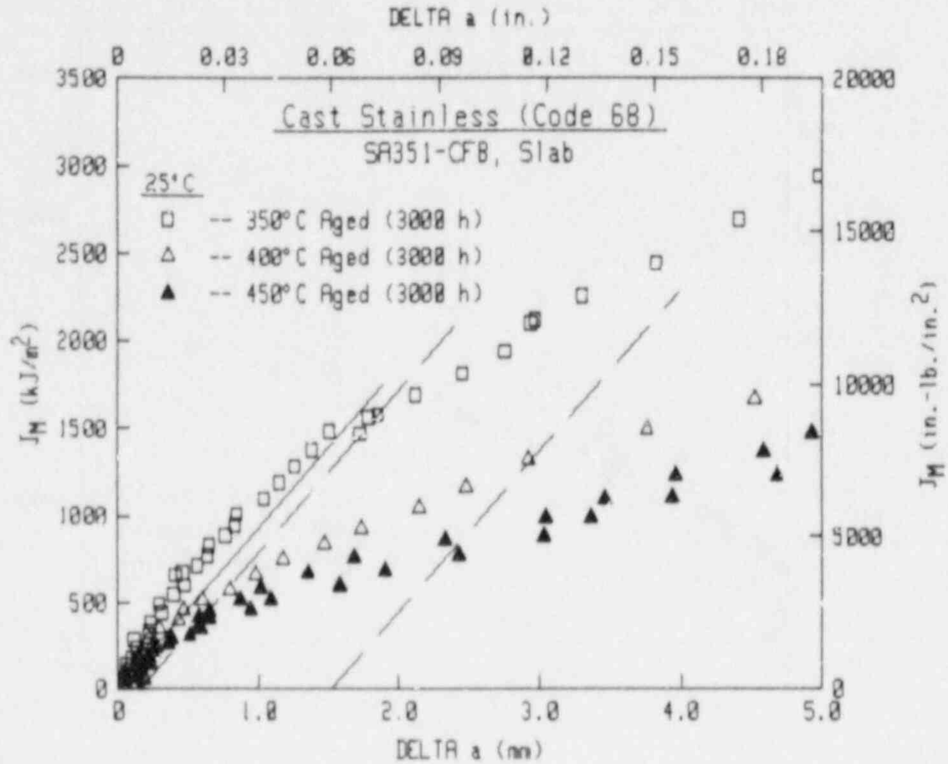

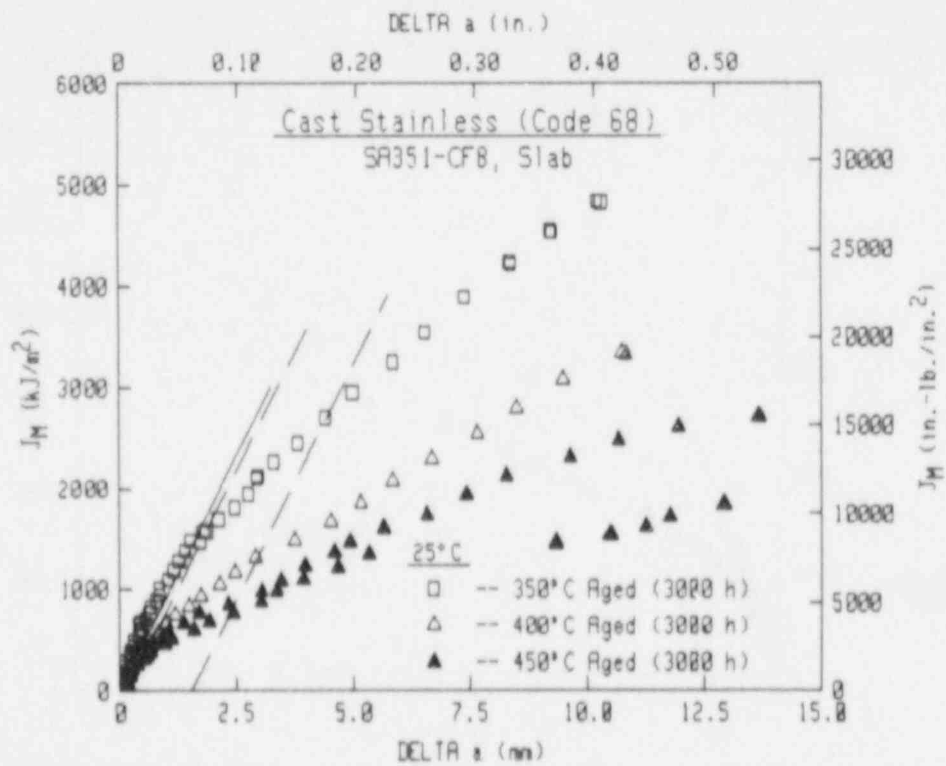

Fig. 87 For the thermally-aged conditions of Heat 68 (grade CF8) at 25°C, higher aging temperatures give successive reductions in J levels.

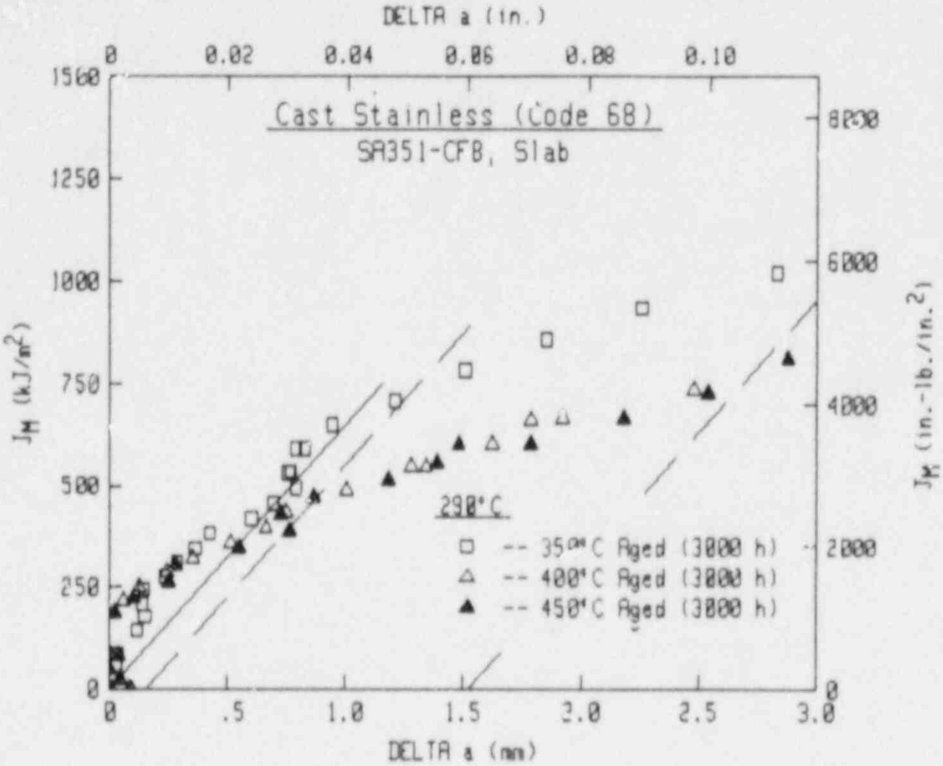

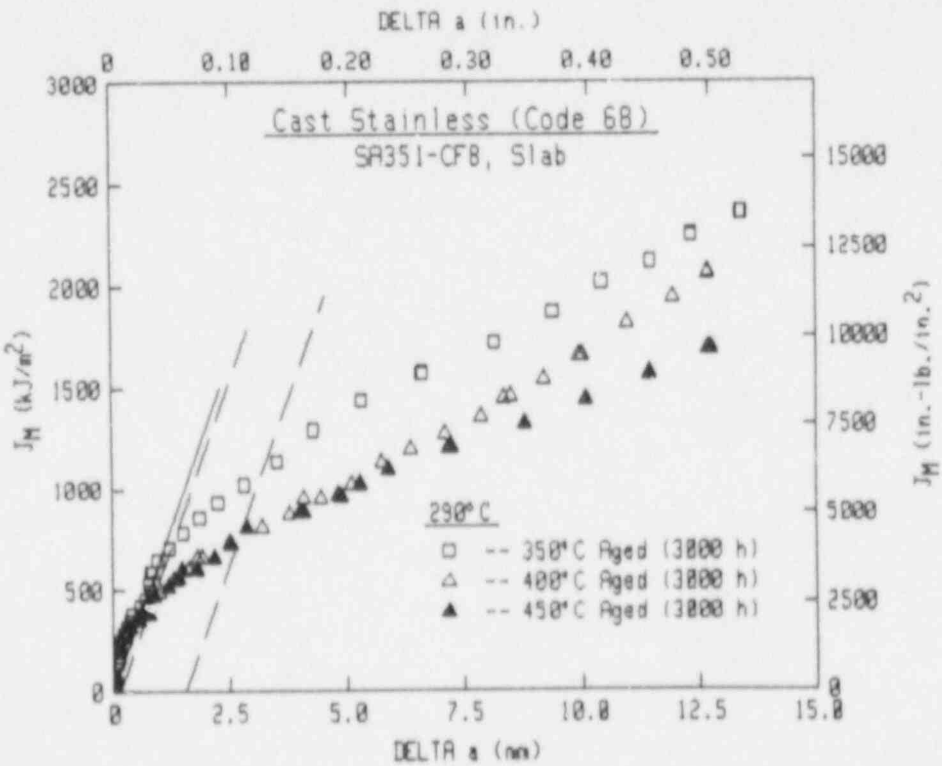

Fig. 88 For the thermally-aged conditions f Heat 68 (grade CF8) at 290°C, higher aging temperature tends to give lower J levels, although by smaller percentages than at 25°C.

Table 29 J-R Curve Results for Code 69 (Cast Stainless Steel Slab, SA351-CF3)

Specimen Number	Test Temp (°C)	$(a/W)_i$	Δa_m (mm)	$\Delta a_p - \Delta a_m$ (mm)	J_{Ic}		T_{avg}		C (kJ/m^2)	n	σ_f (MPa)	Aging Condition	
					MEA (kJ/m^2)	ASTM (kJ/m^2)	MEA	ASTM				Temp (°C)	Time (h)
692-8B	25	0.530	16.07	-2.35	249.4	225.1	267	274	422.6	0.6404	435.5	Unaged	
692-8T	25	0.537	14.60	-1.26	440.8	461.9	299	275	563.7	0.5893	435.5	Unaged	
691-4B	25	0.519	13.61	-1.14	1009.4	993.6	293	287	908.2	0.5058	467.7	350	3000
691-3B	25	0.514	13.65	-0.79	591.2	518.5	214	235	660.1	0.4508	469.1	400	3000
691-5B	25	0.517	14.04	-1.19	640.0	606.9	201	210	692.3	0.4208	472.7	450	3000
693-7T	290	0.532	14.50	-1.63	991.4	926.1	349	388	790.5	0.3860	301.4	Unaged	
691-6T	290	0.530	14.17	-1.20	530.9	520.0	327	309	530.1	0.4458	312.2	350	3000
691-5T	290	0.526	13.42	-0.95	314.3	305.0	325	314	384.8	0.5031	304.4	400	3000
691-3T	290	0.519	13.75	-0.98	325.6	310.2	243	262	391.7	0.4286	327.6	450	3000

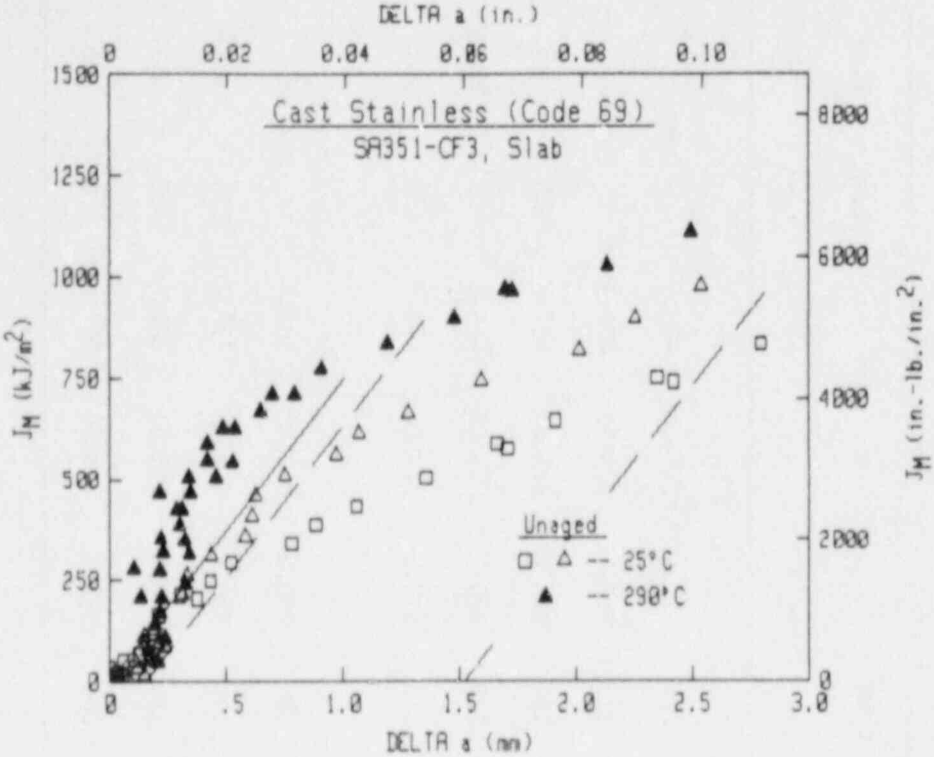

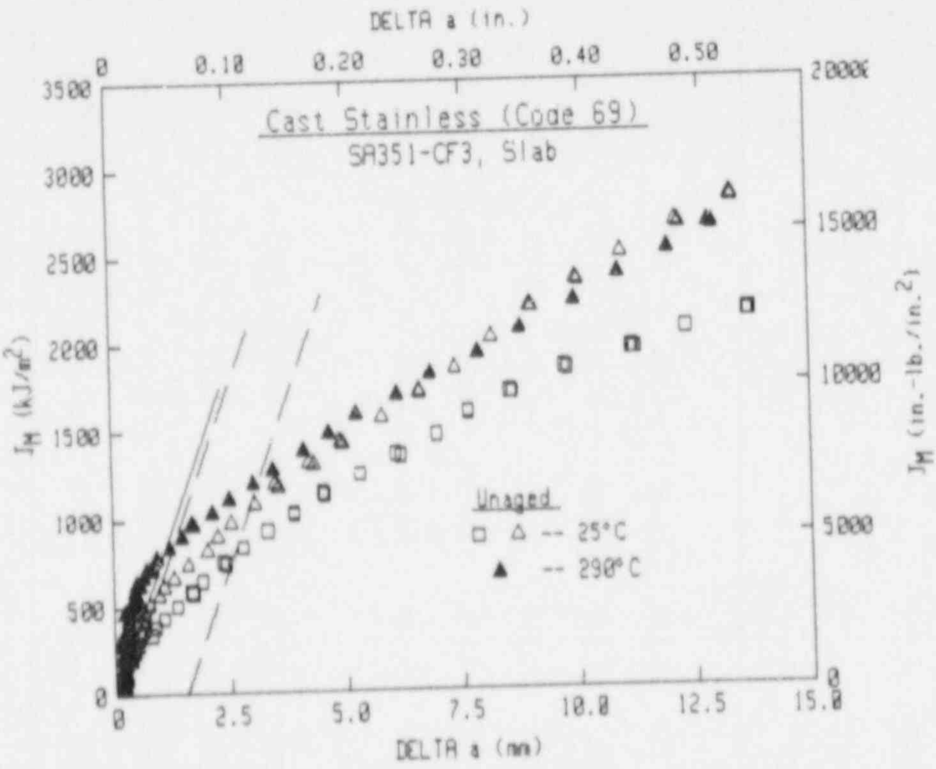

Fig. 89 For the unaged condition of Heat 69 (grade CF3) data at 290°C tend to be higher than those at 25°C.

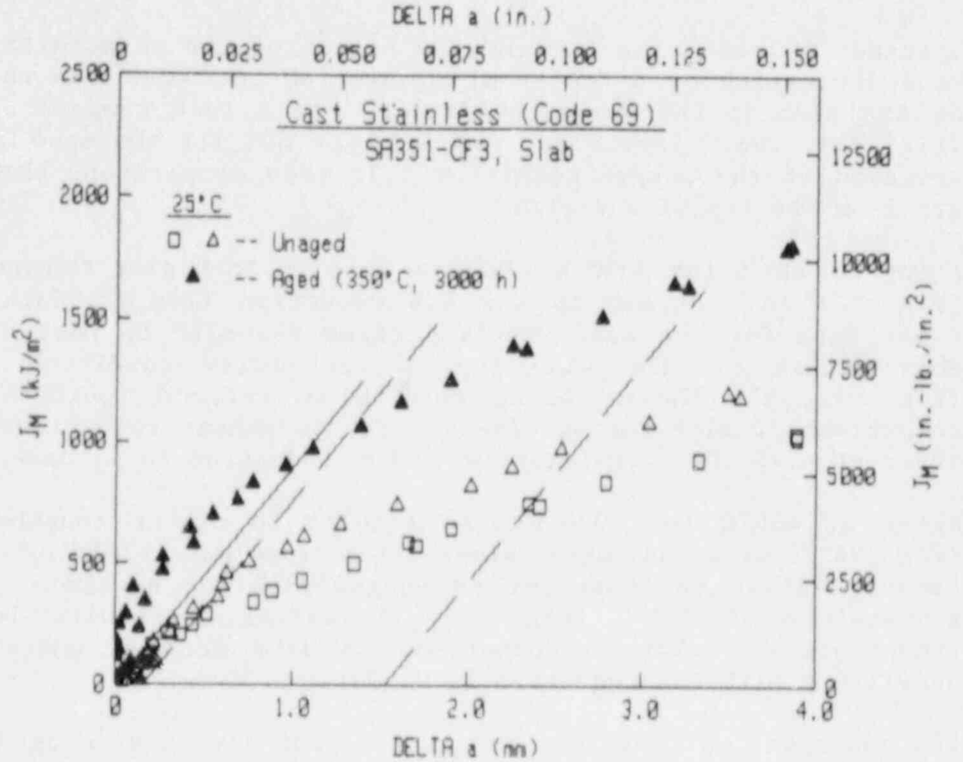

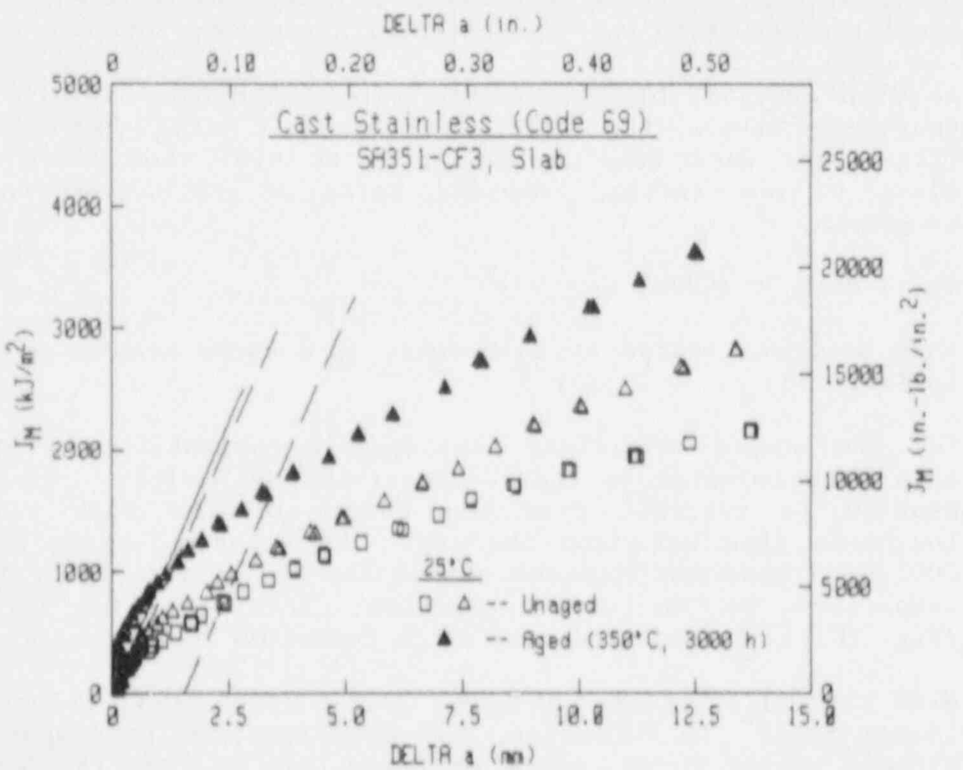

Fig. 90 For Heat 69 (grade CF3) at 25°C, thermal-aging at 350°C for 3000 h results in substantial increases in J levels from trends for unaged material.

specimen in this case is from the bottom of the slab, with the toughness increasing by a factor of almost two in comparison to the bottom of the slab in the unaged condition. At a test temperature of 290°C (Fig. 91), the J levels are reduced by ~ 30% for the aged condition as compared to the unaged condition. In this comparison, both specimens are from the top of the slab.

Aging at 400°C for 3000 h likewise results in higher toughness at 25°C (Fig. 92) in contrast to the 47% reduction from C_v data. In this case, data for the aged specimen (from the slab bottom) are slightly above those for the slab top in the unaged condition. At 290°C (Fig. 93), the thermal-aging results in reduced toughness for this comparison of slab-top specimens. The toughness reductions are on the order of ~ 40-50%, consistent with the reduction in C_v data.

Aging at 450°C for 3000 h also results in higher toughness at 25°C (Fig. 94), with an aged slab-bottom specimen yielding J_M-R curve trends similar to those for an unaged slab-top specimen. At a test temperature of 290°C (Fig. 95), thermal-aging results in toughness reductions of ~ 50% in comparison to data from an unaged specimen, consistent with the reduction in C_v data.

In contrast to results for this heat in the unaged condition (Fig. 89), the three aging conditions demonstrate reduced toughness with higher test temperature (Figs. 96 to 98). The toughness reductions are uniformly on the order of 50%, unlike trends for Heat 68 where the reduction was a function of aging temperature.

As with Heat 68, higher thermal-aging temperature results in reduced toughness levels for Heat 69. At 25°C (Fig. 99) and at 290°C (Fig. 100), data from thermal-aging at 400°C and 450°C tend to be close to one another, whereas aging at 350°C results in higher toughness.

6.2.3 Heat 70 (CF8M)

This heat was tested at 25°C only; J_M-R curve results are summarized in Table 30.

For the unaged condition, considerable variability is apparent for this heat, similar to that demonstrated by Heat 69. In the case of Heat 70, a specimen from the bottom of the slab yields higher toughness than one from the top. With thermal-aging at 350°C for 3000 h, a specimen from the top of the slab gives higher toughness in comparison to an unaged specimen from the top of the slab (Fig. 101). C_v data indicate a 12% reduction in this case.

With thermal-aging at 400°C for 3000 h (Fig. 102), reduced toughness is apparent. In this case, the aged specimen is comparable to the highest unaged curve since each specimen is from the bottom of the slab. C_v data indicate a moderate reduction (30%) in this case.

With thermal-aging at 450°C for 3000 h (Fig. 103), little variability is apparent between specimens from the top and the bottom of the slab,

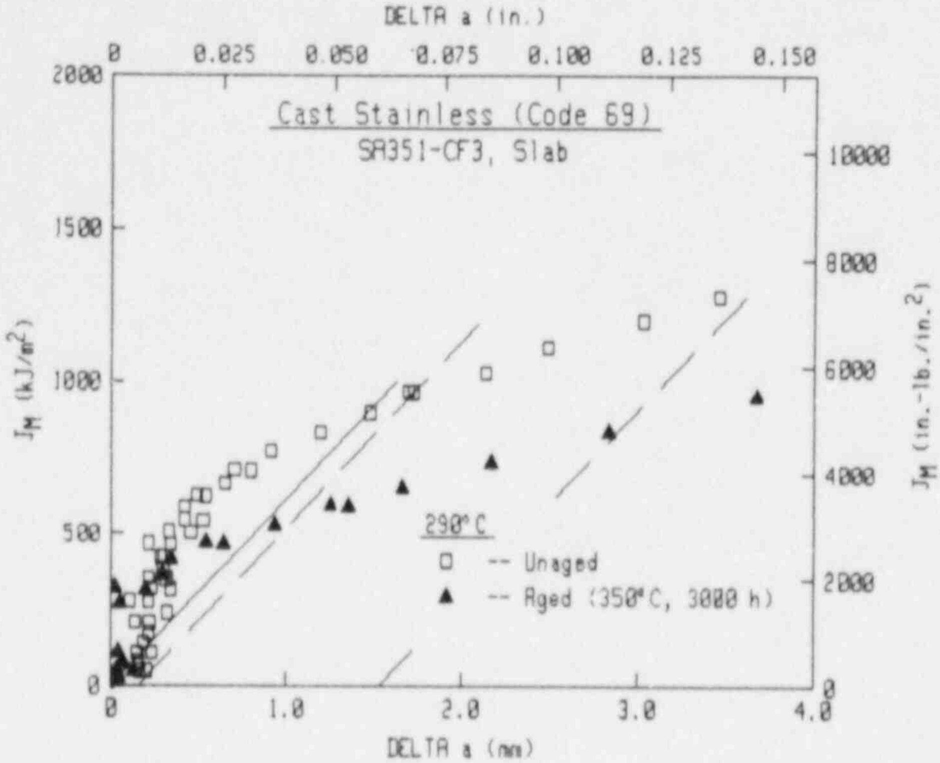

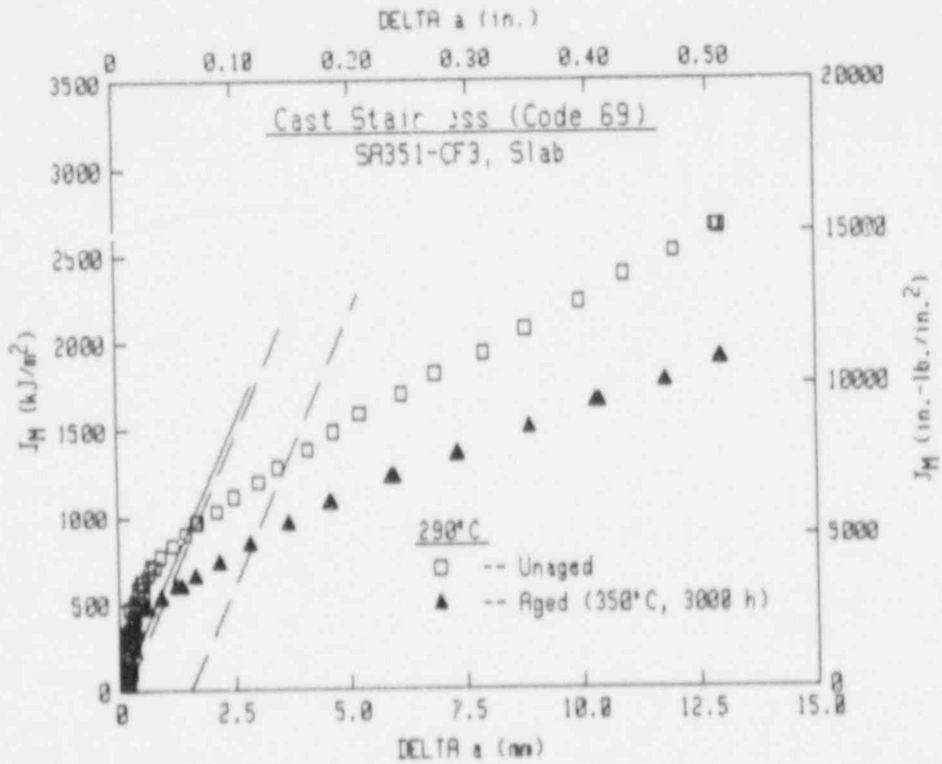

Fig. 91 For Heat 69 (grade CF3) at 290°C, thermal-aging at 350°C for 3000 h results in reductions in J levels of ~ 30%.

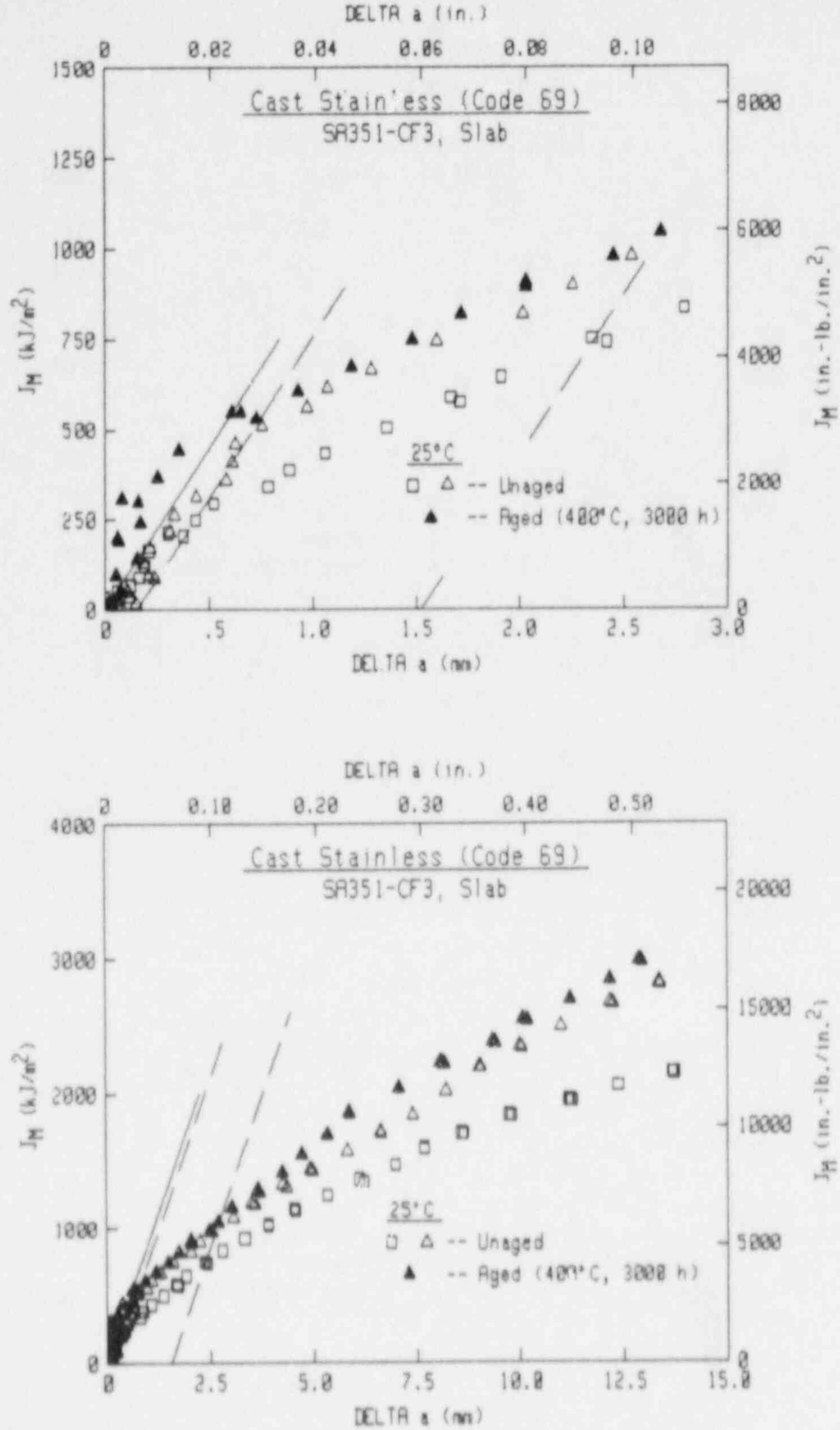

Fig. 92 For Heat 69 (grade CF3) at 25°C, thermal aging at 400°C for 3000 h results in slight elevations in J levels from trends for unaged material.

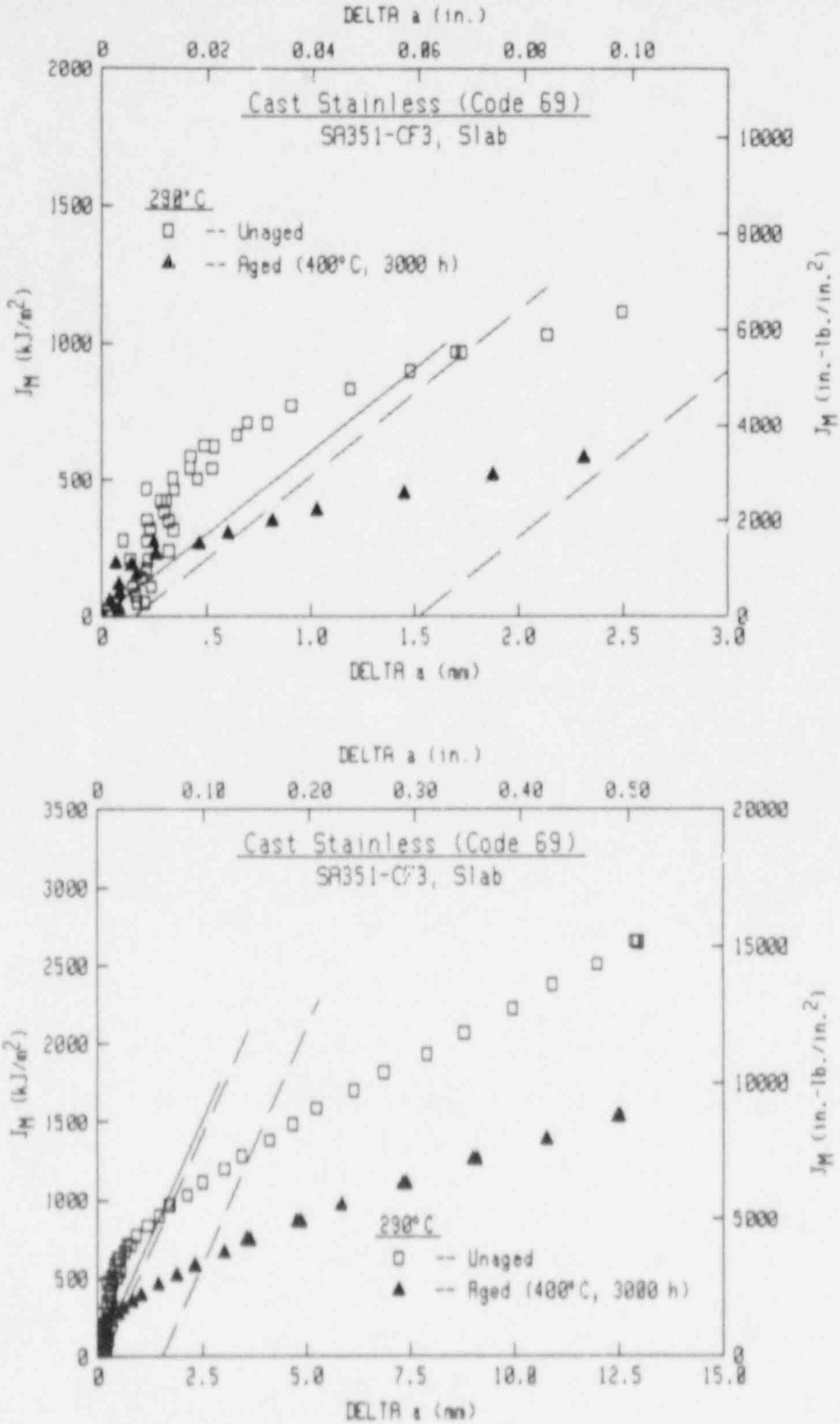

Fig. 93 For Heat 69 (grade CF3) at 290°C, thermal-aging at 400°C for 3000 h results in substantial reductions in J levels, of ~ 40%.

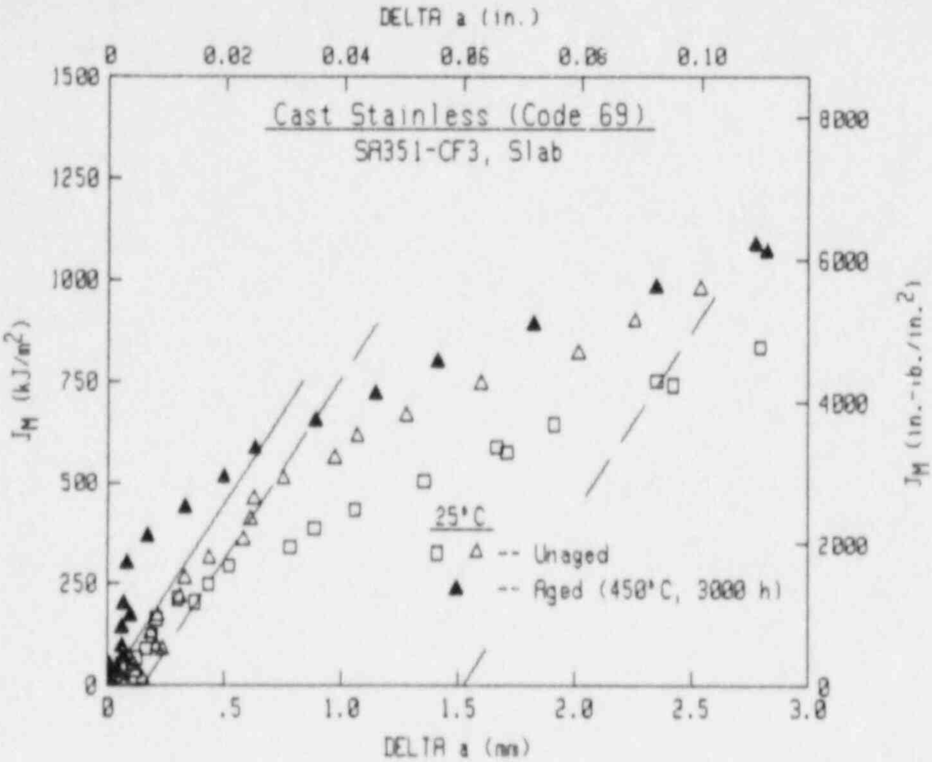

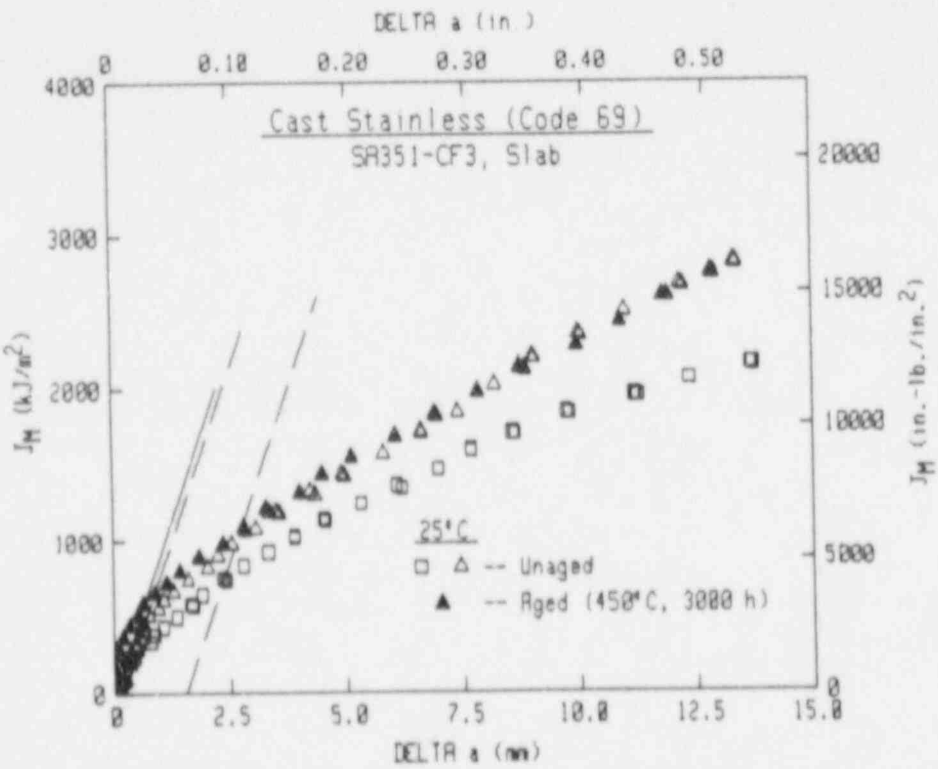

Fig. 94 For Heat 69 (grade CF3) at 25°C, thermal-aging at 450°C for 3000 h results in only a small elevation in J levels from trends for unaged material.

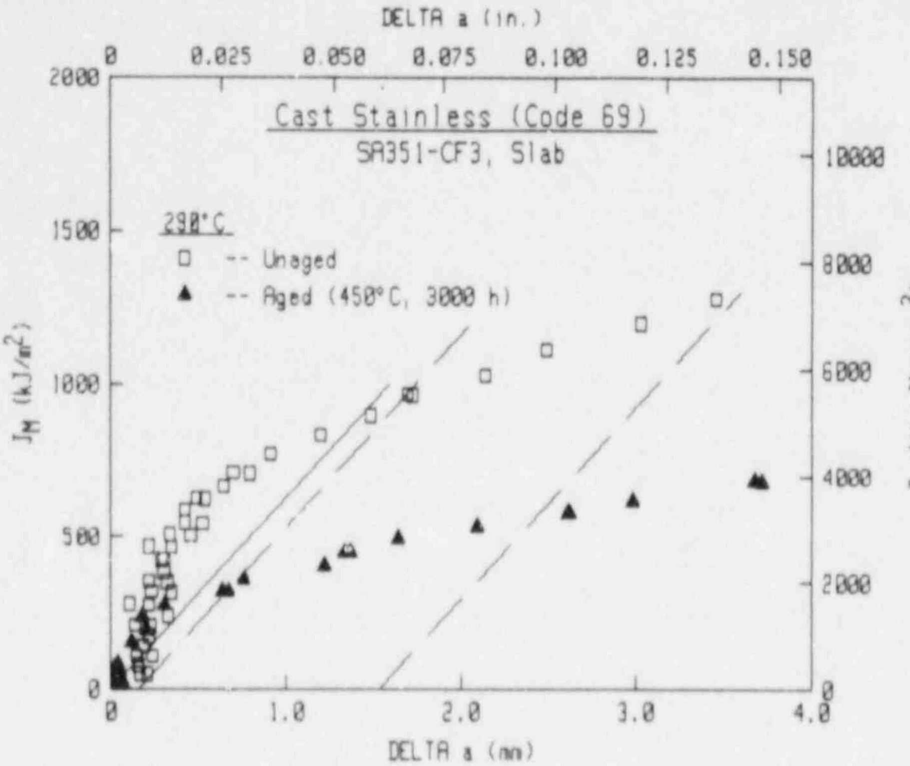

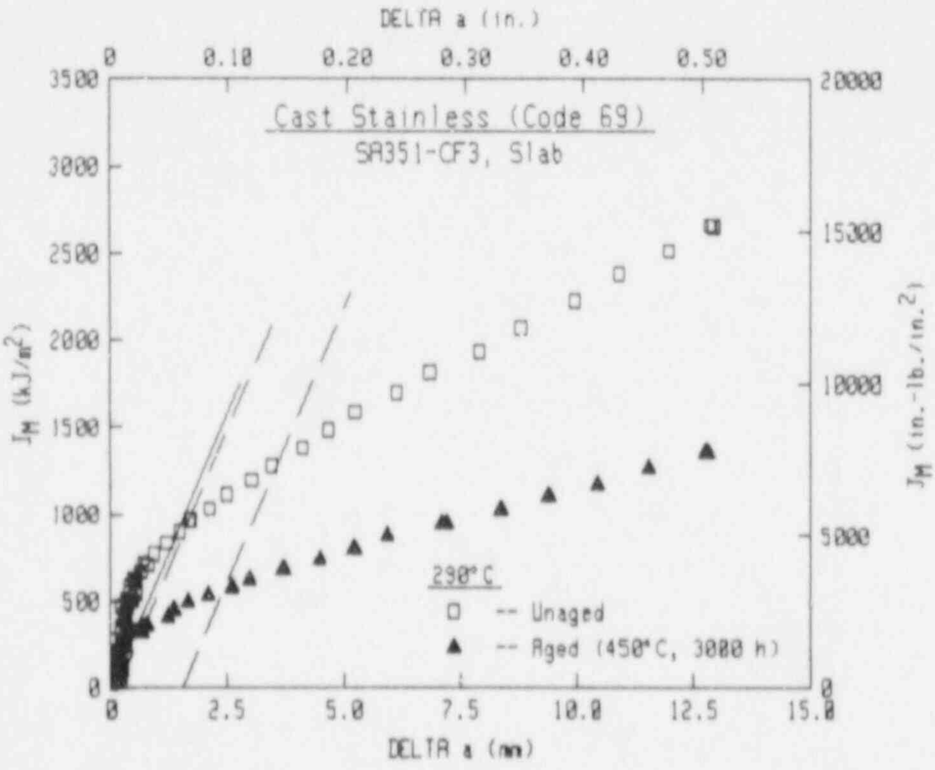

Fig. 95 For Heat 69 (grade CF3) at 290°C, thermal-aging at 450°C for 3000 h results in substantial reductions in J level, of ~ 50%.

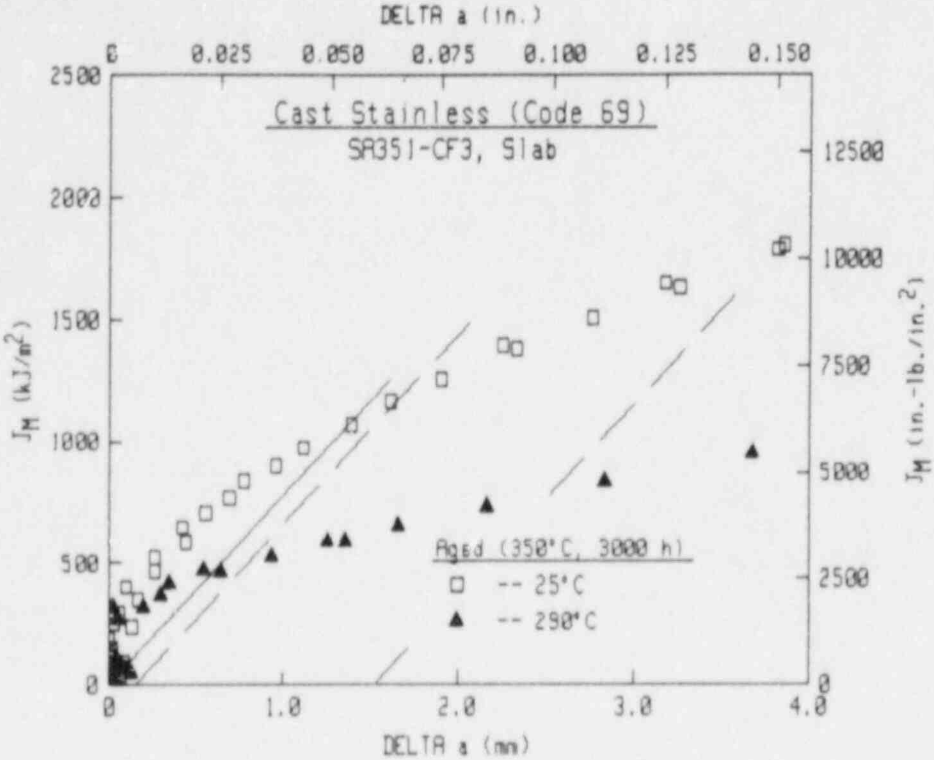

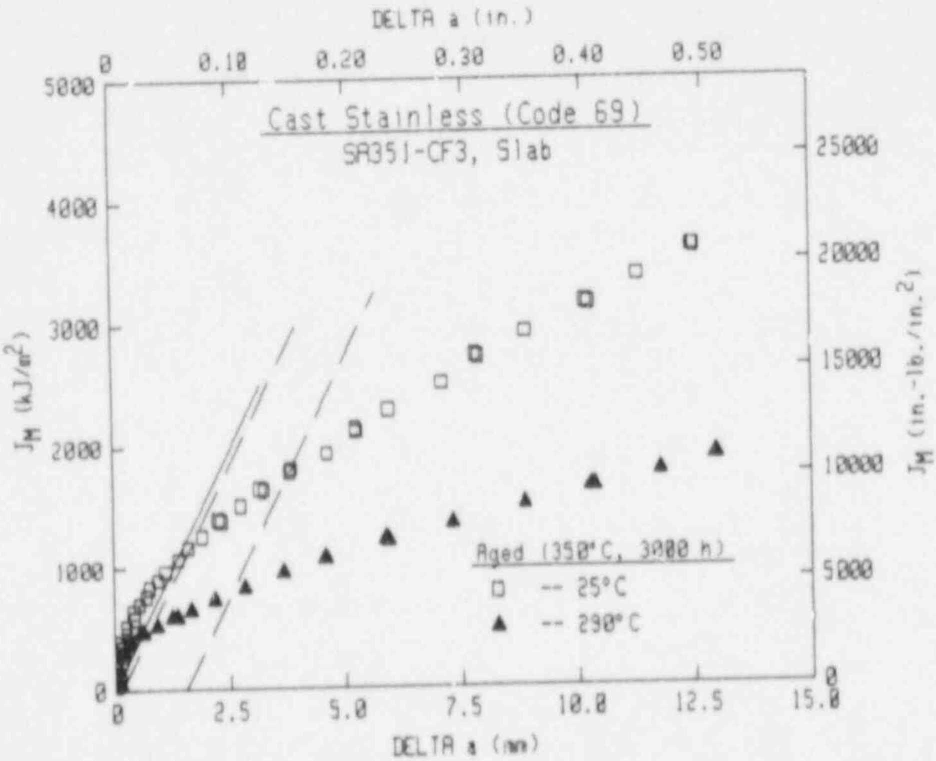

Fig. 96 For Heat 69 (grade CF3) with thermal-aging at 350°C for 3000 h, increasing the test temperature from 25°C to 290°C results in J level reductions of ~ 50%.

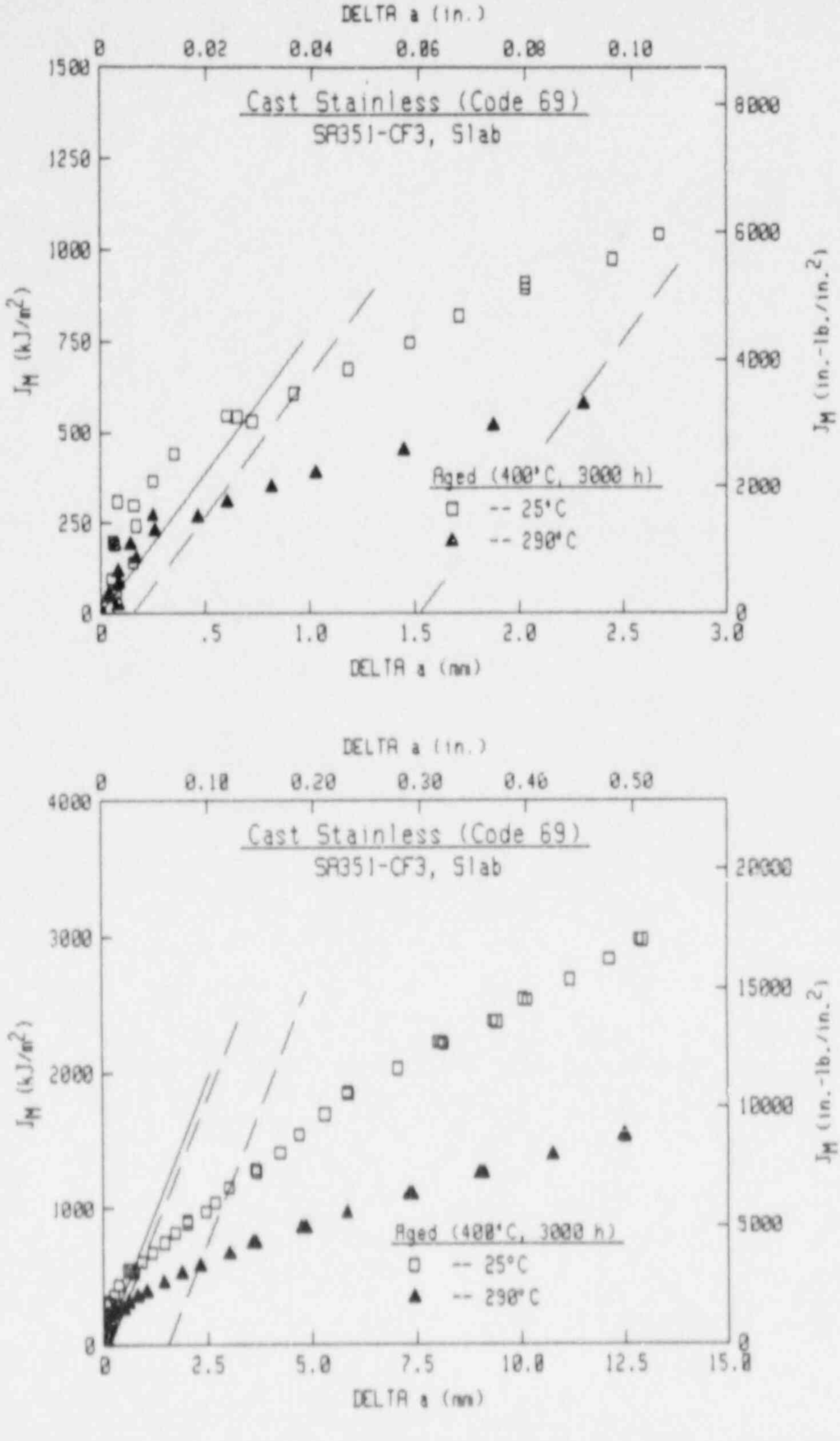

Fig. 97 For Heat 69 (grade CF3) with thermal-aging at 400°C for 3000 h, increasing the test temperature from 25°C to 290°C results in J level reductions of ~ 50%.

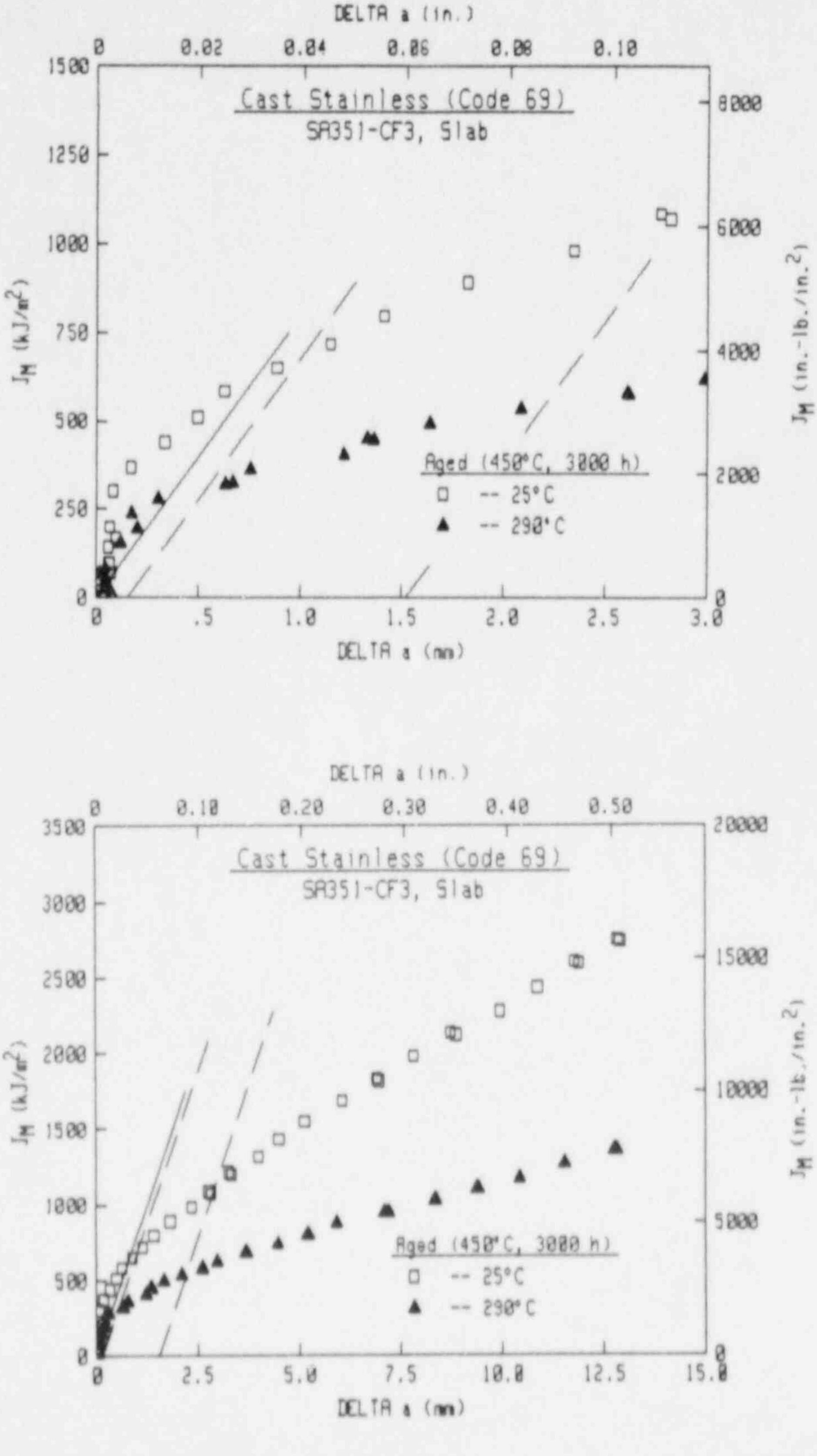

Fig. 98 For Heat 69 (grade CF3) with thermal-aging at 450°C for 3000 h, increasing the test temperature from 25°C to 290°C results in J level reductions of ~ 50%.

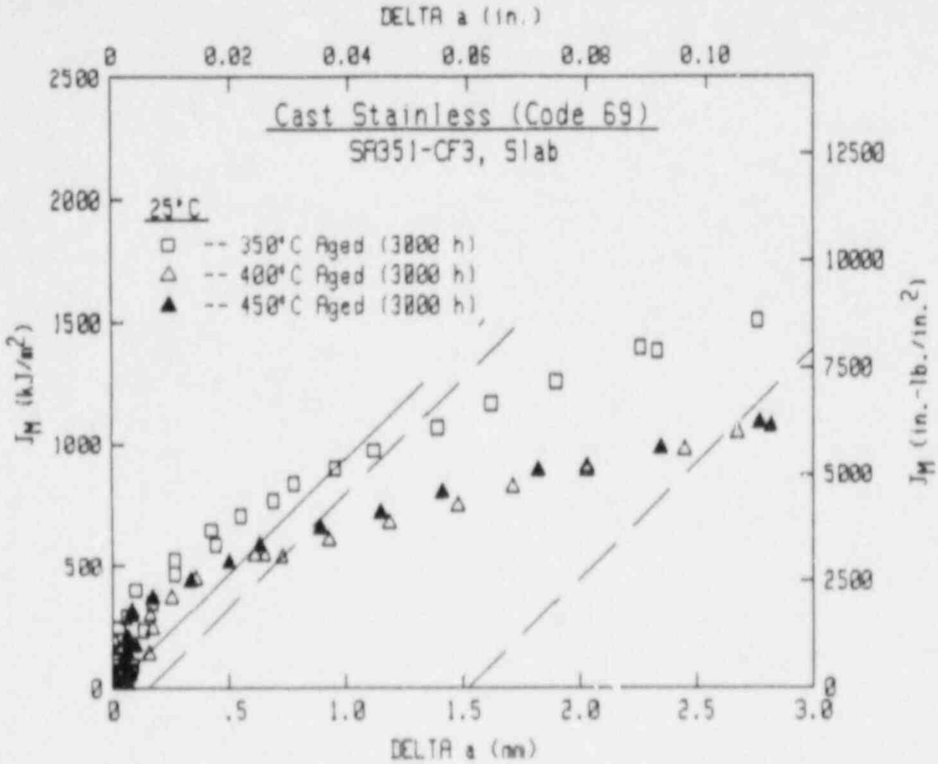

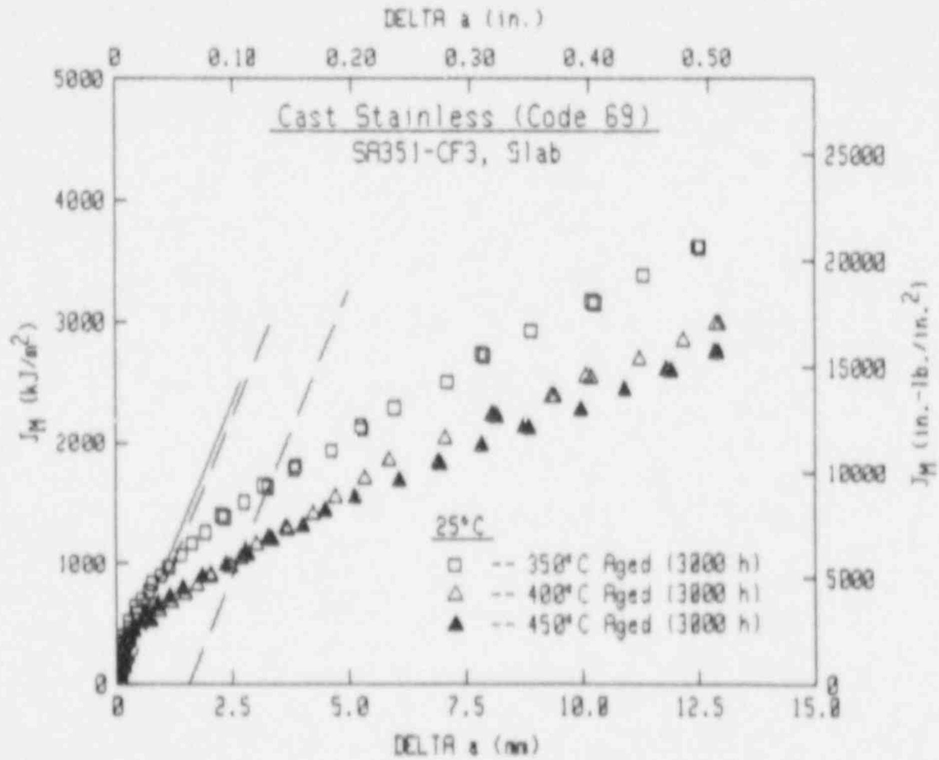

Fig. 99 For the thermally-aged conditions of Heat 69 (grade CF3) at 25°C, higher aging temperature gives lower J_M-R curve levels.

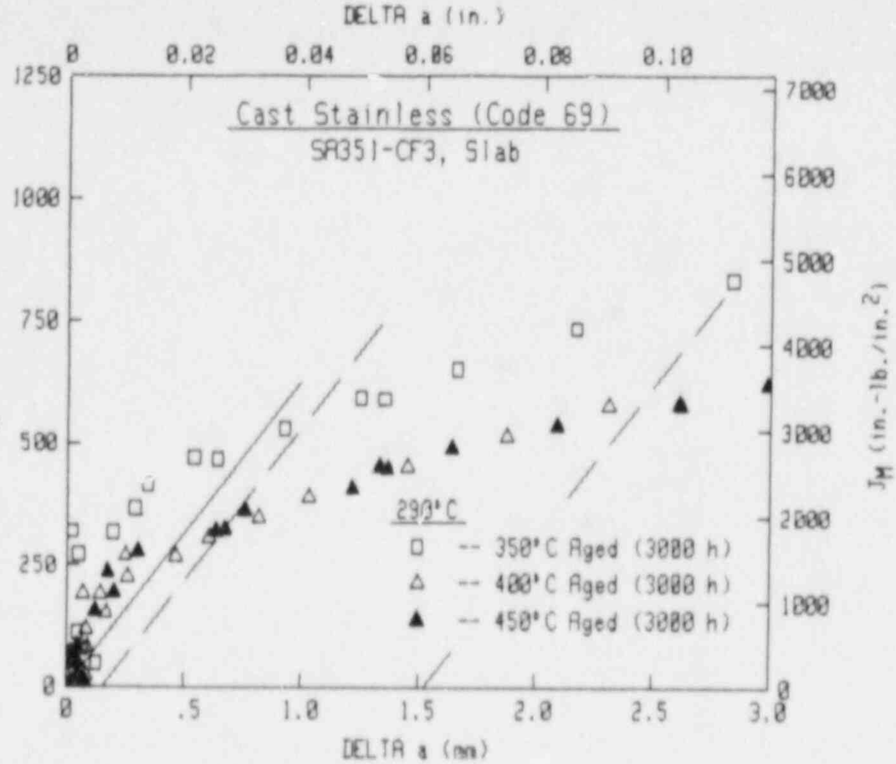

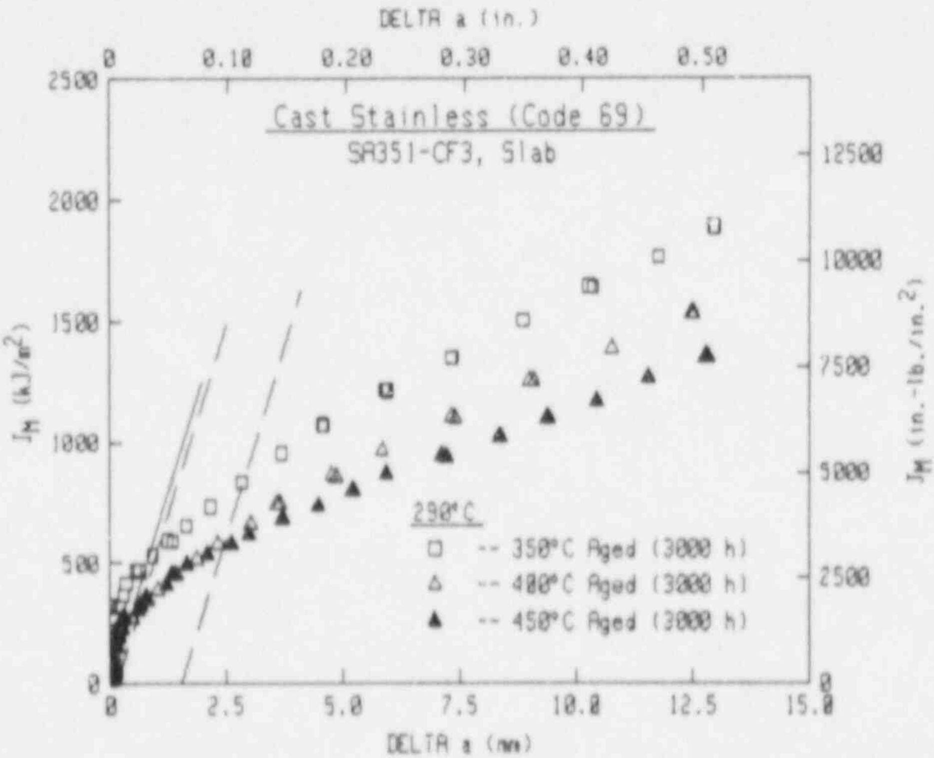

Fig. 100 For the thermally-aged conditions of Heat 69 (grade CF3) at 290°C, higher aging temperature gives lower J_M-R curve levels.

Table 30 J-R Curve Results for Code 70 (Cast Stainless Steel Slab, SA351-CF8M)

Specimen Number	Test Temp	$(a/W)_i$	Δa_m	$\Delta a_p - \Delta a_m$	J_{Ic}		T_{avg}		C	n	σ_f	Aging Condition	
					MEA	ASTM	MEA	ASTM				Temp	Time
	(°C)		(mm)	(mm)	(kJ/m^2)	(kJ/m^2)			(kJ/m^2)		(MPa)	(°C)	(h)
743-5B	25	0.528	14.71	-2.11	967.4	925.7	335	344	833.1	0.4819	399.6	Unaged	
743-5T	25	0.523	14.04	-1.60	789.8	780.4	258	256	748.7	0.4036	399.6	Unaged	
741-6T	25	0.532	14.31	-1.76	1073.7	1102.7	284	265	915.4	0.4158	408.5	350	3000
741-3B	25	0.514	15.18	-2.83	507.8	493.8	234	236	581.0	0.4591	428.2	400	3000
741-5B	25	0.533	13.74	-0.83	291.7	264.3	220	230	424.9	0.5286	431.2	450	3000
741-3T	25	0.522	14.57	-1.49	430.2	421.8	215	225	523.0	0.4557	431.2	450	3000

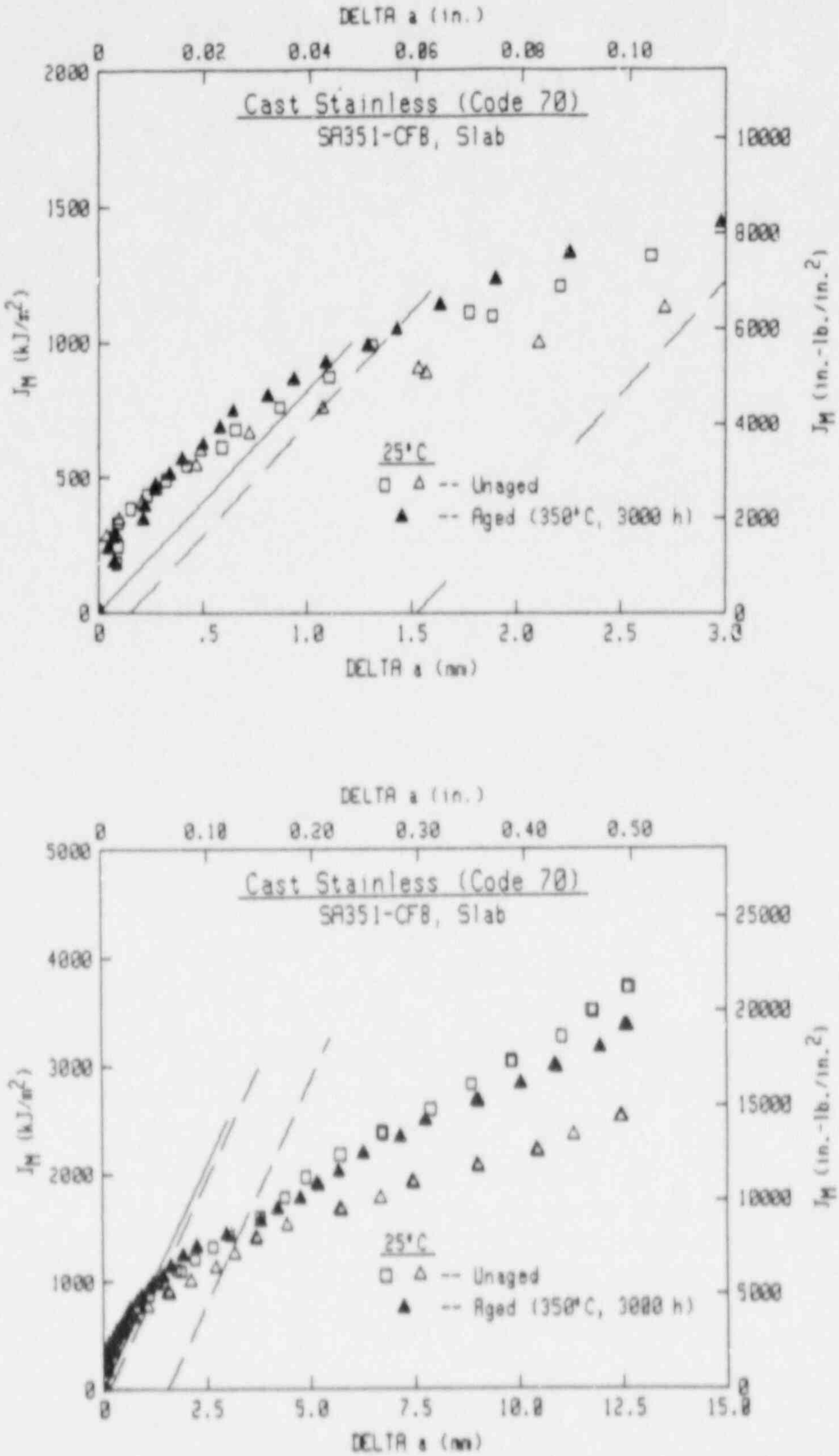

Fig. 101 For Heat 70 (grade CF8M) at 25°C, thermal-aging at 350°C for 3000 h results in no significant change in J_M-R curve trends.

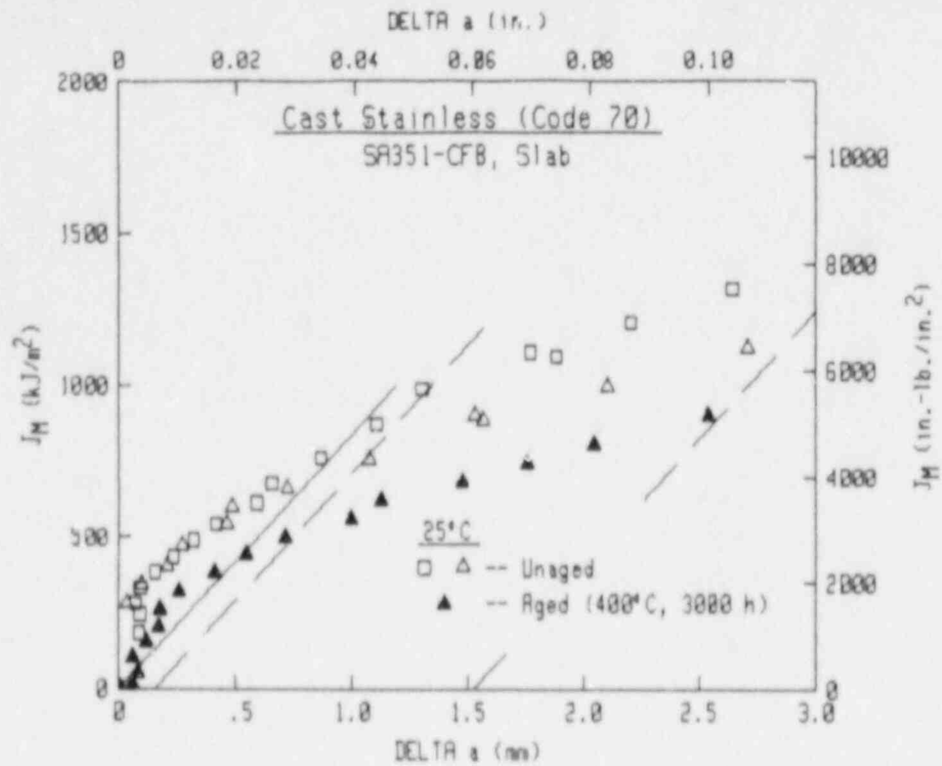

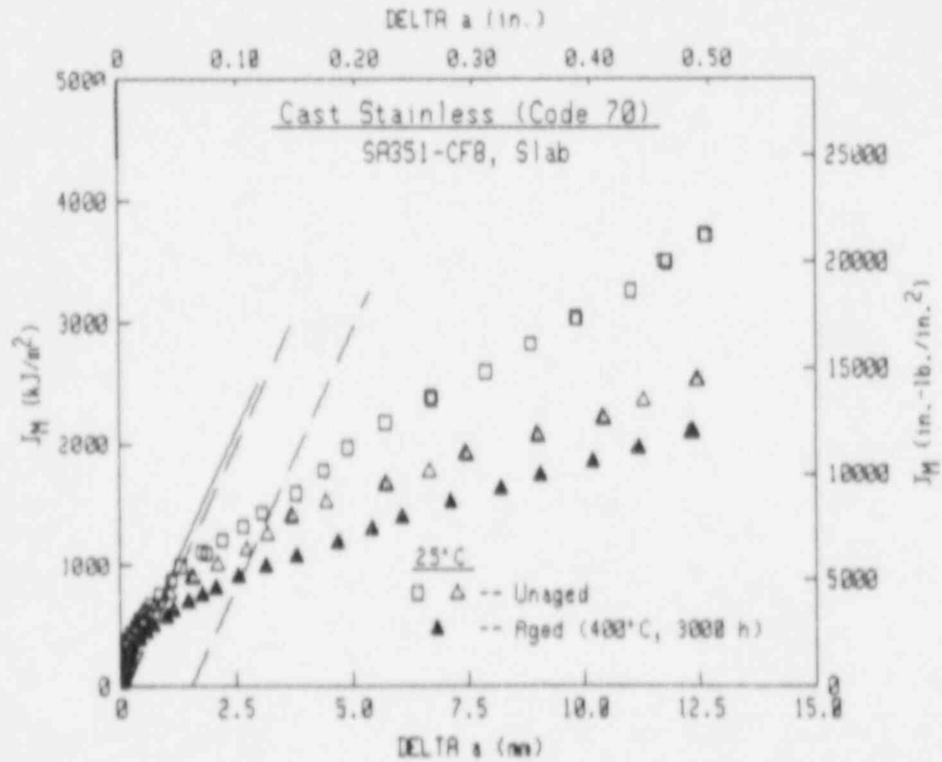

Fig. 102 For Heat 70 (grade CF8M) at 25°C, thermal-aging at 400°C for 3000 h results in considerable reductions in J levels from average trends for unaged material, but only a small reduction in comparison to the lower of the data sets for unaged material.

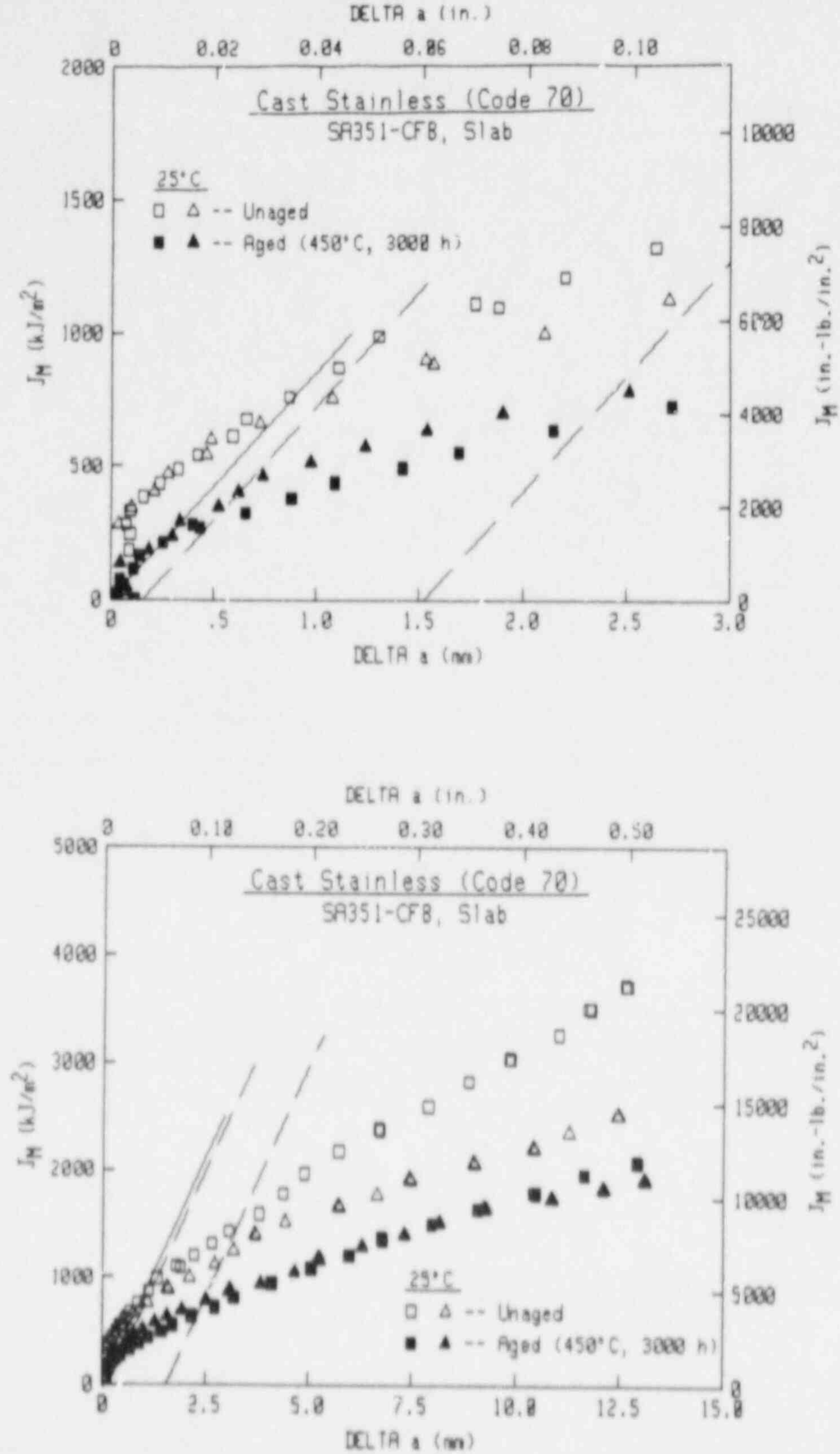

Fig. 103 For Heat 70 (grade CF8M) at 25°C, thermal-aging at 450°C for 3000 h results in considerable reductions in J levels from average trends for unaged material, but only a small reduction in comparison to the lower of the data sets for unaged material.

in contrast to data from unaged specimens. For the aged condition, the top of the slab tends to have higher J levels up to ~ 4 mm of crack growth. Overall the toughness reduction, due to thermal-aging, averages ~ 35%, generally consistent with the C_v data (52% reduction).

Comparison of data for the thermally aged conditions (Fig. 104) follows trends demonstrated by Heats 68 and 69. Specifically, higher aging temperature results in lower J_M-R curve levels, and aging at 400°C and 450°C results in similar J_M-R curve levels.

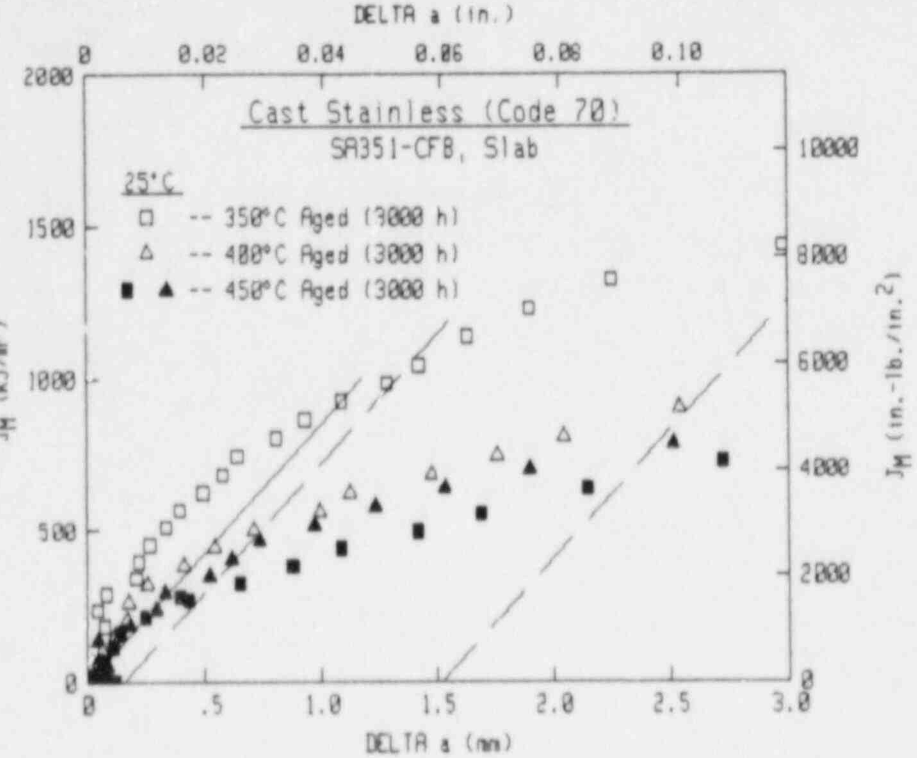

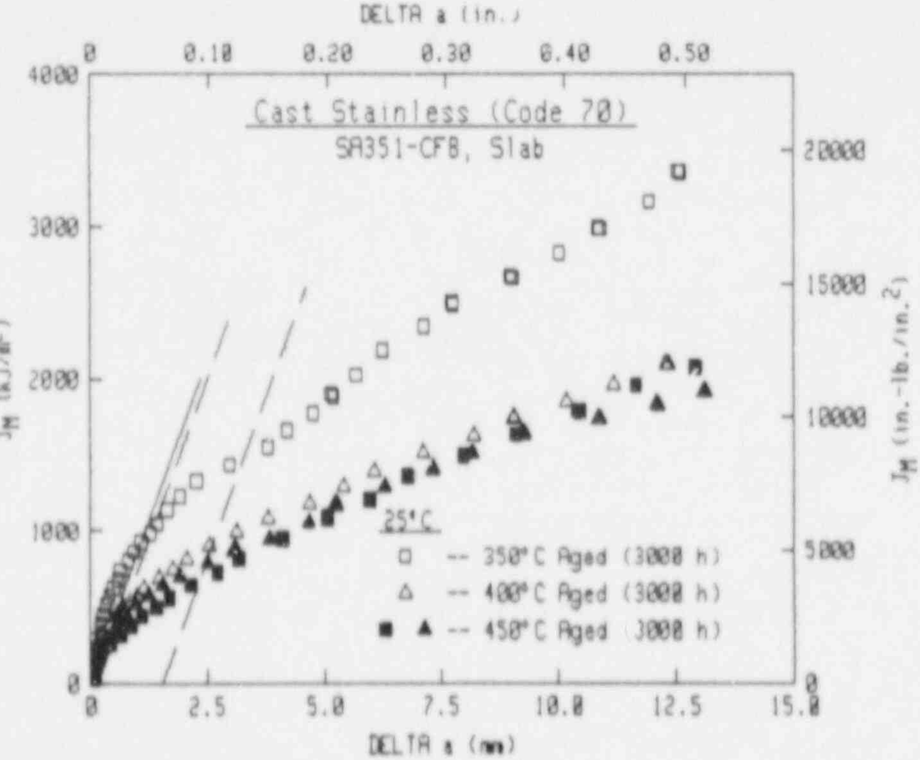

Fig. 104 For the thermally-aged conditions of Heat 70 (grade CF8M) at 25°C, higher aging temperature results in lower J_M-R curve levels, with aging at 400°C and 450°C yielding similar J_M-R curve levels.

7. DISCUSSION

7.1 J-R Curve Testing "Difficulties"

Whereas the J-R curve results described in Sections 5.2 and 6.2 are presented without discussion of details from the testing, mention of several topics is necessary.

The applicable ASTM test standards, specifically E 813 and E 1152, are in reality not applicable to these types of tests. In particular, the maximum J levels permitted to ensure J dominance are ~ 600 kJ/m^2, whereas the "J_{Ic}" values for many of these tests are higher than that level. As illustrated in many of the comparison J-R curve plots, the initial portions of many data sets do not follow the "$2\sigma_f$" blunting line used by ASTM E 813, but instead illustrate steeper blunting trends, whereby less apparent crack advance (due to blunting) occurs per J increment than the ASTM blunting line would indicate. Other investigators have seen similar trends for stainless steels (Ref. 18, 19). Recommendations are to use a "$4\sigma_f$" blunting line or even a 2 ultimate strength blunting line. The latter may be appropriate since ferritic steels which generally follow the "$2\sigma_f$" blunting line typically have a yield to ultimate strength ratio of ~ 0.7 - 0.8, such that the flow strength is 85% - 90% of the ultimate strength. For cast stainless steels, the ratio of yield to ultimate strength is typically ~ 0.4, with a resultant flow strength of ~ 70% of the ultimate strength. The use of 2 ultimate strength is therefore an approximate average of 2 and 4 flow strength for cast stainless steels.

Another problem encountered with these tests is the significant "shape change" exhibited by these materials. As indicated in Fig. 105, these cast stainless steel specimens typically exhibit severe necking at the crack tip as the crack progresses. This results in a trapezoidal cross-section as opposed to the nearly rectangular section for a typical RPV steel. This shape change is thought to be the major reason for the poor correspondence between the crack growth measured optically from the fracture surface (Δa_m) and the crack growth predicted by the unloading compliance method (Δa_p), as indicated in the summary tables. In general the crack growth prediction error (Δa_m-Δa_p) for RPV steels tend to be nearly null, whereas for these cast stainless steels the error tends to be large. This shape change, in combination with the slightly irregular crack front typical of these specimens, would tend to result in a shorter predicted crack length than one would measure optically.

7.2 Modified J (J_M) vs. Deformation J (J_D)

Recent ASTM and ASME discussions have centered on the "proper" J formulation for use in evaluating J-R curves for structural steels. To illustrate the impact of using the various formulations, comparisons of data for high and low toughness cases of these cast stainless steels will be used.

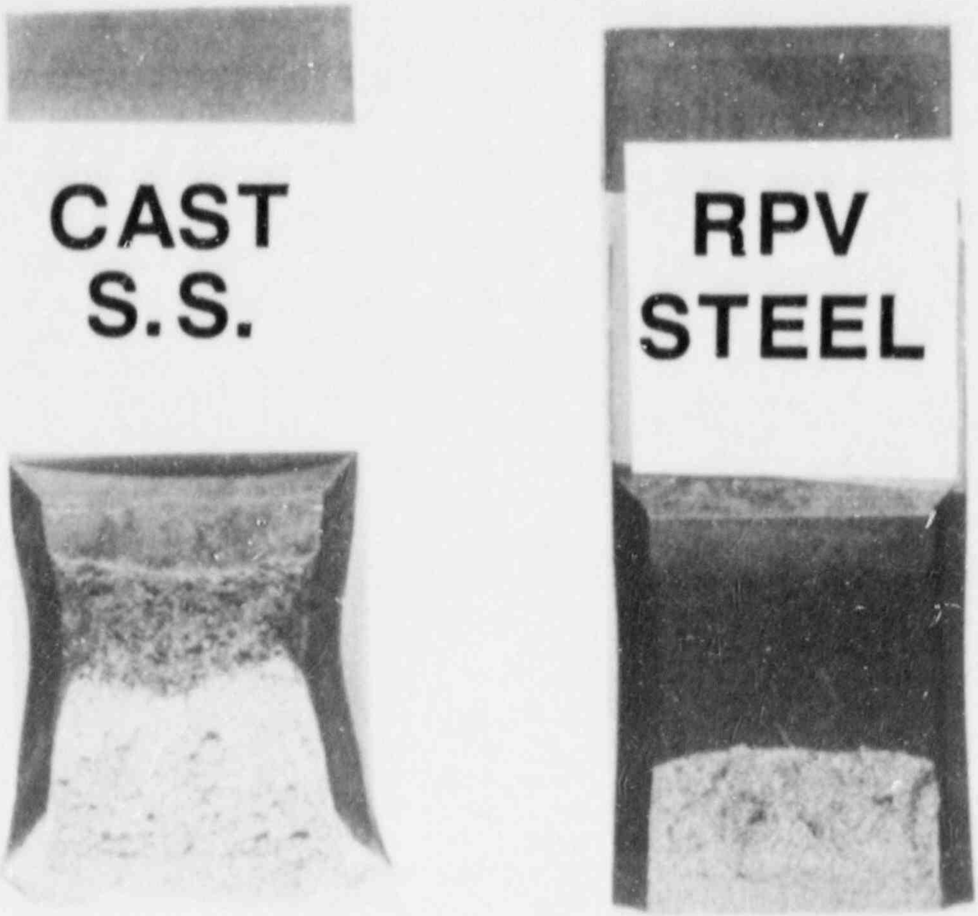

Fig. 105 In contrast to RPV steel specimens, cast stainless steel specimens sustain severe necking and cross-section distortion. The fatigue precrack region in cast stainless steel specimens tends to be irregular due to the large grains, and differentiation of the interface between the precrack region and the stable tearing region can be difficult.

The initial form of the J integral proposed for use with compact specimens was based on an analysis of as deeply cracked beam in pure bending (Ref. 20), as given by

$$J = \frac{2}{b} \int_o^\Delta \left(\frac{P}{B} \right) d\Delta = \frac{2A}{Bb} \qquad (11)$$

with A the area under the load-displacement record for the specimen. However, this form was found to give J values slightly less than G values for the case of failure in the linear range of the load-displacement curve. To correct this discrepancy, Merkle and Corten (Ref. 21) included the effect of axial force in their formulation of the J integral, termed here J_{M-C}. Clarke and Landes (Ref. 22) then simplified the equations to

$$J_{M-C} = \frac{2A}{Bb} \frac{(1 + \alpha)}{(1 + \alpha^2)} \qquad (12)$$

with α a function of a_o/b.

While the J_{M-C} equation was satisfactory for evaluation of J values under conditions of little or no crack growth (such as J_{Ic}), use of the J integral for the case of a growing crack was needed for evaluation of safety margins in nuclear RPV and piping applications. For such applications, the use of J_{Ic} values only would be too severely conservative in providing meaningful assessments of structural integrity. To address the need to account for crack growth in the J integral, Ernst used a deformation theory of plasticity interpretation of J to develop a crack growth corrected form of the J integral, termed here J_D (Ref. 23). The equations used to evaluate J_D are given in Appendix A.

One characteristic of J_D which was quickly found was a tendency towards a size-effect, whereby smaller specimens would give lower J-R curve levels than larger specimens, with negative J-R curve slopes resulting in many cases. To address these concerns, Ernst introduced a modified form of J, termed J_M (Ref. 15). Some of the attributes of J_M cited by Ernst include a better description of the process of deformation and crack growth, specimen-size independence, and a large relaxation of the restructions on the amount of crack extension and/or initial remaining ligament needed to produce valid data. The specimen size independent characteristic of J_M was initially demonstrated in Ref. 15 for an A 508 Class 2A steel using data from 0.5T- to 10T-CT specimens. Confirmation of this can also be found in Ref. 12 and 24.

The J_D and J_M equations described above (and used to calculate the J-R curves in this report) represent "total area" forms of each whereby the area under the load-total displacement curve is used along with a single η term to evaluate J. Recent work indicates that the η term used tends to underestimate the elastic η, η_{el}, for the compact specimens. Therefore, a more appropriate way to evaluate J_D and J_M is to sum the elastic and plastic portions of each:

$$J = J_{el} + J_{pl} \quad (13)$$

In this case,

$$J_{el} = K^2 (1-\nu^2)/E \quad (14)$$

with K from ASTM E 399, ν is Poisson's ratio (0.3) and E is Young's modulus. The plastic parts of the J integral are then evaluated by substituting A_{pl} (area under the load-plastic displacement curve) for A. J_{D*} and J_{M*} are used to differentiate these quantities from J_D and J_M.

For these comparisons, a specimen from heat P2 tested at 25°C (P2-B6LC) represents a high toughness case, whereas a specimen from Heat C1 also tested at 25°C (C1-B1LC) represents a low toughness case. Load-deflection curves for these two specimens are illustrated in Fig. 106. The high toughness specimen exhibits a substantially higher maximum load and high deflection at maximum load than does the low toughness specimen. Likewise for the Δa-deflection curves (Fig. 107), the low toughness specimen exhibits crack growth initiation at lower deflections and in general exhibits more crack growth per deflection than does the high toughness specimen. Both of these specimens exhibit mainly plastic deformation, as given by the closeness of the plastic and total deflection curves. The normalized load-plastic deflection curves (Fig. 108) for these specimens are generally well-behaved, with the low toughness specimen exhibiting the lowest trends overall.

The J-R curves for these specimens (Figs. 109 and 110) are generally consistent with past work. Specifically, J_M and J_{M*} yield the highest J-R curve levels, with J_{M-C} slightly lower; J_D and J_{D*} give the lowest levels in both cases. The "star" quantities, J_{D*} and J_{M*}, give virtually identical trends to their "non-star" forms, J_D and J_M, respectively. This characteristic is illustrated in Figs. 111 and 112, where the ratio of the "star" quantities to the "non-star" quantities, i.e., J_{D*}/J_D and J_{M*}/J_M at each J-R curve data point, is within 2% of unity throughout each J-R curve. These ratios also do not change significantly with the toughness level.

Similarly, the quantities J_M/J_{M-C} (Fig. 113), J_M/J_D (Fig. 114) and J_{M*}/J_{D*} (Fig. 115) do not vary with toughness level. As expected, J_M and J_{M-C} yield similar J levels, with the largest difference ~ 18% at $\Delta a/b$ of ~ 0.5. In this case, a bilinear trend results for J_M/J_{M-C} versus ~a, with the breakpoint at $\Delta a/b$ of ~0.25.

For J_M/J_D (Fig. 114) and J_{M*}/J_{D*} (Fig. 115), the differences become large at low Δa levels, $\Delta a/b_o$ of ~ 0.025. A discernible breakpoint occurs for these data (as functions of Δa) at $\Delta a/b_o$ of 0.35.

As demonstrated through its use in ASTM Standard E 813-87, the power law curve, as given by $J = C\Delta a^n$ with C and n evaluated from regression

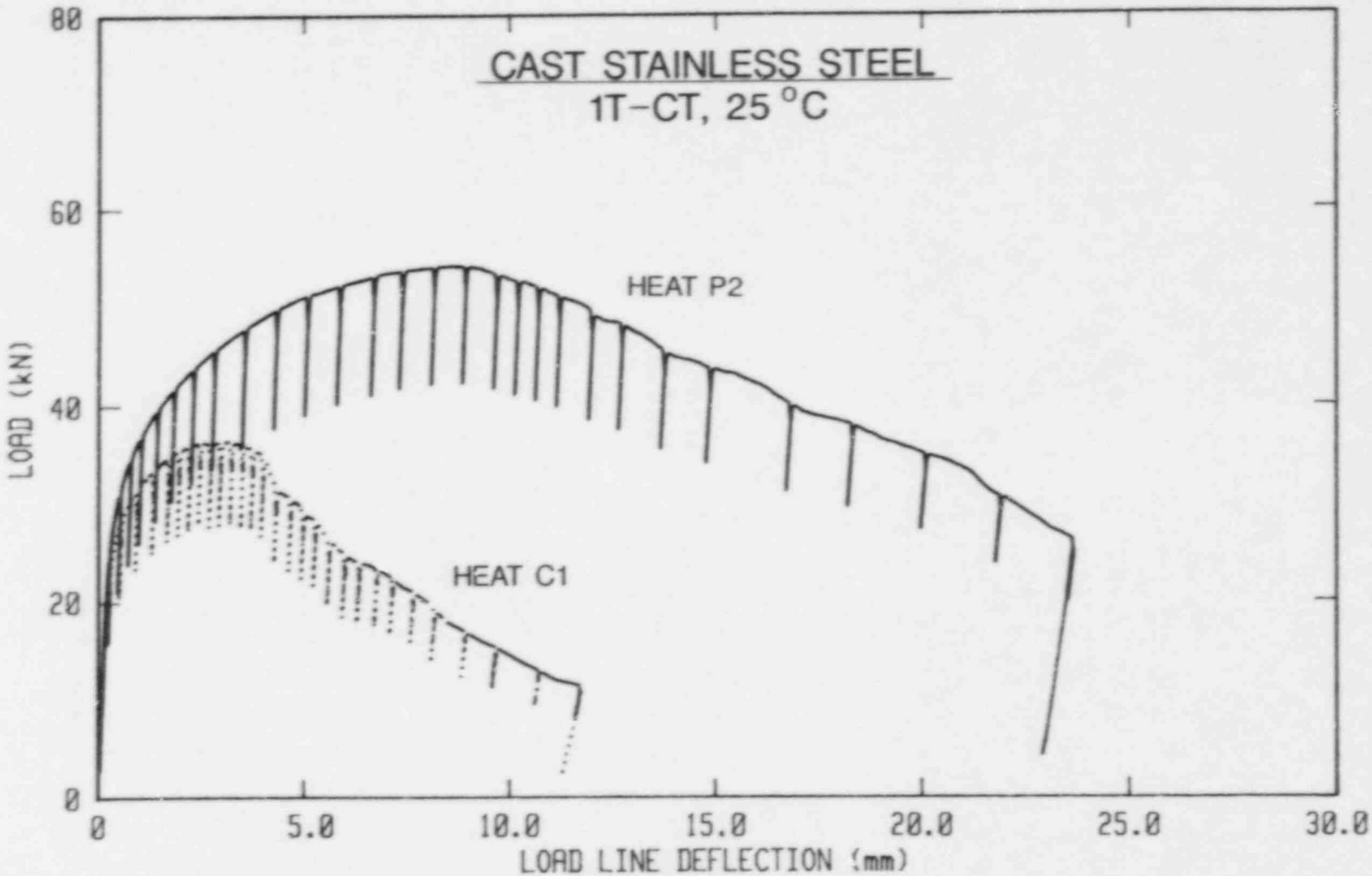

Fig. 106 The load-deflection curve for the low toughness specimen (Heat C1) is dwarfed by that of the high toughness specimen (Heat P2).

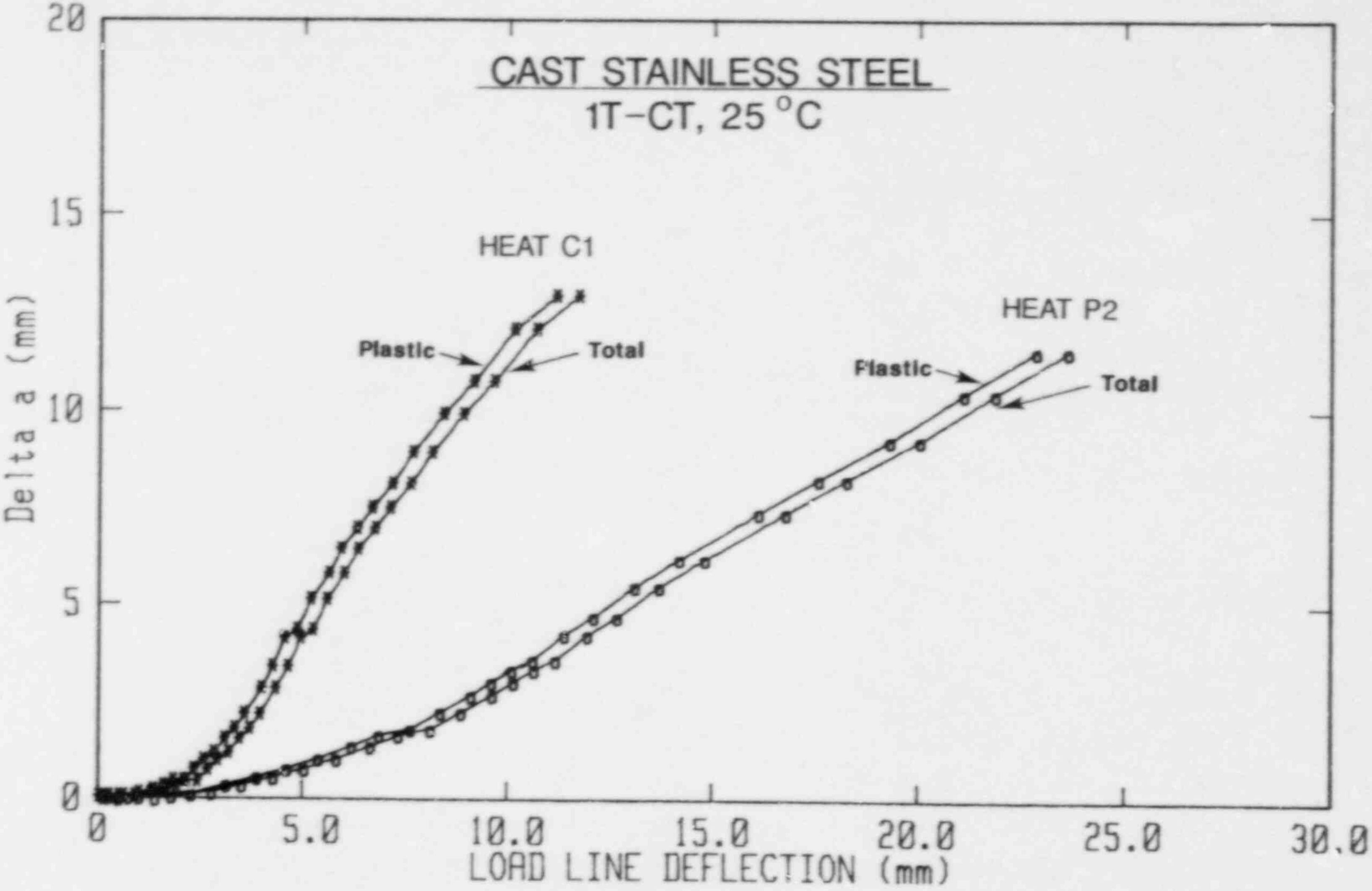

Fig. 107 The Δa-deflection curve for the low toughness specimen (Heat C1) indicates lower tearing resistance in comparison to that for the high toughness specimen (Heat P2). The dominance of plasticity in these tests is indicated by the closeness of the curves for total and plastic deflection.

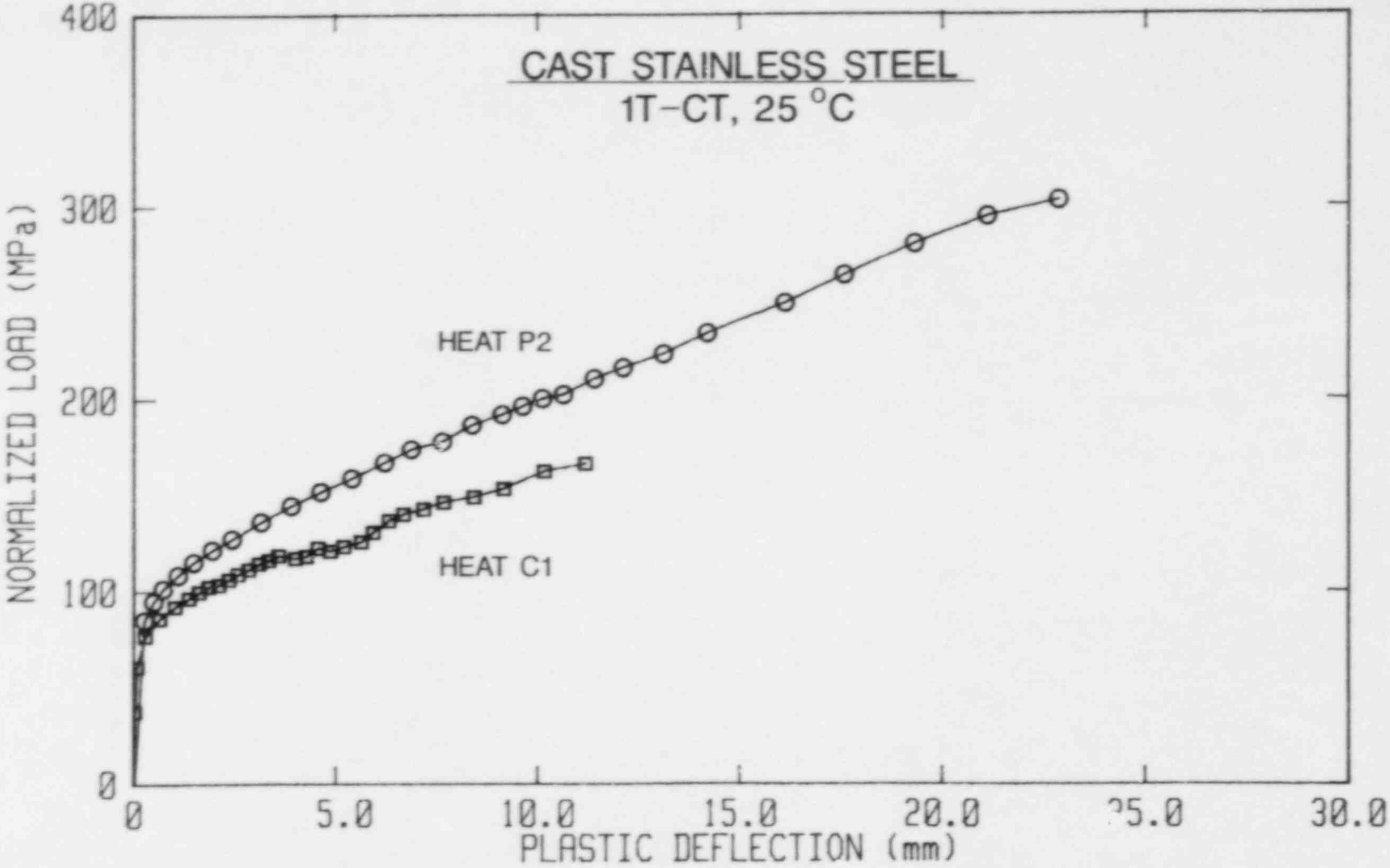

Fig. 108 The normalized load-plastic deflection curves for the high toughness specimen (Heat P2) is only slightly higher than that for the low toughness specimen (Heat C1).

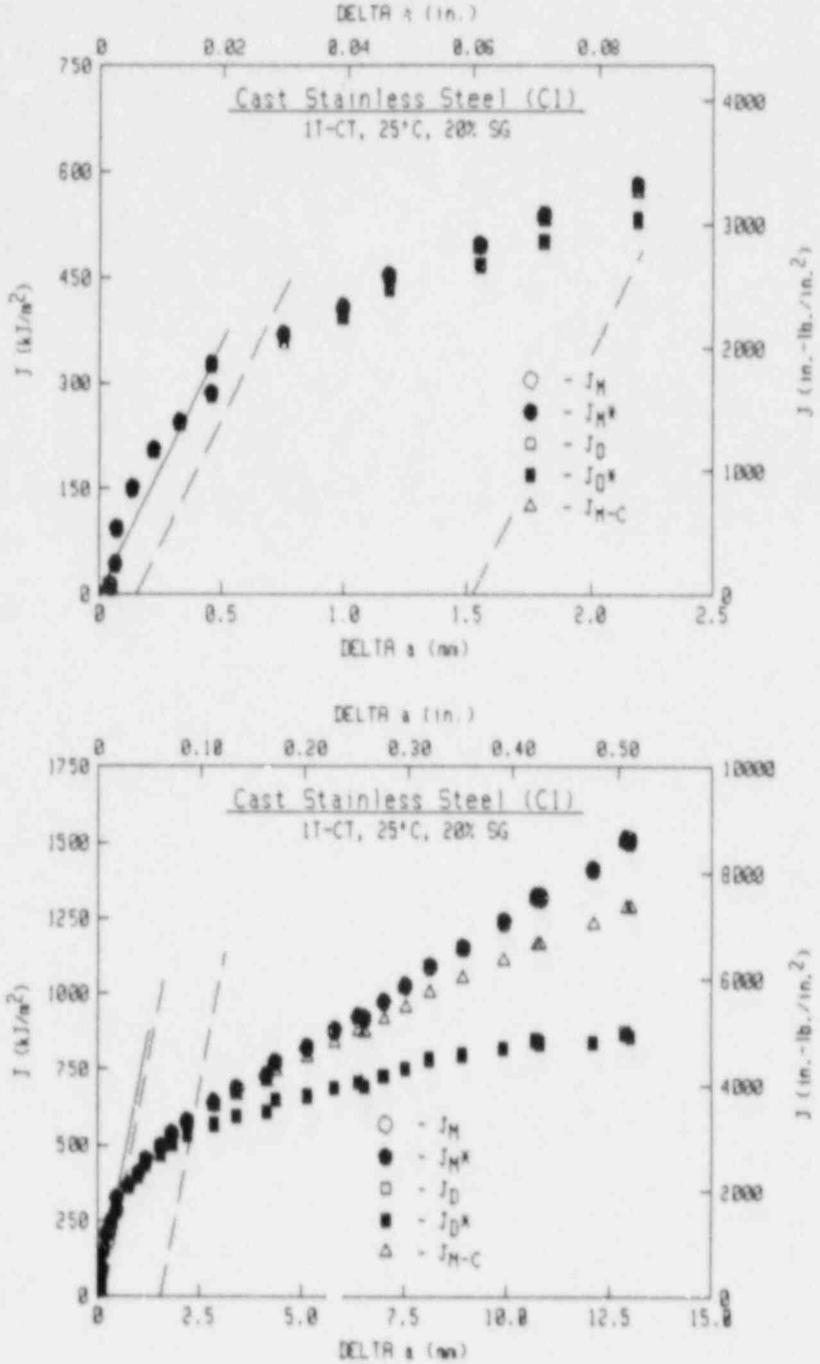

Fig. 109 For the low toughness specimen (Heat C1), J_M and J_{M*} give the highest J levels, whereas J_D and J_{D*} give the lowest J levels.

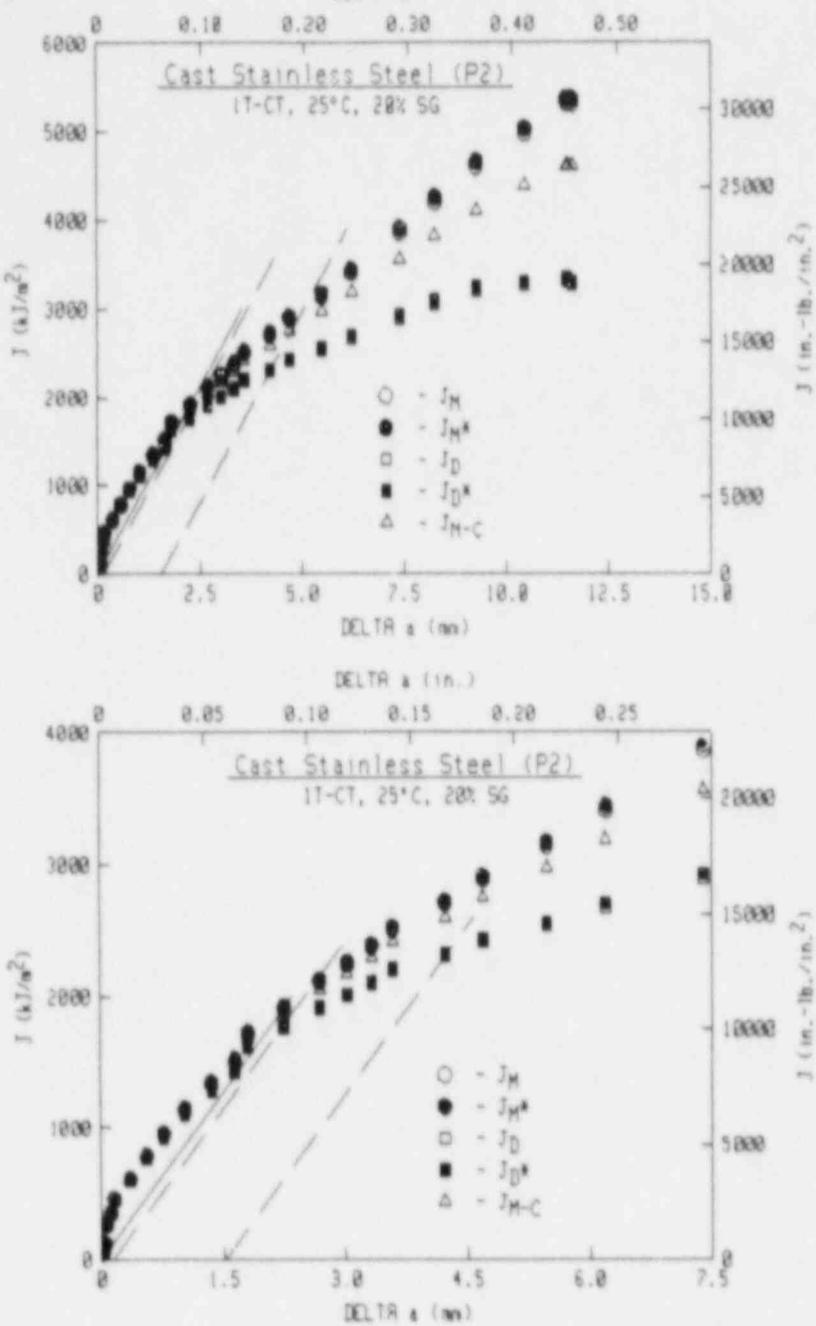

Fig. 110 As for the low toughness specimen, J_M and J_{M*} give the highest J levels for the high toughness specimen (Heat P2) as well, whereas J_D and J_{D*} give the lowest J levels.

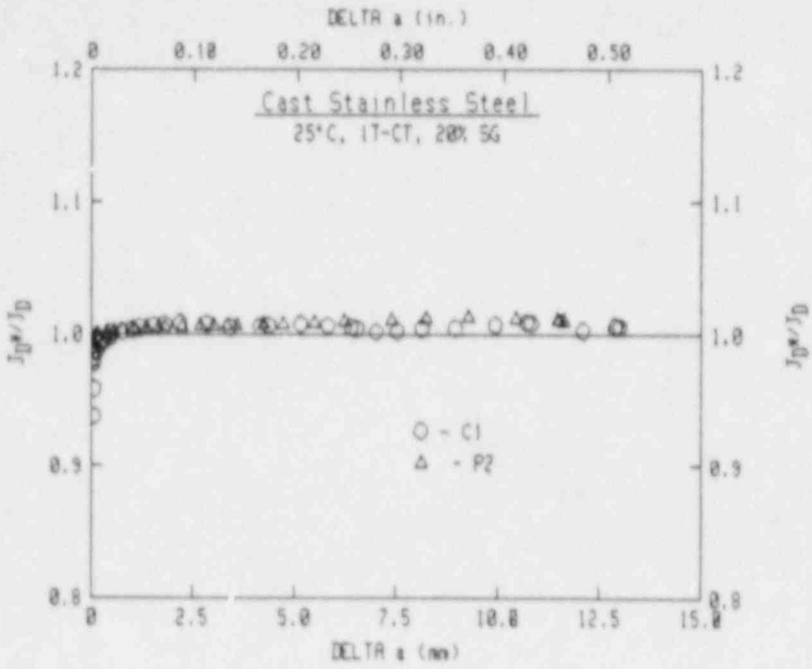

Fig. 111 For both the low toughness (Heat C1) and the high toughness (Heat P2) specimens, J_{D*} and J_D are approximately equal for the entire crack growth interval covered.

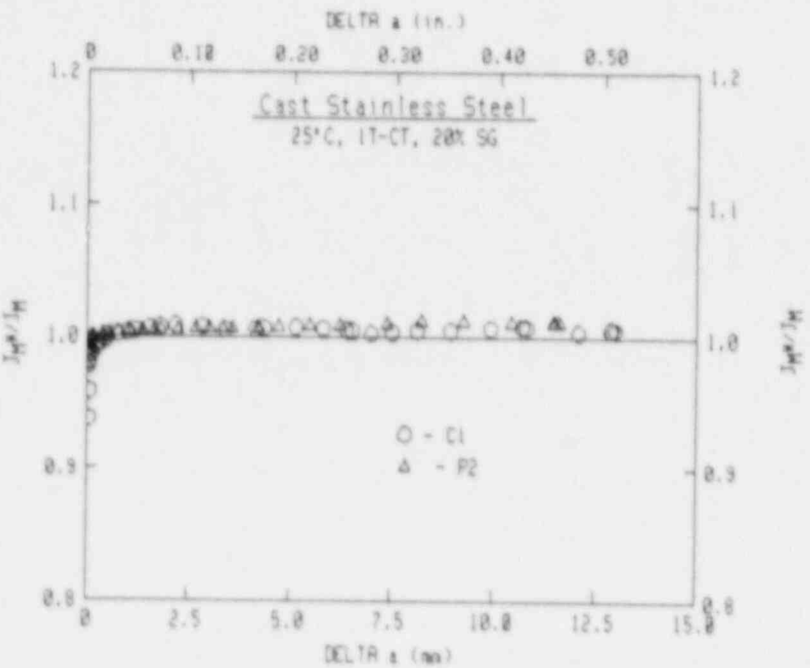

Fig. 112 For both the low toughness (Heat C1) and the high toughness (Heat P2) specimens, J_{M*} and J_M are approximately equal for the entire crack growth interval covered.

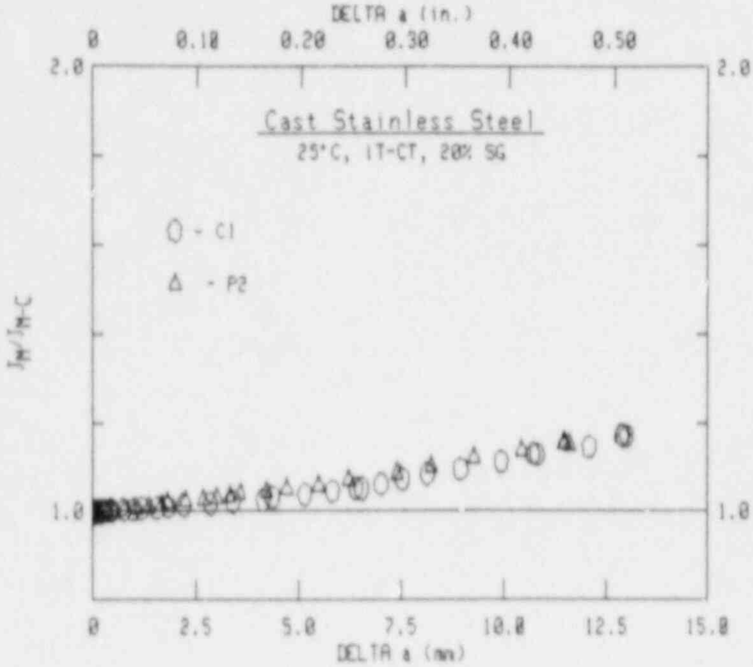

Fig. 113 For both the low toughness (Heat C1) and the high toughness (Heat P2) specimens, J_M and J_{M-C} tend to give similar J levels, although J_M becomes ~ 20% higher at $\Delta a/b_o$ of ~ 0.5.

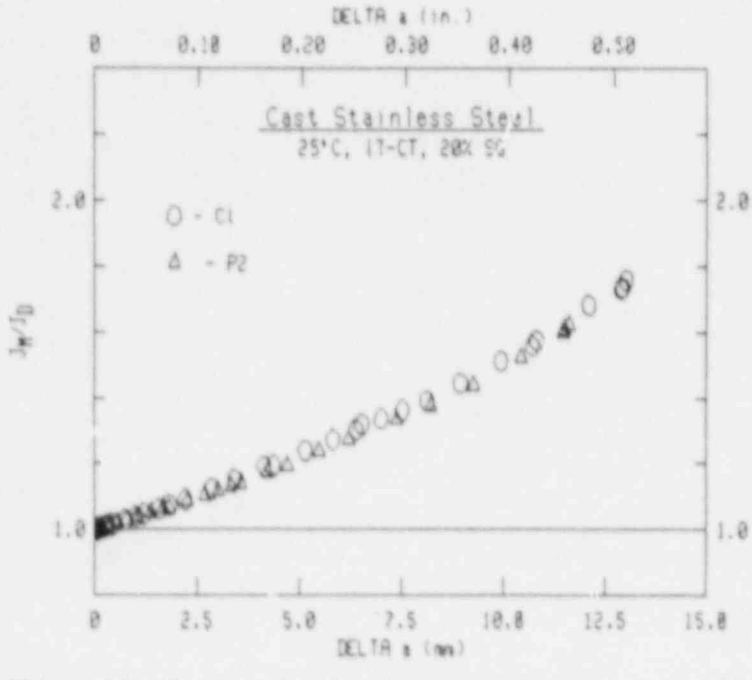

Fig. 114 For both the low toughness (Heat C1) and the high toughness (Heat P2) specimens, J_M becomes much larger than J_D almost as soon as crack growth initiation occurs.

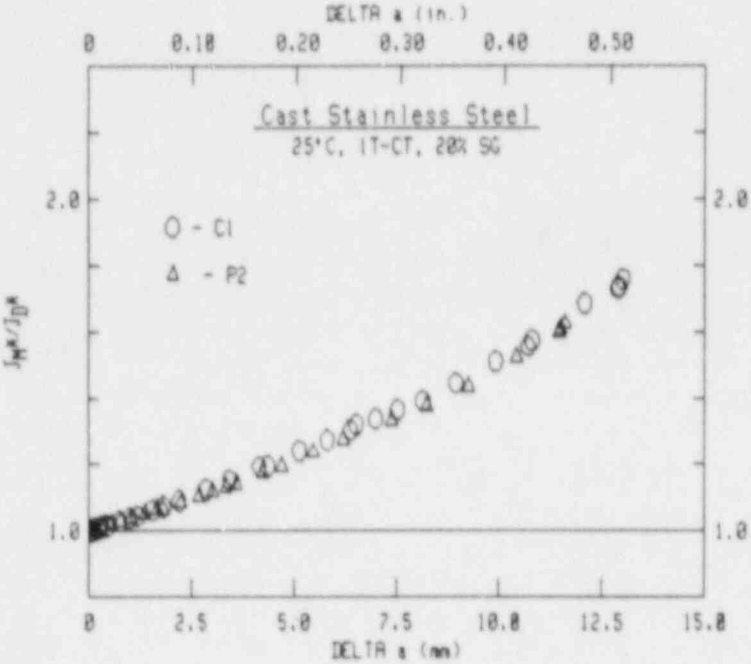

Fig. 115 For both the low toughness (Heat C1) and the high toughness (Heat P2) specimens, $J_{M\star}$ becomes much larger than $J_{D\star}$, in similar proportions to the J_M-J_D comparisons in Fig. 114.

analysis, is a reasonable procedure for approximating the J-R curve. One method for checking the appropriateness of a power law procedure is to plot the J-Δa data in a log-log format. If the data depict a linear trend of J-Δa in this format, then a power law curve will accurately fit the data. For the two sample specimens, J_{M-C}, $J_{M\star}$ and $J_{D\star}$ all demonstrate reasonably linear behavior for Δa increments above 0.25 mm (Fig. 116). However, both $J_{M\star}$ and $J_{D\star}$ tend to diverge from linearity, whereas J_{M-C} remains almost linear throughout all of the data. These trends are more obvious in Fig. 117 for $J_{D\star}$ and $J_{M\star}$, with the latter tending to "hook" upwards and the former tending to "hook" downward. In contrast, the J_{M-C} data tend to remain essentially linear (Fig. 118).

7.3 Correlation of J-R Curve Data and C_v Data

To aid in the interpretation and possible usefulness of the J-R data curve in this report, the J levels at various Δa increments are cross-plotted with the C_v upper shelf energy levels. As opposed to using the C_v energy at the specific test temperature (in particular at 25°C), the upper shelf energy levels are used to avoid the confusion which would result from using upper shelf energy levels in some cases (such as the unaged condition of many of these heats) and possibly lower shelf energy levels for cases in which a large transition temperature increase due to aging has increased the transition region above the test temperature. Since all of the J-R curve tests represent fully-ductile, high toughness behavior, the consistent use of upper shelf energy levels should give the most useful comparisons. In addition, J_{Ic} values are avoided in these comparisons since for these materials, with high toughness and generally low strength, the J_{Ic} measurement points typically occur at large Δa levels (i.e., 1 mm or greater), and the ASTM blunting line clearly does not represent the data in many cases. Therefore, the consistent use of J values at a given level of Δa gives a truer indication of toughness differences.

Comparisons between J level and C_v upper shelf energy have been made at Δa increments of 1.25 mm (Fig. 119), 2.5 mm (Fig. 120) and 5 mm (Fig. 121), with test temperatures of 25°C and 290°C treated separately. Data from aged specimens are denoted by solid symbols in all cases; some additional data from another study (Ref. 25) are given for comparison. (The additional data are not truly comparable to that from this study, since they are evaluated using J_{M-C}; differences should be less than 5% in all cases.) As illustrated at each Δa level, the trend is towards higher J levels with increasing C_v energy. This trend is most representative at 290°C. At 25°C, a cluster of data points for experimental heats 68 and 69 in the unaged condition (at C_v USE levels of 212 and 222 kJ, respectively) are distinctly lower than the remaining data. These two heats demonstrate two other characteristics atypical of the other heats, with both characteristics based upon lower J-R curve levels than would be expected at 25°C. Specifically, the data at 290°C were higher than those at 25°C, and aging at 350°C and 400°C gave higher J-R curve levels (at 25°C) than for the unaged condition. Therefore, if the J-R

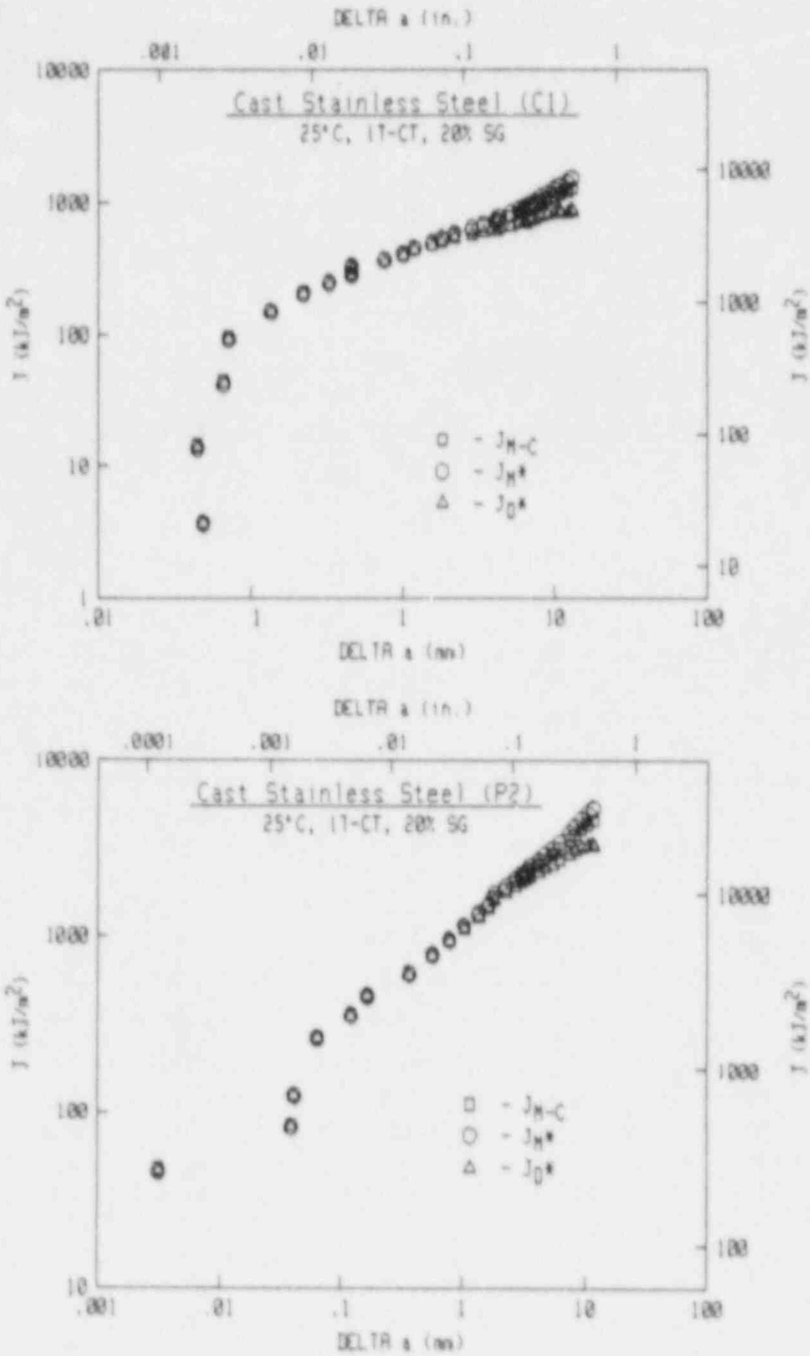

Fig. 116 For both the low toughness (Heat C1) and the high toughness (Heat P2) specimens, J_{M-C} data are virtually linear in a log-log format (indicating conformity to a power law curve), whereas J_{M*} "hooks" up and J_{D*} flattens out.

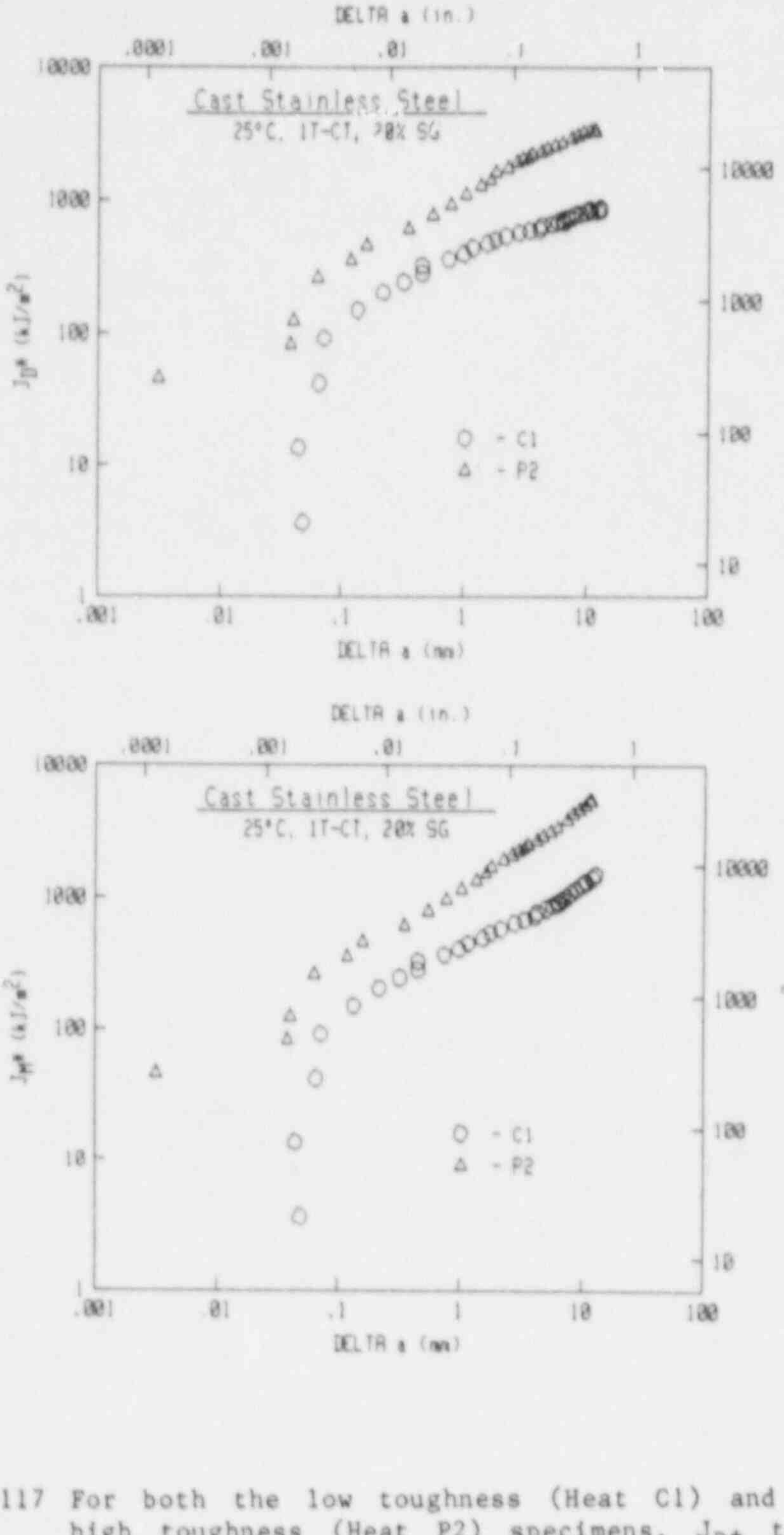

Fig. 117 For both the low toughness (Heat C1) and the high toughness (Heat P2) specimens, J_{D*} tends to flatten out at $\Delta a \sim 2.5$ mm (0.1 in.), whereas J_{M*} tends to give a "hook" up behavior after $\Delta a \sim 7.5$ mm (0.3 in.).

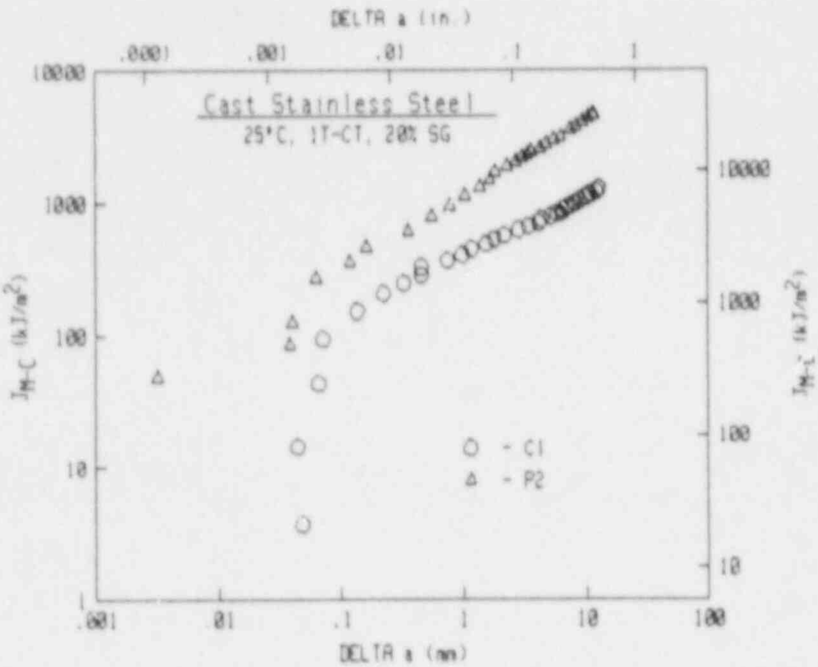

Fig. 118 For both the low toughness (Heat C1) and the high toughness (Heat P2) specimens, J_{M-C} gives the most linear correspondence between J and Δa in a log-log format.

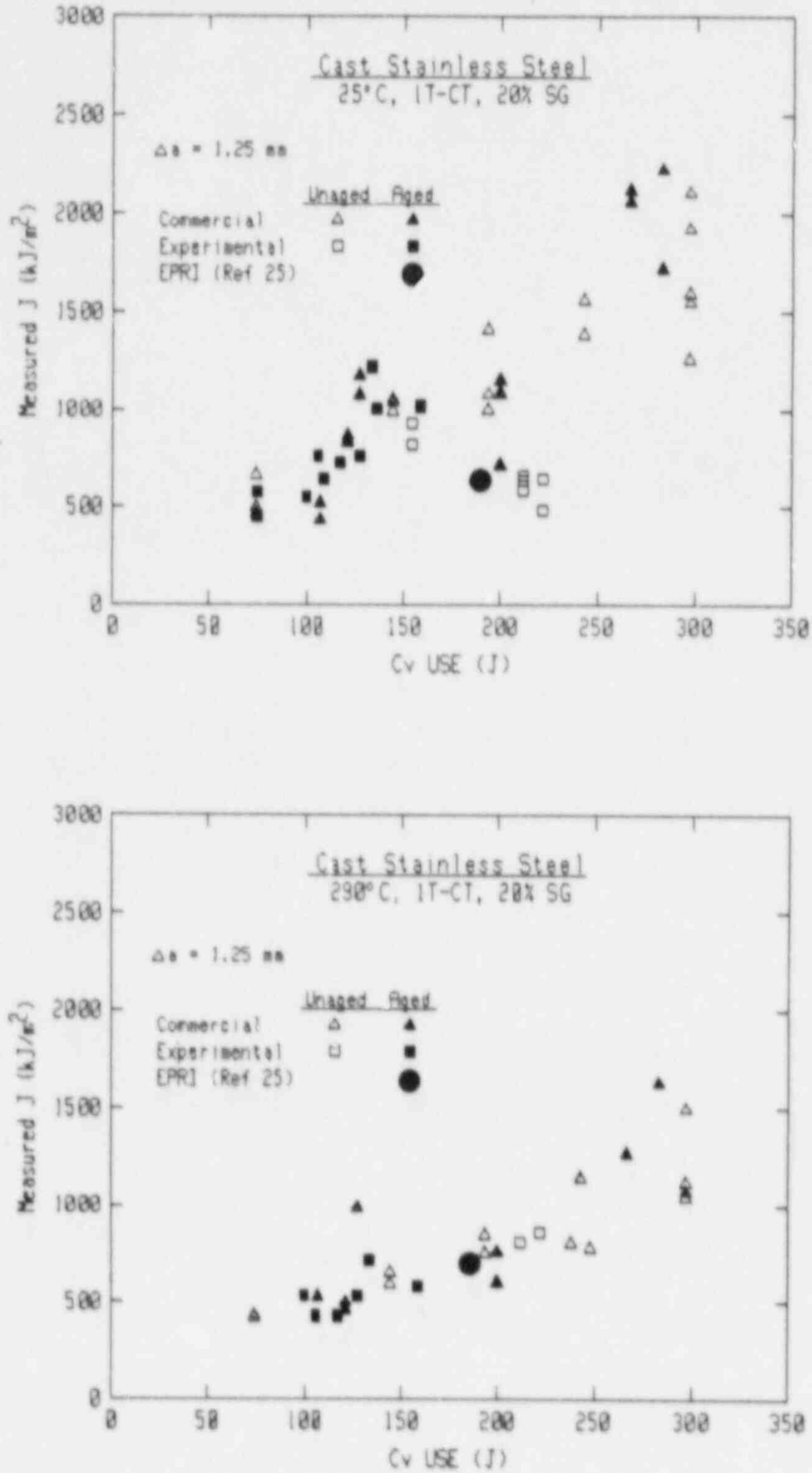

Fig. 119 Comparison of J_M levels at $\Delta a = 1.25$ mm for the cast stainless steels. Higher C_V levels generally correspond to higher J levels, although data for experimental heats 68 and 69 in the unaged condition are notable deviants from the overall trend at 25°C.

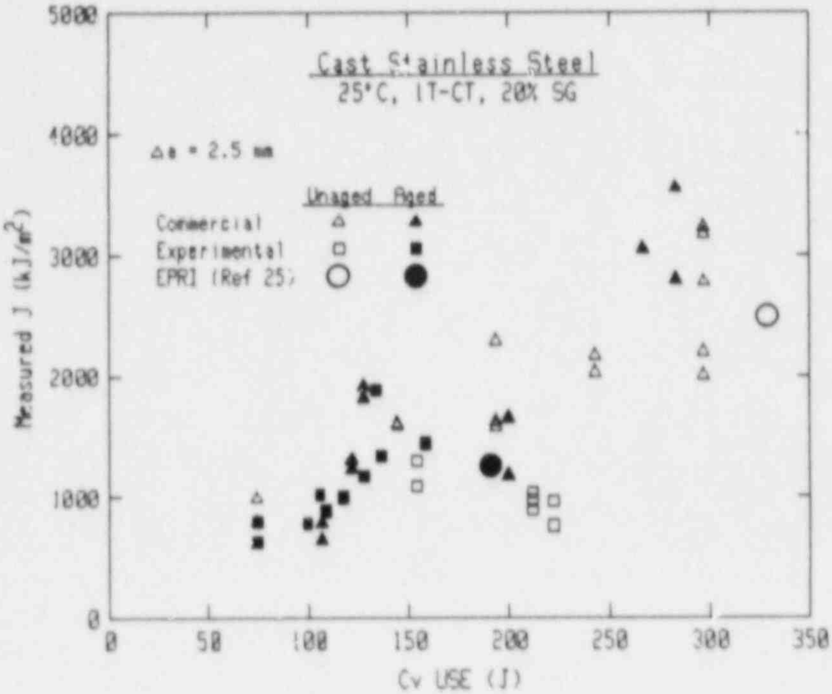

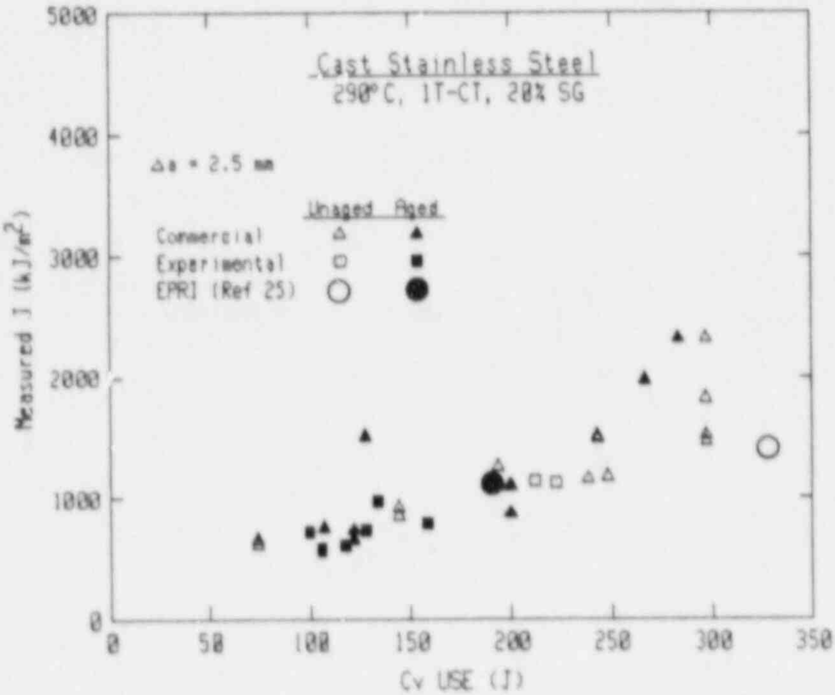

Fig. 120 Comparison of J_M levels at $\Delta a = 2.5$ mm for the cast stainless steels. Higher C_v levels generally correspond to higher J levels, although data for experimental heats 68 and 69 in the unaged condition are notable deviants from the overall trend at 25°C.

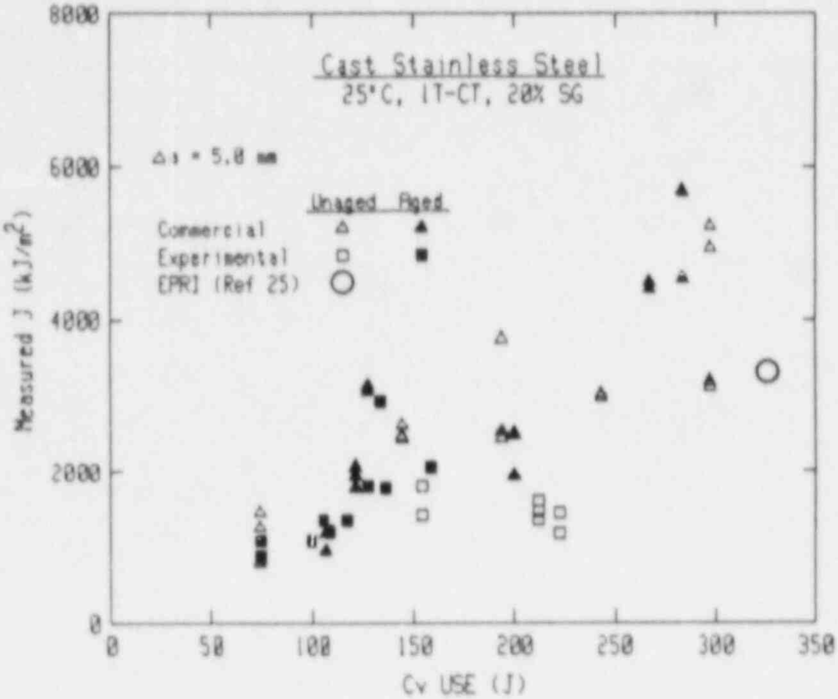

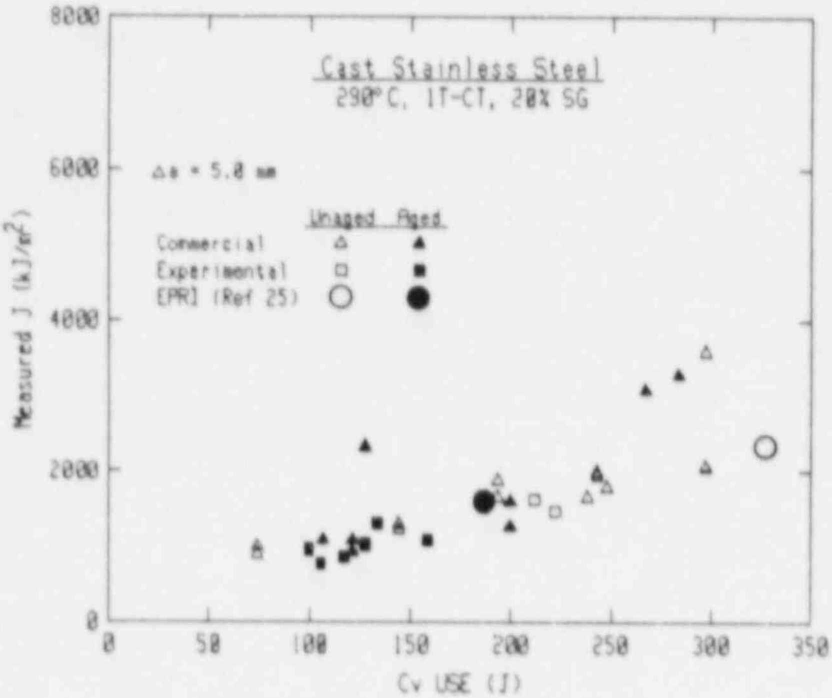

Fig. 121 Comparison of J_M levels at Δa = 5 mm for the cast stainless steels. Higher C_v levels generally correspond to higher J levels, although data for experimental heats 68 and 69 in the unaged condition are notable deviants from the overall trend at 25°C.

curve levels at 25°C for these two heats were to be elevated, then these heats would be consistent with the other heats in all respects. No bases for the lower-than-expected toughness has been found, although the close agreement of data from multiple tests of each heat precludes variability as a possible cause.

As illustrated in Fig. 119 to 121, data from the Electric Power Research Institute (EPRI) study (Ref. 25) are entirely consistent with the data reported in this study.

8. CONCLUSIONS

This study, in conjunction with Argonne National Laboratory, has characterized tensile and fracture toughness (J-R curve) trends of centrifugally and static cast austenitic stainless steels, in the as-cast and various thermally-aged conditions. Conclusions from this study are:

- Increasing the test temperature from 25°C to 290°C resulted in reduced strength (0.2% offset yield and ultimate) and fracture toughness (J-R curve levels) in virtually every case.

- Thermal-aging at 350°C to 450°C generally gave higher strength and reduced toughness in comparison to trends for unaged material; in particular, toughness losses can be exceedingly large.

- Toughness reductions tended to be almost proportional to reductions in Charpy-V upper shelf energy levels, with the notable exceptions of heats 68 and 69 at a test temperature of 25°C (see below).

- Increasing the temperature or time period of thermal-aging generally gave higher strength and lower toughness (indicating greater embrittlement).

- For the same grade, centrifugally-cast heats exhibited higher toughness levels than static cast heats.

- For the commercial heats studied, grade CF3 had the highest toughness and grade CF8 had the lowest toughness.

- Trends between J levels (at a fixed Δa increment) and C_V upper shelf energy levels have been established, covering aged and unaged materials, both commercial and experimental heats.

- Experimental heats 68 (grade CF8) and 69 (grade CF3) in the unaged condition demonstrate lower-than-expected toughness (J) levels at 25°C. No basis for this has been found.

All of these data are available for remote access through the USNRC's Piping Fracture Mechanics Data Base (PIFRAC), an on-line computerized data base (Ref. 26).

REFERENCES

1. A. Tautwein and W. Gysel, "Influence of Long Time Aging of CF-8 and CF-8M Cast Steel at Temperatures Between 300 and 500°C on the Impact Toughness and the Structure Properties," in Stainless Steel Castings, V. G. Behal and A. S. Melilli, Eds., ASTM STP 756, American Society for Testing and Materials, Phila., PA, 1982, p. 165.

2. G. Baudry and C. Pichard, "Evolution During Long Holding Times at 300 and 450°C of the Mechanical Properties of Austeno-Ferritic Steel Castings and Welded Joints Used in Pressurized Water Nuclear Reactors," Troisieme Congres National sur la Technologie des Appareils a Bression, Vol. 2, Materiaux, A.F.I.A.P., 1980, p. 673.

3. E. I. Landerman and W. H. Bamford, "Fracture Toughness and Fatigue Characteristics of Centrifugally Cast Type 316 Stainless Steel Pipe After Simulated Thermal Service," Ductility, and Toughness Considerations in Elevated Temperature Service, ASME MPC-8, 1978, p. 99.

4. G. Slama, P. Petrequin and T. Mager, "Effect of Aging on Mechanical Properties of Austenitic Stainless Steel Castings and Welds," presented at SMiRT Post-Conference Seminar 6, Assuring Structural Integrity of Steel Reactor Pressure Boundary Components, August 29-30, Monterey, CA, 1983.

5. O. K. Chopra and G. Ayrault, "Materials Science and Technology Division Light-Water-Reactor Safety Research Program: Quarterly Progress Report," October-December 1983, USNRC Report NUREG/CR-3689, Vol. IV, ANL-83-85, Vol. IV, Aug. 1984, pp. 129-151.

6. O. K. Chopra and H. M. Chung, "Materials Science and Technology Division Light-Water-Reactor Safety Materials Engineering Research Programs: Quarterly Progress Report," January-March 1984, USNRC Report NUREG/CR-3998, Vol. I, ANL-84-60, Vol. I, Sept. 1984, p. 52.

7. O. K. Chopra and H. M. Chung, "Long-Term Embrittlement of Cast Duplex Stainless Steels in LWR Systems: Annual Report," October 1983 - September 1984, USNRC Report NUREG/CR-4204, ANL-85-20, Mar. 1985.

8. O. K. Chopra and H. M. Chung, "Long-Term Embrittlement of Cast Duplex Stainless Steels in LWR Systems: Annual Report," October 1984 - September 1985, USNRC Report NUREG/CR-4503; ANL-86-3, Jan. 1986.

9. O. K. Chopra. and H. M. Chung, "Long-Term Embrittlement of Cast Duplex Stainless Steels in LWR Systems: Semiannual Report," October 1985 - March 1986, USNRC Report NUREG/CR-4744, Vol. I, No. 1; ANL-86-54, Sept. 1986.

10. G. E. Dieter, Mechanical Metallurgy, McGraw-Hill Book Company, New York, 1976.

11. P. W. Bridgman, Trans. Am. Soc. Met., Vol. 32, 1944, p. 553.

12. A. L. Hiser, F. J. Loss, and B. H. Menke, "J-R Curve Characterization of Irradiated Low Upper Shelf Welds," USNRC Report NUREG/CR-3506, Apr. 1984.

13. A. Saxena and S. J. Hudak, Jr., "Review and Extension of Compliance Information for Common Crack Growth Specimens," International Journal of Fracture, Vol. 14(5), Oct. 1978, pp. 453-468.

14. F. J. Loss, B. H. Menke, and R. A. Gray, Jr., "Development of J-R Curve Procedures," NRL-EPRI Research Program (RP 886-2), Evaluation and Prediction of Neutron Embrittlement in Reactor Pressure Vessel Materials Annual Progress Report for CY 1978, J. R. Hawthorne, Ed., NRL Report 8327, Naval Research Laboratory, Washington, DC, Aug. 1979.

15. H. A. Ernst, "Materials Resistance and Instability Beyond J-Controlled Crack Growth," Elastic-Plastic Fracture, (C. F. Shih and J. P. Gudas, Eds.), ASTM STP 803, Vol. 1, American Society for Testing and Materials, Phila., Pa, pp. 191-213.

16. J. W. Hutchinson and P. C. Paris, "The Theory of Stability Analysis of J-Controlled Crack Growth," Elastic-Plastic Fracture, ASTM STP 668, American Society for Testing and Materials, Phila., PA, Mar. 1979, pp. 37-64.

17. C. F. Shih, "An Engineering Approach for Examining Crack Growth and Stability in Flawed Structures," Proceedings of CSNI Specialists Meeting in Plastic Tearing Instability, USNRC Conference Proceeding NUREG/CP-0010, Jan. 1980.

18. W. J. Mills, "On the Relationship Between Stretch Zone Formation and the J Integral for High Stain-Hardening Materials," Journal of Testing and Evaluation, JTEVA, Vol. 9, No. 1, Jan. 1981, pp. 56-62.

19. J. D. Landes and D. E. McCabe, "Toughness of Austenitic Stainless Steel Pipe Welds," EPRI NP-4768, Electric Power Research Institute, Oct. 1986.

20. J. R. Rice, P. C. Paris, and J. G. Merkle, "Further Results on J Integral Analysis and Estimates," Progress in Flaw Growth and Fracture Toughness Testing, Proceedings of the 1972 National Symposium on Fracture Mechanics, ASTM STP 536, ASTM, 1973, pp. 231-245.

21. J. G. Merkle and H. T. Corten, "A J Integral Analysis for the Compact Specimen, Considering Axial Force as Well as Bending Effects," Trans. ASME, Journal of Pressure Vessel Technology, Nov. 1974, pp. 286-292.

22. G. A. Clarke and J. D. Landes, "Evaluation of J for the Compact Specimen," J. Testing and Evaluation, Vol. 7(5), Sep. 1979, pp. 264-269.

23. H. A. Ernst and P. C. Paris, "Techniques of Analysis of Load-Displacement Recoreds by J-Integral Methods," USNRC Report NUREG/CR-1222, Jan. 1980.

24. F. J. Loss, Ed., "Structural Integrity of Water Reactor Pressure Boundary Components, Annual Report for 1983," USNRC Report NUREG/CR-3228, Vol. 2, Sep. 1984.

25. P. McConnell and B. Sheckherd, "Fracture Toughness Characterization of Thermally Embrittled Cast Duplex Stainless Steel," NP-5439, Research Project 1543-12, Final Report, Electric Power Research Institute, Palo Alto, CA, Sep. 1987.

26. A. L. Hiser and G. M. Callahan, "A User's Guide to the NRC's Piping Fracture Mechanics Data Base (PIFRAC)," USNRC Report NUREG/CR-4894, May 1987.

APPENDIX A

J-R CURVE DATA ANALYSIS PROCEDURES

APPENDIX A

J-R CURVE DATA ANALYSIS PROCEDURES

1. OVERVIEW

J-R curve evaluation requires measurements of applied load, load-line displacement and crack length for the subject test specimen. Load and displacement are readily determined using a load cell and a clip gage, respectively. Instantaneous crack length generally is not directly measureable. Typically, it is inferred by evaluations of some other parameter in collaboration with equations relating that parameter (or changes in it) to the crack length (or changes in it). For static loading conditions, the single specimen compliance (SSC) method, also called the unloading compliance method, normally is used for evaluating crack length; hence the J-R curve can be obtained from a single test specimen.

2. CRACK LENGTH EVALUATION - COMPLIANCE METHOD

The compliance method uses the spring-like nature of the CT specimen (as given by the slope of the elastic load-displacement record) to establish crack length. As illustrated in Fig. A-1, the load-displacement record for a J-R curve test has a linear elastic portion at the beginning of the record, followed by plasticity formation up to maximum load, with decreasing load accompanying increased displacement thereafter. The sloped lines at various points on the record in Figure A-1 represent compliance measurements made during the test. These compliance unloadings represent a decrease in load of ~ 10% of the maximum load (actually a fixed "unload" of displacement), and then a reloading to the previous load value. A linear record of load (ΔP) versus displacement ($\Delta\delta$) results (Fig. A-2). This figure also demonstrates the significant compliance (slope) changes from the initial crack length conditions at the right (a/W ~ 0.52) to the final crack length conditions at the left (a/W ~ 0.78). The $\Delta\delta/\Delta P$ is combined with other terms to give (Ref. A-1):

$$U_{LL} = \frac{1}{\left[\frac{B_e\ E\ \Delta\delta}{\Delta P}\right]^{1/2} + 1} \qquad \text{(A-1)}$$

where $B_e = B - (B-B_N)^2/B$
B = gross specimen thickness
B_N = net specimen thickness
E = modulus of elasticity

The crack length for a load-line mounted clip gage is given by the calibration equation of Hudak-Saxena (Ref. A-1):

$$a/W = 1.000196 - 4.06319\, U_{LL} + 11.242\, U_{LL}^{2} - 106.043\, U_{LL}^{3} \quad \text{(A-2)}$$
$$+ 464.355\, U_{LL}^{4} - 650.677\, U_{LL}^{5}.$$

Two corrections to the compliance crack lengths are made: a rotation correction and a modulus correction.

The calibration equation (Eq. A-2) was determined from elastic specimens which had not been plastically deformed. Since these J-R curve tests result in significant plastic deformation of the specimen, a "rotation" correction must be applied to the measured slope values.

The rotation-corrected compliance, C_c, is evaluated from (Ref. A-2):

$$C_c = \frac{C_m}{\left[\frac{H^*}{R} \sin\theta - \cos\theta\right] \left[\frac{D}{R} \sin\theta - \cos\theta\right]} \quad \text{(A-3)}$$

where (Fig. A-3),

- C_c = compliance corrected for rotation of the specimen
- C_m = measured compliance = $\frac{\Delta\delta}{\Delta P}$
- H^* = initial half span of the load points (center of pin holes)
- R = radius of rotation of the crack centerline, $(W+a)/2$ where a is the last crack length
- D = one-half of the initial distance between the displacement measurement points
- θ = angle of rotation of a rigid body element about the unbroken midsection line, or
  = $\sin^{-1}\left[(d_m/2 + D)/(D^2 + R^2)^{1/2}\right] - \tan^{-1}(D/R)$
- P_m = measured load
- d_m = total measured load line displacement
- P_c = corrected load
- d_c = one-half of the corrected displacement

The modulus correction is used to provide a consistent starting point (initial crack length) between the compliance "measurements" of crack length and the optically-measured initial crack length. A "match modulus" (which matches the compliance and optical initial crack lengths) is evaluated from Eq. A-1 and A-2 in an iterative manner, by first determining the proper U_{LL} to give the optically-measured initial (pre-test) crack length. Using an initial (pre-test) compliance value (C_o), the match modulus, E_M, is determined by inverting Eq. A-1:

$$E_M = \left[\frac{1}{U_{LL}} - 1\right]^2 / (B_e C_o) \qquad \text{(A-4)}$$

Combining these two corrections, a corrected definition of Eq. A-1 results:

$$U_{LL,C} = \frac{1}{\left[B_e E_M C_c\right]^{1/2} + 1} \qquad \text{(A-5)}$$

This corrected value of U_{LL} is then used with Eq. A-2 to determine the crack length and, after subtracting the initial crack length, the crack growth for the specimen. These crack growth values are typically referred to as "predicted" crack growth values, or Δa_p.

3. J INTEGRAL EVALUATION - J_D and J_M

Values of the deformation theory (J_D) and modified (J_M) forms of the J integral are calculated using the following equations (Ref. A-3):

$$J_{D\ i+1} = \left[J_{D\ i} + \left(\frac{\eta}{b}\right)_i \frac{A_{i,i+1}}{B_N}\right] \left[1 - \left(\frac{\gamma}{b}\right)_i \left(a_{i+1} - a_i\right)\right] \qquad \text{(A-6)}$$

η = 2 + 0.522 b/W for compacts

γ = 1 + 0.76 b/W for compacts

b = unbroken ligament = W-a

W = specimen width

A = area under load-loadline displacement record

a = crack length

$$J_M = J_D - \int_{a_o}^{a} \left.\frac{\partial\ [J_D - G]}{\partial a}\right|_{\delta_{pl}} da \qquad \text{(A-7)}$$

where

J_D = deformation theory J

G = Griffith linear elastic energy release rate

= $K_I^2\ (1-\nu^2)/E$

a_o, a = the initial and current crack lengths

$J_D - G$ = J_{pl}, the plastic portion of the deformation theory J

δ_{pl} = the plastic portion of the displacement

ν = Poisson's ratio

and $K_I = P \; f\left(\frac{a}{w}\right) (WBB_N)^{-1/2}$

where P is the hold load at a partial unloading, $f(\frac{a}{w})$ is given in ASTM standard E 399, and W, B, and B_N are the specimen width, thickness, and net thickness, respectively.

Reference A-3 also provides an incremental form of Eq. A-7:

$$J_{M\,i+1} = J_{D\,i+1} + \Delta J_{i+1} \quad \text{(A-8)}$$

where

$$\Delta J_{i+1} = \Delta J_i + \left(\frac{\gamma}{b} J_{pl}\right)_i (a_{i+1} - a_i) \quad \text{(A-9)}$$

Deformation theory J, i.e., J_D, is the formulation of the J integral specified for use in the ASTM standards E 813 and E 1152. The severe validity criteria associated with J_D render J_D-R curve evaluations virtually useless for application to structural stability determinations, primarily due to the limits on crack extension. Evaluation of J_D-R curves for different sizes of CT specimens have demonstrated a specimen size dependence as well. In this report modified J is used as the primary form because it has been shown to be specimen size independent under greatly relaxed validity requirements, with much greater crack growth increments still yielding acceptable results.

4. J-R CURVE EVALUATION

A typical J-R curve is illustrated in Fig. A-4. The J-R curve format is in accordance with that of ASTM E 813-81. The line emanating from the origin, called the blunting line, is given by $J = 2\sigma_f \Delta a$, where σ_f is the flow strength (the average of the 0.2% offset yield strength and the ultimate strength). The exclusion lines are constructed parallel to the blunting line, but offset by 0.15 mm (0.006 in.) and 1.5 mm (0.060 in.).

By ASTM E 813-81 procedures, a straight line is fit to the test data between the 0.15 and 1.5 mm exclusion lines. This line is extrapolated back to the blunting line; the intersection is termed J_Q. J_{Ic} equals J_Q if various validity criteria are satisfied. In the present investigation, the overall (small) specimen sizes and the test materials (i.e., low strength and high toughness) preclude determination of J_{Ic} values valid per ASTM E 813.

In the power law evaluation of the J-R curve data, an equation of the form $J = C\Delta a^n$ is fit to the data between the exclusion lines. The power law J_{Ic} is defined as the intersection of the power law curve with the 0.15 mm exclusion line. Previous experience has shown that the power law definition of J_{Ic} tends to give values nearly equivalent to the ASTM E 813-81 values for low alloy (ferritic) steels.

The tearing modulus, T_M, is used to characterize the tearing resistance of structural materials. T_M is given by

$$T_M = \frac{E}{\sigma_f^2} \frac{dJ}{da} \qquad \text{(A-10)}$$

where dJ/da is the slope of the J-R curve. Since the J-R curve conforms to a power law, the value of T_M changes (decreases) with increasing crack growth. For comparison purposes, average values of T_M, termed T_{avg}, typically are used. The ASTM T_{avg} value (as defined by MEA) uses the slope of the linear fit curve as dJ/da; the power law T_{avg} value is determined from a fit of the power law curve to a straight line, defining dJ/da as an average slope evaluated in a closed-form manner (see Appendix H of Ref. A-4).

REFERENCES

A-1. A. Saxena, S. J. Hudak, Jr., "Review and Extension of Compliance Information for Common Crack Growth Specimens," International Journal of Fracture, Vol. 14, No. 5, Oct. 1978, pp. 453-468.

A-2. F. J. Loss, B. H. Menke, and R. A. Gray, Jr., "Development of J-R Curve Procedures," NRL-EPRI Research Program (RP 886-2), Evaluation and Prediction of Neutron Embrittlement in Reactor Pressure Vessel Materials Annual Progress Report for CY 1978, J. R. Hawthorne, Ed., NRL Report 8327, Naval Research Laboratory, Washington, DC, Aug. 1979.

A-3. H. A. Ernst, "Material Resistance and Instability Beyond J-Controlled Crack Growth," Elastic-Plastic Fracture: Second Symposium, Vol. I: Inelastic Crack Analysis, ASTM STP 803, American Society for Testing and Materials, Philadelphia, PA 1983.

A-4. A. L. Hiser, F. J. Loss, and B. H. Menke, "J-R Curve Characterization of Irradiated Low Upper Shelf Welds," USNRC Report NUREG/CR-3506, Apr. 1984.

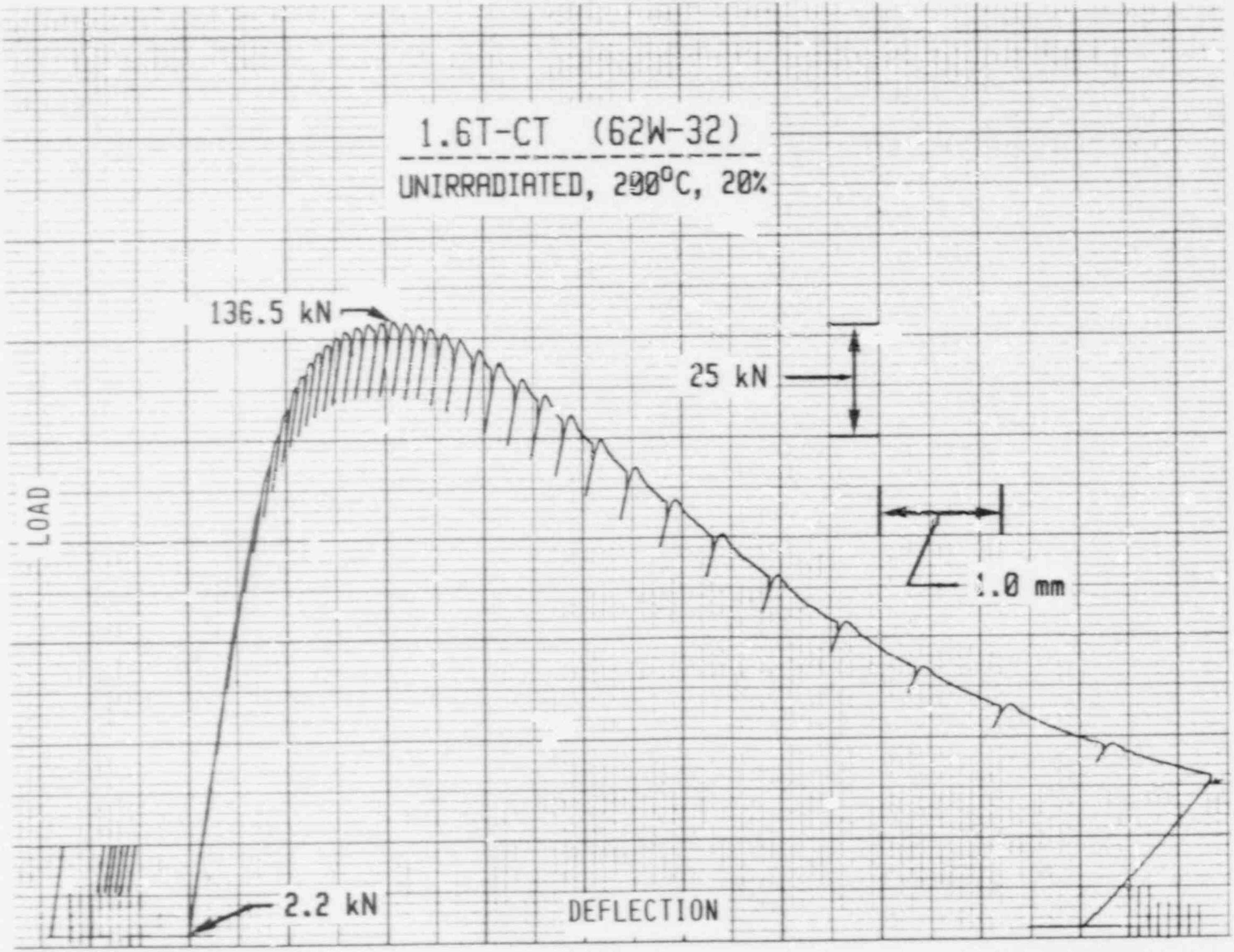

Fig. A-1 Typical load-displacement record for a J-R curve test. The test record is for a low-alloy steel specimen.

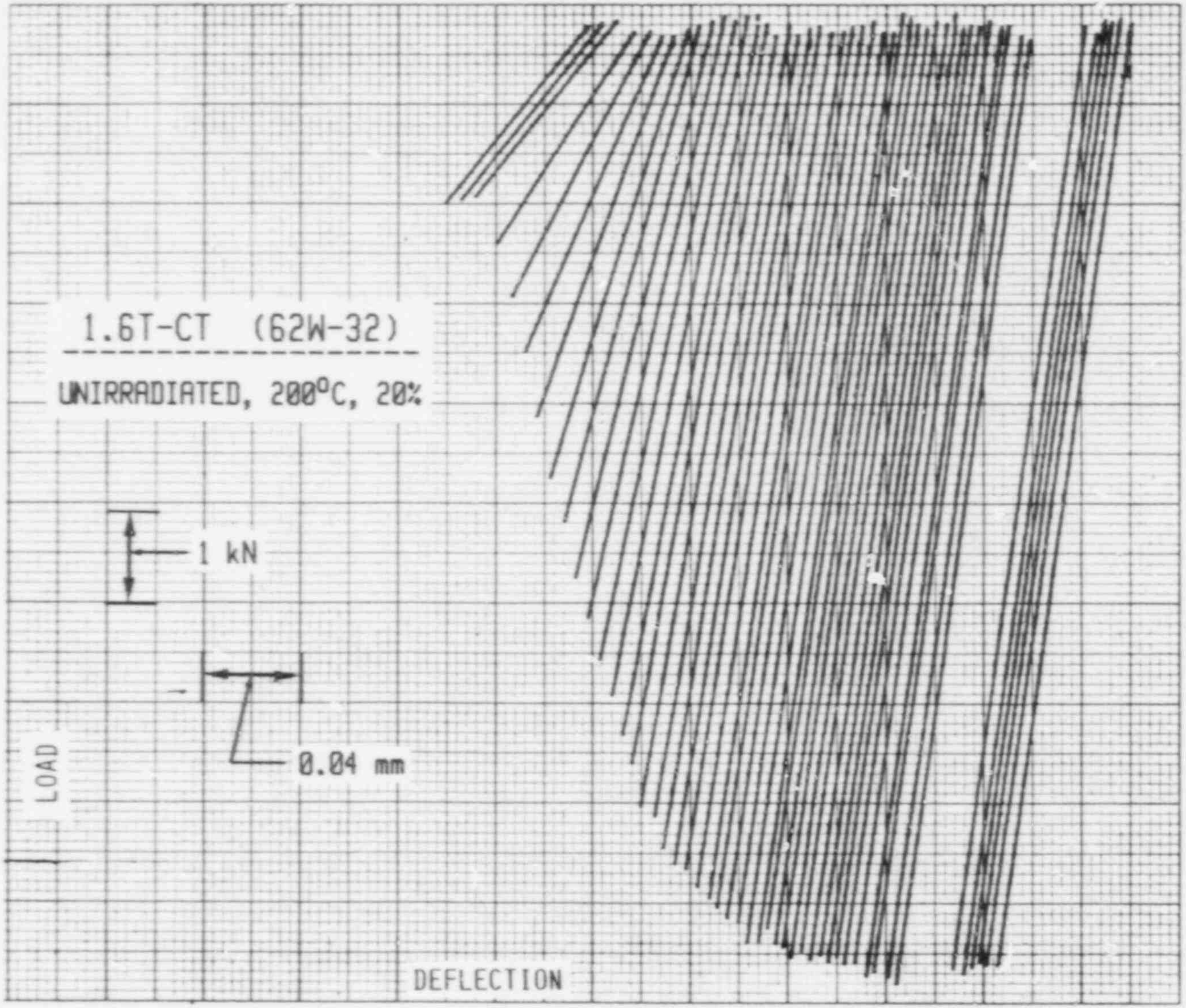

Fig. A-2 Unloading compliance traces for the J-R curve test in Fig. 1. In this case, the test data progress from right to left chronologically. Significant slope changes are apparent.

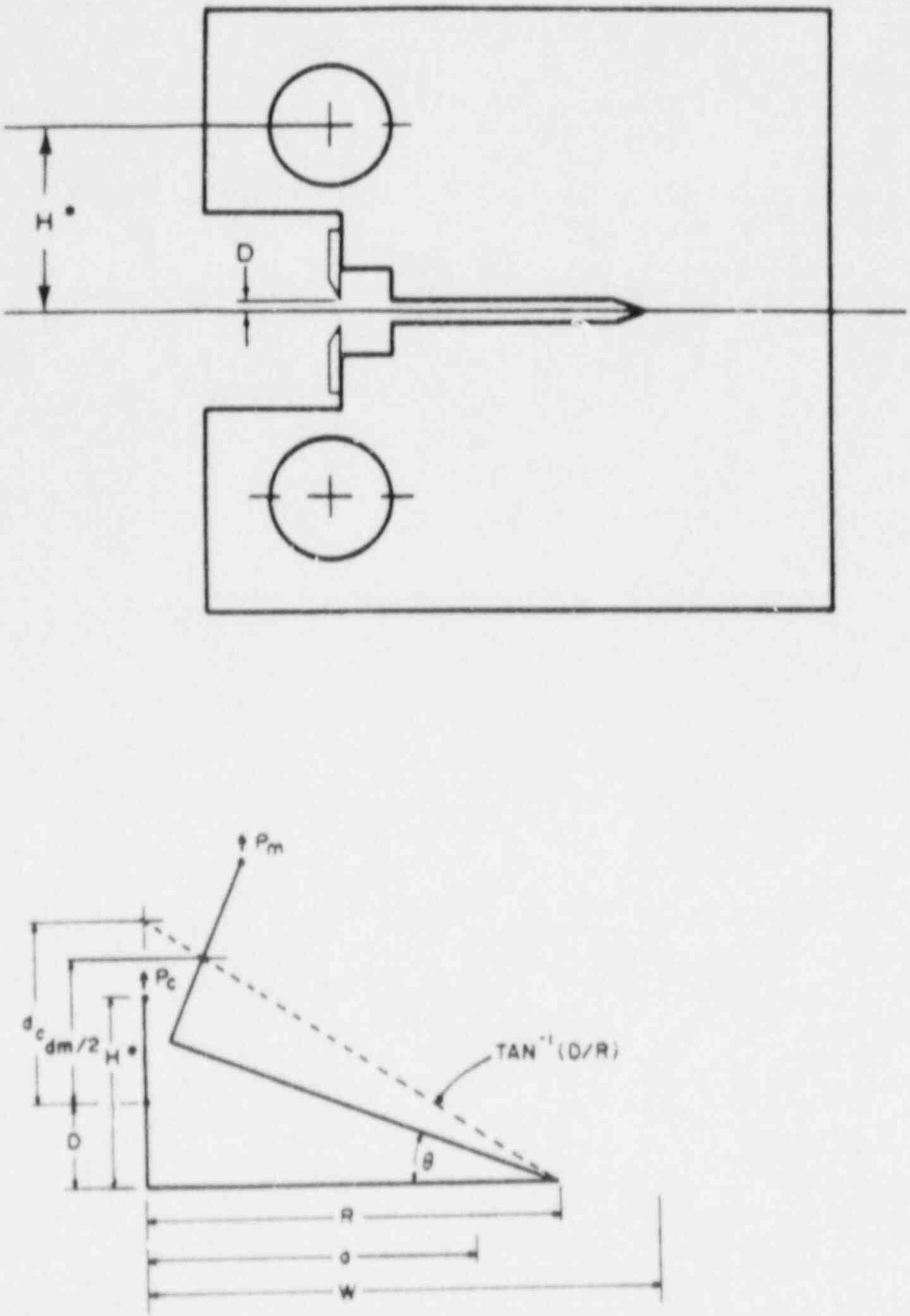

Fig. A-3 Elastic compliance correction for specimen rotation.

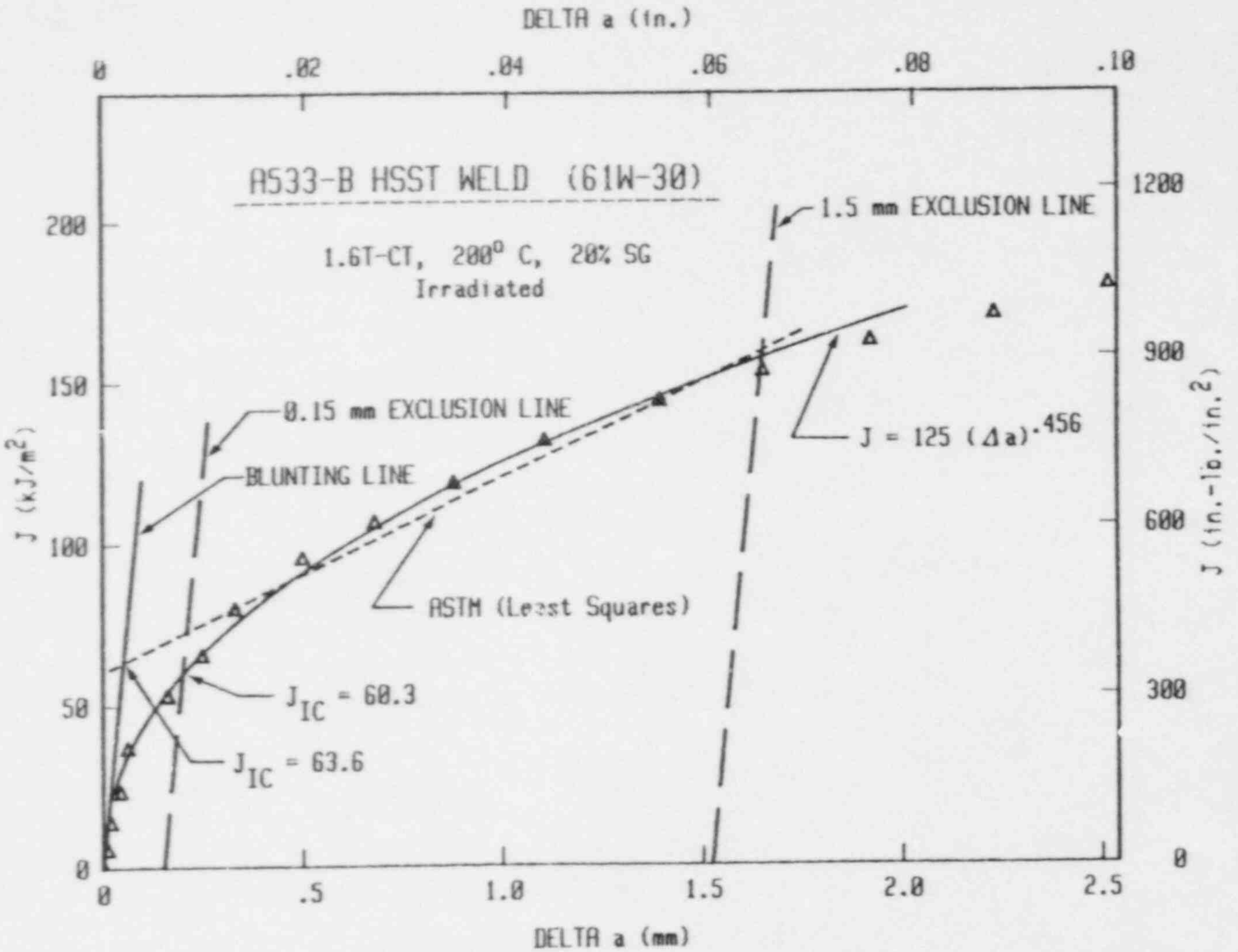

Fig. A-4 Example of a typical J-R curve. The ASTM E 813-81 format is used in these cases.

NRC FORM 335 (11-81) U.S. NUCLEAR REGULATORY COMMISSION **BIBLIOGRAPHIC DATA SHEET**	1. REPORT NUMBER (Assigned by DDC) NUREG/CR-5024 MEA-2229
4. TITLE AND SUBTITLE (Add Volume No., if appropriate) Tensile and J-R Curve Characterization of Thermally Aged Cast Stainless Steels	2. (Leave blank)
	3. RECIPIENT'S ACCESSION NO.
7. AUTHOR(S) A. L. Hiser	5. DATE REPORT COMPLETED MONTH August YEAR 1988
9. PERFORMING ORGANIZATION NAME AND MAILING ADDRESS (Include Zip Code) Materials Engineering Associates, Inc. 9700-B Martin Luther King, Jr. Highway Lanham, Maryland 20706-1837	DATE REPORT ISSUED MONTH September YEAR 1988
	6. (Leave blank)
	8. (Leave blank)
12. SPONSORING ORGANIZATION NAME AND MAILING ADDRESS (Include Zip Code) Division of Engineering Office of Nuclear Regulatory Research U.S. Nuclear Regulatory Commission Washington, DC 20555	10. PROJECT/TASK/WORK UNIT NO.
	11. FIN NO. B8900
13. TYPE OF REPORT Technical Report	PERIOD COVERED (Inclusive dates)
15. SUPPLEMENTARY NOTES	14. (Leave blank)

16. ABSTRACT (200 words or less)

Although cast stainless steels have excellent properties in the as-received or pre-service condition, significant degradation of the properties, principally fracture toughness (J-R curve), can occur after extended exposure to elevated temperatures typical of service conditions.

The NRC is sponsoring work to study the significance of in-service embrittlement of thermally aged, cast stainless steel. This report summarizes the results of tensile and J-R curve tests of commercial and experimental heats of these steels. The materials were supplied by Argonne National Laboratory (ANL), who have conducted microstructural studies to identify the degradation mechanisms.

The loss in Charpy-V upper shelf energy can be quite large, up to 57% for aging at 450°C for 9980 h. The decrease in fracture toughness, specifically J levels on the J-R curve, can be even more severe, with a reduction of 75% in some cases.

Data from this study are accessible through the NRC's Piping Fracture Mechanics Data Base (PIFRAC), an on-line system available at MEA.

17. KEY WORDS AND DOCUMENT ANALYSIS	17a. DESCRIPTORS
cast stainless steels, thermal-aging, low temperature aging, fracture toughness, J-R curve, correlations, tensile strength	

17b. IDENTIFIERS/OPEN-ENDED TERMS

18. AVAILABILITY STATEMENT	19. SECURITY CLASS (This report)	21. NO. OF PAGES
Unlimited	Unclassified	
	20. SECURITY CLASS (This page) Unclassified	22. PRICE $

NRC FORM 335 (11-81)

UNITED STATES
NUCLEAR REGULATORY COMMISSION
WASHINGTON, D.C. 20555

OFFICIAL BUSINESS
PENALTY FOR PRIVATE USE, $300

SPECIAL FOURTH-CLASS RATE
POSTAGE & FEES PAID
USNRC
PERMIT No. G-67

120555139217 1 1AN1RF1R5
US NRC-OARM-ADM
DIV FOIA & PUBLICATIONS SVCS
RRES-PDR NUREG
P-210
WASHINGTON DC 20555